CRANFIELD UNIVERSITY

Bertrand SAINT-RAMOND

LOW MASS PLATINUM ALUMINIDE BONDCOAT FOR THERMAL BARRIER COATING

SCHOOL OF INDUSTRIAL AND MANUFACTURING SCIENCE

Supervisor : J.R. NICHOLLS

Mphil THESIS

Academic Year 2000-2001

Abstract

During the last 30 years, Thermal Barrier Coating systems (TBCs) have been extensively used to protect the hottest part of aero-engines. They can extend significantly the lifetime of high pressure turbine blades and combustor walls by decreasing the superalloy substrate temperature by up to several hundreds of degree C.
TBCs are duplex systems consisting of a thermal insulative ceramic toplayer and an intermediate metallic bondcoat layer, whose function is to protect the substrate against corrosion and oxidation and to promote the ceramic adherence by forming an alumina scale at the interface with the ceramic.
The lifetime of the TBCs is however limited by chemical, mechanical and thermal stresses in the coatings due to bondcoat oxidation and the mismatch of thermal expansion coefficient (CTE) between the ceramic, the bondcoat and the substrate.

The bondcoat consideration is therefore of a substantial importance for the TBCs lifetime extension, and the present work has been focused on the development of a novel and innovative intermetallic overlay bondcoat, having a much thinner thickness than conventional bondcoats, acting as a diffusion barrier for substrate harmful elements, and promoting the formation of a pure, slow-growing and adherent alumina scale.

The low-mass bondcoat system has been based on a 3-15 microns thick **$PtAl_2$** intermetallic layer, with the ternary addition of a **reactive element** (Hafnium, Zirconium, or Yttrium).
Aluminium and Platinum are deposited sequentially by the **sputtering process** (Physical Vapor Deposition). The bondcoat is thus a **multi-layer coating**, and the layers react one with another exothermically by diffusion after a subsequent heat treatment at a relatively low temperature.

The temperature of reaction between the layers and the stability of the obtained intermetallics has been studied by using Differential Thermal Analysis.
Different platinum aluminides have been developed as bondcoats and the number of layer has been varied (up to 350 layers) in order to study the influence on the coating structure.
Finally, the most successful systems have been cyclically tested to be compared to industrial bondcoats systems.

These experimentations have led to the development of a highly controllable bondcoat deposition and formation process. Different morphologies and compositions can be accurately obtained by varying the individual layer thickness and Al/Pt thickness ratio within the coatings.
A reactive element, which consists of either zirconium, yttrium or hafnium has been introduced into the aluminium layer by sputtering co-deposition and it has been therefore

demonstrated the possibility of improving the efficiency of the low-mass bondcoat by adding such an element evenly through the coating.

Whatever the composition or its structure, the low-mass bondcoat is adherent to the substrate and does not interact with the substrate during the deposition and the formation process.
The bondcoat is thermally stable for a significant time of aging at 700°C, 900°C and 1100°C, but do not withstand cyclic oxidation testing better than industrial bondcoats. Nevertheless, to really assessed the potential of the low mass bondcoat, a cyclic oxidation test has to be performed after ceramic topcoat deposition, which would modify the local stress gradients on the thermally grown oxide, during cooling.

Acknowledgements

The author would like firstly to express his gratitude to his academic supervisor, Prof. J.R. Nicholls, for his skilful support, contribution and belief at any time of the project.

The author is also indebted to Snecma Moteurs Villaroche for making possible his employment at Cranfield University .
The author is particularly grateful to Mr Y. Jaslier and S. Alperine from Snecma Moteurs, who have trusted and motivated him from the beginning.

The author wishes to express his gratitude to Mr K.J. Lawson for his technical support and knowledge in sputtering and coatings technology.
Thanks are also due to Dr Sue Impey for useful discussion and help in coating characterisation and thermal analysis.
The author has also benefited from the experience of Mr Tim Rose in sputtering technology.

The author is very thankful to the following technical support staff at Cranfield for their contribution to the present work: Mr Jeff Rao, Mr. Tim Prior, Mr John Hedge, Mr Colin Matthews, Mr Andrew Dyer, Mr Dennis Timpson.

Special thanks to Vitor Pereirra, my favourite office mate, for his natural kindness and his very helpful computer assistance.

Finally, the author acknowledges to have benefited from working within a team of eminent scientists, with complementary technical expertise and skill.

Nomenclature :

ρ	[g/cm^3]	density
κ		adiabatic exponent
η_{th}		thermal efficiency
q	[kJ]	heat/ enthalpy
p	[Pa]	pressure
T	[K]	temperature
k'	[cm²/s]	parabolic rate constant
x	[µm]	oxide layer thickness
t	[s]	time
D	[m^2/s]	diffusivity
Z		metal volume
µ'		chemical potentials of oxygen at the bondcoat-oxide
µ"		chemical potentials of oxygen at the oxide-gas interfaces
V	[cm^3]	volume
k''		volumic parabolic constant
m	[g]	mass
M	[g/mol]	atomic mass
S	[cm^2]	surface
a	[µm]	thickness
mol		number of molecules
G		heat transfer coefficient

Table of contents

List of tables

List of figures

Introduction

The blades and vanes of the high-pressure turbine section of aero engines are among the most highly stressed parts in engineering components. Internally cooled airfoils of state-of-the-art nickel based superalloys operate at temperature of about 1000°C with short-term peaks leading to hot spots above 1100°C, close to 90% of the alloy's melting points[90].

The continuing need for advanced gas turbine engines has led to improved thrust and fuel efficiency, and a reduction of emission rates, resulting in reduction of cooling air and the **increase in turbine entry temperature (TET).**

These demanding conditions have therefore required the utilization of advanced air-cooling technology, the continuing development of improved strength and higher temperature capability nickel base superalloys, and the use of **Thermal Barrier Coatings.**[12;113]

The Thermal Barrier Coating (TBC) concept consists of a thermal insulative ceramic top-layer along with an intermediate metallic bondcoat layer, deposited on top of the nickel-based substrate of combustion and turbine parts.
This coating system reduces the actual temperature of the metal introducing a large temperature gradient (up to 100°C) through the ceramic coating and allowing higher operation temperatures.

Thanks to its extremely low thermal conductivity and good phase stability, **Yttrium-stabilised zirconia** is the most successful ceramic top-layer, when combined with a metallic interlayer. This interlayer acts on the one hand as a bond coat (a glue between the ceramic layer and the metallic substrate) and on the other hand as an oxidation and corrosion protective barrier.[101]

Two deposition processes for ceramic layer are currently in use:

Plasma spray, which gives relatively thick, low cost and low conductivity coatings, well adapted to combustion chambers. The thermal barrier coating applied by Plasma Spraying have been used successfully for more than 20 years to extend life of combustion chambers and annular platforms of high pressure nozzle guide vanes within the turbine section of the engine.

However, the thermal spray deposition process is not tailored for **turbine blade applications**, because it results in poor surface finish, high heat transfer coefficient, low erosion resistance and poor mechanical compliance.[72]

The use of **Electron Beam Physical Vapor Deposition** (EB-PVD) has thus been introduced, giving a good surface finishing, a columnar microstructure with high strain compliance, a superior tolerance against thermal shock, and a good resistance to erosion and foreign object damages.[72;90]

The lifetime of the thermal barriers is however limited by chemical, mechanical and thermal stresses in the coatings due to **bondcoat oxidation** and **the mismatch of thermal expansion coefficient** (CTE) between the ceramic, the bondcoat and the substrate.[41]

The bondcoat consideration is therefore of a substantial importance for the TBC life improvement, because it is the key for the ceramic adherence. Indeed, the first role of the bondcoat is to form an intermediate layer of a high-stable aluminium oxide at the interface with the ceramic.

Overlays and Diffusion coatings have been so far extensively used as bondcoats, because of their excellent resistance against oxidation and corrosion and a sufficient content in aluminium to form the required alumina scale[40]. However these coatings were originally developed for **protective coating** application and the needs actually differ between a bondcoat and an environmental protection coating:
Bondcoats must develop **a pure, slow-growing alumina scale** that **does not spall** (spallation would lead to the loss of the TBC and coating failure). For environmental protection coatings, isolated spallation is less important, provided the coating can self-repair.

To meet at best the demanding requirements of the scale, the bondcoat has to be thermally stable and to act as an **effective diffusion barrier** for the transition metal and refractory metal elements from the substrate (Tungsten, Molybdenum, Titanium and Tantalum)[99]. Their outward diffusion and incorporation within the scale can indeed compromise adhesion.

Finally, coating thickness and weight have to be seriously considered to reduce manufacturing cost and to enhance blade design tolerances.

These considerations have led to the development of a new type of bondcoat for Thermal Barrier Systems applied to nickel-based, rotating turbine blades.

Based on the $PtAl_2$ barrier work published by Cranfield and DERA[22;23], and originally developed for the protection of titanium alloys and titanium aluminide, a **thin intermetallic layer** has been developed to act as a diffusion barrier to stop the outward diffusion of deleterious scale forming elements from the superalloy substrate.

The low-mass bondcoat system has been based on a 3-15 microns thick **$PtAl_2$** intermetallic layer, with the ternary addition of a **reactive element** (Hafnium, Zirconium, or Yttrium). These elements have been shown in the recent works to be beneficial by either reducing the rate of scale growth or increasing the adhesion of the alumina scale.

Aluminium and Platinum are deposited sequentially by the **sputtering process** (Physical Vapor Deposition). The bondcoat is thus a **multi-layer coating**, and the layers react one with another exothermically by diffusion after a subsequent heat treatment at a low temperature.

The following figure summarizes the coating formation process (it can be used with more than 2 layers):

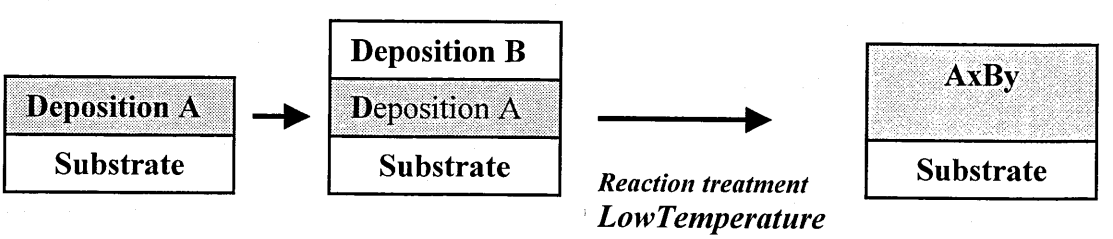

Figure 1: Low-mass bondcoat deposition and formation

The low temperature of the deposition process and the relatively low reaction temperature of the studied intermetallic compounds **prevent any interdiffusion** between the substrate and the coating.

The reactive element has been introduced by codeposition with either aluminium or platinum, allowing a control of its concentration and distribution in the coating.

The temperature of reaction between the layers and the stability of the obtained intermetallics has been studied by measuring their heats of formation using a 1600°C DTA apparatus.

Different platinum aluminides have been developed as bondcoats and the number of layer has been varied (up to 350 layers) in order to study the influence on the coating structure.

Finally, the most successful systems have been cyclically tested to be compared to industrial bondcoats systems.

1. TBC concept and technologies

1.1. The need for Thermal Barrier Coatings

This chapter aims to explain the demanding blade operating condition in the high-pressure turbine section and to highlight the need for high-temperature resistant coatings.

1.1.1. The Brayton cycle

High thrust at low weight (i.e. high thrust-to-weight ratio), low fuel consumption and pollution control are the principal requirements for a jet engine. This has resulted in a continuing and progressive increase of the Turbine Inlet Temperature (TIT) over the last 20 years.[48;114]

In order to understand the need for a higher combustion exhaust gas temperature, a thermodynamic study has to be made regarding the gas turbine process.

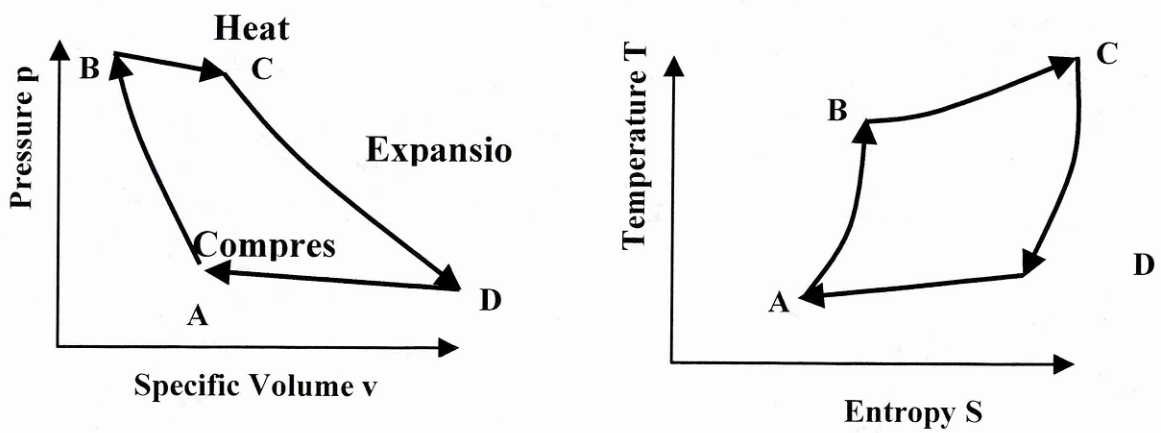

Figure 2: Pressure/specific volume and Temperature/entropy diagrams of the real Joule (or Brayton) process

The engine cycle is referred to as the Joule or Brayton thermodynamic process, which consists of 4 steps (Figure 2). A first isentropic compression (A=>B) is carried out in the compressor section, followed by an isobaric heat addition (B=>C) in the combustion

chamber; then the hot gas expands isentropically in the turbine section, and finally reverts to its original condition in the atmosphere.[48;86;101]

The thermal efficiency of the engine cycle is expressed as follows:

$$\eta_{th} = 1 + \frac{q_{in}}{q_{out}} = 1 - \frac{T_D}{T_C} = 1 - \frac{(p_D)^{\frac{\kappa-1}{\kappa}}}{p_C}$$

The power efficiency of the engine can be therefore enhanced by increasing the turbine inlet temperature T_D, while keeping a constant cooling level.
The TIT of aero-engines have thus risen by about 100°C over the last 20 years and a much greater increase is predicted for the next 5-10 years as more powerful large aero-engines are developed.[114]

1.1.2. Cooling considerations in the combustor

The highest temperature in the engine is reached in the combustion chamber and in the first stage of turbine blades. These strongly stressed components have to be protected in order to avoid high cost maintenance. High-temperature resistant materials have been developed along with improved air cooling technology; however, the more demanding conditions will still lead to an increase in cooling airflow.

Nowadays, the atmosphere pollution by the harmful exhaust emissions is a topical issue and engines have to be designed with this environmental consideration.[3;41;48] The gas turbine engine uses hydrocarbons as fuel and the oxygen of the ambient atmosphere as oxidant. The injected fuel is however not burned completely because apportioning the exact amount of air is difficult to achieve. Therefore, due to this incomplete combustion, and to the heat of combustion process (as discussed in the previous section), the exhaust gases contain pollutants, some of which are considered as hazardous:

- Carbon monoxide (CO)
- Unburned hydrocarbons (CH_n)
- Unburned carbon (C)
- Nitric oxide (NO_x)

The unwanted emission of pollutants is also caused by the loss of pressure in the combustor (ideal combustion is isobaric), and by cooling airflow, which makes the combustion temperature dropped near the combustor walls[3].

In a typical combustor (Figure 3), 20-30% of the air is mixed and burnt with the fuel in the primary zone and 70% bypasses this zone in order to cool the hot combustor parts and to be diluted in the secondary and tertiary zones.[48;86]

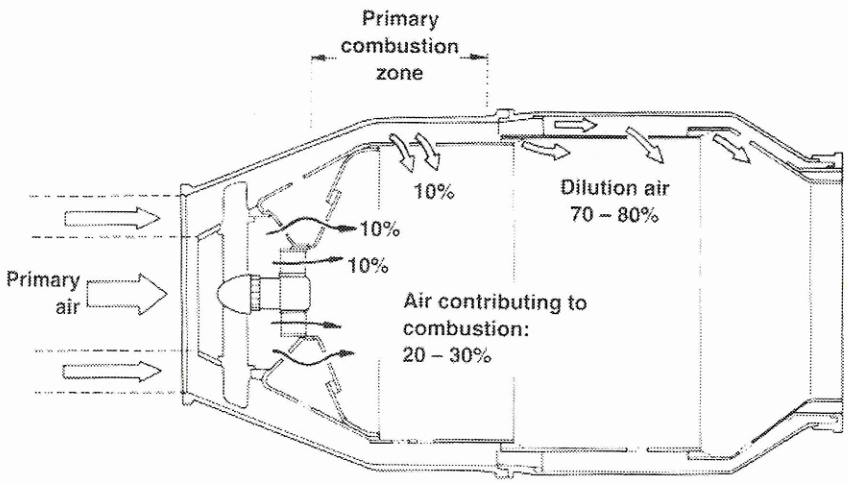

Figure 3: Schematic flow in combustion chamber [48]

The air introduced through the liner wall (10%), downstream of the dilution jets, may not be effective in the combustion process, therefore contributing to combustor inefficiency. Low pollutants emission and improved specific fuel consumption can therefore be achieved by the **reduction of cooling air** in the combustor chamber [3].
Even if more efficient cooling technology has to be introduced, the need to use less cooling air, along with an increase in TIT, constitutes nowadays a conflicting challenge for the material designed to withstand the operation conditions.

1.1.3. Superalloy development

The materials use to manufacture the hot sections of the HP turbine, such as the blades and the vanes have been continuously developed to resist the increasing **thermo-mechanical stresses**. This evolution has been carried out by **chemistry variation** and **structural development** (single crystal).
In 1941, the blades of the first Whittle engine consisted of austenitic stainless steel and were aimed to resist to thermomechanical stress up to a TIT of 700-750°C. Nickel base alloys, such as Ni-20Cr replaced the stainless steel due to the increased strength required for the turbine blades. However, even if the high presence of chromium was beneficial for

protection against hot corrosion, it was at the expense of the creep resistance. It has thus led to alloys with lower amount of chromium (as little as 8%wt).
The content of γ'-forming elements, such as aluminium and titanium, have conversely increased, progressively improving the strength at high temperature. Refractory elements, such as molybdenum and tungsten have also been added for solution strengthening, leading to an even less corrosion resistant material.[39;64]

In parallel to these chemical composition variations, a structural evolution has taken place. To replace the conventional cast material, new processing techniques such as directional solidification (DC) and single crystal techniques (SC) have been introduced, preventing grain boundary corrosion and crack initiation at grain boundaries (Figure 4).[101]

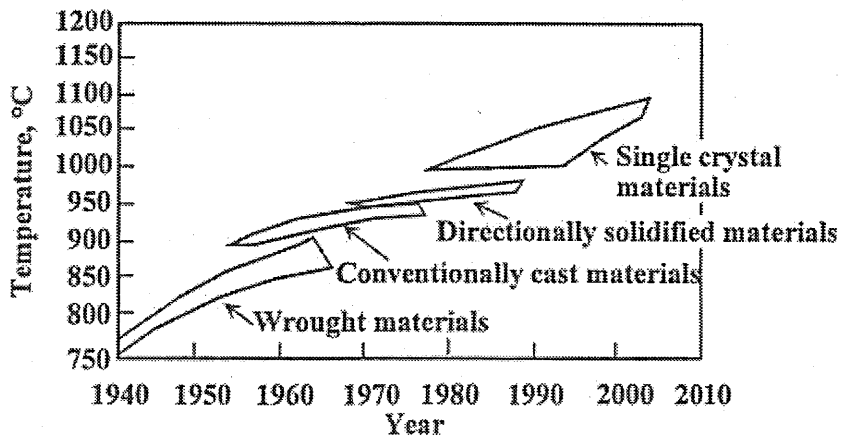

Figure 4: Temperature improvements of gas turbine alloys [101]

Directionally solidified materials were introduced in the 70s and consist of directionally grown grains in the high creep resistant (001) crystallographic orientation.
In the 1975-1985 period, many new competing materials appeared such as cast single crystal cast superalloys, directionally solidified eutectic superalloys, directionally recrystallized extruded powder alloys and fibre reinforced superalloys. However, major aircraft engine producers, because of technical and economical interest adopted **single crystal** materials for turbine blades and vanes.[46]

The next development in single-crystal superalloy technology was the introduction of **rhenium** for further improved stress rupture and creep resistance. Rhenium strengthens the

alloy matrix and retards the coarsening of fine γ' (rafting) with time at high temperature[12;13;46] by reducing dramatically diffusion in the superalloy at high temperature.

All these advances in superalloy technology have thus raised their high temperature capability to about 1100° C, which corresponds to 90% of the average superalloy melting point (T_{Ni}= 1433°C)[90;101].
The TIT of modern gas turbine may reach however temperature as high as 1500°C, and even with the introduction of complex air cooling systems, the superalloys have to be protected against these high temperatures

Furthermore, the development in superalloys has shown that any improvement in mechanical strength and creep properties at high temperature is associated with a decrease in oxidation and corrosion resistance.

The superalloys reveal therefore crucial performance limitations for the future engine enhancements, and the application of a suitable high-temperature coating is actually the best technical and economical solution to tackle this problem.

1.1.4. The need for high-temperature coatings

The previous sections have highlighted and discussed the even more demanding conditions suffered by the hot section materials of the HP turbine:

- The TIT has to be increased to improve engine thrust and efficiency.
- Air-cooling has to be reduced in the combustor to prevent pollution and improve the combustion process.
- The superalloy innovations (for combustor liners, vane and blade materials) are about to reach their limitations[114]. The current thermal capability (1100°C) can virtually not be increased any more, and even if the creep resistant is better than ever, the oxidation resistance is not good enough to withstand the even higher temperature.

During the last 30 years, TITs have indeed increased by about 500°C. 30% of this increase is due to improved superalloys and casting process, while the other 70% is due to more efficient design in air-cooling (introduction of serpentine convection, thin cooling), but also to the use of **protective coatings**.[13]

By the mid-1950s, high temperature coatings were being applied to hot section gas turbine aerofoils. The use of various types of **aluminium diffusion coatings** became increasingly common in the 1960s[39], because of their high oxidation resistance.
These coatings were essentially applied by the pack cementation techniques and they consisted firstly of simple aluminides, followed by modifications with silicon, chromium and platinum.[40]
In the late 1970s, the **MCrAlY** (M = Fe, Co, Ni) **overlay coatings** were introduced to protect the superalloys from hot corrosion.

The protective coatings have thus inhibited for many years the interaction between the superalloy substrates and the potentially damaging environment: metal recession, oxidation, corrosion and harmful species diffusion in the superalloys have been largely reduced.[116]

However, the continuing increase of operating temperatures in the hottest part of the engine has led to the limitation of the protective coatings and the so-called **Thermal Barrier Coatings (TBC)** have been introduced. The TBC is a duplex system consisting of an intermediate metallic coating and a ceramic top layer, which reduce the effective temperature of the superalloy.
The TBC allows, therefore, either the engine to operate at higher temperature, or to reduce the air-cooling flow, or a compromise thereof.
Different classes of coatings compositions, and deposition processes have evolved to meet the various applications, as discussed in the following chapters. These high-temperature resistant coatings have been thus applied for 20 years on the static part of the combustor, and recently on the vanes and blades of the HP turbine.[114;116]

1.2. The TBC Technology

In this chapter, the concept and properties of the thermal barrier coatings are being reviewed. An emphasis is given to the ceramic deposition technique challenge to coat the turbine parts of the engine.

1.2.1. TBC concept

In spite of the dramatical progresses made in material development and cooling technology in the last 20 years, the continuing increase of TIT has led to the development of a new protection for the turbine blades and the combustor parts of aircraft engines. This solution consists of protecting the metallic parts, which are exposed to high temperature, with a thin and insulative ceramic coating, called a Thermal Barrier Coating.

1.2.1.1. General concept

The thermal barrier coating is actually a multi-layer system. It consists of an insulative ceramic outer layer (topcoat) and an intermediate metallic layer (bondcoat) deposited between the superalloy substrate and the ceramic[116].

The function of the ceramic top-layer is to protect the metallic substrate (bondcoat + superalloy) from the high temperature of the combustion gas in contact with the coating surface. Depending on the thermal conductivity and the coating thickness of the ceramic, a temperature gradient, which may exceed often 100°C, can be created through the coating. As shown in the Figure 5, a large part of the temperature drops across the boundary layer of gas at the ceramic surface[67;72], which is actually a better thermal insulator than the ceramic. The temperature gradient across the ceramic is then assessed either between the ceramic surface and the bondcoat interface or between the ceramic bondcoat interface of both ceramic coated or ceramic free bondcoats. The latter reference is more relevant because the metal surface temperature drives the life of the TBC.

The TBC benefits for the engine operation can be either[39;51;117]:

- The increase of the gas temperature: The TBC allows the substrate material to tolerate higher temperature.
- The reduction of the cooling air flow, leading to an increase in turbine efficiency
- The lowering of the metal temperature: the lifetimes of cooled components, which are limited by creep damage, are prolonged.

- The decrease of the magnitude of thermally induced strains: Because the coating reduces the thermal gradients in the metal substrate, it reduces also the driving force for thermal fatigue.

The ceramic material usually used for TBC is **Yttria stabilised Zirconia** (Z_2O_3- 8wt% Y_2O_3) and is deposited either by Plasma Spraying or Electron Beam Physical Vapour deposition (EB-PVD). The resulting coatings have a structure relative to the deposition technique and have a thickness, which varies in the range 120-400 microns. These deposition processes are detailed and compared in a subsequent section.

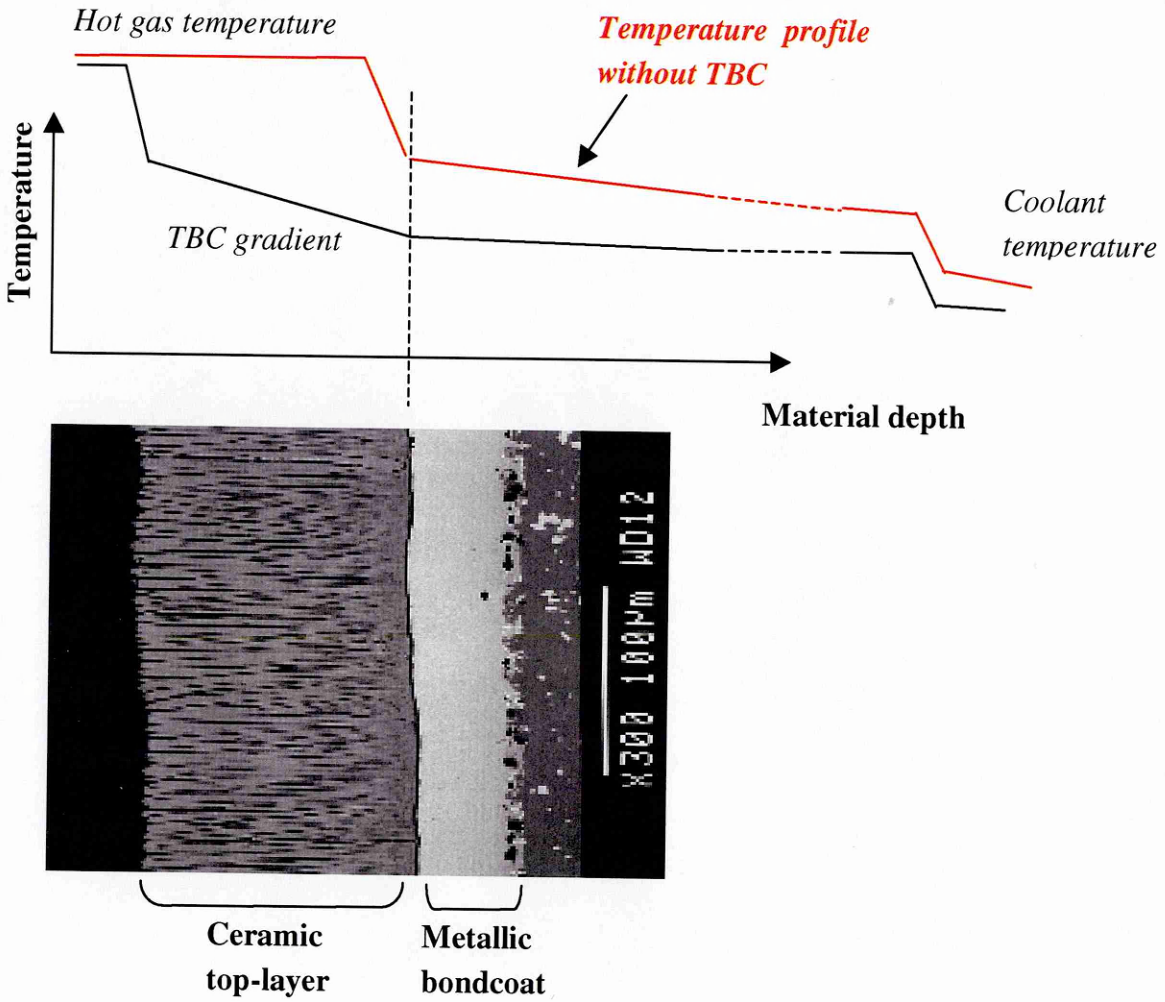

Figure 5: Backscattered micrograph of an EB-PVD ceramic layer and a platinum aluminide bondcoat. A schematic of the TBC principle is represented beside the photograph.

The metallic bondcoat function is threefold[6]:

- Its main purpose is to provide a mean of adherence for the ceramic layer. Especially in the case of the EB-PVD TBCs, the bondcoat must contain a sufficient amount of aluminium to form and maintain an alumina oxide scale at the bondcoat/ceramic interface. This few microns thick layer is commonly known as the TGO (Thermally Grown Oxide) and acts as a "glue", which promotes the adherence of the ceramic on the metallic substrate.
- Due to the formation of the oxide scale, the bondcoat is oxidation and corrosion resistant and protects therefore the superalloy substrate.
- The bondcoats can be designed to palliate the expansion mismatch between the ceramic and the superalloy

The bondcoat is usually deposited by Chemical Vapour Deposition (CVD), Physical Vapour Deposition (PVD) techniques, low-pressure plasma spraying or electroplating and has a thickness varying in the range 50-225 microns.

1.2.1.2. The ceramic top layer

This part will focus on the stabilised zirconia, which is the commonly used ceramic material for TBCs.
Zirconia ceramics have been chosen as thermal insulator for superalloy substrate because they have a much lower thermal conductivity than the metals, but a higher thermal expansion coefficient than many other ceramic phases. Their main drawback is however like many ceramics, that they are relatively brittle.
Zirconia exists in 3 different allotropic forms:

1. **Monoclinic** up to 1170°C
2. **Tetragonal** in the range 1170°C-2370°C
3. And **cubic** up to its melting point at 2680°C

The polymorphism of zirconia has a catastrophic effect on the ceramic TBC topcoat because the tetragonal to monoclinic transformation is accompanied by a large volume variation[2;7;28]. To avoid the effects of this phase change, it is common to use calcium, magnesium or yttrium oxides to **stabilise** the structure of zirconia.

Early TBC's were manufactured from magnesia (MgO) or calcia (CaO_2) stabilised zirconia, because they performed well in service at operating temperature below approximately 1000°C.

Above this temperature, significant diffusion of the magnesium or calcium ions occurs and precipitates of magnesium or calcium oxides are formed, which results in an increase of the thermal conductivity[67].

Early combustor coatings consisted of an outer insulative layer of air plasma deposited, 22 wt% MgO stabilised ZrO_2 on an inner metallic bondcoat of air plasma deposited Ni-Cr or Ni-Al. By replacing the magnesia with 7 wt% yttria, the spallation life at high temperature has been improved substantially.[3]

The **Yttria partially stabilised zirconia** (ZrO_2 with 8wt% Y_2O_3), which was firstly deposited by APS (air plasma spraying), has finally been chosen for the refractory ceramic layer because it offers the best combination of properties[6;61]:

- Thermal stability: with only 8wt% yttria, a form of tetragonal zirconia, called the metastable tetragonal phase t', can be retained at room temperature. This phase can be decomposed but only by heating to 1400°C or above for long periods.
- Refractory and chemical stability
- Low thermal conductivity
- Relatively high coefficient of thermal expansion, which matches with the metallic substrate

APS technologies have been used to deposit TBCs on combustor and afterburner parts and **LPPS** (Low Pressure Plasma Spraying) was applied to highly thermally loaded parts like vane platforms and vane airfoils. However, these techniques were not adapted to the application on blade platforms and airfoils, which are subjected to high thermal and additional mechanical loads. The **EB-PVD** technology has therefore been developed, offering a much better strain tolerance.

1.2.1.3. The bondcoat intermediate layer

The major role of the bondcoat is to provide a means of adherence for the ceramic layer to the superalloy substrate that depends on the ceramic deposition technology:

- Air plasma sprayed TBC need a rough bondcoat surface, which act as a mechanical key for the ceramic layer.
- On the other hand, the adherence of EBPVD ceramic layer is achieved by the growth of an oxide scale during the processing at the interface bondcoat/ceramic; the oxide providing the bond between the ceramic and the bondcoat.

Along with the adherence requirement, the bondcoat has to provide hot corrosion and oxidation resistance as well as to accommodate the expansion mismatch between the metallic substrate and the ceramic.
Two main different types of bondcoat have therefore been introduced, referring to the usual classes of protective coatings:

- The diffusion coatings, which consist usually of aluminide or modified-aluminide intermetallic compounds. Their formation involves an interdiffusion with the substrate.
- The overlay coatings, which are also known as MCrAlY. Conversely to the diffusion coatings, they have a very little interaction with the substrate and are designed as oxidation and corrosion resistant alloys.

APS and LPPS ceramic layers have usually been applied on MCrAlY overlay bondcoats[51]. EB-PVD TBC's are applied on either diffusion, platinum aluminides, or MCrAlY overlay bondcoats.

1.2.2. The properties of a thermal barrier coating system

There are actually two classes of property required for a TBC system.

- The assets or the benefits of the TBC in the operating environment, which are those required functions of the innovative high-temperature coating.
- The properties related to the life-limiting factors, that the coating system must have to prevent failure.

These properties are summarised in these following tables:

Benefits	
Improved component life expectancy	Low thermal conductivity of the ceramic layer develops a temperature gradient between the substrate and the environment.
Higher operating temperature	
Reduce need for active cooling	
Improved engine performance	More complete combustion associated with operating at higher temperatures.
Lower Nox emission	
Protection against oxidation and corrosion	Bondcoat properties.

Table 1: Benefits of Thermal Barrier Coatings

Life-limiting factors	
Ceramic sintering	At high temperature, a possible densification can occur in the ceramic layer leading to an increase in thermal conductivity.
Erosion	Dependent on the ceramic layer deposition technique.
Ceramic Surface finishing	
Ceramic strain tolerance	
Strain mismatch	Dependent on the bondcoat deposition methods and properties
Poor adhesion at the bondcoat/substrate interface	
Poor adhesion at the ceramic/bondcoat interface	

Table 2: TBCs life-limiting factors

1.3. The competitive deposition processes

In the aeronautical field, TBCs were firstly applied on the combustor parts of the engine, and the ceramic top-layer was deposited by plasma spraying. As the combustion temperature has continuously increased, the need to coat first the nozzle guide vanes and now the turbine blades has become critical. However ceramic deposition using plasma spraying was not suitable to this turbine blade application and the EB-PVD has been introduced.

This chapter is aimed at detailing these two line-of-sight processes, as well as their respective properties and consequences for the TBC system.

1.3.1. Plasma spraying

Thermal spraying was the first process to be chosen to deposit TBC on combustor parts. It is the generic name for a family of thick overlay coating processes, which consist of melting the material powder to be deposited using a thermal source (flame, electric arc, or plasma), and then to project it at high velocity to the substrate to be coated. The resulting coating is formed by overlapping molten droplets (called splats), which have been flattened out during the impact[14;29;53;116].

Most metals, alloys, many ceramics, cermets and even plastics can be deposited by a thermal spraying process. The only condition is that the material to be deposited can melt[53].

The following table gathers the most common thermal spray processes[14;20;53]:

Flame Spraying (FLSP)	Powder, rod, or wire are melted by an oxy/fuel flame at a temperature around 2500°C.
Electric Arc Spraying (EASP)	A wire is melted by an electric arc at 5500°C. The melted droplets are projected to the substrate by a gas.
Detonation gun (d-Gun)	Powder is melted in a gun by spark ignition of explosive gas.
High-velocity oxy/fuel (HVOF)	Powder is melted in a combustion chamber by a O_2/H_2 flame or O_2/fuel supersonic flame. The coatings are characterized by lower residual stresses, a strong adherence to the substrate and a lower porosity.
Plasma Spraying	Powder is melted by an arc-generated plasma within the plasma spray gun.

Table 3: Thermal spraying processes

Plasma spraying has the advantage of being able to deposit a wide range of metals, ceramics, or a combination thereof to generate homogeneous coatings with microstructures consisting of fine, equi-axed grains, without columnar/leader defects[73]. This makes this process the most versatile of the thermal-spraying techniques. For this reason, and along with its cost-effective advantage, it was chosen as deposition technique for ceramics and bondcoats of TBC systems.

In the plasma spraying process, a non-transferred arc is created between a tungsten electrode and the anode, which serves as a nozzle. The gas passing through this high current density arc are then ionised resulting in a plasma jet, which is ejected from the nozzle at velocities of several hundred meters per second.
Most guns use nitrogen, argon or helium as the main plasma gas.
The material powder is introduced in the plasma and sprayed in the form of semi-molten particles because of the high temperature and inert nature of the plasma.

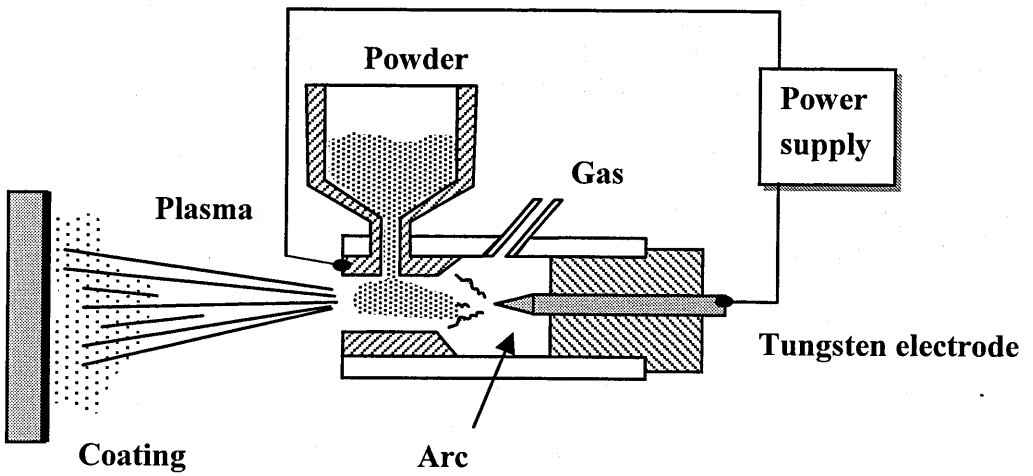

Figure 6: an arc plasma spraying torch device

One common disadvantage of all thermal-spraying techniques is that there can be some interaction between the molten particles and the ambient atmosphere. Even if plasmas are essentially inert, turbulence can entrap air resulting in unacceptable levels of oxide in some coatings. Thus, Air Plasma Spraying (**APS**) coatings contain internal globular oxides (Cr an Al-rich) and filamentous oxides (Y and Al-rich) due to the oxidation of airborne particles.

Various modifications to air plasma spraying (APS) have then been introduced to minimise this oxidation effect[20;53]:

LPPS (Low Pressure Plasma Spraying) or **VPS** (Vacuum Plasma Spraying) processes rely on the modification of the spraying atmosphere by spraying a reduced pressure in an enclosed chamber. This leads to the reduction of the oxygen/particle interaction and reduces the oxide formation. The coatings that result also have a denser structure.

Limitations:

The thermal spray application is a line of sight coating application process, and the areas to be coated must be directly accessible to the spray apparatus. The rate of deposition is therefore dependent on **the angle of impact** of the spray jet[88].

Complex robotic manipulations are required for complete coverage of workpieces.

Porosity problems can largely be overcome using post-coating thermo mechanical treatments.

Cooling holes can be rapidly obstructed and technical solutions have to be implemented to cover them during the deposition.

The plasma sprayed ceramics have a lamellar structure build up by splat overlapping. The structure can contain voids arising from outgasing, shrinkage or topographical effects (shadowing)[53]. Unmelted material, as well as oxides [61] can be also present especially if the deposition was processed in air.

The structure exhibits also a micro crack network consisting of:

- **Cracks perpendicular to the coating surface**: which originate from cracking of individual splats and expand during cooling.
- **Cracks parallel to the coating surface**: which are due to a lack of adherence between the overlapped splats.

1.3.2. Electron Beam Physical Vapour Deposition (EB-PVD)

Physical vapour deposition emerged in the 1960s as the primary overlay coating production technique. It refers to the deposition of metals by transport of vapour in a vacuum without the need for a chemical reaction[11;59]. PVD processes involve atom-by-atom or molecule-by-molecule deposition of various materials on a solid substrate. The PVD processes of most importance are thermal evaporation, sputtering and ion plating[14] and are detailed in a subsequent chapter.

Electron Beam Physical Vapour Deposition belongs to the **thermal evaporation processes**. In this technique, the material to be deposited is either placed on a refractory metal boat or used in the form of a rod ingot. A directed high-energy electron beam then melts and evaporates the rod in the vacuum chamber. The *evaporant* forms an atomic cloud (shaped like an ice cream cone, with the tip of the cone at the source), that coats all surfaces in the line-of-sight of the rod.

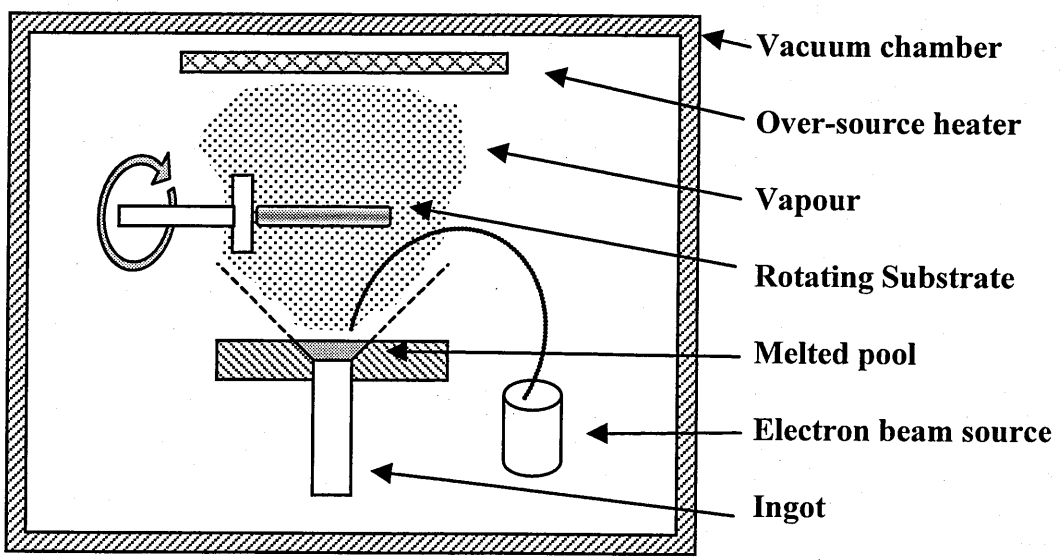

Figure 7: EB-PVD apparatus

Because of the geometry of most components to be coated, it is necessary to rotate them because EB-PVD is a line-of-sight process.

EB-PVD is a high deposition rate process and deposition rates for a rotated substrate of >25μm/min have been reported[11].

The deposition of compounds is possible but the composition of the deposited coating will often be different from that of the starting ingot, due to differences in vapour pressure of the elements in a typical coating alloy. The transition in the gaseous phase leads generally to dissociation and a subsequent recombination of the species on condensation.

Therefore, during the deposition of thermal barrier ceramic, the bleed of an oxygen containing gas is introduced in the coating chamber in order to compensate for the dissociation of zirconia[49]. The need of oxygen in the chamber is also prompted by the need to establish, before the ceramic deposition, a thin film of aluminium oxide on top of the bondcoat onto which the ceramic condensate can chemically bond.

The EB-PVD technique is moreover particularly suitable for the deposition of thermal Barrier Coatings, due to the relatively high deposition rate and the possibility of influencing the coating microstructure. Indeed, through a combination of substrate heating and work pressure control, evaporation technique can lead to fibrous, columnar or equiaxed morphologies [60;65;107].

However, a **columnar growth** is most often chosen because it results in a very strain tolerant microstructure compare to that of the plasma sprayed coating. This morphology is therefore characterised by a little bonding between adjacent columns, but strong bonding with the substrate[28;51].

The EB-PVD TBC eventually fails at the thermally grown aluminium oxide layer that develops on the bondcoat at the ceramic-bondcoat interface after prolonged cyclic exposure.

1.3.3. Adhesion to the bondcoat

In the case of the plasma sprayed topcoats, the bondcoat surface has to be **grit-blasted** prior to ceramic deposition[92]. The effective bond strength of the coating depends on the number of molten particles that impact, flow and solidify on the grit blasted surface.
The bonding mechanism of thermally sprayed coating is then predominantly **physical** rather than metallurgical or chemical. Because of rapid cooling, there can only be limited interdiffusion between the deposit and substrate materials.
Although the molten particles will deform to the surface roughness, producing a degree of **mechanical interlocking**, grit blasting does not significantly increase the surface area, but does create a very active surface.
In the case of the EB-PVD TBC, it is the role of the bondcoat to provide a means of adherence for the ceramic layer. A thermally grown oxide (**TGO**) develops at the bondcoat-ceramic interface during processing and acts as a glue between the bondcoat and the topcoat. Conversely to the plasma sprayed TBC, the bondcoat surface has to be smooth to promote the correct ceramic growth morphology.

1.3.4. Strain compliance

The ceramic materials such as zirconia are known to provide excellent thermal insulation but their structure is very brittle. However, during engine operation, the strain tolerance is directly related to the resistance to thermal cycling and therefore to coating life achievable on turbine components.
Putting a ceramic coating mechanically into **tension** by substrate deformation does not lead to the spallation of the coating. It leads to through coating cracking. However, when a substrate is deformed mechanically to produce **compression** in the coating, spallation occurs very rapidly[7].

In the case of the thermally sprayed ceramic coatings, the strain tolerance is achieved using the extended network of micro crack, but it is not as efficient as in the case of the EB-PVD

coatings. Grain boundaries between individual columns are weak but they provide an excellent tolerance to the compression and tension waves suffered by the brittle ceramic during operation[25;67;101].

Cyclic burner rig testing by the major aero-engine manufacturers has demonstrated significant life improvement (**approximately 10 times**) with EB-PVD TBC coatings[6].

1.3.5. Surface finish influence

The surface finish or the roughness of the blade affects directly the gas flow and therefore the turbine efficiency of the engine. As related by Morell, P. and Rickerby, D.S. (1997)[67], the coefficient of friction C_f of the surface of the blades is also directly related to the roughness and in turn the C_f value influences the heat transfer coefficient and efficiency of the turbine.

Provided the bondcoat has a good surface finish, the ceramic roughness is controlled by the tips of the columnar grains. EB-PVD ceramic coating surface is thus very smooth (1μm Ra) compare to the much rougher surface (10 μm Ra) of air plasma-sprayed ceramic layer[6;67].

A subsequent polishing of the thermal sprayed ceramic surface can make some improvements, but erosion in service, which is detailed in the next section, brings back quickly the initial surface roughness.

1.3.6. Erosion

Due to incomplete combustion or ingestion of foreign objects by the engine, high velocity particles are formed and flow with the hot gas through the compressor, the combustor and the turbine. These particles can then cause erosion of the protective coating and TBC by impacting and spallation.

Erosion does not affect greatly the combustor parts, because the gas flow is parallel to the coating surface. However, turbine blades and nozzles, which have normal surfaces to the gas flow can be seriously damaged by the particles impaction[67].

Erosion of the **ceramic topcoat** is considered as a **life-limiting factor**, because it leads to the progressive loss of thickness during operation, which is directly linked to its efficiency.

As related by Nagaraj (1995)[68], TBC spallation due to erosion is observed generally on substantial sections of the blade leading edge and in local regions of the trailing edge and tip of the blades.

On the other hand, TBC's are more susceptible to erosion than fully dense ceramics because their microstructure contains many crack-like features, which can growth and expand until spallation of coating pieces.

Moreover, the erosion rate has been shown to be dramatically dependent on the ceramic deposition process. As studied by Tabakoff (1989), Nicholls (1997, 1999) [71] and related by

Morell and Rickerby (1997)[67], EB-PVD TBC is **7-10 times more erosion-resistant** to normal impacts than is an APS coating, whatever the size of the particle and the test temperature.
This difference in performance is caused by the strain tolerant microstructure relative to both processes. In the case of the APS system, the strain tolerance is introduced through the inclusion of porosity and micro crack, whereas it is achieved using a columnar microstructure in the case of the EB-PVD coatings.
The APS coating fails by propagation of cracks around splat boundaries and through the micro crack network. The erosion rate is high, because the erodant needs a low amount of energy to generate expanded micro cracks and cause the spallation of platelets. In contrast, the erosion of EB-PVD TBC requires the generation of a new crack surface across individual columns, which needs a relatively high amount of energy and leads to lower erosion rates.
In addition, the **surface finish** of the plasma sprayed ceramics, which have been polished, reverts quickly to its initial state, whereas it is not affected for the EB-PVD coatings.

1.3.7. Thermal conductivity

The thermal conductivity values for zirconia based coatings belong to the lower (within the range 0.5-2 W/m.K) range of thermal conductivity for oxides. This is moreover significantly lower than values determined on bulk zirconia (2-4 W/m.K)[2].
The structure of the ceramic coating is at the route of this property difference and explains also why **EB-PVD ceramic have higher thermal conductivity than the plasma sprayed coatings** having the same composition[25;61;67;72].
The plasma sprayed coatings contain two different types of micro cracks. The first type is perpendicular to the coating surface, and does not affect the thermal conductivity. Conversely, the second type of cracking, parallel to the coating surface help reducing the thermal conductivity because the resulting expanded porosity is perpendicular to the heat flow.

In the case of EB-PVD coatings, the reduction in thermal conductivity comes mainly from the intracolumnar fine porosity, the intercolumnar porosity being much less effective as it is arranged perpendicular to the surface. Schematically[2], the columnar coating can be considered in an electrical analogy, more as a set of parallel resistances than a series set which gives a closer image of the sprayed coatings.

Furthermore, conversely to plasma sprayed ceramic coatings, the thickness of the EB-PVD coatings affects the thermal conductivity of the ceramic[56;61]. The microstructure evolution

during the coating growth starts indeed from a multitude of small columns and intercolumnar voids to a denser structure with less but wider columns. The ceramic coating structure comes progressively closer to the bulk zirconia structure and results in an increase of the thermal conductivity. It causes thus a dilemma because for both types of deposition, thick coatings are needed to enlarge the temperature gradient. As showed by Nicholls and al (1997)[72], it is possible to lower the thermal conductivity of EB-PVD coating by layering the columns. The principle relies on introducing interfaces into each column structure without disrupting the overall columnar structure, which gives the good strain tolerance properties.

1.3.8. Final comparison

Technical comparison

The first table gathers the main structural and technical differences between the plasma sprayed TBCs and their EB-PVD counterparts.

	Plasma Spraying	EB-PVD
Structure	lamellar	columnar
Surface finish	Good but extra polish	excellent
Bondcoat roughness	Grit blasted (10μm)	Smooth (1μm)
Bonding mechanism	mechanical	Chemical
Typical ceramic thickness	0.2-3mm	0.1-0.3mm
Cooling hole closure	poor	Excellent
Large parts predicable	favourable	costly
Investment costs (%)	100	100-400
Parts per charge	1	1-10

Table 4: Structural and processing comparison

Benefits comparison

The following table compares the properties of the TBC in service

	Plasma Spraying	EB-PVD
Thermal conductivity	0.6-0.8 W/m.K	1.6-2 W/m.K
Strain tolerance	poor	excellent
Resistance to erosion	Poor, when the impact is normal to the coating surface	good
Turbine efficiency	Can be affected by erosion	Not affected by erosion

Table 5: Properties comparison

The operation conditions suffered by the High Pressure turbine blades are severe. These rotating parts must withstand relentlessly thermal cycling and creep constraints. The introduction of TBC reduces the harmful effect of these conditions by reducing the substrate temperature. As the superalloy substrate temperature decreases, the blade strain is reduced but still exists, leading to different deformation of the TBC layers, relatively to the difference in thermal expansion coefficient, and plasticity. Therefore the ceramic has to withstand the generated stresses otherwise it breaks and spalls resulting in the TBC failure. Because of its columnar morphology, the EB-PVD ceramic can tolerate thermal strain much better than the plasma sprayed ceramic and even if its thermal conductivity is a bit higher than the plasma-sprayed coatings one, this coating highlights the most suitable technique for turbine blade application. Methods exist to reduce the thermal conductivity of EB-PVD coatings, even if these methods are not commercially available at present.

2. Bondcoat considerations

2.1. Bondcoat requirements for EB-PVD TBCs

As described in the previous sections, the multi-layer TBC system insulates the superalloy substrate from the high temperature of the combustion gas. However, spallation of the ceramic toplayer leads to the failure of the TBC system because it can not self-repair. **A strong and reliable bond between the ceramic and the bondcoat must therefore be created.**

In the case of the EB-PVD TBCs, this bond is produced chemically using the growth of an alumina scale at the smooth ceramic/bondcoat interface.

This chapter aims thus at describing the EB-PVD TBC scale formation as well as the failure factors related to it.

A bondcoat specification is given in order to underline the requirements for a durable and reliable TBC system.

2.1.1. TBC failure mechanisms

In order to understand the failure mechanism of the TBC, it is substantial to describe the deleterious interactions and evolutions between the different parts of the TBC system, and their environment[101] through time, high temperature exposure and temperature variation.

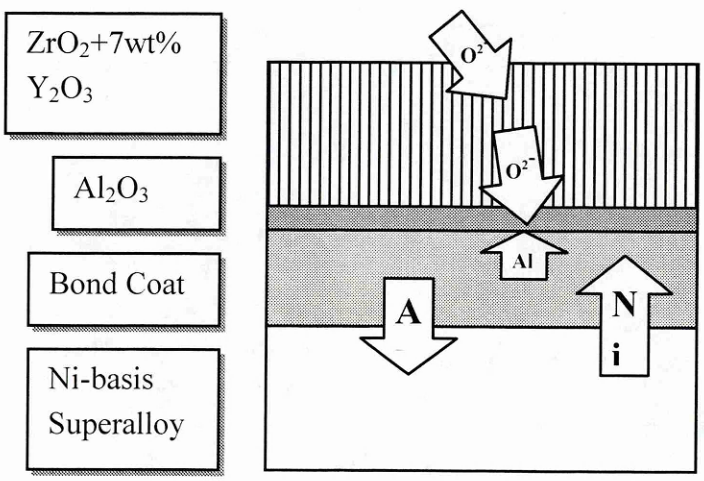

Figure 8: Interaction and interdiffusion in the TBC system

As mentioned earlier in the report, the ceramic layer must be **strain tolerant** to avoid instantaneous delamination[117] under thermo-mechanical cycling conditions of the turbine components.
Failure can occur also because of the high temperature and erosive environment. High temperature condition leads to **sintering** of zirconia, which is characterised by changes in porosity and crack morphology and by an increase of elastic constant. Long time exposure at these high temperature leads also to **phase transformation**, which is extremely deleterious because it is followed by an up to 10% volume variation.
Crack growth and **thermo-mechanical fatigue** are also caused by temperature changes.

As the zirconia's ceramic layer used for TBC is a fully oxidised material, oxidation does not affect it[7]. However, oxygen can diffuse through the ceramic top layer by two mechanisms:

- An ionic transportation through the lattice by reverse movement of oxygen ion vacancies.
- A gaseous diffusion along the columnar morphology boundaries and along the tortuous networks of interconnected micro cracks and pores.

The oxygen diffusion depends thus on the structure of the ceramic and influences the oxidation rate of the bondcoat. Depending on the bondcoat chemical composition, and diffusion kinetics, the oxides scales formed can consist of Al_2O_3, Cr_2O_3 and/or spinel phases, but the usual expected oxide is **α-Al_2O_3** , because of its high stability.

The oxidation mechanism will be detailed in the next section, but it has to be kept in mind that **the oxide scale is the weakest part of the TBC system** and can be affected by the outward diffusion of elements from the bondcoat or substrate and also by the development of **compressive stresses** during the growth of the scale[6;51].
The most likely failure location is therefore the TGO/bondcoat interface but TBC breakdown can also occur near the ceramic/TGO interface, leaving a thin, white layer on the bondcoat. This type of spallation is commonly called the **white failure** and is caused by the growing oxide scale stresses[101].

Differences in chemical activities of the elements in the bondcoat and substrate lead to **interdiffusion**[21;93]. In general, Ni from the Superalloy substrate diffuses outwardly into the bondcoat, and Cr and Al from the bondcoat diffuse inwardly into the substrate (Figure 8).

The actual chemical composition of the surrounding alloy matrix (bondcoat and substrate) determines the diffusion constant and therefore the diffusion rate of each individual element[101].
Thus, different diffusion rates from either side of the bondcoat/substrate interface are responsible for the originating **Kirkendall-pores**[50;101;109]. The extension of these pores along with the generated internal stress and material deformation can lead to the destruction of the interface with the substrate. The deleterious effect of Kirkendall voids has also been observed at the bondcoat/oxide scale interface[50].

Even though the TBC ceramic layer can spall due to foreign object impact, erosion thermal fatigue or extended sintering, **the most usual failures** are the edge or buckling delamination[101] at **the interface TGO/bondcoat,** which are due to:

- the strain mismatch between the ceramic, the scale and the bondcoat leading to stress build-up through the coating during thermal cycling.
- the properties and adherence of the TGO growing at the ceramic-bondcoat interface.

2.1.2. Bond coat oxidation mechanism

Scale formation[30;52;99;112;117]:

As explained in the previous section, the growth of the oxide scale is controlled by the inward diffusion of oxygen and the outward diffusion of aluminium.
When oxygen is in contact with an alloy surface at elevated temperature, nuclei of all possible oxides are formed, and the amounts of these oxides are such that the proportion of metal atoms is essentially the same as that of the alloy surface. These oxides grow laterally and outwardly during the first oxidation sequence usually called **the transient phase**.

However, the oxide with the greatest stability continues to grow laterally, until the alloy surface is covered with a continuous layer of this oxide. From this point, the growth of the other metal oxides stops and the oxidation rate is controlled by the growth of the predominant oxide. This growth occurs predominantly at the TGO/alloy interface by inward diffusion of oxygen through the oxide grain boundaries, for the growth of an alumina scale under a thermal barrier coating.
This final oxidation phase is often referred as to the **selective oxidation**, developing a protective scale of the most stable oxide.

As related by Felten (1976) or Smialek (1987), during the oxidation mechanism of a NiCrAl alloy (whose oxidation is comparable to that of the commonly used superalloys), a transient oxidation is firstly observed at the early stages, with the formation of external NiO, $NiCr_2O_4$ and Cr_2O_3 before the formation of the continuous aluminium oxide layer.

In the case of the TBC system, the formation of transient oxides is however deleterious. Their growth rate is not predictable, they are not thermally stable (sometimes volatile) and their formation can therefore lead to the TBC failure. It is thus desirable to develop a **pure and unique stable oxide scale** with no other oxides on the alloy surface, which is **the role of the TBC bondcoat.**

α-Al_2O_3 is regarded as the most stable oxide even at high temperature and is usually formed as protective oxide or TGO scale, because diffusion through it is relatively slow compare to most other oxides and because its growth rate is also slow. Cr_2O_3 scales are also very stable, but they are susceptible to degrade by volatilisation at very high temperatures under an oxygen-containing atmosphere:

$$Cr_2O_3(solid) + \frac{3}{2}O_2(gas) = 2CrO_3(gas)$$

When Cr_2O_3 is grown as protective layer, this evaporation of CrO_3 leads to the continuous thinning of the Cr_2O_3 scale.

In parallel with the oxidation transient phase, the formation of α-Al_2O_3 is not instantaneous. **Metastable cubic phases**, such as γ, δ, **or** θ have been shown to form at temperatures from 700°C to 1200°C, affecting the oxidation behaviour of the alloy[79;82].
The following phase formation sequence gathers the various transient aluminas observed when an NiAl intermetallic oxidises:

$$\gamma - AlO(OH) \xrightarrow{500°C} \gamma - Al_2O_3 \xrightarrow{750°C} \delta - Al_2O_3 \xrightarrow{900°C} \theta - Al_2O_3 \xrightarrow{1000°C} \alpha - Al_2O_3$$

The scales grow by different transport mechanism and have different microstructures. θ-Al_2O_3 scales are thus less dense and faster growing than α-Al_2O_3. The phase transformation from cubic to hexagonal (θ- or δ-Al_2O_3 to α-Al_2O_3) results in a **13% volume reduction** in the scale, generating tensile residual stresses and cracking. Transverse cracks through the scale thickness allow rapid oxidation and ultimately, the **formation of ridges** and convolutions in the scale.

The presence of the ridges radically modifies the localised stress field[36] and provides out-of-plane tensile stresses at the peak of the ridges and in-plane compressive stresses at the shoulder of the ridges.
However, this phenomenon appears to be unique to nickel aluminide and can be partially avoided if the oxidation is performed at a temperature above 1100°C.

The scale formation for an EB-PVD TBC is performed before the deposition of the ceramic, during the pre-heating stage. It is formed by predominantly inward diffusion of oxygen ion transport, mainly along grain boundaries. A significant flux of aluminium ions diffuses also in the opposite direction through the alumina grains. A reaction with oxygen can thus occur in the grain boundaries and lead to the lateral growth of the oxide scale. This can moreover result in scale convolution.
The oxidation reaction occurs therefore in the region of oxide grain boundaries, especially near the bondcoat/oxide interface.

Scale growth:

Under isothermal condition, the growth of the scale is approximately parabolic and follows the equation[99]:

$$dx / dt = \frac{k'}{x}$$

where k' is the **parabolic rate constant** with units cm^2/sec
and x is the growing oxide layer thickness.

The instantaneous growth rate of the scale is therefore an inverse function of its thickness[30].
Assuming that the oxide layer is compact and that a thermodynamic equilibrium is established at the metal-oxide interface, at the gas-oxide interface and throughout the scale, the parabolic constant is expressed as follows:

$$k' = \frac{1}{RT}\int_{\mu'}^{\mu''}(D_O + \frac{Z_A D_A}{2})d\mu$$

where D_A and D_O are the diffusivities of aluminium and oxygen, Z_A is the metal volume and μ' and μ" are the chemical potentials of oxygen respectively at the bondcoat-oxide and at the oxide-gas interfaces.
The constant k" is also often introduced because it takes the equivalent volume V of the oxide into account:

$$k'' = \left(\frac{8}{V}\right)^2 k'$$

The parabolic rate constant k' and k" are usually used to compare the relative oxidation rates of the various oxide layers. The following figure gathers the rates of the commonly encountered oxides and show the **relative low parabolic rate of the alumina scale**:

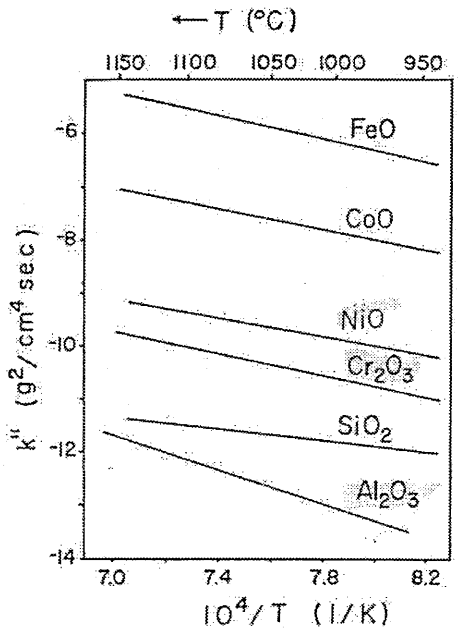

Figure 9: Order of magnitude of rate constants for the growth of selected oxides

A slow-growing oxide scale is an important factor to increase the life of the TBC system. After a critical thickness which depends on the thermal conditions (1-5 μm for aeronautical engine and 5-10 μm for industrial gas turbine), the scale indeed breaks and the TBC fails.

2.1.3. Causes of Failure at the scale-bondcoat interface

2.1.3.1. Voids formation

The formation of voids at the TGO/bondcoat interface during oxidation growth has been observed in virtually every externally-grown oxide scale[80;112;113]. During the high-temperature oxidation, the metal-scale interface is a **dynamic location** of reaction,

diffusion, boundary migration, stress and segregation. The combination of these factors leads to the nucleation of interfacial voids, which limit the contact between the metal and the scale.
The void growth is an important factor in **determining scale adhesion**: when the voids remain small (20-50 nm), they have little effect on scale adhesion, but when they grow to a sufficiently large size, they can bring about **failure**.

B.A. Pint(1996) [76]proposed a realistic model to explain the formation and growth of these interfacial voids.
The oxide scale grows predominantly by inward diffusion of oxygen through the scale grain boundaries, and the intersection between the oxide grain boundary and the metal-oxide interface appears thus to be a preferred location for void formation.
When a interfacial void nucleates and grows, the metal substrate and oxide lose contact in that region. New oxide can still form as a result of the **evaporation of Al** across the void and the reaction occurs primarily near scale grain boundaries.

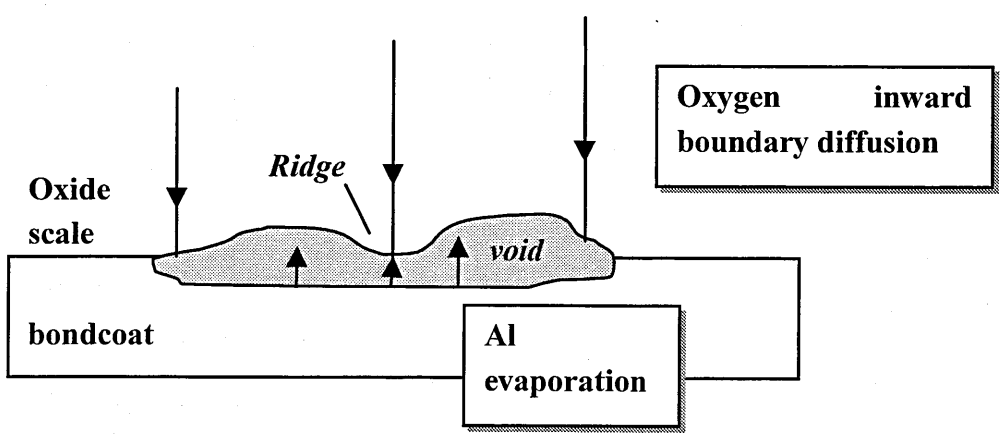

Figure 10: ridges formation within an interfacial void

When lateral surface diffusion can not keep up with the formation of new oxide near the grain boundary, the oxide surface does not remain flat and **oxide ridges** begin to form along scale grain boundaries above interfacial voids.
As the valleys continue to deepen, the growth of the ridges can eventually lead to necking and sealing off the valleys between the ridges, which can create large voids in the centre of oxide grains.
The presence of these voids is closely connected to the lifetime of the scale. The increase of porosity generates indeed defects interaction and leads to the mechanical failure of the scale[113].

The same mechanism can occurs at the gas /scale interface. At a lower rate than oxygen, aluminium diffuses indeed outwardly along the scale grain boundaries and generates surface ridges. These ridges have to be differentiated with the ridges caused by alumina phase transformation.

Another void formation mechanism has been related by Golightly and al. (1976)[38]and Katsman and al. (1996)[50]. Accumulation or condensation of vacancies in the scale and beneath the interface lead indeed to the formation of void channels, which allow a fast penetration of oxygen by surface diffusion. These vacancies can be generated by the **Kirkendall effect**, when the diffusion of the less-noble component is higher than the diffusion of the second component.
Penetration of oxygen through the voids may cause new oxide formation following additional consumption of the less-noble component, generating more vacancies and voids.
This mechanism is therefore **self-propagating** and can lead to the displacement of the metal-oxide interface and the growth of the voids.

2.1.3.2. Tramp and refractory elements outward diffusion

The oxide scale adhesion is sharply affected by the outward diffusion of impurity elements such as sulphur which are known to be indigenously (caused by the manufacturing process) present within nickel and nickel-based alloys at tramp levels[96](<100ppm). These harmful elements can also be introduced during aluminising or platinum plating processes.
Among all the impurities commonly present in commercial Superalloys, **sulphur** is actually considered to be the most deleterious:
As related by many papers, the sulphur **weaken** indeed dramatically **the interfacial bond** of the scale/bondcoat interface[47;57;80].
It is also believed that the sulphur diffusing from the substrate, **segregates at grain boundaries and at the scale-bondcoat interface** and enhances interfacial void formation by reducing the surface energy of those voids[47;58;76].
However, Khanna and al [52] (1989), related that the main effect of the presence of sulphur in the alloy is to **increase the growth rate** of the scale, which can spall at a later stage when a critical thickness is reached. He showed also that the addition of reactive element was decreasing this growth rate by gettering the sulphur and was also improving the adherence.

The reasons for the detrimental effect of the sulphur are actually unclear, but however it has been demonstrated that the scale adherence can be dramatically improved if the sulphur

level is reduced, either by **H_2 annealing desulphurisation** [47;98] or by the introduction of **reactive elements**[91;96;99] in the coating.
As studied and reviewed by Smialek (2000), a good scale adhesion can be produced simply by removing sulphur without any reactive element addition.

Sulphur is not the only element harmful for the scale adherence and growth. The refractory elements present in the superalloy substrate can have a deleterious effect when they diffuse outwardly. **Tungsten**, **molybdenum** and **vanadium**[99] decrease alloy interdiffusion rates and therefore may have an adverse effect on selective oxidation. On a second hand, these refractory elements react with oxygen to form **non-protective oxides** (low melting points, volatiles, high diffusivities), which is undesirable for a TBC TGO system.

2.1.3.3. TBC CTE mismatch

The TBC failure at the TGO/bondcoat interface is also due to residual stresses accumulated within the oxide scale[80;101].
These stresses arise from two sources:

- **Growth stresses** generated isothermally during the TGO formation and does generally not exceed 1GPa. They are caused by the deformation of the substrate during oxidation and to the convolutions and ridges generated by phase transformations.
- **Thermal stresses** generated during thermal cycling due to the **thermal expansion mismatch existing between the bondcoat, the TGO and the ceramic.**

As shown in the following table, the thermal expansion of the bondcoat is higher than that of both TGO and ceramic.

	Ceramic ZrO_2 7wt% Y_2O_3	*TGO* α-Al_2O_3	**Bondcoat**
Thermal expansion coefficient, α (C^{-1})ppm	11	8-9	13-16
Young's Modulus, **E** (GPa)	0-100	350-400	200
Misfit compression, σ (GPa)		3-4	

Table 6: TBC material properties[117]

With changing temperature, the stress varies due to the different thermal expansion coefficients. Thus, the system is nearly stress-free at high temperature (above 700°C), because the bondcoat start to creep and soften.
However, during cooling, the plastic deformation is irreversible and the bondcoat is hard again. This leads then to the formation of **compressive residual stresses** in the ceramic and TGO layer, and **tensile residual stresses** in the bondcoat.

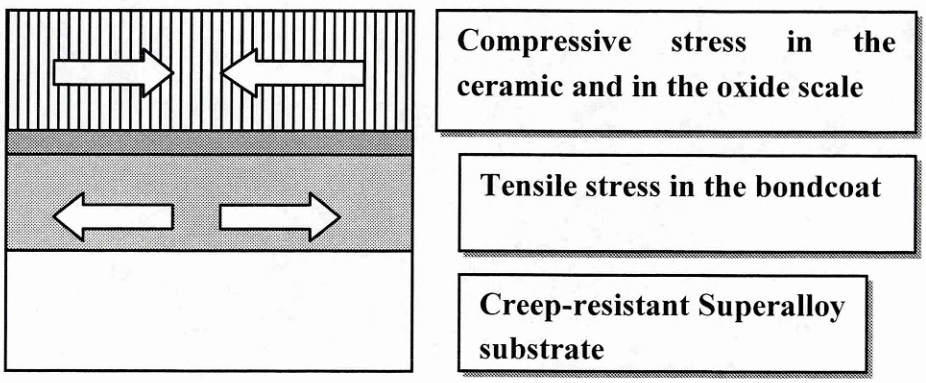

Figure 11: Residual stresses in the TBC caused by thermal cycling

Extremely large residual compressions (3-5 Gpa) are thus generated in the oxide scale as the system cools down to the ambient temperature[117]. These stresses are generally orientated in the plane parallel to the metal-scale interface and the adherence can be maintained. However, in the **concave curvature** or at free edges, extremely high out-of-plane tensile stresses can develop[34;80]and they can lead much easier to crack nucleation, and failure.

2.1.3.4. Bondcoat chemistry and degradation

In order to maintain an external Al_2O_3 scale, a coating must contain more than 17 wt% of aluminium for binary alloys[99]. Chromium addition are sharply beneficial, since 10 wt% enable the alumina scale to form with a concentration as low as 5 wt% of aluminium.
However, the breakdown of the scale can strongly affect the chemistry of the bondcoat[115]. Repetitive spallation leads to continuous alumina re-formation and bondcoat aluminium consumption.

Once the coating does not contain sufficient aluminium to ensure the coating reformation, oxygen react with the other elements present, either initially in the coating or after outward diffusion from the substrate.

The bondcoat degradation can also be affected by other mechanisms.
As described earlier in the thesis, the oxygen diffuses through the oxide scale and reacts with aluminium mostly at the TGO/bondcoat interface. Usually, the scale growth is expected to be parabolic and therefore slow once a continuous layer has been formed. However, if aluminium diffuses inwardly into the substrate, a depletion begins at the outer part of the bondcoat and oxygen can form oxide with the other elements present. The oxidation of nickel, chromium, refractory elements (Mo, W, Ta, V,...)[93], or combination thereof is generally not controllable, and high growth rates can be observed leading to the thickening and unavoidable spallation of the TGO.

2.1.4. Delamination mechanism

Generally caused by the simultaneous effect of the previously detailed mechanism:

- namely the voids formation and impurities segregation at the interface,
- the continuous growth of the scale
- and predominantly the increasing compressive stress in the scale.

the spallation of the ceramic occurs leading to the ineluctable TBC failure.

The delamination sequence consists usually of three different steps[15;110;117]:

1. **formation of separations at the TGO/ bondcoat interface:**

   The separation begins by the nucleation of cracks at the defects and heterogeneities of the scale/bondcoat interface. As described in the following figure, a bondcoat convoluted surface can generate separation at the apex of the **wrinkles** upon high temperature. Heterogeneities of the scale lead on other hand to the formation of **Small Scale Buckles** (SSB, 20-100µm diameter), which expand along the interface. Their expansion is usually stopped by similar heterogeneities

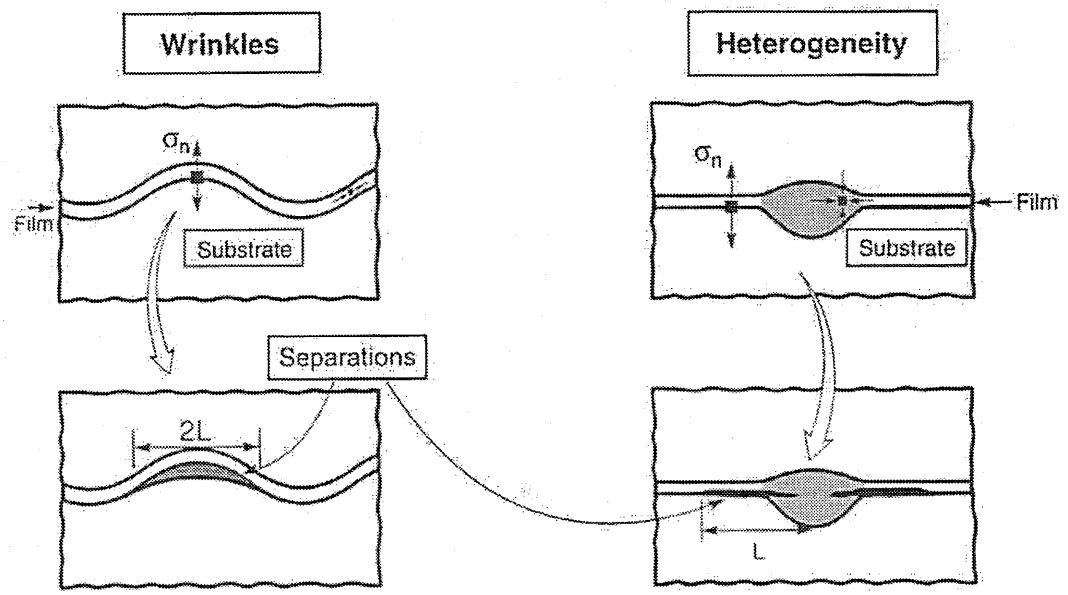

Figure 12: Crack nucleation modes

Bondcoat grain boundaries, and interfacial voids account also for crack nucleation location.

2. Buckling and Separation propagation

Once nucleated, the cracks extend and coalesce but the ceramic toplayer still remain attached at **remnant ligaments**.

The buckle growth is a manifestation of fatigue at the TGO/bondcoat interface. The scale in compressive residual stresses triggers tensile stresses along and at the edge of the separation.

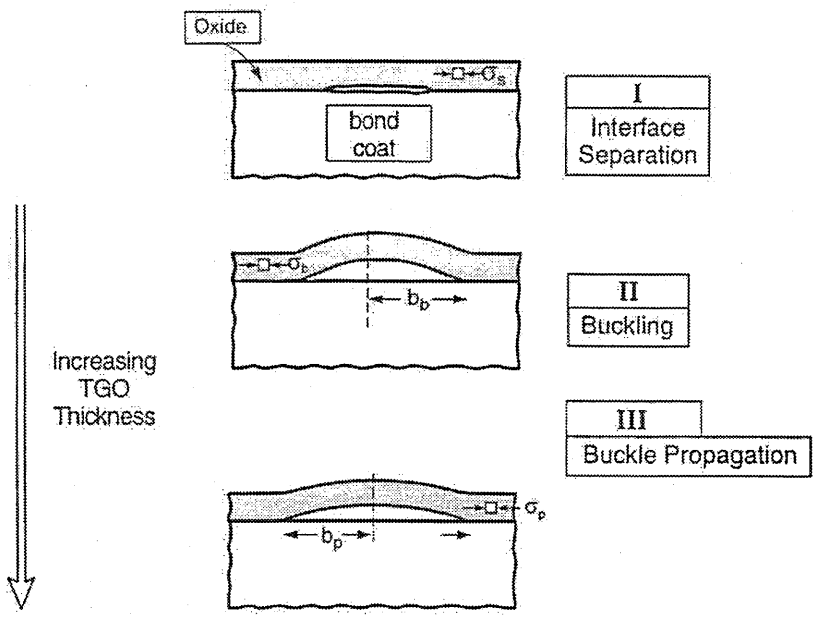

Figure 13: Crack propagation

As the buckle propagates, the initial compression in the TGO is relaxed

In some cases, interfacial voids formed during oxidation can coalesce and lead to extended separation. This occurs especially when impurities such as sulphur segregates at the interface.
In other cases, interaction between defects occurs also leading to extended defective regions.

3. Spallation

Failure happens when remnant ligaments are detached, causing a separation large enough to create either **large scale buckle** or **edge delamination** that results in spalls.
Cracks through the coating thickness appear then either at the edge of the large buckles (**kinking failure**) or at the apex of the buckles.

As studied by Bull[15], another mechanism of spallation occurs at the scale interface. It is caused by nucleation of **compressive shear crack** through the scale thickness, and is referred as to the **wedging spallation**. This type of failure is more likely to occur when the interface is strong but the scale is weak, conversely to the buckling mechanism, which involves a stronger scale with a weaker interface.

Such spallation failures have sloping edges and are most common for thicker and adherent scale.

2.1.5. The need for a suitable bondcoat

HP turbine blade operation condition

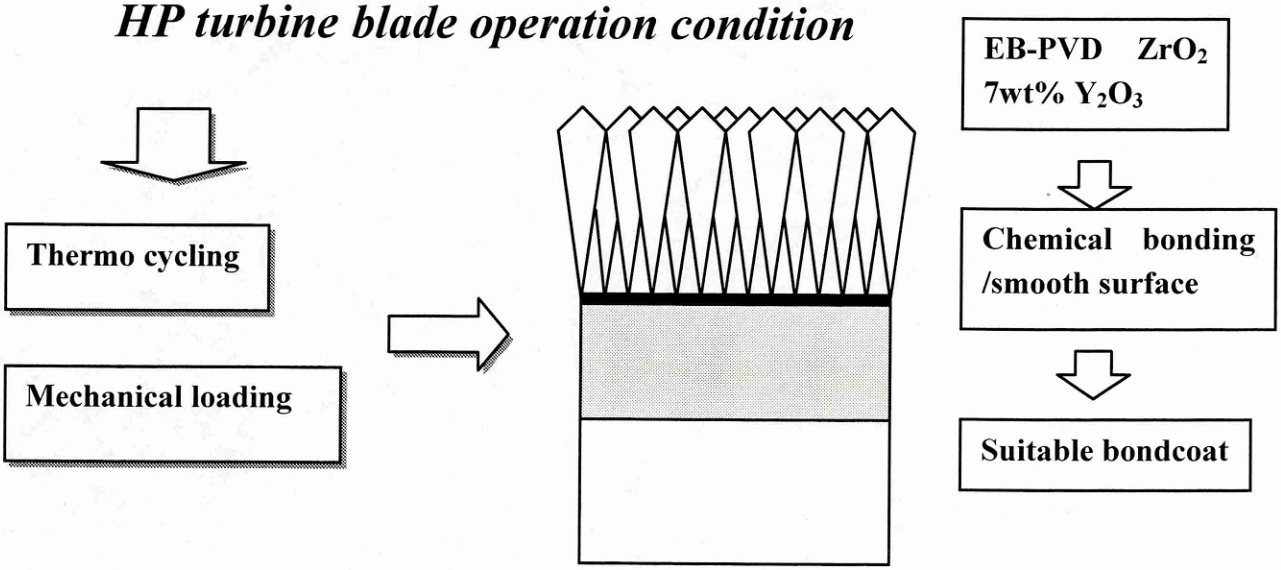

Figure 14: Environment of an EB-PVD TBC's bondcoat

The previous section has described the different mechanisms and causes of failure during formation and operation of an EBPVD-TBC system. The formation of the chemical bonding between the bondcoat and the ceramic layer has been detailed in particular and 3 main causes of failure have been explained:

- **Cooling stresses**, generated by the difference in thermal expansion coefficient between the scale and the bondcoat
- **Growth stresses**, which develop during oxidation because of phase transformation, and lead to convolution and cracking.
- **Defects, impurities and voids**, which accumulate or segregate at the scale-bondcoat interface, limiting the contact of the two layer, generating tensile stresses and initiating cracks throughout the scale.

Taking into account the tough operation condition of the TBC system and the failure mechanisms, which are initiated at the scale/bondcoat interface, requirements for a optimal EB-TBC's bondcoat are given subsequently:

Alumina-forming alloy

The bondcoat must form an oxide, which thickens at a slow rate and which must remain adherent to the alloy surface. Al_2O_3 is generally regarded as the best TGO, because diffusion through it is very slow in comparison to other oxides and since it is also stable, it is not difficult to find an alloy containing sufficient aluminium, to provide a continuous layer of Al_2O_3. [112]

Creep resistant

A route to minimise the misfit stresses and improve spallation resistance is to make the bondcoat more creep resistant. Which will bring more stability to the TBC root area on thermo mechanical cycling[51]. It is possible by reducing the CTE of the bondcoat.

Thermal stability:

No interdiffusion with the substrate

It is important to avoid:

- refractory elements outward diffusion
- aluminium depletion

Control of the Thermally Grown Oxide

- **Adhesion**

Elimination of void formation; an adherent alumina scale having a relatively flat, void free, metal-scale interface.

- To maintain compressive stresses in the parallel plane and reduces out-of plane tensile stresses (to avoid scale convolution)
- Re-doping or desulphurizing to limit interfacial voids.
- **Growth rate**

The TGO is the long-life factor.

The nature of the bondcoat metal surface is of prime importance as it controls the nucleation and growth of the oxide film.

2.2. Bondcoat selection

This chapter is aimed at describing the bondcoats currently chosen for EB-PVD TBC systems. Bondcoats suitable for this use must provide an adherent and reliable chemical bond to the ceramic and the common **protective coatings**, such as MCrAlY overlays, aluminide and modified aluminide diffusion coatings, meet usually this criteria depending on the temperature, the time of exposure and the environment.

This chapter will detail with these well established protective coatings, which have been used for many years to provide hot corrosion/oxidation protection for turbine components. Their advantages, as well as their limitations and improvements to act as a TBC bondcoat will also be emphasized.

2.2.1. Protective coatings

The need for protective coatings has appeared when it became apparent that superalloy substrate compositional requirements for improved high temperature strength and optimum high temperature environmental protection were not compatible. Increasing operating temperatures caused excessive oxidation of the high creep resistant nickel and cobalt superalloys used for turbine blades and vanes. This led to the development of **simple aluminide diffusion coatings** that solve the oxidation problem[39;40;116].

These coatings are however inefficient in hotter or more aggressive corrosive environment, such as in marine or desert conditions. To inhibit the severe hot-corrosion attack, **overlay coatings** based on **MCrAlY** (M = Co, Ni), CoCr and MCrSi(Al) applied by EB-PVD or plasma spraying have been introduced as protective coatings.

The recent discovery of low-temperature hot corrosion along with the even more severe operating conditions has finally led to the development of modified type of the 2 classical protective coatings.

2.2.1.1. Simple aluminide diffusion coatings

The aluminide coatings were the first protective coatings used to extend the lifetime of turbine blades and vanes.

The concept of the aluminide formation relies on the diffusion of aluminium into a substrate surface and a wide variety of deposition processes exist. Slurry-fusion and pack cementation were the first methods to be used , but recently Chemical Vapour Deposition (CVD) processes have been proven to be beneficial for numerous application.

Pack cementation[95 73;116]

Pack cementation is the traditional route to deposit diffusion coatings onto turbine components, and was introduced into aero engine service during the 1950s. This class of coating is still extensively used and satisfy probably around 80-90% of the current world market[73].

In this process, the parts to be coated are buried in a **'pack'**, contained in a sealed resort. The pack is a mixture consisting of:

- aluminium or aluminium alloy powders (**donor**)
- an **inert filler**, which is generally an aluminium oxide (to prevent pack sintering)
- a **halide activator**

When heated to sufficiently high temperatures (650°C or more), the halides react with the aluminium to form gaseous aluminium halides. These vapours condense onto the metal surface, where they are reduced to elemental aluminium. Interdiffusion between the deposited aluminium and the substrate alloy results then in the formation of **stable intermetallic aluminides** (NiAl and Ni_2Al_3 on nickel alloy substrates and CoAl and Co_2Al_5 on cobalt alloys).

There exists actually two types of coatings formed by this deposition route, and they are usually referred to as **high activity** and **low activity**. Their differentiation depends on the operating parameters, mainly temperature and aluminium activity:

High activity coatings are obtained at a relatively moderate temperature(<950°C), and the deposition rate is controlled by aluminium diffusion from the cement to the substrate (**Inward diffusion**). The process lead to the formation of a δ-Ni_2Al_3 phase containing substrate elements such as carbides and a further heat treatment is required to convert this brittle surface layer to NiAl (Figure 15).
The final morphology of these coatings is thus characterised by:

- an external zone constituted of a β-NiAl matrix along with substrates elements (carbides and α-Cr) which have diffused and concentrated near the surface during the diffusion treatment. This outer layer contains also inclusions from the 'pack'.
- an intermediate zone constituted of β-NiAl.
- and an internal zone (interdiffusion zone) constituted of nickel-depleted alloy, which induces precipitation of intermetallic compounds.

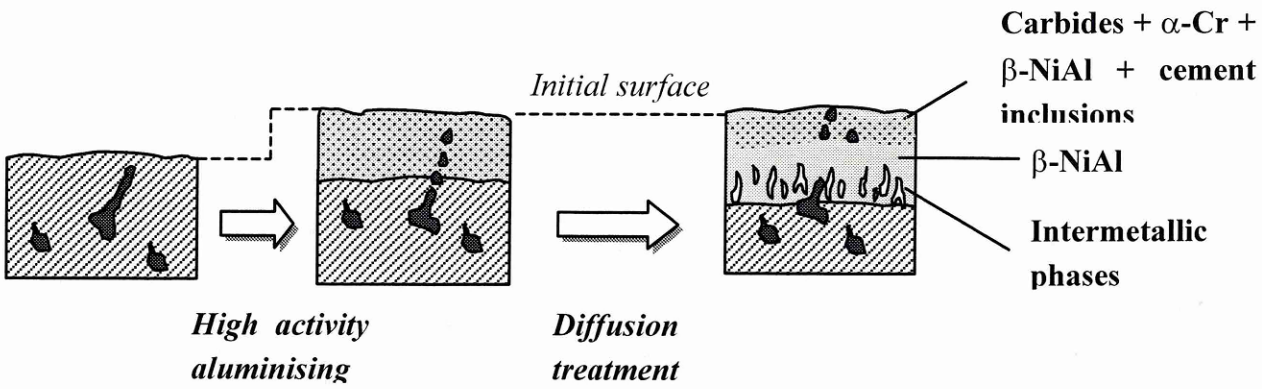

Figure 15: ***High activity Low temperature aluminising (Al inward diffusion)***

Low activity coatings are obtained at higher temperature (>1000°C). In this case, NiAl formation is controlled by nickel diffusion from the substrate towards the pack (**outward diffusion**). The initial surface of the substrate remains approximately in the middle of the final coating (Figure 16).

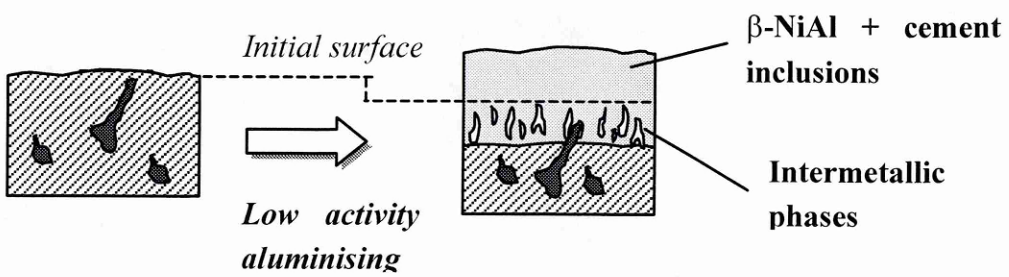

Figure 16: ***Low activity High temperature aluminising (Ni Outward diffusion)***

Both coating types contain the high-melting point β-NiAl phase, which is a very stable phase: aluminium concentration can vary from 45 to 60 at%, but an hyperstoichiometric NiAl is often chosen to improve the oxidation resistance.
On another hand, the solubility of substrate elements apart from nickel is very small in NiAl. These elements are therefore largely rejected from the NiAl outer layer and usually precipitate as **carbides** ($M_{23}C_6$, M_6C, MC), **metals** (α-Cr) or **topologically close-packed phases** (σ, η) in a discrete interdiffusion zone between the outer layer and the substrate. In the case of *High activity coatings*, precipitates are also present in the NiAl outer layer.

Vapor phase aluminising[45 116]

Vapor phase aluminising is a CVD process, which involves - as for the pack cementation process - the formation of gaseous halide to condense on the substrate surface. Compared to pack cementation however, the pack of reactants are **not in contact** with the components to be coated.
The major advantages of CVD over pack cementation are then :

- the absence of pack inclusions in the outer layer of the coating
- its ability to coat serpentine internal cooling passages of airfoils

SNECMA has developed a CVD route to produce aluminide protective coatings on turbine blades, which is called APVS (Aluminisation Phase Vapeur Snecma)[62].
It consists of a 3h-vapour phase aluminising at 1150°C of a low activity (outward diffusion of nickel) aluminide carried out under fluoride and argon atmosphere. This type of coating has been applied to military engine (ATAR, M53) and to civil engine (CFM-56).
A low activity coating is formed but because parts do not come in contact with the cement, inclusions usually present in the external zone of the pack cementation coatings are not observed.
Typically, aluminide coatings contain in excess of 30wt% Al and are deposited to thicknesses between 30 and 70μm[73].

Slurry aluminising

The slurry consists of aluminium powders mixed in an acidic water-based solution of chromates and phosphates[64]. The slurry, or *binder* can be applied by brush or conventional spray methods. When heated at a temperature of about 260°C to 540°C, the binder transforms to a glassy solid which bonds the metal powder particles to one another and the substrate. If heated at about 980°C, the aluminium powder melts and diffuses into the component to produce a protective aluminide, that is NiAl on a nickel alloy and CoAl on a cobalt alloy.

Whichever the deposition and formation way, when exposed at high temperatures the aluminides oxidize in contact with air as described in a previous chapter. The spallation of the oxide scale leads to the consumption of aluminium from the coating, which diffuses outwardly to reform the scale. The degradation of the aluminide is then driven by the depletion in aluminium and the outward diffusion of nickel and the other substrate elements. **β-NiAl usually converts to γ'-Ni_3Al and eventually to γ- Ni solid solution.**

When the aluminium level drops to below about 4-5 wt.%, the continuous Al_2O_3 scale can not be formed and more rapid oxidation occurs[116].
Moreover, the outward diffusion of substrate elements such as Ti, V, W, or Mo is very deleterious to oxidation resistance of the coating surface.

The low activity and high activity simple aluminide have been extensively used in the aeroengine field, because their cost is relatively low (5% of the component cost) and their adherence is perfect due to the diffusion process. However, their resistance in corrosive and high temperature oxidation environment is not very high, their composition is not easily controllable, their DBTT is relatively high (700-800°C), and the interdiffusion zone which forms with the substrate weakens the thin walls of internal cooled turbine blades.
These limitations have therefore led to modify their composition or to replace them by different types of coating.

2.2.1.2. Overlays

Overlay coatings or MCrAlY (M refers to Fe, Co, or Ni) deposited by EB-PVD or plasma spraying have been developed to provide a protection system essentially independent of the substrate and with composition optimised to provide increased hot corrosion resistance and in some instances improved mechanical properties such as thermal fatigue resistance[66].
The usual structure of the MCrAlY consists of β-NiAl and α-Cr phase in a matrix of γ-Ni and γ'-Ni_3Al[102].
The use of MCrAlY overlays put forward the following advantages[63;116]:

- Their Ductile to Brittle Transition Temperature (DBTT) is lower than that of the aluminide. It means thus that the risk of cracking is reduced, especially for the low temperature-operating engine.
- The composition is determined directly by the deposition material, compare to the thermo chemical coatings, which are formed by diffusion between both the deposition material and the substrate material. It is therefore easier to adapt the overlay composition to the specific engine need.
- The overlay deposition processes enable an extended range of coating thicknesses and several hundred microns thick coatings can be considered. In the case of the aluminide, the thickness is more or less limited to 100 microns, because the processes are driven by element diffusion.

The MCrAlY are usually deposited by plasma spraying (APS, LPPS) or HVOF, but can be also deposited by EB-PVD to obtain a better surface finish.

The NiCoCrAlY overlays have been considered as the most efficient overlay in high temperature application [20]. A comparative study between RT22 type platinum aluminide and NiCoCrAlYTa (produced by Turbomeca) has shown that the latter have a better resistance to high temperature corrosion and oxidation (1000°C and 1100°C).

The properties of the MCrAlY depends on its composition and consist usually of the combination of element properties[20]:

- The nickel base inhibits the interdiffusion mechanisms (on nickel-base superalloys).
- The cobalt improves the ductility and stabilisation of the β phase.
- The chromium improves the hot-corrosion resistance by the formation of stable chromium sulphides.
- The aluminium improves the high temperature resistance by forming a stable alumina layer.
- The yttrium improves the adherence and thermal properties of the alumina layer.

During exposure at high temperature, the MCrAlY overlays oxidize in a similar way to the diffusion aluminide coatings and interaction with the substrate occurs. The aluminium-rich β phase gradually convert to islands of γ' and eventually only the γ phase remains. Moreover, the large grain boundary area present in fine-grained overlay coatings affords a large network of diffusion paths for base metal elements[116].

2.2.1.3. Modified aluminide

Simple aluminide coatings have shown a limited protection under severe hot corrosion conditions (in the presence of condensed alkaline salts), or at temperatures above 1100°C. In order to extend their lifetime by improving their high temperature resistance and by limiting the substrate-coating diffusion phenomena, modified aluminide coatings have thus been developed [5;27;73]and have gained renewed interest because they offer an economical alternative to EB-PVD and plasma sprayed deposition processes.
They can involve an element co-deposition during the pack cementation, a pre-treatment of the substrate surface, or a metallic pre-deposition before aluminising.
The modifications, which have been applied for protective coating are numerous and strongly depend on the superalloy composition, the aluminising process and the environment. Of most relevance chromium and platinum modified aluminides are detailed subsequently:
The presence of **chromium** in the aluminide improves significantly the hot corrosion resistance and it has been introduced either by co-deposition with aluminium during the

pack cementation process –or vapour phase process-, or by a chromizing pre-treatment prior to the aluminising process.
In the C1A process developed at SNECMA, the vapour phase chromizing treatment is carried out at 1050°C for 3 hours with a cement containing granules of chromium and NH_4Cl as an activator. The substrate is then subjected to a vapour phase aluminising treatment at 1200°C for 2 hours with a cement containing Cr 30wt.%Al alloy and NH_4F[27].

One of the most important developments in modified-aluminides is the incorporation of a noble metal such as **platinum**, which strongly increases the high temperature, hot corrosion and thermal cycling resistance.
The platinum aluminide formation process begins usually by the deposition of a 5-10 microns platinum layer by electro-deposition, plating or sputtering. It is then followed directly, or subsequently to a diffusion treatment, by an aluminising treatment.
Different platinum aluminide structure can therefore exist depending on the platinum diffusion before aluminising and the type of aluminising (low or high activity)[103;104]. These structures are classified usually in three main categories referred as to commercial types:

1. the LDC-2 type which exhibits a homogeneous outer layer of **single phase $PtAl_2$**
2. the RT 22 type which exhibits a two-phases outer layer of (Ni,Pt)Al and **$PtAl_2$**
3. the RT-69 (or Chromalloy's CN91), which consists of a single phase(Ni,Pt)Al

The formation of a LDC-2 type platinum aluminide implies the deposition of a first 5-10 microns thick layer of platinum (usually by electroplating). A subsequent **low activity aluminising** (1050°C) results in a 3-zone coating (Figure 17) characterised by:

- An outer single phased layer of **$PtAl_2$**
- An intermediate layer of **β(Ni, Pt)Al**
- A interdiffusion zone consisting of intermetallic **σ-CoCr** phase in a matrix of **β-NiAl**

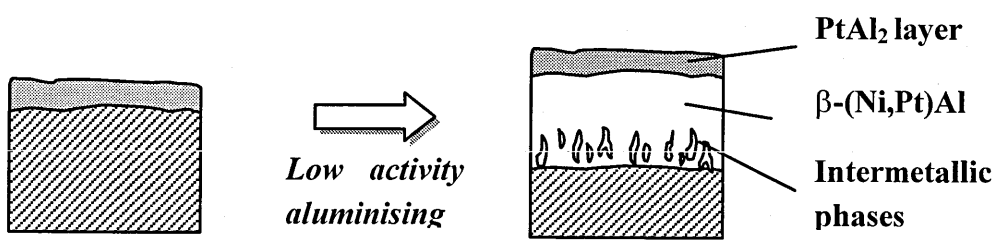

Figure 17: Type LDC-2 Platinum aluminide formation[63]

The formation of a RT 22 type of platinum aluminide begins also by the deposition of a platinum layer (5-10 microns), but prior to aluminising, a diffusion treatment at 1000°C is carried out to form a outer layer of **γ-(Pt, Ni)**. The following **low activity aluminising** leads to a 3-zone coating (Figure 18) characterised by:

- a bi-phased outer layer consisting of $PtAl_2$ precipitates in a **β-(Ni,Pt)Al** matrix
- an intermediate **β-(Ni,Pt) Al** layer
- a interdiffusion zone similar to that of the LDC-2 type

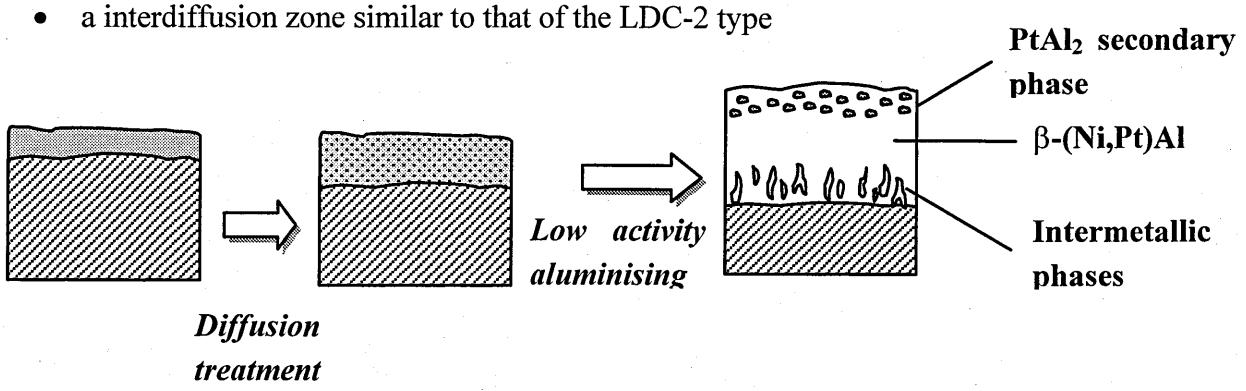

***Figure 18*: Type RT 22 Platinum aluminide formation[63]**

If the low activity aluminising step is replaced by a high activity one for both diffused or undiffused platinum layer, a similar structure is obtained at the outer part of the coating, but the platinum distribution is different through the rest of the coating. Indeed the structure observed beneath the platinum rich region is depleted in platinum and very similar to the unmodified 3-zone high activity aluminide structure (formed by inward diffusion of aluminium).

The thickness of the initial platinum layer influences also the outer structure of the coating. As reviewed by Krishna, G.R.[54], in the case of a high activity aluminising if the platinum layer is as thin as 1 micron, the NiAl phase close to the surface retains all the platinum in solid solution. When the thickness is in the range 2-10 microns, a two-phase structure is present, but if the platinum layer thickness is further increased, a single-phase outer layer $PtAl_2$ appears whatever the pre-aluminising diffusion treatment.

Finally, a new generation of platinum aluminide has appeared and consist of a single phase of β-(Pt,Ni)Al usually referred as to CN91 by Chromalloy and RT69 by Rolls-Royce[31]. These coatings are produced by CVD low activity aluminising and by a subsequent heat treatment (Figure 19). During the deposition process, the gas introduced is formed at low temperature but the parts to be coated are heated above 1000°C.

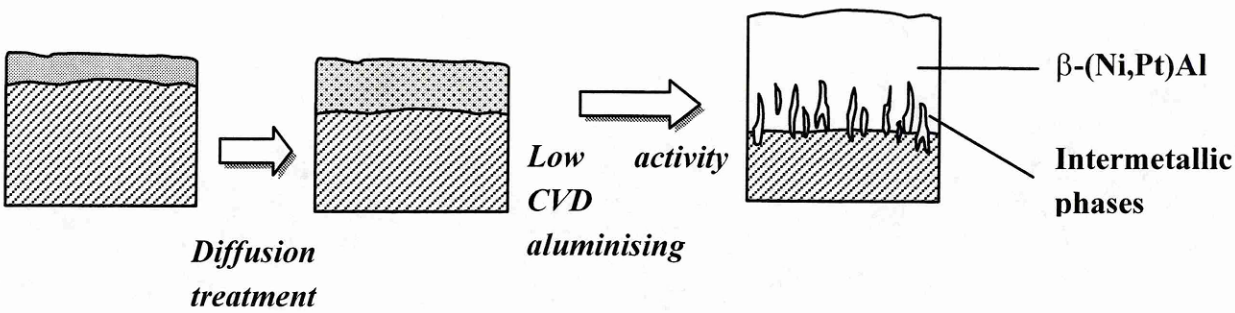

Figure 19: single-phase platinum aluminide formation

Berstein and **Allen**[8] worked on cracked Gas turbine Blades coated with Platinum aluminide (β (Ni,Pt) Al matrix and $PtAl_2$ phase in the outermost layer) and observed degradation phenomenon.

The degradation of a platinum aluminide coating occurs by consumption of aluminium from the coating to form aluminum oxide on the surface. The aluminum oxide actually protects the coating and base metal by acting as a barrier between the coating and the environment. As the aluminum oxide spalls off due to thermal cycling, erosion, etc... the coating supplies additional aluminum to form a new aluminum oxide layer.

As the aluminum (as well as platinum) content of the coating is reduced, the phases of the coating microstructure change to accommodate the lower aluminum levels.

The depletion in aluminium is also due to its inward diffusion in the substrate.

The degradation process of the platinum aluminide is described below.

Degradation process [19;69]**:**

1. The **$PtAl_2$ particles** in the outer part of the coating dissolve in the **NiAl** to form a single phase **(Ni, Pt) Al or β phase**.
2. The beta phase breaks up into a two phases structure of γ' **$(Ni, Pt)_3$ Al** and β **phase**.
3. There is insufficient aluminium to maintain the β phase and **a single γ' phase is left**.
4. The single γ' phase breaks up into a γ **phase** (**Ni + solid solution** elements and γ').

The γ phase is left and the coating is completely consumed.

2.2.2. Application as bondcoat for EB-PVD TBCs

As described in the previous chapter, the suitable bondcoat for EB-PVD TBC applied on turbine blades must have a controlled oxidation, so that a pure, strongly adherent, and slow-growing alumina scale develops and chemically bonds to the ceramic top-layer. The

bondcoat must on another hand withstand, absorb and palliate the thermo-mechanical cycling stresses and strains, which develop in the overall TBC during the turbine operation. This section will explain how the protective coatings can meet these requirements and will provide a comparative review of their limitations to act as bondcoat.

2.2.2.1. Benefit of platinum

In most of the TBC failure cases, the spallation occurs because the alumina scale is not adherent to the bondcoat. The lack of adherence is usually caused by a brittle interface weakened by the outward diffusion of substrate elements, by the degradation of the bondcoat and by the development of stresses within the scale.
Platinum can improve dramatically the adherence of the scale, the oxidation kinetic and the thermal stability of the bondcoat.

Influence on the scale growth and adherence:

During oxidation and thermal cycling of a simple aluminide, lateral growth stresses and thermally induced stresses develop in both bondcoat and scale and lead to the scale decohesion by propagation of cracks and voids. The addition of platinum to the aluminide composition modifies the oxidation mechanism and the scale growth, so that the adherence is improved[1;30;33;104].
Felten and Petit[30] studied the oxidation of platinum aluminide Pt_5Al_3 and Pt_2Al and observed the formation of a very adherent scale **mechanically keyed or pegged** in the alloy. This improved adherence compare to classical aluminide is due to the metallic protrusions, which extend into the scale at sites where grain boundaries are not present. The scale is thus thicker at grain boundaries, which highlights that the oxidation growth is a grain boundary-controlled transport process during which the oxygen diffuses inwardly along the scale grain boundaries.
It has been observed [104] that the growth of alumina scale on platinum aluminium alloy is not homogeneous and that grain size vary considerably through the scale thickness. The outermost part of the scale consists thus of fine grains resulting from initially nucleated oxide, whereas relatively large, columnar grains are observed in contact with the alloy.
The columnar grains are formed later when the overall thickening rate of the oxide is low.

As related by Fountain, J.G.[33], the platinum enhances the isothermal stability of the scale by preventing the lateral growth of the oxide, which gives rise to a **convoluted scale morphology**. Furthermore, the platinum promotes the stress relief mechanism at

temperature via an enhanced diffusional creep process or enhanced grain boundary sliding, which reduces growth stresses generation.
Wood, G.C.(1978)[115]related also the isothermal stability (900 and 1000°C) of the scale produced on LDC-2 platinum aluminide but did not observe a convoluted surface. The scale appearance was rather nodular with many whisker-like growths from the surfaces of nodules. He reported as well an irregular scale thickness with small oxide intrusions in the coating, which maintains a close contact at the scale/platinum aluminide interface during isothermal oxidation and thermal cycling.

Influence on the thermal stability:

The thermal stability refers to the influence of temperature on the structure and composition of the bondcoat. During operation of a gas turbine engine, coated blades are exposed to an average temperature of about 1000°C.. However, due to hot spot conditions, the temperature may rise locally to about 1100-1200 °C.. At temperature **below about 1000°C**, interdiffusion between the bondcoat and superalloy substrate was suggested to play an insignificant role in coating degradation. In this case, **oxide formation** and **spallation** could play an important role. At temperatures **above 1000°C**. , however, **interdiffusion** could be the most important variable influencing the performance capability of the bondcoat.

Tawancy, **Shridhar** and **Abbas**[105]compared classical aluminide and Pt-aluminide coating on a nickel-based superalloy. The two types of coating were exposed in air atmosphere for up to 1000 hours at 1000, 1050 and 1100 deg C.

After heat treatment, analysis of the **aluminide coating without platinum** (Figure 20) detected the presence of:

- **W** and **Ta** within the grains of the beta phase
- **Hf -rich phases** at the grain boundaries of the beta phase
- **Alpha-Cr** phase within the beta phase

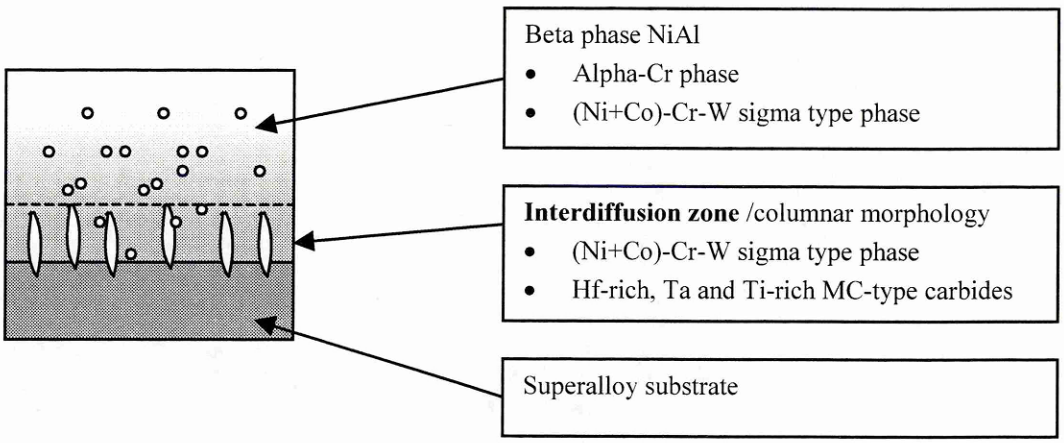

Figure 20*: *Simple aluminide oxidised at 1100°C

In the case of the **Pt-aluminide** (Figure 21), theβ-phase contained substrate elements, as observed for the conventional aluminide, such as Hf, Cr, Ti and Co, but their concentrations were **generally lower in comparison** with the aluminide coating. The coating surface was free of both W and Ta and there was no evidence for the presence of the alpha-Cr phase at the coating surface.
Furthermore, the Pt-aluminide had a much **finer grain structure** than the equi-axed grains of the classical aluminide.

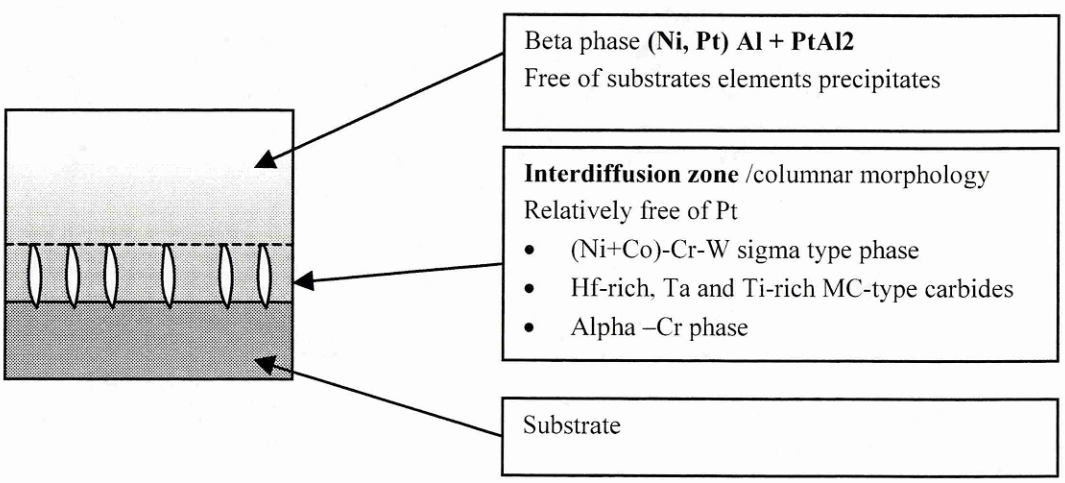

Figure 21*: *Platinum aluminide oxidised at 1100°C

In comparison with the Pt-aluminide[105], the aluminide coating was found to develop a less protective scale. The scale spalled off quicker and reveal **Cr-rich spinel type oxide** with a

substantial concentration of **W**. Other non-protective oxides included **Ni- and Ti-rich oxides** and especially **large Hf-rich oxide pegs**.
The scale formed on Pt-aluminide was more compact and consisted almost entirely of α-Al_2O_3. The subscale contained **fine particles of Hf-rich oxide** rather than large pegs.

Gobel (1994)[37]studied the interdiffusion between single-crystal superalloys and a RT-22 coating at 1000°C and 1200°C. Two different substrates were assessed: CMSX-6 (poor in W) and SR99 (rich in W; 9.5wt%).
The formation of **plate-like precipitates** (Figure 22) just beneath the interdiffusion zone was pointed out at 1000°C. These plates are an acicular phase[4], (most likely sigma, σ) and form preferentially at an angle of about 45° to the substrate/coating interface. They are rich in **Cr**, **Mo** and **W** (elements from the substrate).

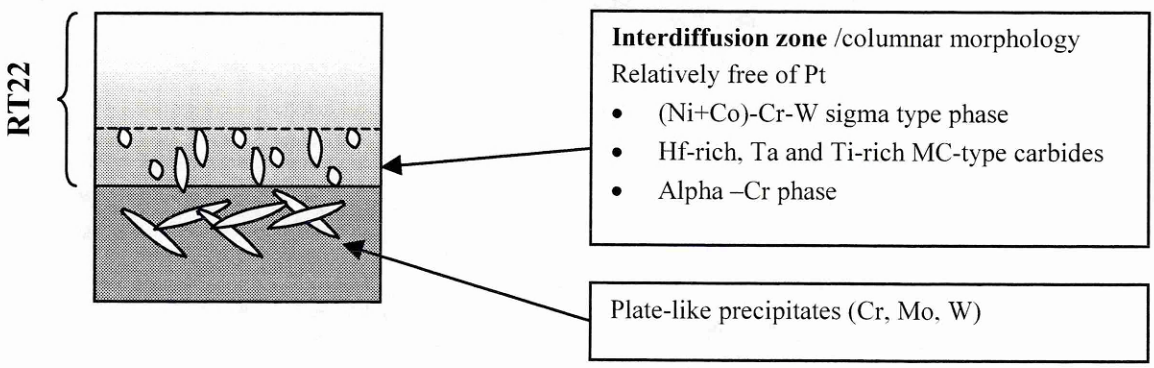

Figure 22: Plate-like precipitates at 1000 °C

At 1000°C, the RT22 coatings are remarkably stable. The refractory metals, such as Mo, W, Ta and to some extend Cr are relatively immobile because they are mainly fixed in precipitates. The solubility of intermetallics and carbides is still relatively low at 1000°C.
At 1200°C, the precipitates of intermetallics rich in Cr, Mo and Ni become dissolves in the system (with CMSX-6 substrate), but **Precipitates extremely rich in W** develop at this high temperature and act as a **diffusion barrier** (with SR99 substrate). The substrate composition has therefore a distinct influence on the rate of degradation.

Tawancy and **Rhys-Jones**[106] studied the thermal stability of a platinum aluminide coating applied on the directionally solidified MAR M 002 and the single crystal alloy SRR 99. The coating was a RT 22LT-type(which nominally contains 35%-55% Pt), it means a matrix of hyperstochiometric β- NiAl (aluminium rich) with a secondary phase of $PtAl_2$.

The different heat treatments emphasized that at 1100°C, ***$PtAl_2$ become thermodynamically unstable***. The platinum diffuses inwardly and γ-phase(Ni_3Al) appears in the outer coating layer as described in the degradation model of 2.2.1.3.

Platinum aluminide performance

The addition of platinum to aluminide has dramatically improved the static and cyclic oxidation and hot corrosion of these coatings[17;102;115]. First generation platinum aluminide bondcoats, produced by inward diffusion pack aluminising processes, have been reported to provide a 4-fold life advantage in cyclic oxidation and a more than 2 times improvement in hot corrosion over simple aluminide coatings. They have also proved reliable in TBC system used on turbine components, even if phase changes and interdiffusion with the superalloy occurs during operation.
Recent thermal cycling testing have however shown that more stable and pure platinum aluminide can now been produced using high temperature low activity CVD type aluminising processes[114]. The TBC life is improved because the bondcoat microstructure is formed by outward diffusion and superalloy elements are retained within the inner part of the coating.
The superiority of the single phase, $PtAl_2$ outer layer, systems has furthermore be demonstrated by Streif et. al. [103], who studied the hot corrosion behaviour of different platinum aluminides. He concluded that the pre-aluminising diffusion treatment of the initial platinum controls the Pt distribution through the coating and that the hot corrosion resistance is improved when the platinum diffusion is small, leading to a single $PtAl_2$ outer layer.
The single $PtAl_2$ phase is however brittle and **crack formation may occur during thermal cycle and service as emphasised by Bauer et. al.;** the LDC-2 coating type is more prone to crack failure than the RT-22 coating type[5].

The initial platinum layer thickness affects also the life of thermal cycled platinum aluminide. Krischna[54]has reported that a minimum content of Pt (corresponding to a 6 microns thick initial Pt layer) in the coating is necessary to have a beneficial effect.

Platinum modified MCrAlY

Platinum deposited on top of MCrAlY provides also an improvement in the bondcoat performance. It has been established[102;114] that very stable phases can be formed between the platinum and the aluminium from the underlying MCrAlY. During time at temperature,

as the alumina scale grows, the platinum scavenges the aluminium to maintain the phase composition. The most stable system was formed by depositing platinum onto a CoNiCrAlY composition and has been evaluated as a TBC bondcoat[6;114]: Thermal cycle rig testing at 1135°C of platinum modified vacuum plasma sprayed CoNiCrAlY bondcoat /EB-PVD ceramic layer system on MAR-M002 (directionally solidified) and CMSX-4 (single crystal) superalloys revealed significant improvement in spallation life as compared to unmodified CoNiCrAlY and outward or inward platinum aluminide diffusion bondcoats.

2.2.2.2. Benefit of reactive elements

One of the major improvements in the protective coating development has been the incorporation of a small amount (<1%) of reactive element in the coating composition. This innovation has been firstly applied in the MCrAl[96;99] coating systems with the introduction of Y, but are currently assessed in the aluminide and platinum aluminide coatings. These elements consist mainly of Yttrium, Zirconium and Hafnium and provide extremely beneficial effects for the bondcoat requirements:

- Improvement of the scale adherence
- Reduction of the scale growth
- Inhibition of the sulphur segregation

Reduction of the scale growth rate[75;112]:

The reactive elements (RE) are Oxygen active[75]. They diffuse outwardly from the coating to the gas interface (Figure 23), following the scale grain boundaries which are the fastest path of diffusion (the grain boundary diffusion for a typical 1-µm grain size is about 4 orders of magnitude greater than the lattice diffusion[99]).

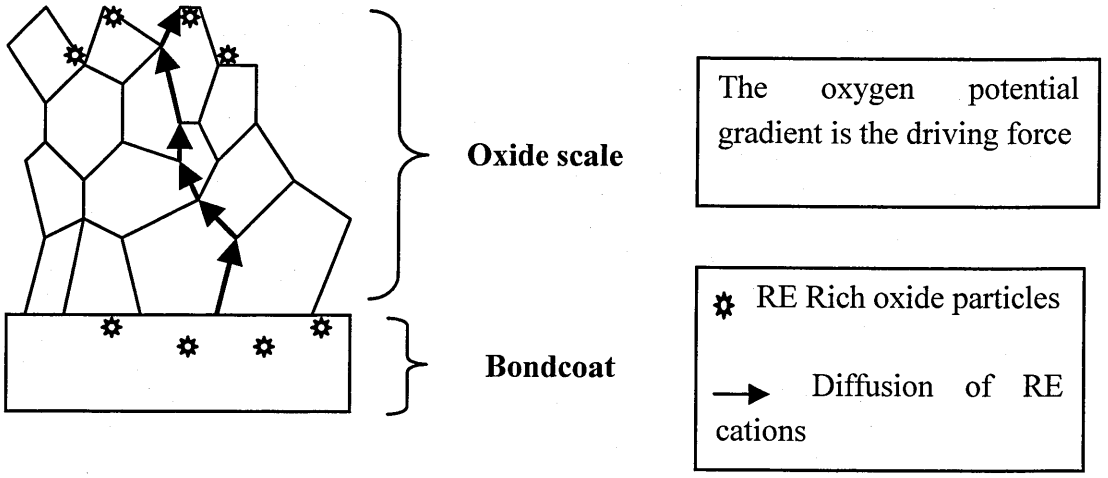

Figure 23: Outward diffusion of reactive elements

RE ions become enriched in oxygen in the scale grain boundaries near the gas interface. When a critical supersaturation is reached, **RE-rich oxides particles** are nucleated. RE ions leave the boundaries and are incorporated into particles, resulting in a lower steady-state segregation level.

RE effect begin when transient stage of oxidation is over and a complete α-Al_2O_3 layer is formed. However, above 1300°C, the RE effect begins to breakdown.

At high temperature (1200°C), undoped scales are observed to grow by a mixed diffusion mode involving simultaneous Al and O transport. New oxide appears to form at both metal-oxide and oxide-gas interface.
With the addition of Zr or Y, aluminium diffusion is reduced and the scale is observed to grow mainly by inward oxygen transport[78]. This can be explained by the slow diffusion of the large RE ions compare to the native cation (either Cr or Al) diffusion.
There is thus an inhibition of the normal outward short-circuit transport of cations along the scale grain boundaries and it affects **the parabolic oxidation rate**:

- For α-Cr_2O_3, reduction **10-100 X**
- For α-Al_2O_3, reduction **2-4 X**

Furthermore, this change in the oxidation mechanism leads also to a microstructure modification characterised by **the formation of columnar grains**[75;112] adjacent to the alloy.

The RE doping leads also to a finer grain microstructure and enhances therefore **the scale plasticity**[58](grain boundary sliding).
Hafnium and Yttrium reduce the duration of the initial transient oxidation stage and speed up the establishment of a continuous α-Al_2O_3 layer. However, once this stable scale is formed, the reactive element reduces the oxidation rate[112].
Under isothermal conditions Hafnium has a better effect on scale growth with small addition, and under cyclic condition, it has a better effect with higher addition (0.3%-1%)

Reactive elements can be incorporated and co-deposited as a powder in the pack aluminising process. In the case of the plasma sprayed overlays, they can also be introduced in the powder mixture to be melted and sprayed.
Other method using the powder metallurgy technique consist of adding an oxide dispersion in the coating[77;79]. This generally produces a uniform distribution of reactive elements throughout the coating.
Dispersed oxide addition act as **nucleation sites** for the first formed oxides and reduce therefore the duration of the transient oxide stage.

Improvement of scale adhesion[32;58;75;91;112]

The presence of small voids with compressive growth stress at the metal-scale interface can weaken the scale adhesion and lead to scale buckling. The segregation of RE ions at the metal-scale interface and in the scale grain boundaries[38;76]**does not eliminate the void nucleation** at the metal-scale interface, **but it can prevent them** from growing rapidly such that metal-scale adhesion is maintained for a longer period.
The void formation prevention may be promoted by internal oxide particles in the coating which act as **vacancy sinks**[38;58;112]. The oxide particles may be present as a dispersion in the coating or may be formed by internal oxidation of the yttrium or other reactive element addition.
Another improvement in oxide adhesion is explained by the phenomenon of **oxide pegging or keying**[58] (Internal oxidation of the active alloying addition) which occurs in the latter stages of oxidation: It corresponds to the formation of dispersoid particles growing in size to form oxide stringers of thin elongated oxide intrusions extending into the alloy substrate (therefore between scale and bondcoat).=> **HfO_2, ZrO_2, Y_2O_3**

Another cause of spallation prevention, is that the development of convoluted oxide does not occur on a reactive element containing coating.

In a RE element free coating, reaction between the inward and outward diffusing species results in the formation of oxide within the existing oxide layer, the reaction taking place in the oxide grain boundaries. Consequently, in addition to general thickening, lateral oxide growth occurs[38], leading to convolutions. The segregations of reactive element in the oxide grain boundaries inhibit the aluminium outward diffusion and therefore the lateral growth. This reduces the high compressive growth stresses and the risk of spallation due to scale convolution.

The effects of dopants level on isothermal and cyclic oxidation are summarized in the following figure (Figure 24). The isothermal curve accounts for the scale growth and the cyclic one accounts for the adherence.

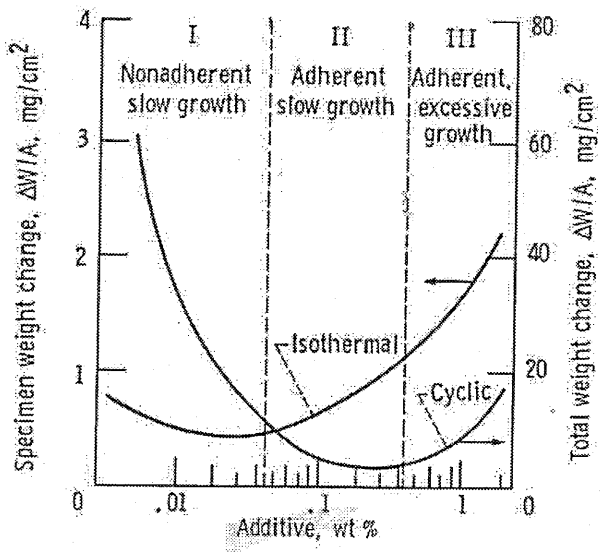

Figure 24: influence of reactive element content on scale growth and adherence[99]

There are **2 conflicting requirements**:

- Low active elements contents minimize thickening of the scale by inward growth around the internal oxide and prevent the formation of large oxide pegs.
- Higher active elements contents are necessary to ensure sufficient pegs needed for efficient scale retention.

Small additions (area I) are found to reduce the rate of scale growth and the amount of compressive stress within the scale, but rapid spallation occurs during thermal cycling.

In the range 0,05-0,5 wt% (area II), the reactive element level is optimum and the doped alloys show excellent isothermal and cyclic performance having excellent adherence and minimal growth rate.
In the area III, higher dopant levels cause excessive weight change due to the formation of less protective oxides.

Small amount of RE leads to **micropegs** formation. Higher additions leads to **macropegs**, which are detrimental to scale adhesion.
Hafnium additions seem **more efficient than Yttrium**, and this is related to the shape of the pegs as much as to the concentration; with the Hf additions, the internal growth of Al_2O_3 around the Hf-rich internal oxide particle takes on a branched, **dendritic form** as opposed to the **relatively smooth interface** between the Al_2O_3 surrounding the Y-rich particles in the original alloy. Yttrium tends to segregate to grain boundaries as **an intermetallic Yttride**. Hafnium is completely in solid solution, and thus leads to a very fine distribution of small internal oxide precipitates, which then promote the branching growth of Al_2O_3 around them.

As reported by Pint[80], the improvements associated with platinum addition begin to breakdown relatively quickly at 1200°C, but reactive element additions such as hafnium or zirconium provide an additional benefit to platinum. He related also that nickel aluminide with small amount of hafnium (0,05 at%) and without platinum could form a very adherent scale.

However, the reactive effect is still not fully understood and could be dependant on the incorporation process and on the distribution through the coating.
G.Fisher, P.K.Datta, J.S. Burnell-Gray studied in 1998 [32] the consequences of **the ion implementation** of **either Y or Hf** on the isothermal oxidation performance at 1100°C of **a low-aluminium-activity platinum aluminide/MarM002 system.**
They observed that the addition present as a thin layer of RE did not acted to either increase the adhesion of the scale or decrease the oxide growth rate.
The spallations were associated with the excessive formation of **Hf-rich pegs** at the oxide/coating interface. The pegs resulted from the outward diffusion of Hf from the MarM002 substrate to the oxide interface.
This highlights the relative complexity of an intermetallic coating/ superalloy system as compared to a simple bulk intermetallic, where the outward diffusion of elements from the superalloy, such as Hf, will act to modify the potential effects of active element additions.

Detrimental role of sulphur[52;58;96;97;99]

Indigenous impurities such as sulphur known to be present at tramp level (<100 ppm) within nickel and nickel-based alloys can segregate to the coating surface and reduce significantly the scale adherence.
By lowering the metal-scale interfacial energy, the presence of S at the interface increases the growth of interfacial voids, leading to their propagation and to the scale spallation.

Sulphur increases also the growth rate of the scale, because it promotes the outward diffusion of aluminium along the scale grain boundaries. Khanna, A.S.(1989)[52] reported that when sulphur enters the oxide lattice as a singly charged negative ion, it can cause a corresponding increase in aluminium ion vacancies. This increase in the aluminium vacancies would cause a change in the aluminium ion vacancy gradient across the oxide scale, thereby increasing the mobility of the aluminium ions and hence the availability of aluminium at the oxide-gas interface.

Sulphur removal from the coating (to < 1 ppm) by vacuum annealing, by repeated oxidation and polishing, or by hydrogen annealing has been proven efficient to eliminate its detrimental role[47]. However, the presence of reactive element in the coating enables also the neutralisation of the sulphur[52].
Yttrium has been reported to be an exceedingly strong sulphide former, stronger than nickel, chromium or aluminium. In the presence of small amount of yttrium, internal oxidation occurs underneath the scale and leads to the formation of $YAlO_3$, $Y_3Al_5O_{12}$, and $Al_2Y_4O_9$[91]. Sulphur segregates then to these phases, which are actually more stable than alumina. The sulphur is therefore tied up in the coating and can not diffuse to the coating-scale interface.

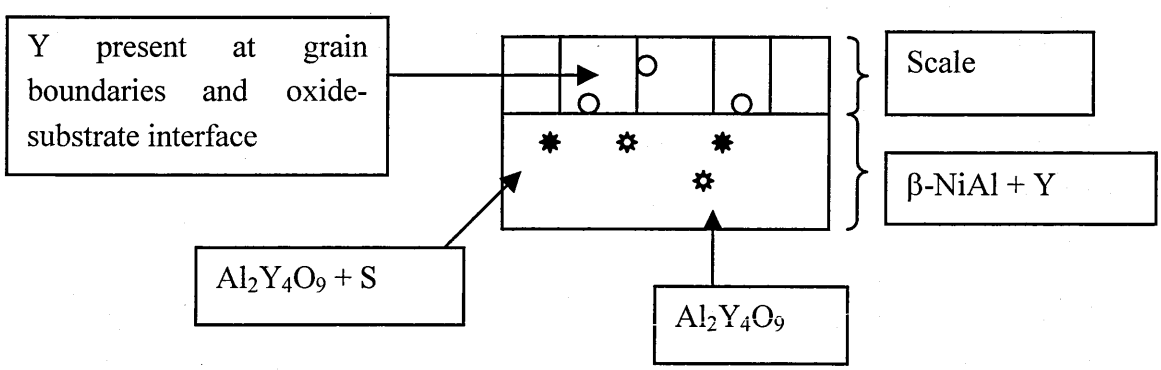

Figure 25: Inhibition of the sulphur segregation

Yttrium appears also to be more effective than cerium or hafnium[52] to prevent the detrimental roles of sulphur. Its presence in the coating induces an improvement in scale adherence but also a tremendous reduction in scale growth rate.

As reported by Pint (1996)[76], RE dopant effect and desulphurisation are temperature dependant and maintain an adherent scale in the range 900-1200°C. Above 1200°C, the desulphurisation is no longer effective and above 1300°C, RE dopants do not improve the scale adhesion anymore.

2.2.2.3. Bondcoat comparison:

The early application of TBC's was the protection of combustor parts. This application involved applying a ceramic coat on top of an MCrAlY coating used as a bondcoat, both deposited by air plasma spraying. In the early 1960's, plasma-sprayed calcia and magnesia-stabilised zirconia TBC's have been extensively used on combustion chamber walls and burner. In the 80's, they were however replaced by the outstanding yttria-stabilised zirconia and 2 generations of TBCs have been successively introduced: APS MCrAlY/APS 7YSZ and LPPS MCrAlY/APS 7 YSZ[90]. The main advantage of the air plasma spraying was to provide the MCrAlY with a rough surface on which the air plasma sprayed ceramic could mechanically bond[20;49].
The application of TBC's on the rotating turbine blades has then led to the introduction of the more strain tolerant EB-PVD ceramic layer. Thus, EB-PVD YSZ ceramic layer with an LPPS NiCoCrAlY bondcoat offers a roughly three-fold improvement in blade life or a surface temperature increase on the hot sections of foils of approximately 150°C.
The adherence of the EB-PVD ceramic requires a smooth bondcoat surface to enable the growth of a strong and adherent alumina scale. In order to improve the life capability of EB-PVD TBCs, it is then substantial to select the right bondcoat, taking into account the engine operating conditions and the diffusional stability of the superalloy/bondcoat system.
For some applications, a simple aluminide coating will be suitable, but other applications will require advanced diffusion coatings or MCrAlY overlays; Bell and Wing[6] reported that platinum modified MCrAlY overlays show excellent high temperature performance and can meet the most demanding conditions.

In general, the aluminides are most often limited by oxidation and corrosion behaviour, while overlay coatings are most susceptible to thermal fatigue cracking because of their low strength in highly cyclic applications[116].

The new challenges for the development of optimal bondcoats for EB-PVD ceramic top-coats are the reduction of the growth stresses by controlling the scale growth and the reduction of the diffusional mechanism by preventing interdiffusion with the substrate.
As the oxidation resistance of aluminides can be strongly improved and controlled by the incorporation of platinum and reactive element, they appear also suitable to be chosen as bondcoat for EB-PVD TBC applied on turbine blades. Outward diffused platinum aluminides modified with yttrium or zirconium will tightly compete relatively to cost and performance with MCrAlY bondcoats in the near future.

3. The low-mass bondcoat concept

3.1. Development of a low-mass bondcoat

3.1.1. General concept of the low-mass bondcoat

Because even higher operating temperatures limit the lifetime of EB-PVD TBC applied on high pressure turbine blades, a new type of bondcoat has been developed and detailed in this report.
Its concept relies on three main objectives:

- To reduce the process and material cost
- To reduce the weight of the whole TBC system
- To prevent the interdiffusion with the superalloy substrate during the deposition process as well as during service at high temperature.

The cost effectiveness of a processed coating has always to be considered relatively to its function. In all cases, it must be as low as possible, but it is however bound to the thickness, the deposition process, the microstructure and the performance of the coating.
The low-mass bondcoat concept is aimed at reducing the manufacturing and material cost by decreasing the whole thickness of the coating without losing the bond effectiveness required by the application of an EB-PVD ceramic on top of it.
Furthermore, the use of a thin efficient bondcoat would reduced the whole TBC system weight and could enhance as well the blade design tolerances.

Another advantage expected for the low-mass bondcoat is a higher thermal stability than usual commercial bondcoat.
As operating temperatures are increased, the use of diffusion coating becomes indeed ineffective and dramatic degradation of the bondcoat by interdiffusion with the substrate leads to TBC failure. Overlay coatings are then the only route possible, but even within the MCrAlY systems, diffusion of elements between the substrate and coating can have a major influence on coating performance.
Therefore, to provide long-term stability, the development of a **diffusion barrier**[22;73] becomes necessary to minimize the interdiffusion between the coating and the substrate.
This diffusion barrier can be produced by combining overlay and diffusion coating advantages:

- Using an overlay deposition route to form the bondcoat independently of the substrate. Some interdiffusion is only necessary to give good adhesion.
- Forming stable intermetallic compounds to act as the diffusion barrier in itself.

3.1.2. Suitable deposition process

As explained previously, the use of an overlay route to deposit the bondcoat is the best way to prevent the interaction between the coating and the substrate at the coating deposition and formation stage.
Moreover, another advantage of this deposition technique is an accurate control of the coating thickness and stoichiometry.
There exists many different process including plasma spraying, EB-PVD, electroplating or sputtering and all these techniques are detailed and assessed in a subsequent chapter.
The relevant criteria of choice are:

- A low temperature process: to prevent diffusion initiation between the as-deposited coating and the underlying substrate.
- An efficient process with a minimal waste of material to be coated.
- A universal process, which can deposited a wide range of material with the highest deposition rate possible.
- the most economical process, which meets the previous criteria.

3.1.3. Diffusion barrier

The purpose of a diffusion barrier is to separate physically two materials and to prevent the interdiffusion between them. A relevant review of diffusion barrier mechanism has been made by De Reus (1994)[83].

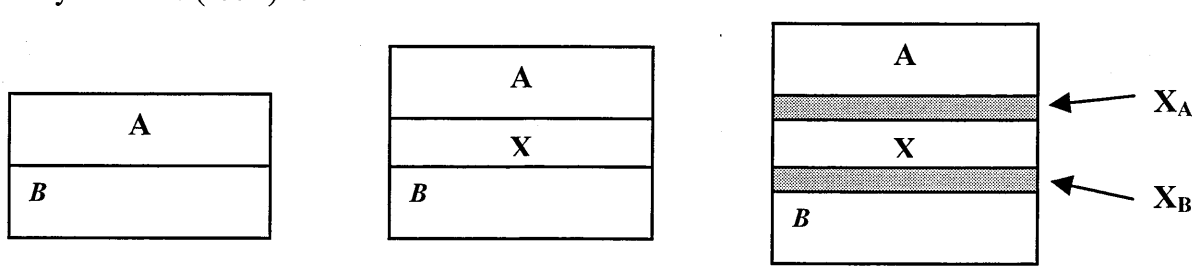

Figure 26: Diffusion barrier concept[83]

The simplest system is to add a layer between two materials, A and B, to stop direct interdiffusion (Figure 26). However, a typical engineering approach is to separate the

functions and add layers at the interfaces to optimise the performance of the structure (X_A and X_B). These added layers could for instance improve the adhesion between X and A/B.

Diffusion barrier have already been applied in many technical fields:

- in microelectronics to improve the conductivity of electrical contacts,
- in macroscale joining operations to increase the wettability or adhesion of braze alloys,
- for fibre composites improvement: by coating the fibre, the interdiffusion with the matrix is prevented.

To understand the operation of a diffusion barrier it is substantial to review the different type of diffusion and their evolution with temperature.
There exists two main types of solid-state diffusion:

- Diffusion via surface or line defects, such as grain boundaries
- Bulk Diffusion via lattices

According the work of Tammann (1923) reviewed by De Reus[83], the diffusion mechanism is temperature dependant: below about two third of the melting point of the solid, atomic diffusion may be dominated by defects diffusion (grain boundaries, dislocations) rather than by bulk processes. At higher temperature, bulk diffusion increases significantly but remains the slowest type of diffusion.
The aim of most diffusion barriers is then to eliminate diffusion along extended defects, but also to slow lattice diffusion.

The ideal diffusion barrier is therefore a defect-free and dense layer (such as a single crystal layer) of an inert or highly stable compound.
Different type of diffusion barrier have already been developed, such as:

- stuffed barriers, which imply the incorporation of foreign atoms in the extended defects in order to block the diffusion.
- sacrificial barriers, which allow a partial consumption of the barrier without short circuiting the substrate and the overlayer.
- inert barriers, whose performance relies on their low reactivity to minimize interdiffusion.

3.1.4. The use of intermetallics

Intermetallics are suitable for diffusion barrier, because of their high thermal stability and their limited solubility, which leads to a slow diffusion rate through them.
The intermetallic compounds can be defined as ordered alloy phases formed between two metallic elements[26;89;111] (An alloy phase is ordered if two or more sublattices are required to describe its atomic structure)
Their superlattice structure reduces then the **dislocation mobility** and the **diffusion processes** at high temperature.

The applications of intermetallics relied also on their **outstanding hardness** and **wear resistance** together with **their metallic properties.**
The outstanding hardness of intermetallics is however accompanied by an unusual brittleness, which has limited their use structural materials in the past.
A successful structural material development was though based on **the nickel aluminide Ni_3Al** that is the strengthening second phase in the superalloys. Other relevant applications are gathered in the following table:

Since approx.	Material or process	Phase	Application
2500 B.C.	cementation	Cu_3As	Coating of bronze tools
1931	Alnico	NiAl-Fe-Co	Permanent magnet material
1938	Cu-Zn-Al	CuZn-Al	Shape memory alloys
1950	Pack aluminide coating	NiAl, CoAl	Surface coating for protection from environment
1961	A15 compound	Nb_3Al	Superconductors

Table 7: Applications for intermetallic compounds[89]

Intermetallics form because the strength of bonding between the respective unlike atoms is larger than that between like atoms. Accordingly, intermetallics form particular crystal structure with **ordered atom distributions** where atoms are preferentially surrounded by unlike atoms.
Some intermetallics are however subjected to an intermediate or low temperature degradation phenomenon referred to as the pest effect. This phenomenon causes the fragmentation of the intermetallic specimen by the combined effects of oxidation and external or residual stresses.

Another benefit of intermetallics such as modified nickel and platinum aluminide, is an excellent oxidation behaviour (transient oxides consist mainly of the transition Al_2O_3 phases), which makes them suitable for EB-PVD TBC bondcoats.

3.1.5. The formation of intermetallic by exothermic reaction

As related by Larikov (1994)[55], intermetallics can be formed by crystallisation from the liquid state and also as a result of **reactions in a solid phase**. In this latter case, the formation by reactive diffusion is a typical first-order transition: intermetallic formation is realised by the formation and growth of at least one new phase due to diffusive interaction between two initial phases.

The intermetallic phase appears however only when the solubility limit of the solid solution is reached in the boundary layer of the solvent metal at a given temperature. This formation can furthermore be modelled and predicted relatively to the enthalpy of formation of the different compounds likely to be formed[83].

Furthermore, the transformation, which follows the diffusion and leads to the intermetallic phase formation has been reported to be exothermic[22;74]. A patented processing route has thus been developed by Deakin and Nicholls[23] whereby continuous intermetallic layers such as the platinum aluminide $PtAl_2$ can be produced. This process consists of the sequential deposition by the sputtering technique of a layer of two materials A and B followed by a reaction treatment at 700°C for 2 hours.

An exothermic reaction occurs during the heat treatment and leads to the formation of the intermetallic compound.

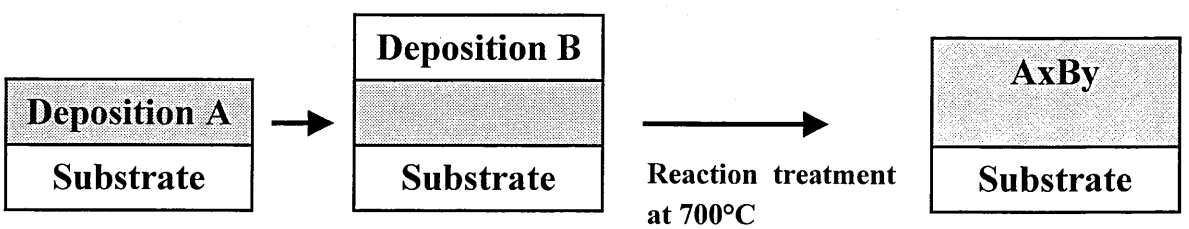

Figure 27: Intermetallic exothermic formation[74]

The stoichiometry of the coating is controlled by the initial thickness of each layer, which allows the formation of a range of binary intermetallic A_xB_y. A thickness ratio of the layer can then be defined as follows:

$$\frac{x.M_A}{\rho_A} : \frac{y.M_B}{\rho_B}$$

where M_A and M_B are the atomic weights and ρ_A and ρ_B are the densities of the species A and B.

3.1.6. A multi-layer coating

The low-mass bondcoat relies for its initial composition on aluminium and platinum in order to form a platinum aluminide EB-PVD TBC bondcoats, which will act as a diffusion barrier as well as a reservoir in aluminium to develop a stable outer layer of α-Al_2O_3 oxide scale.

Layers of platinum and aluminium will thus be deposited sequentially by the sputtering route and a subsequent heat treatment at a relatively low temperature will be carried out to trigger the exothermic reaction between the layers.

The formation of platinum aluminide by exothermic transformation is an interfacial reaction. The increase in numberof layers in the coating should then promote the reaction by increasing the number of interfaces between platinum and aluminium.

Therefore the quicker the intermetallic bondcoat is formed without interacting with the underlying superalloy substrate, the quicker the bondcoat should be efficient as a diffusion barrier and the outward diffusion of substrate elements such as tungsten, molybdenum, titanium and tantalum should be prevented.

3.1.7. Addition of reactive element

Reactive elements have been proven to be beneficial to platinum aluminide bondcoats, because they prevent the sulphur segregation, improve the oxide scale adherence and control its growth.

Their incorporation in the low-mass bondcoat has thus to be considered and should be promoted by the multi-layer initial structure.

3.2. Sputtering route for low-mass bondcoat deposition

This part is focused on the different deposition methods used in the aeronautic field and explains why the sputtering process has been chosen for the development of new low-mass bondcoats.

3.2.1. Deposition routes for turbine blades protective coatings

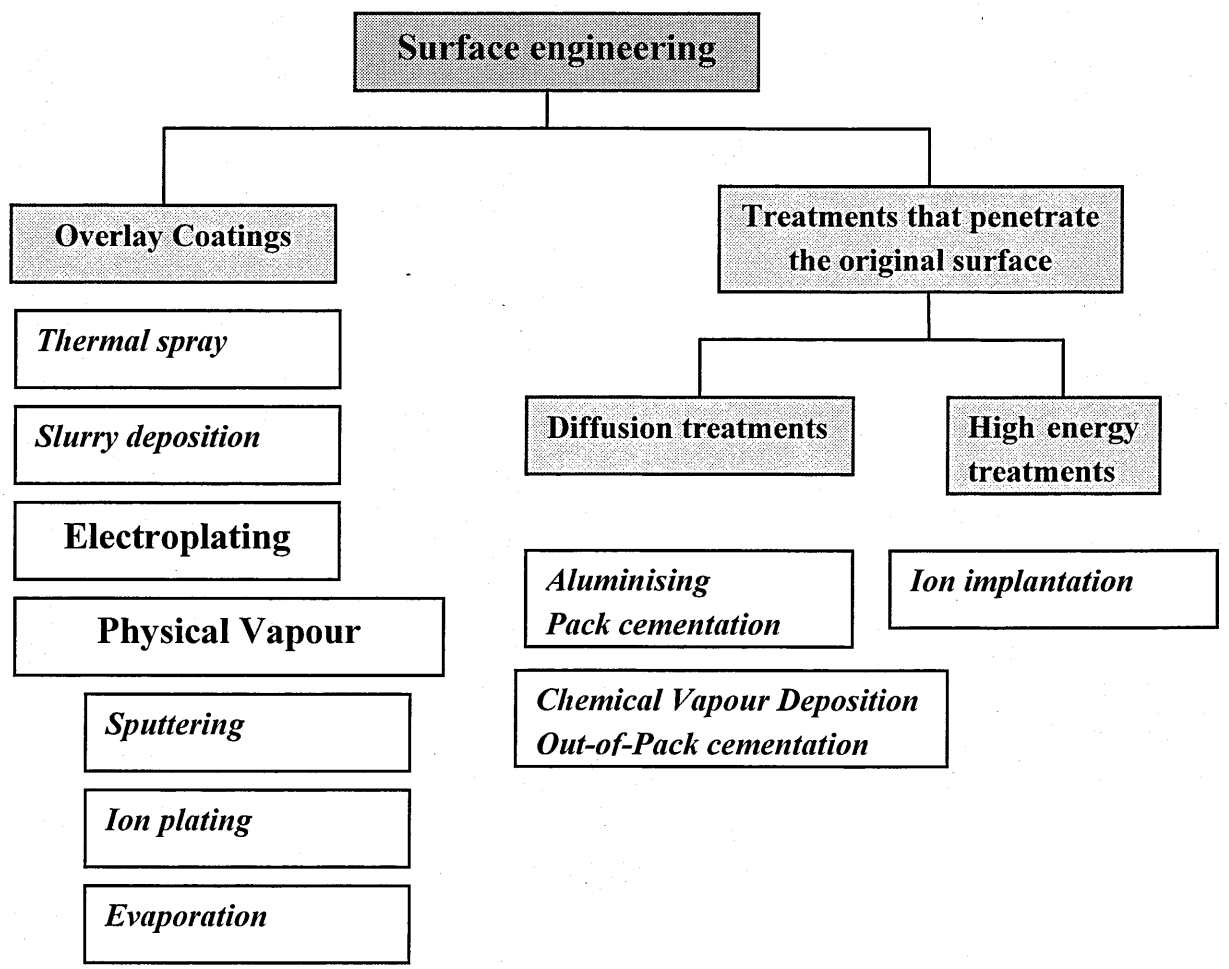

Figure 28: Deposition techniques for high temperature coatings

The deposition techniques can be set apart in two main categories:

- the techniques which involve an interaction with the substrate during deposition (e.g. diffusion coating techniques)
- the overlay techniques

3.2.1.1. Diffusion and penetration deposition techniques

The first category of deposition techniques includes the diffusion processes usually used for diffusion protective coating and bondcoat deposition. The pack cementation as well as the out-of-pack cementation have already been described in the 'bondcoat selection' chapter.
In the CVD processes[10;42], a gas mixture is introduced into a reactor. Near or on the usually heated substrate, a chemical reaction occurs, which yields the solid material to be deposited. In addition to the solid material, also volatile reaction products are formed which are exhausted from the reactor.
Depending on the deposition temperature, various solid-state reactions may take place during CVD and interdiffusion with the substrate occurs most of the time and leads to the final coating.

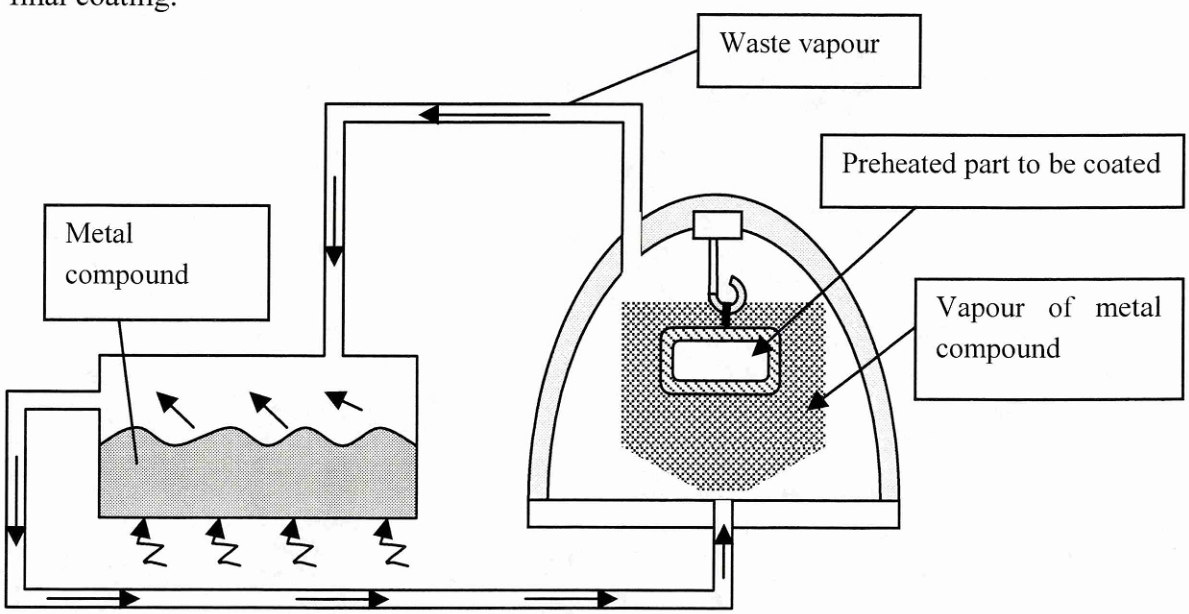

Figure 29: Chemical Vapor Deposition process

Ion implantation involves the use of directed beam of energetic ions in a vacuum. The electrical acceleration of the ions gives them sufficient energy to penetrate into the material that is being treated (about 0.3µm deep)[24;43]. Ion implantation is not really a coating

process, but it can be readily combined with a PVD process in order to change the property of the deposited coating or add a small amount of another element.
The advantage of ion implantation is that it can be carried out at low temperature (typically below 200°C) and it is also highly reproducible.

This category of techniques has however not been considered because interdiffusion between the substrate and the coating occur most of the time during deposition.

3.2.1.2. Overlay deposition techniques

Thermal spraying and PVD are the most common techniques. Thermal spraying has already been described in a previous part and the following section is focused essentially on physical vapor deposition techniques:

PVD[11] processes involve atom-by-atom, molecule-by-molecule, or ion deposition of various materials on a solid substrate. All these processes are performed in vacuum systems.

Thermal evaporation[14;59] is the simplest and oldest of the PVD processes. In this process, the metal to be deposited is placed in a refractory metal "boat" (crucible). The boat is heated to melt the evaporant forming a cloud, which coats all surfaces in the line-of-sight of the crucible.

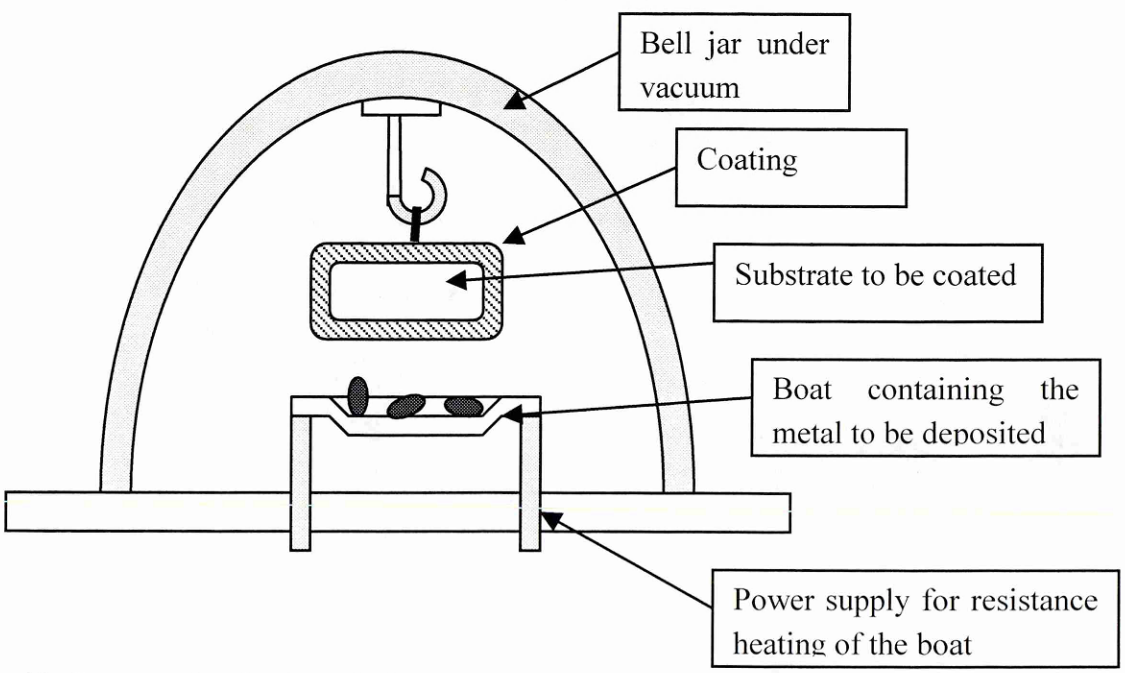

Figure 30: Evaporation basic technique

Thermal evaporation is used to apply relatively thick (up to 1 mm) coatings of heat-resistant materials, or MCrAlY's on jet engine parts. However for this latter application, sophisticated rod fed, electron beam sources would be used to provide sufficient deposition material.

The material to be coated can also be heated using an electron beam (EB-PVD). This variation of the process called EB-PVD has already been detailed in a previous part and is extensively used to deposit the ceramic of TBCs for turbine blades.

Ion plating[44] is a variation of the two previous processes. A metal is evaporated as in thermal deposition, and a plasma is also established to ionise the evaporating species. Evaporant ions bombard the substrate with such energy that they physically implant into the substrate to produce an extremely strong coating bond strength.

Sputtering[18;85] is a process wherein material is sputtered from the surface of a solid or liquid because of the momentum exchange associated with bombardment by energetic particles. The bombarding species are generally ions of a heavy inert gas. Argon is most commonly used. The source of ions may be an ion beam or a plasma discharge into which the material to be bombarded is immersed.
Sputtering may be used as a method of surface etching or coating.

Although Thermal spraying and PVD techniques are the most used processes, other deposition techniques exist.
Electroplating[14] for instance is used to deposit thin layer of material such as platinum and is usually combined with another process(aluminising) in order to form coatings. It employs two electrodes immersed in an electrolyte and connected to a power supply. The metal 1 from the first electrode is dissolved, forming ions, which are attracted by the second electrode (substrate to be deposited).
Electroplated coatings are however not uniform on edges and do not go into holes.

3.2.2. The sputtering deposition technique

The coatings deposited by sputtering consist of atoms dislodged from a material surface by ion bombardment. The source of ions is provided by the formation of a plasma within a vacuum chamber.

3.2.2.1. Use of a plasma in sputtering deposition technologies [18;87]

A plasma can be defined as a system containing atoms, ions, and electrons in a gas phase dynamic equilibrium. Its total charge is virtually neutral, and it exists roughly an equal number of ions and electrons in the body of the plasmas. Perturbations of this neutrality can occur within the plasma on a small scale, or at the edge of the plasma on a major scale.
The plasmas are used for a number of applications, but are usually distinguished in two classifications. On a first hand, the plasma can generate metastable species, such as excited states of atoms and ions which cause various surface phenomena and are used for reactive etching for instance. On a second hand, and in the case of the **sputtering application**, the ions present in the plasma are accelerated by an electric field. The energy gained by these ions is then used to erode, implant ions or sputtered materials.
The terms 'plasma' and **'glow discharge'** are often used almost interchangeably in thin film processing.
Electrons are the dominant charge carriers in processing plasmas. Owing to their low mass, they can respond much more quickly to electric fields than can the heavier ions.
There are a number of inelastic collision processes that are possible in plasmas. The most important one is **ionisation** and occurs as follows:

$$e^- + Ar \rightarrow Ar^+ + 2e^-$$

This reaction results in the emission of an electron by the atom. It is also possible to multi-ionise species by removing additional electrons but this requires significant additional energy and usually ions of charge greater than 2^+ are not observed.
In addition to the phenomenon of ionisation, a second very common process occurs within the plasmas, which is the excitation of an atom or an ion into an electronically excited state. The following equation depicts the excitation process:

$$e^- + Ar \rightarrow Ar^* + e^-$$

These excited state lifetimes are very short for most species and are followed by a radiative decay and the emission of a photon. This gives a bluish colour to the plasmas, and explains why they are also known as glow discharges.

3.2.2.2. The sputtering mechanism

The sputtering mechanism is a pure mechanical process generated by the acceleration of ions from the plasma to the material to be coated (usually called the target). During the impact, a mechanical energy transfer occurs, as the ion is attracted by the target and gives up its motion quantity.

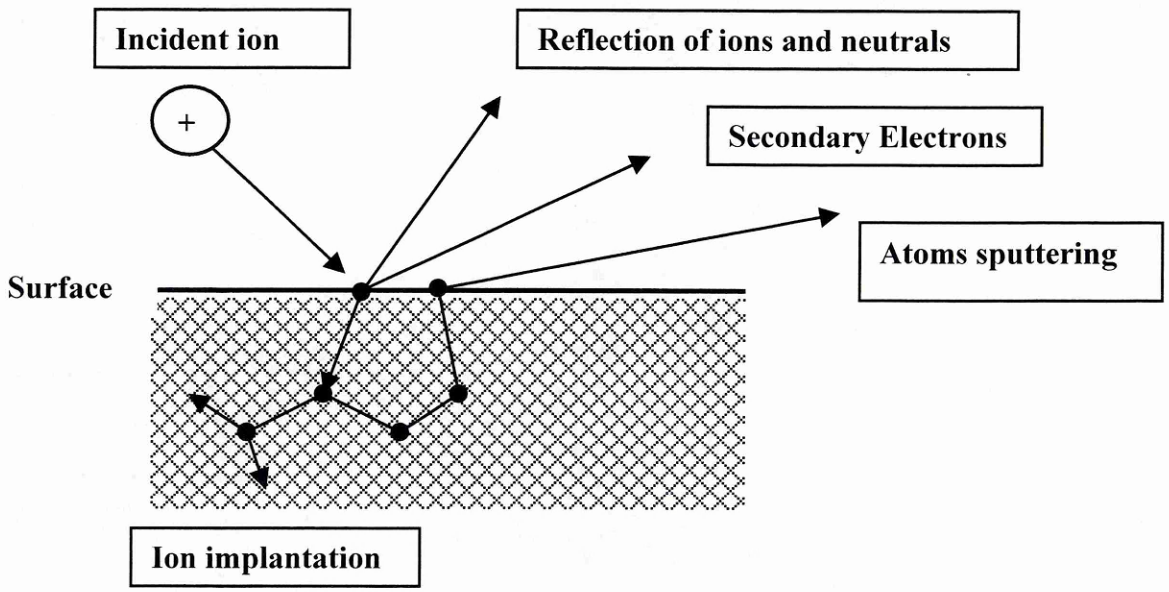

Figure 31: Ion impact consequences[18]

Several phenomena may then follow the impact (Figure 31)[18;108]:

- The ion may be reflected, and neutralised in the process at the same time
- The impact may cause the target to eject an electron, usually referred as to a secondary electron.
- The ion may be buried in the target, which is referred as to ion implantation.
- The ion impact may cause a series of collisions between atoms of the target, possibly leading to the ejection of one of these atoms. This latter process is called the sputtering process.

3.2.2.3. The sputtering techniques

Formation of the plasma[9]

The basic sputtering technique involves the use of a plasma as a source of ions. A pair of electrodes is therefore required to form this plasma by ionisation of the gas introduced. The mechanism of this formation is described as follows:
The gas which flows between the two electrodes always contains a few free electrons stemming from ambient ultraviolet radiation. When an electric field is applied between the electrodes, the electrons are accelerated. During their motion, they collide with gas molecules and ionise them by impact.
These ions (positively charged) are then attracted by the negative electrode, which is the sputtering target and where they dislodge atoms and electrons. The latter usually called secondary electrons are accelerated in turn by the electric field and collide with other gas molecules, producing even more ions and electrons.
The plasma is therefore generated by a chain reaction of impacts and is maintained by the secondary electrons emission.

DC sputtering

As schematised in Figure 32, the sputtering technique is processed in a sealed chamber, which is pumped by an array of vacuum pumps to pressures well below the desired operating pressure. At this base pressure, gas is added back to the chamber to obtain the desired pressure.

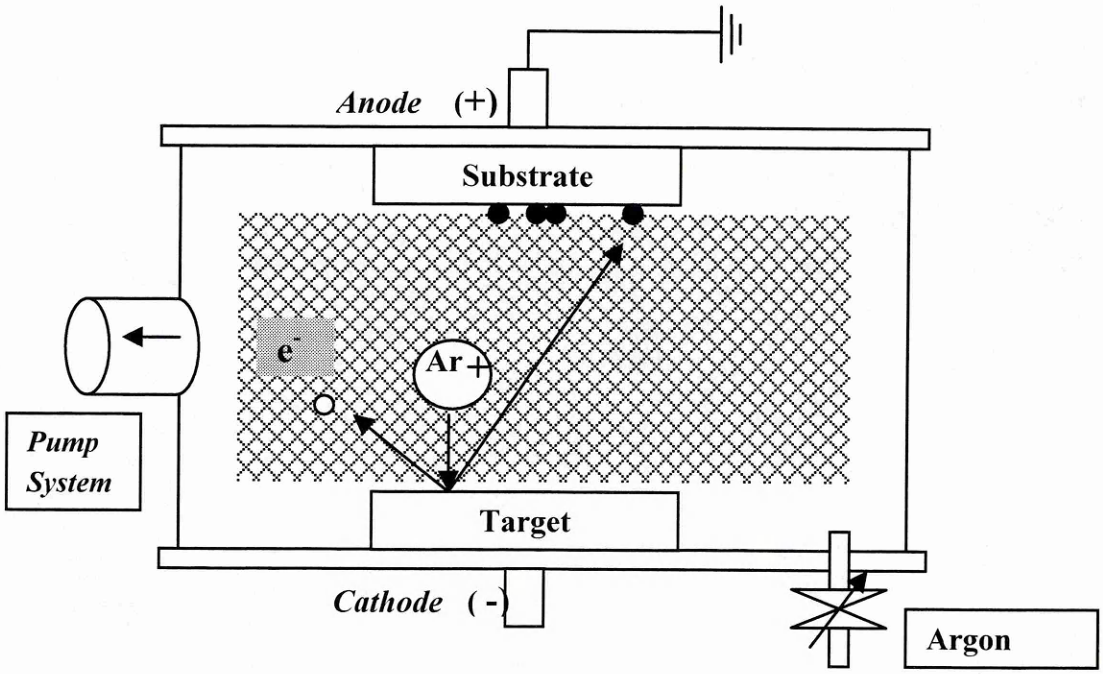

Figure 32: DC sputtering process

The material to be sputtered is made into a sputtering target which becomes the cathode of an electrical circuit.
The substrate to be coated is placed on an electrically grounded anode a few centimeters away.

In DC sputtering, a high negative voltage V is continuously applied to the target. It triggers the discharge and help maintaining the plasma.
The discharges operate at voltages in the range of 0.5 to 5 kV. Ions accelerated by this voltage impact on the target and cause ejection sputtering of the target material.
The substrates are positioned so as to intercept the flux of sputtered atoms, which may collide, repeatedly with the working gas atoms before reaching the surface where they condense to form a coating of the target material.

RF sputtering[9;18]

The use of alternative voltages appeared in sputtering systems because of the need to sputter dielectric or non-conductive materials. The technique of RF sputtering uses an alternating voltage power supply at RF frequencies around 10 MHz, so that the sputtering target is alternately bombarded by ions and then electrons so as **to prevent a dramatical charge build-up**.

At low frequencies,(<50kHz)[9], the ion mobility is sufficient to reach the cathode and to behave as in the DC system during each half-period. However, because each electrode is alternately anode and cathode, both are sputtered!
At higher frequencies, the electrons of the plasma oscillate in the electrical field with a sufficient energy to ionise the atoms, which reduces the dependence on secondary electrons emission from the target. This leads to the use of lower operating voltage and a decrease in the work pressure.
The most efficient frequencies stand above 10 MHz, however 13.56 and 27 MHz are commonly used, since they are the only frequencies allowed for medical and industrial applications.
At such high frequencies, the ions of the plasma are virtually motionless because of their relatively high mass and the ion bombardment of the target is negligible. If an impedance (insulative material or capacitor) is though coupled with the target, the electron load can not be evacuated and a pulsed negative voltage (known as the **dc offset voltage)** develops.
The target acquires a self-bias and become positive for only a very short fraction of each cycle, which leads to a virtually continuous ion bombardment of the target[18].
This is usually accomplished by connecting the RF generator to ground and by grounding the chamber wall and the substrate fixtures. An impedance matching network is also needed between the RF generator and the load to introduce the proper inductance required to form a resonant circuit[85].

The use of magnetron[9;18;94]

The development of sputtering sources with magnetic plasma confinement, called magnetrons has greatly enhanced the capability of sputtering process. These devices can provide order-of-magnitude increases in sputtering rates.
In this technique, the majority of the plasma is confined to a region near the target surface by using strong magnetic fields to bend the trajectories of the secondary electrons ejected from the target surface into spiral-like patterns across the target surface.
The magnetic fields are usually produced using permanent magnets placed under the target.

There several advantages of confining the plasma; which include:

- An increase in the deposition rate because the confined plasma near the target surface promotes the ionisation and the chance of sputtering atoms from the target.
- Reduced sputtering from the substrate and the chamber walls
- Reduced substrate heating during deposition
- Reduced work pressure requirement

3.2.2.4. Coating characteristics

Surface cleaning

In order to improve the adherence and the purity of the film deposited by sputtering, it is substantial to clean the substrate before placing them in the deposition chamber but also once the vacuum is achieved because contamination and oxidation always occur in an air atmosphere.
The same types of contamination can affect the targets and it is necessary to clean them as well.
The cleaning technique consists of removing a thin layer of the substrate and the target and 2 main techniques are detailed here:

Glow discharge cleaning:

Glow discharge cleaning involves placing the substrates to be cleaned in the glow so that they are **bombarded by low energy ions and electrons**.
The precise energy of bombardment will depend on whether the substrates are insulating or conducting, whether the discharge is RF or DC excited. **Impurities** are removed from the surface due to the ion and electron bombardment, or due to the heating associated with these bombardments. The most efficient results are obtained using **an oxygen glow discharge**.
This cleaning involve the negative bias (-50/-100V) of the substrate to increase the ion bombardment.

Sputter cleaning / sputter etching:

Sputter etching is commonly used to clean the target prior to deposition.

The target is exposed to **energetic ions** and to **low energy electrons**. In contrast to glow discharge cleaning, sputtering is encouraged and the target is cleaned by removal of material (contamination + target surface material).

Target cleaning is referred to as **presputtering**, which process is also used to heat the system and bring it to a steady state, whilst protecting the substrate from deposition with a **shutter**.

Bias sputtering

In order to improve the adherence of the coating at the early stage of the deposition, the substrates are biased to cause ion bombardment during deposition; This technique helps removing loosely bonded contamination or modifying the structure of the resulting coating. Furthermore, the ion bombardment increases the temperature on the substrate surface, so that the mobility of the atoms to be deposited is higher. Rearrangement of atoms occurs and leads to the formation of a denser coating. The deposition rate is however reduced and the bias is usually switched off once a continuous adherent layer is deposited. The bias is also usually lower than for glow discharge cleaning in order to avoid a complete backsputtering of the atoms to be deposited.

Coating growth

In sputter deposition, as with the other standard vacuum deposition technique of evaporation, material arrives at the substrate mostly in an atomic or molecular form. The atom diffuses around the substrate with a motion determined by its binding energy to the substrate and is influenced by the nature as well as the temperature of the substrate.
During the nucleation stage of the film growth, atoms join together on the surface, forming quasi-stable **islands**. The islands grow then in size and eventually coalesce until the film reaches continuity.
On single crystal substrate, the growth and coalescence can lead to a single crystal film. This phenomenon called **epitaxy** occurs however only above a specific temperature.

The structure of the film is therefore strongly dependant on the substrate temperature and has been modelled by Mochvan and Demchishin[65] and Thornton[107].
Mochvan and Demchishin (1969)[65] have studied the effect of substrate temperature on the coating structure during sputtering deposition. They have divided the different structures in three zones (relatively to T/Tm, where T is the substrate temperature and Tm is the coating material melting point measured in °K):

1. Zone 1 (T/Tm <0.3): it consists of tapered crystallites with domed tops which increase in width with temperature.
2. Zone 2 (0.3 <T/Tm) < 0.45): it consists of columnar grains with a smooth mat surface.

3. Zone 3 (T/Tm>0.45): it consists of equiaxed grains and a bright surface

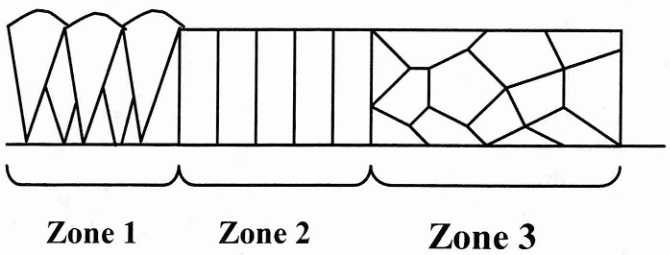

Figure 33: Mochvan and Demchishin's Model (1969)

Thornton (1973)[107] also studied as well the coating structure dependence on temperature but further discovered that the argon pressure also influenced the morphology. Thus, at low argon pressure a new zone (called zone T) appears between the pervious zone 1 and 2 and consists of densely packed fibrous grains (see figure).

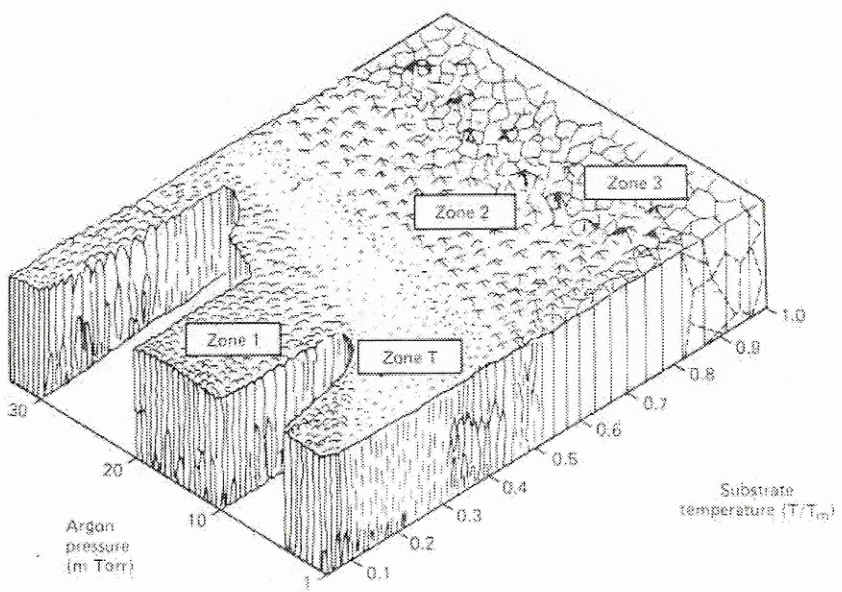

Figure 34: Thornton's Model (1973)

The coatings that are subjected to energetic reflected atom or ion bombardment during growth and that have the zone T structure often exhibit **high compressive internal stresses.**
The coatings deposited under conditions that yield the zone 1 structure are often in **tension,** apparently because they are underdense with wider than equilibrium interatomic spacings.

Coating uniformity

The sputtering technique is a **line-of-sight** deposition process. Depending on their complexity, the substrates must usually be rotated to obtain an overall uniform thickness.
The thickness uniformity is also affected by the target shape, the target-substrate distance and the position of the substrate in front of the target.
Relatively to evaporation, the sputtering technique has however an advantage in that the position and the shape of the target can be varied. Cylindrical magnetron targets for instance enable the deposition onto different substrate sides at the same time.

Deposition rate

The deposition rate of the films is affected by many factors, which include:

- The power applied to the target: the deposition rate is directly proportional to the RF or DC power density.
- The apparatus geometry: target shape / position of the substrates relatively to the target(s)
- Working gas pressure: high pressures limit the passage of sputtered flux to the substrates, low pressure may be unable to sustain the plasma;
- Use of a magnetron: when a magnetron is coupled to the target, the deposition rate can 50 times as high as for DC planar diode mode deposition.
- Sputtering yield of the material to be deposited.

The sputtering yield is defined as the number of target atoms (or molecules) ejected per incident ion[18]. It is dependent on the masses of the colliding species and on the energy of the incident ion, but not on the temperature.

$$S = \frac{sputtered\ atoms}{incident\ ions}$$

The sputtering yield is also proportional to the surface binding energy of the target and to the nuclear stopping power s(E), which corresponds to the energy transferred to the surface of the bombarded target by the incident ion (whose energy is E).

The following table gathers relevant sputtering yield for the low-mass bondcoat deposition:

Element	Sputtering yield
Aluminium	1
Platinum	1.1
Nickel	1.3
Yttrium	0.77
Zirconium	0.63
Hafnium	0.79

Table 8: Sputtering yield of low-mass bondcoat elements

3.2.3. Sputtering as low-mass bondcoat deposition process

Relatively to the process requirement listed in the 'low-mass bondcoat development' part, the sputtering process has been chosen as low-mass bondcoat deposition technique for these following reasons:

- Sputtering is a low-temperature **overlay** process, which does not induce interaction with the substrate during deposition.
- The most striking characteristic of the sputtering process is its **universality**. Because the coating material is transformed into the vapour phase by a mechanical process rather than a chemical or thermal process, virtually any material is a candidate for depositing as a coating.
- Since it is an overlay technique, the coating thickness is controlled by the deposition power and time and thus the stoichiometry of a sputtered multi-layer system can be defined accurately.
- Depending on the substrate initial surface roughness, the coating surface can be relatively smooth and suitable for EB-PVD ceramic toplayer adhesion.
- Co-deposition of several materials is possible and can be undertaken for instance as a mean to introduce a reactive element.
- Sputtering is however a line-of-sight process, which implies the rotation of the samples to obtain a uniform coating.

4. Experimental procedure

The goal of this chapter is to describe the experimental procedure, which has been followed to produce the low-mass bondcoats. The main lines of the basic procedure are gathered in the following organigram:

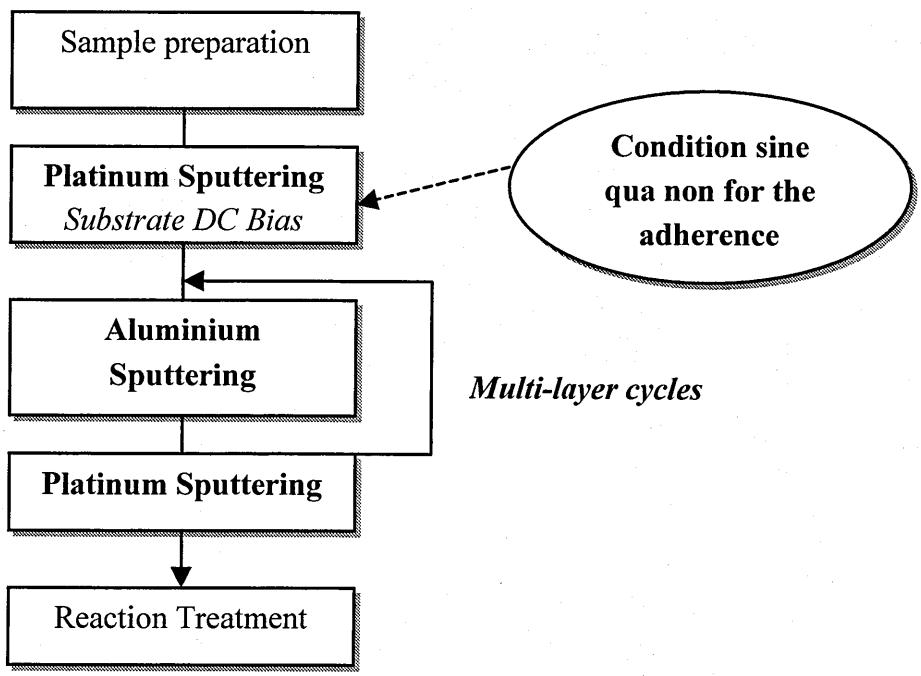

Figure 35: Low-mass bondcoat formation steps

The chapter outlines as well the tests and analysis, which have been carried out on the as-coated and as-reacted samples, and gives a brief description of each analysis method.

4.1. Coating Deposition

In this following section are detailed the deposition steps (Figure 35) as well as their variations and improvements.

4.1.1. Substrates

Materials:

The multi-layer coating depositions have been carried out on various substrate materials in order to suit the analysis and test requirements.

Glass plates have been deposited onto, because of their smooth surface in order to measure accurately the coating thicknesses.

Alumina squares (10*10*1mm) have been used because they are an inert material and do not interact with the coatings during heat treatment.

Superalloy coupons have been used extensively to assess the bondcoat performance and evolution on an industrial blade material. The alloy need was a first generation single crystal nickel-base superalloy AM1 (Acier Monocrystallin 1) provided by SNECMA

Its composition is detailed in the following table (concentration in weight %):

	Ni	Co	Cr	Al	Ti	Ta	Mo	W
AM1	Bal.	6.5	7.5	5.3	1.2	8	2	5.5

Finally, deposition have been also undertaken on thin aluminium foil to be used for thermal analysis:

- 6.5 microns thick; purity of 99.5 %
- 1.5 microns thick; purity of 99.1 %

Substrate preparation before deposition:

The superalloy substrates were usually prepared as follows:

1. polishing of both sides of the coupons in order to have a smooth surface
2. Ultrasonic cleaning in isopropyl alcohol

The foil, glass and alumina substrates were cleaned by the same way.

After cleaning, all the specimens were kept in a vacuum dessicator until they were loaded into the chamber.

4.1.2. Multi-layer coating deposition

The sputtering apparatus, which has been used to deposit the multi-layer coatings, is schematised in the Figure 36:

The sputtering is a process carried out under vacuum. The deposition chamber is therefore connected to a pumping system consisting of:

- A roughing pump, which evacuates the deposition chamber down to 10^{-1} mbar.
- A diffusion pump, which switches on automatically when the pressure reaches 10^{-1} mbar and which evacuates the chamber down to 10^{-6} mbar.

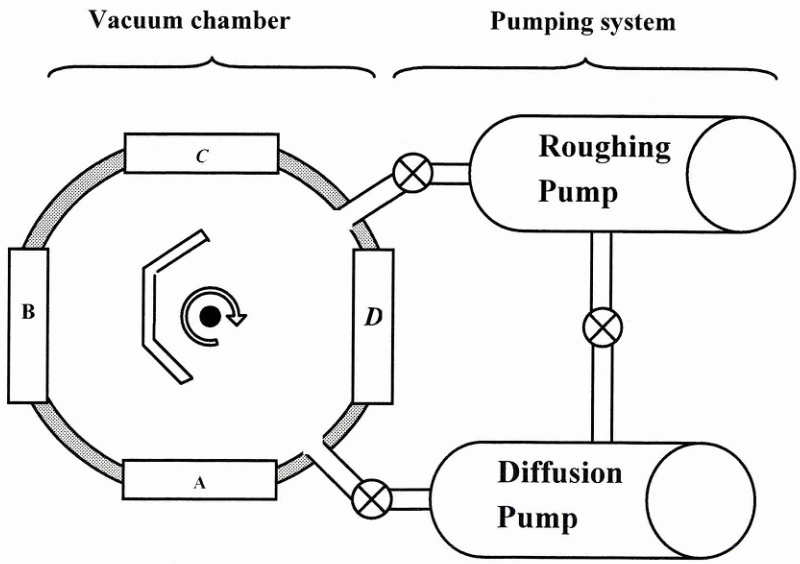

Figure 36: Sputtering apparatus

4 different targets of material to be sputtered can be mounted in the vacuum chamber. The samples to be deposited are held on a sample holder which can rotate and be placed in front of each target. This rotation can be done either manually or automatically. **This apparatus allows the production of multi-layer coatings without opening the chamber between the different layer depositions.**

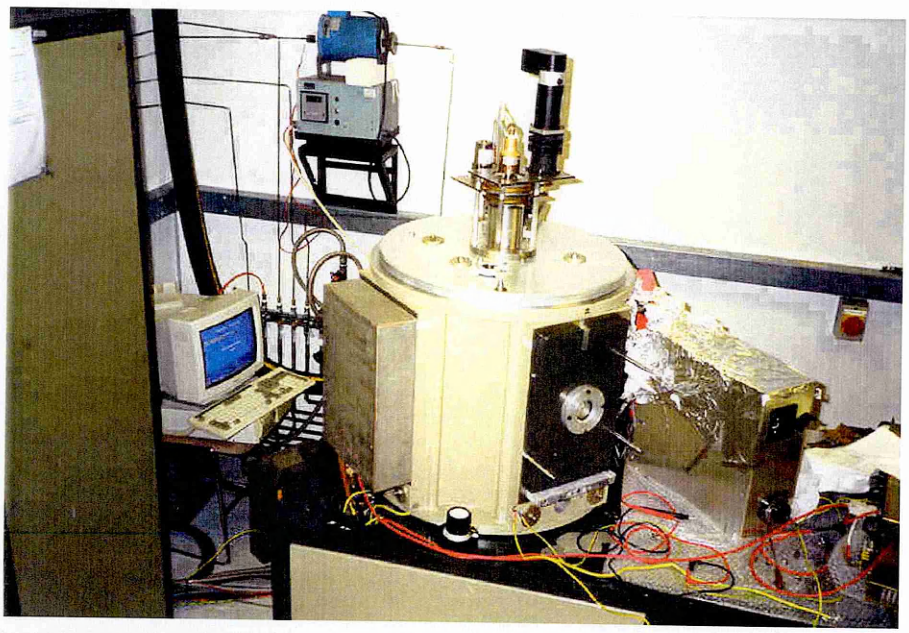

Figure 37: Sputtering apparatus

Once the substrates are clamped on the sample holder, the vacuum chamber is evacuated to a base pressure of approximately 10^{-6} mbar (using the pumping system). An inert gas, which is usually Argon, is then introduced. By throttling the diffusion pump, the chamber pressure is finally decreased down to 10^{-2} mbar, which is the chosen process pressure.

A potential is then applied between the substrate and the facing target in order to ionise the inert gas. The ions of Argon are accelerated towards the target and dislodge atoms of the target material due to the high energy of the impact. The dislodged atoms are eventually deposited on the substrate samples.
The platinum metal is deposited by RF sputtering and the power is chosen in the range 350-450W.
The aluminium metal is deposited by DC sputtering. The applied potential varies between 250 and 350V at a current of 1.7 A.

The following flow chart depicts the steps to follow at the first stages of a deposition run

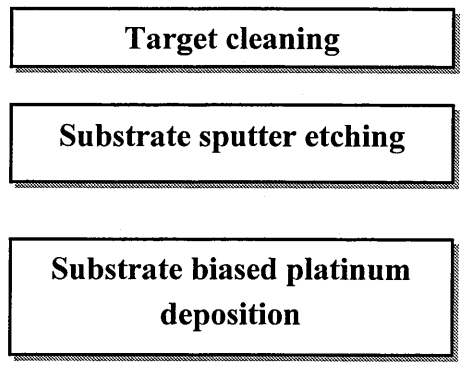

Figure 38: precautions of deposition

All the targets, which have to be used, must be cleaned, because they may have been oxidised or contaminated during the air exposure. Sputtering the material on a shutter placed between the samples and the target is used to carry out this cleaning.
The substrate samples can be cleaned as well using a high ion bombardment. To achieve this, the deposition power is sharply decreased and a negative bias is applied to the substrates. This procedure is called sputter etching.
Once the target and the samples to be coated have been cleaned, a first deposition of platinum is carried out with the substrate bias still activated. Platinum has been chosen to be the first layer because aluminium could diffuse in the substrate.
The bias is very important at the first deposition stage because it promotes dramatically the adherence at the coating/substrate interface. This bias is generally chosen in the range of -50/-150V.

Subsequent to the first platinum deposition, the bias is switched off and alternate thin layers of aluminium and platinum are applied by sputtering.
The last layer of the multi-layer coating has been chosen to be platinum because it does not oxidise in air atmosphere.
The stoichiometry of the multilayer is controlled by the thickness ratio between aluminium and platinum layers. The thickness of both the platinum and aluminium layer is controlled by the deposition rate of the metal, and by the deposition duration.

This method has been used to deposit 3, 5 and 9-layer coatings on alumina and superalloy substrates. These multi-layer coatings consisted of alternative platinum and aluminium layers.

In parallel to these depositions, another coating systems have been produced using an aluminium foil substrate. Platinum has been deposited, either on one side or on both sides of the thin foil leading to the formation of a multi-layer coating without a substrate. These coatings were aimed at the thermal analysis.

4.1.3. Samples automatic rotation implementation

In increasing the number of layers (keeping the same bondcoat thickness) in the coating, the number of interfaces and therefore the surface of reaction are also increased. The reaction between aluminium and platinum is thus improved.

In order to research this theoretical concept, a rotative motor has been linked to the sample holder of the deposition chamber (Figure 39).
The main aim of the process is to place automatically the samples to be coated in front of each sputtering target for a **short programmed time**.
A computer program (UNIDEX®) monitors the rotation of the sample holder and allows setting up of a specific time spent in front of each target as well as a rotation speed.

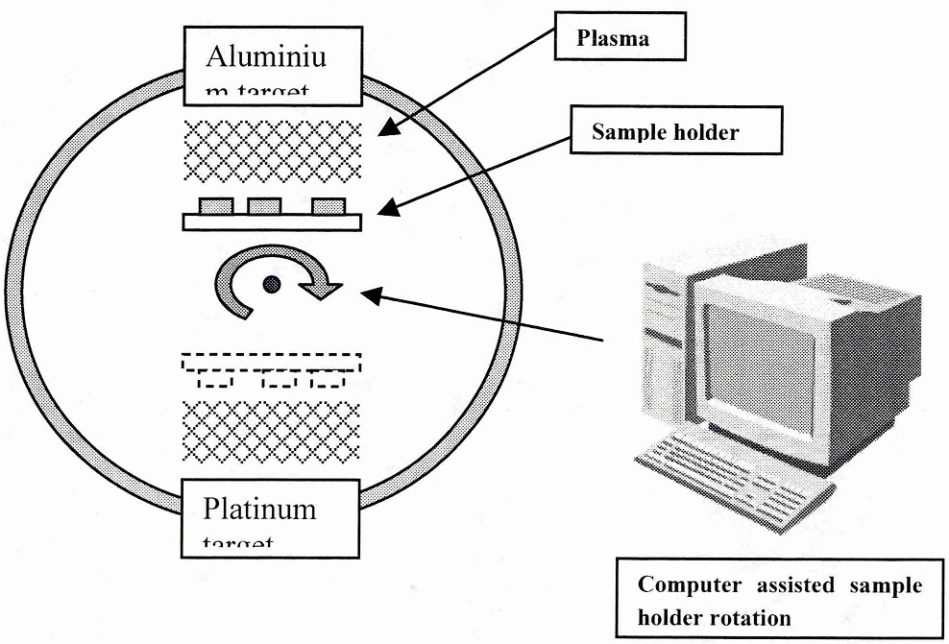

Figure 39: Sample holder's rotation monitoring

The time spent in front of each target is calculated relatively to:

- The deposition rate of the material to be deposited

- The stoichiometry of the expected compound

This method has been used to deposit coatings with up to 300 layers. These multi-layer coatings consisted of alternative platinum and aluminium layers and were applied on superalloy coupons.

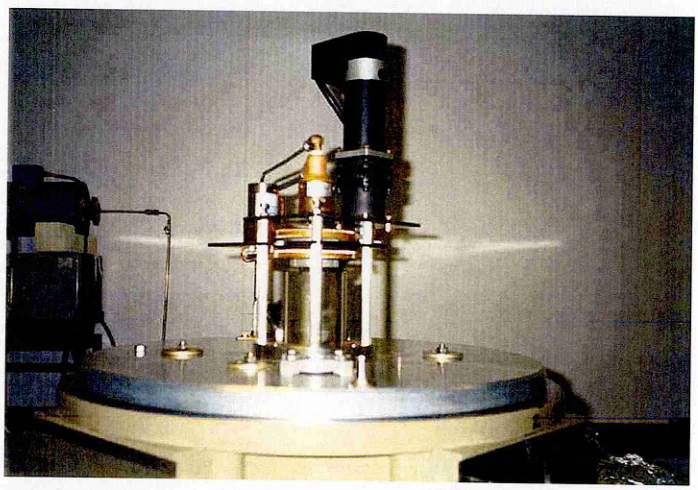

Figure 40: rotative motor mounted at the top of the chamber

4.1.4. Introduction of a reactive element

The addition of a Reactive Element (**RE**) into the composition of the low-mass bondcoat has been studied and experimented.
In order to introduce evenly a small concentration of RE in the coating, the co-sputtering of aluminium and RE (and platinum plus RE) has thus been implemented by clamping a small piece of RE material on either the platinum or the aluminium target.
The study has been carried out using wire of zirconium, yttrium and hafnium:

	Zirconium	**Yttrium**	**Hafnium**
diameter	1mm	1mm	1mm
Purity (wt%)	99.2%	99.9%	97%

As the reactive elements (Zirconium, Hafnium, Yttrium) are very expensive materials, aluminium was firstly co-deposited with platinum, to research the appropriate methodology.

A clamp system was then developed to be able to place a piece of wire on the aluminium or platinum target (

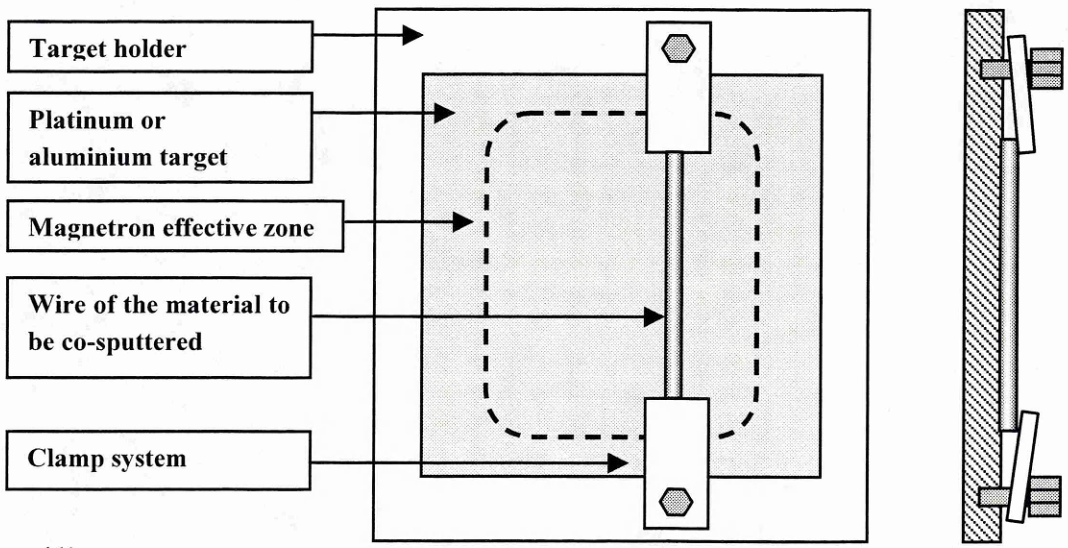

Figure 41).

Figure 41: co-sputtering arrangement

4.2. Heat treatments and oxidation tests

This section relates to the heat treatments carried out on the as-deposited multi-layer coating.

4.2.1. Reaction treatments

The reaction treatment is the last step of the low-mass bondcoat formation. It triggers an exothermal reaction between the deposited layer leading to the formation of a stoichiometry-controlled platinum aluminide.

This reaction treatment has been set at 700°C for 2 hours, referring as to the work of M.J.Deakin[22] and has been performed in an Argon atmosphere.

4.2.2. Post reaction treatments

Other heat treatments have been performed at 700°C, 900°C and 1100°C for variable duration and an argon atmosphere was used to prevent coating oxidation.

4.2.3. Cyclic Oxidation test

Cyclic oxidation runs at 1200°C and 1100°C have been carried out under air atmosphere in order to compare the oxidation behaviour of the low-mass bondcoats to the bondcoats currently used at SNECMA.
The cycle consisted of 1 hour at temperature and 15 min cooling under ambient atmosphere.

4.3. Differential Thermal Analysis

Thermal Analysis was carried out in order to assess the transformation temperature of the intermetallic coatings and to provide information about their heats of formation.
A **DSC2920** apparatus equipped with a **1600DTA** head was therefore used to study the coatings deposited on alumina substrates and aluminium foil.
The following section describes the analysis process.

4.3.1. Introduction

Thermal analytical methods monitor differences in the properties of samples as the temperature increases or differences between a sample and a standard as a function of added heat (or as a function of the temperature). These methods are usually applied to solids to characterise the materials.

3 different methods are relevant[81;100]:

Thermogravimetry (TG):
Thermogravimetry is the measurement of the mass of a sample as the temperature increases. This method is useful for determining sample purity and water, carbonate, and organic content; and for studying decomposition reactions.

Differential Scanning Calorimeter (DSC):

According to the ICTA Nomenclature Committee, the **D**ifferential **S**canning **C**alorimeter (**DSC**) is "a technique for recording the energy necessary to establish a zero temperature difference between a substance and a reference against either time or temperature, as the two specimens are subjected to identical temperature regimes in a environment heated or cooled at a controlled rate".
In other words, DSC devices measure the amount of energy (heat) absorbed or released by a sample as it is heated, cooled or held at a constant (isothermal) temperature.

These devices are used to find the melting point, transition temperature and other thermal properties of materials. The system at Cranfield had a temperature range from **-100°C up to 550°C.**

Differential Thermal analysis (DTA):

According to the ICTA Nomenclature Committee, the **D**ifferential **T**hermal **A**nalysis (**DTA**) is "a technique for recording the difference in temperature between a substance and a reference material against either time or temperature, as the two specimens are subjected to identical temperature regimes in a environment heated or cooled at a controlled rate".

The DTA apparatus is used for the same purposes than the DSC apparatus, but it can be operated at higher temperature. Some apparatus are able to heat samples **up to 2400°C,** the Cranfield system can heat to 1600°C.

The DTA experiments are performed for different applications:

- Endothermic and exothermic reactions
- Phase diagrams
- Phase transitions
- Purity and identification
- Thermal decompositions
- Measurement of heat capacity

4.3.2. DTA apparatus

To carry out a DTA run, the piece of material to be analysed is placed in a small crucible made up of an inert material. A second crucible, referred as to the reference holder, is filled with a piece of inert material having the same weight as the sample.
The two crucibles are placed in a furnace tube, which is heated at a control rate by the temperature programmer. A differential thermocouple records the temperature difference between the 2 crucibles.

4.3.2.1. DTA apparatus[35;81]

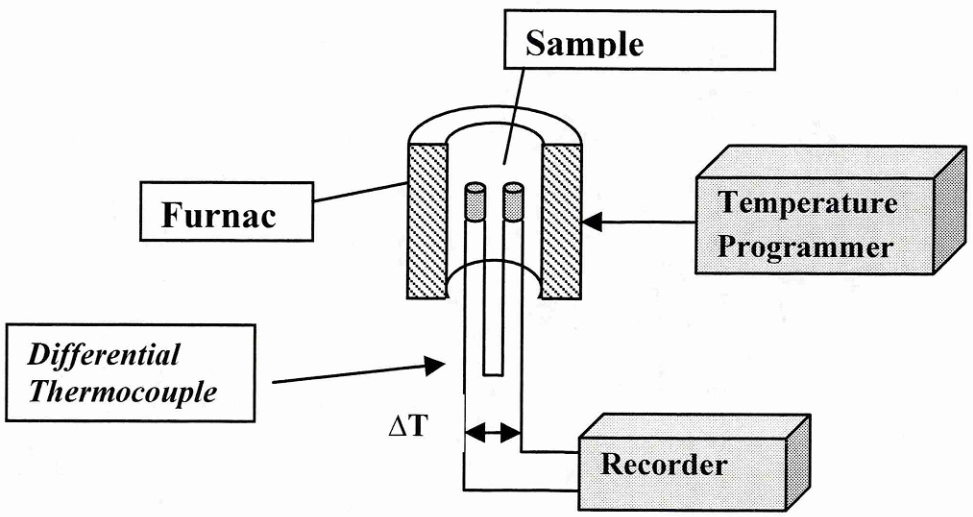

Figure 42: DTA apparatus

Sample holders

The most common materials used for the crucibles are pyrex, silica, alumina, and platinum. Sensitivity of the method is increased if the heat capacity of the sample holder is very small because the metal of the sample holder will not, for example rapidly absorb heat during an exothermic reaction, which would thus reduce the exothermic effect measured.

Thermocouples

In early DTAs, the thermocouples were immersed in the sample and in the reference.
In modern DTAs (principles set out by **Boersma**[100]), the differential thermocouples are in intimate contact with vessels containing the test and reference materials.

Thermocouples commonly used in DTA and DSC:

ISA type	Positive metal	Negative metal	Thermoelectric power (μV/K)	Approximate maximum temperature (°C)
Y, J	Iron	Constantan	51	450
K	Chromel	Constantan	41	1350
S	Platinum	Platinum-10% Rh	5.5	1600
-	Tungsten	Tungsten-26% Re	3.3	2400

Samples

According to the works of **Barral** (1973)[100], the use of very small samples minimises the thermal gradients. (with weight range between 5 an 50 mg).
In practice, it is important to keep a **steady weight** and a **steady Surface /Volume ratio** for each sample.

Furnace (atmosphere)

The furnace must have a large and uniform hot zone; it must be able to heat up and cool down with a rate specified by the temperature programmer.
It must also have a design such that it can be removed easily from the equipment whilst still hot and can be located in the same position for each experiment.

Recorder

The recorders are made up of an amplifier (the most sensitive with 25 μV, and the least with 500μV; this voltage corresponds to the smallest voltage difference gathered by the thermocouple).
Nowadays, modern DTA systems use computerised data processing.

Temperature programmer

It generally offers a large range of programmed rates (1-20°C.min^{-1}).
It should be capable of heating, cooling and isothermal control.

4.3.2.2. DTA results

An endothermic reaction would slow the rate of heating, because this reaction needs energy. It would lead to a negative temperature difference between the sample and the reference. On the other hand, an exothermic reaction would increase the rate of heating, because of the added heat and would lead to a positive difference.

The data gathered by the differential thermocouple –connected to both the reference and the sample holder- are displayed as a differential Temperature curve as a function of the time or the furnace temperature (Figure 43).

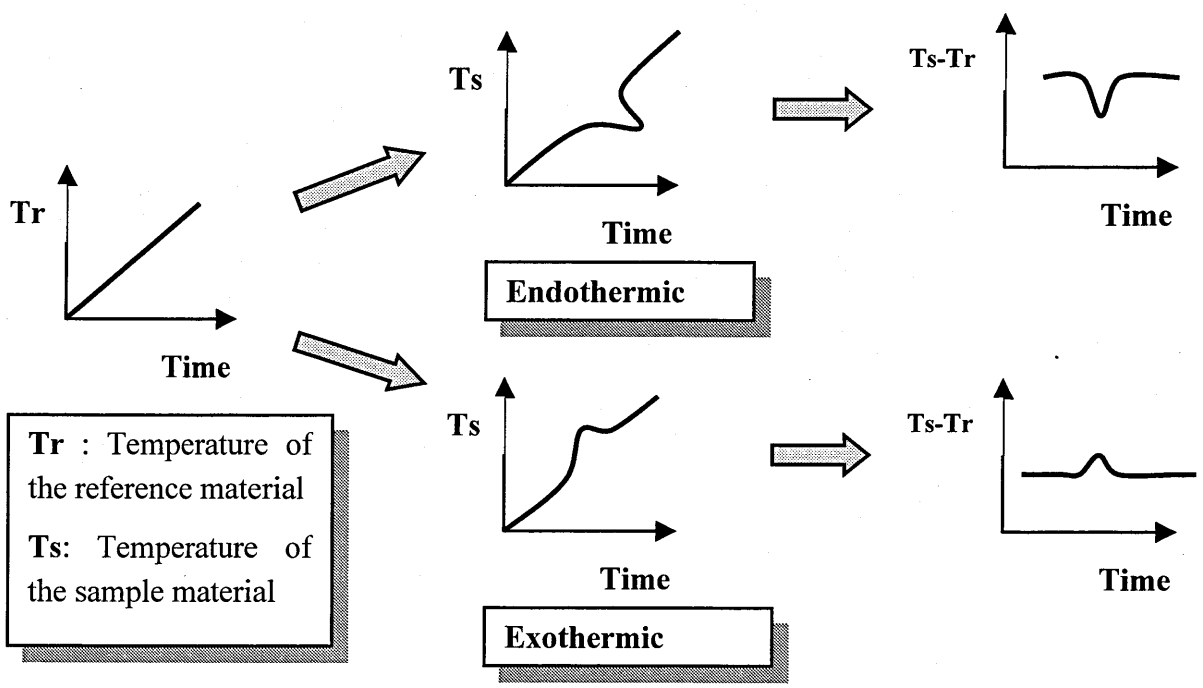

Figure 43: Differential result of a transformation

4.4. Coating characterisation

4.4.1. Coating adherence and strength

In order to assess the adherence and the brittleness of the as-deposited and as-reacted coatings, a pull-off test was carried out (Scotch Tape test)[84]. It consists of sticking a strip of adhesive tape on to the coating and drawing it off suddenly.

4.4.2. X-Rays diffraction analysis[16]

X-ray diffraction was carried out on all the as-deposited coating as well as on the as-reacted and as-tested coatings in order to determine the formed intermetallic compounds.

X-rays are electromagnetic radiation (very much shorter wavelength than light). They are produced when any electrically charged particle of sufficient kinetic energy are rapidly decelerated.

Electrons are usually used for this purpose. The radiation is produced in a X-ray tube, which contains a source of electrons and two metal electrodes. The high voltage maintained across these electrodes (some tens of thousands of volts) rapidly draws the electrons to the anode, or target, which they strike with very high velocity.
X-rays are produced at the point of impact and radiate in all directions.

The X-ray diffraction work was carried out with a Phillips X-ray diffraction analyser system PW1840, using copper K-alpha radiation. The coatings were analysed at 40kV, 20mA and data were produced in the range 20 to 90 degrees.

4.4.3. Metallographic examination

Metallographic examination was carried out on coating sections after the deposition process, and all the subsequent heat treatment or oxidation tests.
The coatings deposited on alumina substrate were impregnated with epoxy resin, because of their high brittleness.
Conductive bakelite was used to impregnate the as-coated superalloy substrate.
The mounted samples were prepared using standard metallographic techniques on a Buhler Metaserv 12 semi automatic grinder/polisher.
The structures were examined using a Cambridge 250 and ISI-ABT55 scanning electron microscopes.

4.4.4. Diffusion profile analysis

Quantitative analysis was carried out on a Cambridge 250 electron microscope, using EDX analysis, coupled with ZAF software.
Digipoint analysis was performed as well to determine the diffusion profile through the coatings. This analysis mode allows quantifying the composition automatically at different points previously chosen.
10 and 20 points digipoint analysis were performed from the outer surface of the coating until the end of the interdiffusion zone in the substrate.

4.4.5. Auger spectroscopy

Auger spectroscopy was carried out in order to determine the elements and compounds present at the interfaces between the coating layers.

Auger electron spectroscopy (AES)[16] identifies elemental compositions of surfaces by measuring the energies of Auger electrons. Auger electron emission is stimulated by bombarding the sample with an electron beam. The Auger electron energies are

characteristic of the elements from which the electrons come. Auger electron spectroscopy is a widespread method for analysis of **surfaces, thin films, and interfaces**.

The basic Auger process starts with removal of an inner shell atomic electron to form a **vacancy**. Several processes are capable of producing the vacancy, **but bombardment with an electron beam** is the most common. A second atomic electron from a higher shell fills the inner shell vacancy. Energy must be simultaneously released. A third electron, the Auger electron, escapes carrying the excess energy in a radiationless process.

To analyse samples in depth, Auger instruments incorporate ion beam sputtering to remove material from the sample surface. One cycle of a typical depth profile consists of sputtering a small increment into the sample, stopping, measuring relevant portions of the Auger spectrum, and using the equation for elemental quantification.

The surface of the analysed sample is usually slightly etched in order to remove any impurities or thin oxide layer.

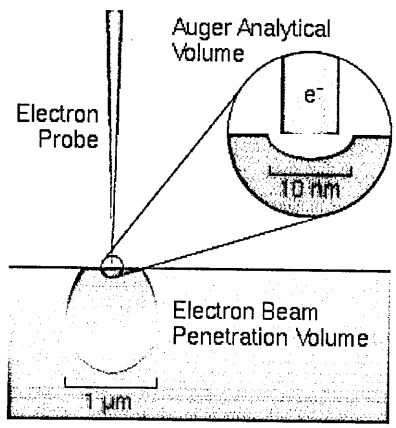

Figure 44: the Auger spectroscopy technique

Electron beams disperse into small volumes, typically about one cubic micron (1e-12 cc). X-rays are emitted from most of this volume. Auger signals arise from much smaller volumes, down to about 3e-19 cc.

The X-ray analytical volume increases with electron beam energy and decreases for materials with higher atomic numbers. The Auger analytical volume depends on the beam diameter and on the escape depth of the Auger electrons.

5. Predeposition considerations

This chapter introduces the deposition and formation of platinum aluminide overlays. The first part is focused on the formation by interface reaction and the theoretical stability of various intially multi-layer platinum aluminides.
The second part concerns the characterisation of platinum aluminide compounds and the third part gathers the thermal analysis work performed to highlight and analyse the multi-layer exothermic reaction.

5.1. Platinum aluminide formation

5.1.1. Platinum aluminide compounds

The different compounds that can possibly formed with platinum and aluminium are collated in the following binary phase diagram:

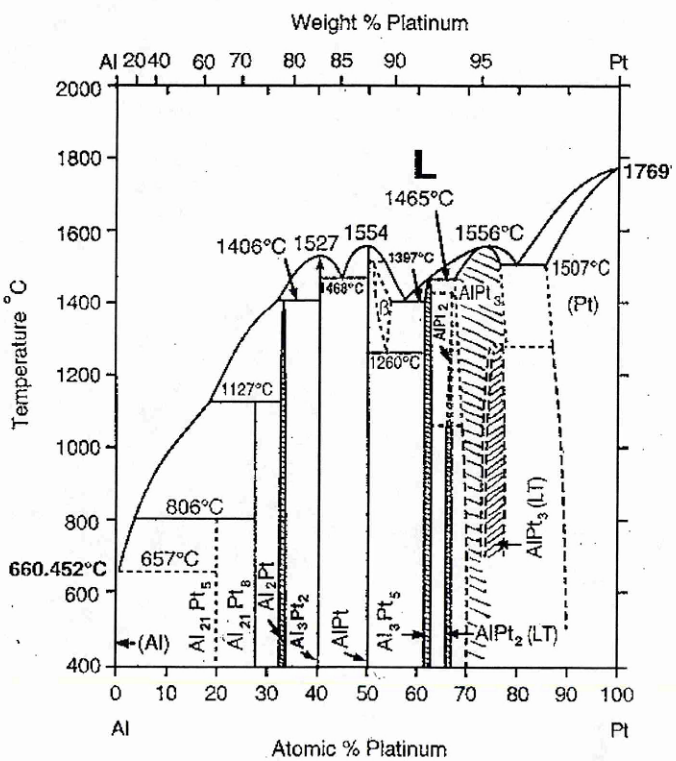

Figure 45:Pt-Al binary phase diagram

Even though they contain aluminium, these compounds have a relatively high melting points because of the platinum alloying element (Table 9).

Phases	Melting point (°C)	Enthalpy of formation (kJ/g.atom)	Composition wt % Pt	
Al	660.45		lower	upper
Pt_6Al_{21}	806	55	63.2	
Pt_8Al_{21}	1127	71	72.8	
$PtAl_2$	1406	84	76.9	78.5
Pt_2Al_3	1527	95	82.8	
PtAl	1554	100	87.9	
Pt_5Al_3	1465		92	92.5
Pt_2Al	1430	88	93	94
Pt_3Al	1465-1556	70	93.7	96.18
Pt	1507-1769		97.4	100

Table 9: platinum aluminide characteristics

The stability of a compound can be compared or assessed by plotting the energy of formation in function of the melting point. The most stable compound is then the compound with the best compromise of values.

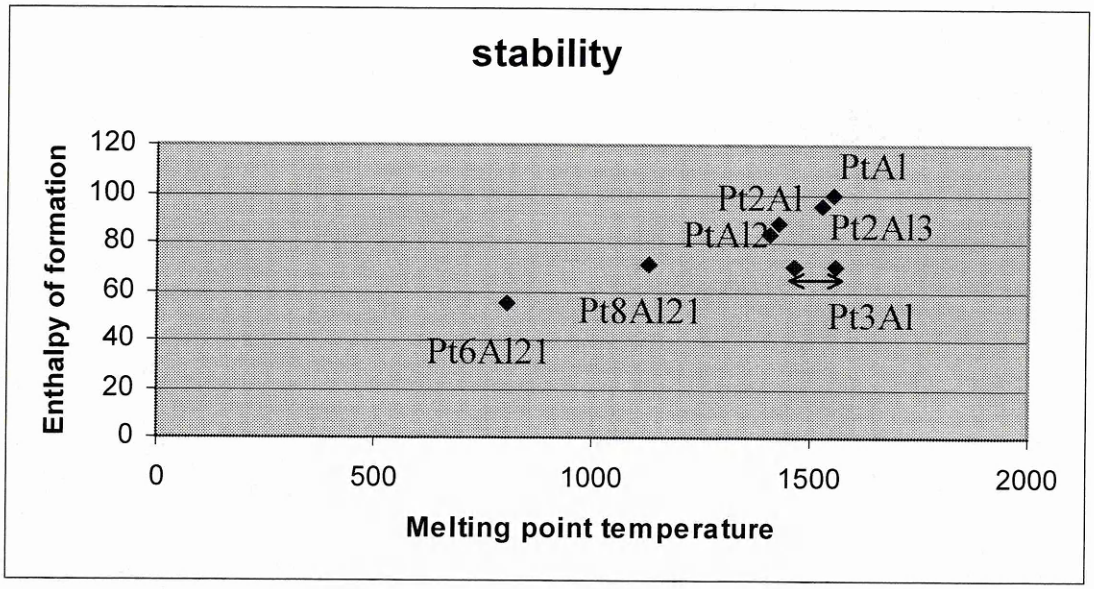

Figure 46: Enthalpy of formation in function of the melting point of various platinum aluminide compounds

Such a representation results in the Figure 46, which shows that :

- PtAl is the most stable compound
- $PtAl_2$ is less stable than PtAl, but it is easier to form because of its wider range of composition (Table 9).
- The aluminium-rich compounds Pt_6Al_{21} and Pt_8Al_{21} are relatively unstable

5.1.2. Thickness ratio calculation:

As explained in the 'experimental procedure' chapter, the formation of the low-mass bondcoat final structure involves the interdiffusion and interaction of successive layers of platinum and aluminium. The stoichiometry of the desired compound is thus controlled by the thickness ratio between platinum and aluminium, assuming that no interaction with the substrate occurs.

In a layer of the compound Pt_xAl_y, containing n moles, it has to be found n.x moles of platinum and n.y moles of aluminium.

The number of moles can be connected to the volume of coating, by equaling two formulation of the coating weight:

$$m = mol \times M = \rho \times V$$

The thickness of each layer can be then introduced by replacing the volume by:

$$V = S \times a$$

For each material, it gives:

$$a = \frac{M}{S \times \rho} \times mol$$

The thickness ratio is then defined by:

$$Thickness\ ratio = \frac{a_{Al}}{a_{Pt}} = \frac{y}{x} \times \frac{M_{Al}}{M_{Pt}} \times \frac{\rho_{Pt}}{\rho_{Al}}$$

x and y depends on the compound, M and ρ are given in the following table:

	Aluminium	Platinum
Density (g/cm^3)	2.7	21.45
Atomic weight (g/mol)	26.98	195.09

Table 10: density and atomic weight for aluminium and platinum

The numerical values for platinum aluminides thickness ratios are gathered in the following table, as the ratio of the Al thickness to that of Pt:

Phases	**Pt_6Al_{21}**	**Pt_8Al_{21}**	**$PtAl_2$**	**Pt_2Al_3**	**PtAl**	**Pt_5Al_3**	**Pt_2Al**	**Pt_3Al**
Thickness ratio (Al/Pt)	3.83	2.87	2.19	1.64	1.10	0.66	0.55	0.37

Table 11: thickness ratios calculated for the platinum aluminide compounds

5.1.3. Formation mechanism and sequence

A reaction between two elemental metals through an interface is however not as simple as it seems. In order to control the formation of chosen compounds, a thermodynamical study has been carried out to predict the different reactions possible at the interfaces of the multi-layer coatings.

Pretorius et al (1990,1991,1992,1993)[83] has developed **a model of prediction** based on the effective heats of formation. This concept enables the calculation of heats of formation as a function of concentration and has been successfully applied in many cases, such as silicide and **aluminides**. [22:83]

The Gibbs free energy:

The phase formation at an interface during solid-state interaction is a **non-equilibrium process** because one phase forms at the interface. During a equilibrium process, simultaneous phases are formed leading to the lowest energy state of the system.
Although standard rules in equilibrium thermodynamics can not be applied to predict phase formation at the interface, the effective heat of formation model makes direct use of thermodynamic data.

The change in **Gibbs free energy** is the driving force for a process to take place

$$\Delta G° = \Delta H° - T\Delta S°$$

Since the change in entropy is quite small for a solid-state formation of an ordered compound, **the Gibbs free energy can be approximated by the change in enthalpy.**
The **enthalpy of formation** (or heat of formation) can be therefore used to predict a phase formation or transformation.

Effective concentration and effective heat of formation:

The following picture accounts for a simple diffusion couple between two materials A and B ,which are expected to react in order to form an intermetallic compound $\mathbf{A_{1-x}B_x}$.

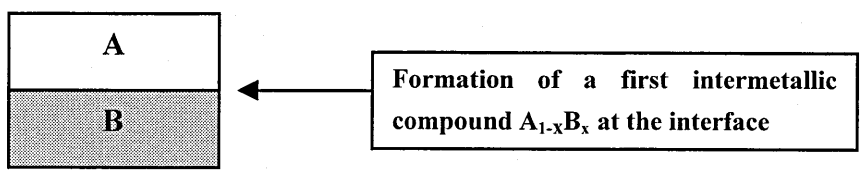

At the interface between the 2 materials, a compound forms as the temperature increases, but at an unknown ***effective concentration***.
The effective concentration **x'** is the concentration at which the reaction occurs. It differs from the physical compound concentration **x** because the reaction is affected by many factors (lowest eutectic, impurities, atomic mobility...).

The effective concentration expresses the availability of the *limiting element* of the reaction at the growth interface.
B is defined as the **limiting element** in the reaction if **x' < x .**

The compound $\mathbf{A_{1-x}B_x}$ is thus to be formed at an effective concentration x' of the limiting element B. The heat released during compound formation will be dictated by this effective concentration. An **effective heat of formation ΔH'** can therefore be defined as:

$$\Delta H' = \Delta H^{\circ}\left(\frac{\textit{effective concentration of Limiting element}}{\textit{compound concentration of Limiting element}}\right) = \Delta H^{\circ}\left(\frac{x'}{x}\right)$$

where ΔH° is the heat of formation of the compound

Prediction rules:

The activation energy for solid-state interdiffusion is directly proportional to the melting point of the solid (Brown and Ashby, 1980) and it determines therefore the mobility of the atoms. The greatest mobility is expected to take place at the composition of the lowest eutectic (or liquidus) of the binary system; it corresponds to the point where the mixing of materials at the interface is the most effective and the concentration of this lowest-temperature eutectic are thus chosen to be the effective concentrations of the reaction.
The rule for the first-phase formation states (Pretorius *et al*, 1990, 1991):

"The first compound phase to form during metal-metal interaction is the phase with the most negative effective heat of formation (ΔH^*) at the concentration of the lowest temperature eutectic (or liquidus) of the binary system."

And the phase formation sequence is formulated as follows (Pretorius *et al*, 1993):

"After the first phase formation in metal-metal binary systems, the effective concentration moves in the direction of the remaining element and the next phase to form at the growth interface is the next phase richer in the unreacted element."

Prediction model:

- **Heat of formation diagram**: for each compound of the phase diagram, the known enthalpy of formation is plotted at its stoichiometric concentration and is triangulated with the end points of the concentration axis.

- The effective concentrations of the interacting atoms at a growth interface are chosen to be those of the lowest temperature eutectic or liquidus. **If an eutectic is absent in the phase diagram, an arbitrary, but non-zero concentration close to the lowest liquidus is chosen.**

- The first phase to be formed is the compound with the most negative effective enthalpy of formation at the concentration of the lowest eutectic, expressed by the higher triangulation edge on the heat of formation diagram.

- The next phase to be formed at the interface is the next phase richer in the remaining element , and so on.

Application to the platinum aluminide compounds:

The effective heat of formation model can be applied to an interface between a layer of platinum and a layer of aluminium:
The intermetallic heats of formation are plotted and triangulated in the Figure 47.
The next step of the method consists in finding the lowest-temperature eutectic or liquidus. The most likely solution is the lowest liquidus at 657°C. It corresponds to a temperature close to the melting point of aluminium (660.45°C), but this point is actually coupled with an eutectic, because the solubility in aluminium is low but not nil.

If we consider this point for the *Effective Heat of Formation Model*, the effective concentration of platinum has to be chosen so that it is not zero but close to the concentration of the limiting element (platinum in this case) at the lowest liquidus.
Platinum is the limiting element because its concentration at the liquidus is always less than the concentration of the expected intermetallic (whatever the intermetallic in this case)
To sum up, the reaction, which occurs at the interface, needs a very low concentration of platinum to form the first intermetallic.
If we assume that the effective platinum concentration is is less than 1 at%, the most negative heat of formation at this point of the binary diagram is the one of the Pt_6Al_{21} intermetallic compound.
According to the model first rule, Pt_6Al_{21} is obviously the first-formed phase;
The sequence is then:

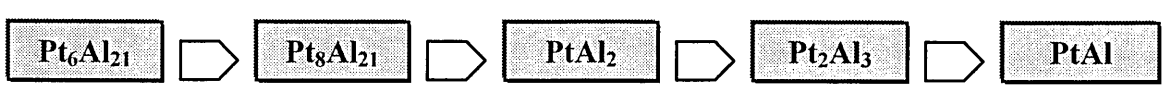

Remark: Pt_6Al_{21} has not been well studied and its relative thermodynamical data have to be used very carefully. Indeed, Pt_6Al_{21} has never been detected experimentally in this project

The model has emphasised that at each interface in the multi-layer coating, the first compounds to form are rich in aluminium, and that all the compounds richer in aluminium than the expected one, are formed before the layers have completely diffused one in each other.
With this concept, the whole consumption of both aluminium and platinum **layers by exothermic reaction** leads to the formation of an intermetallic compound with a determined stoichiometry (dependent on the thickness ratio Al/Pt).

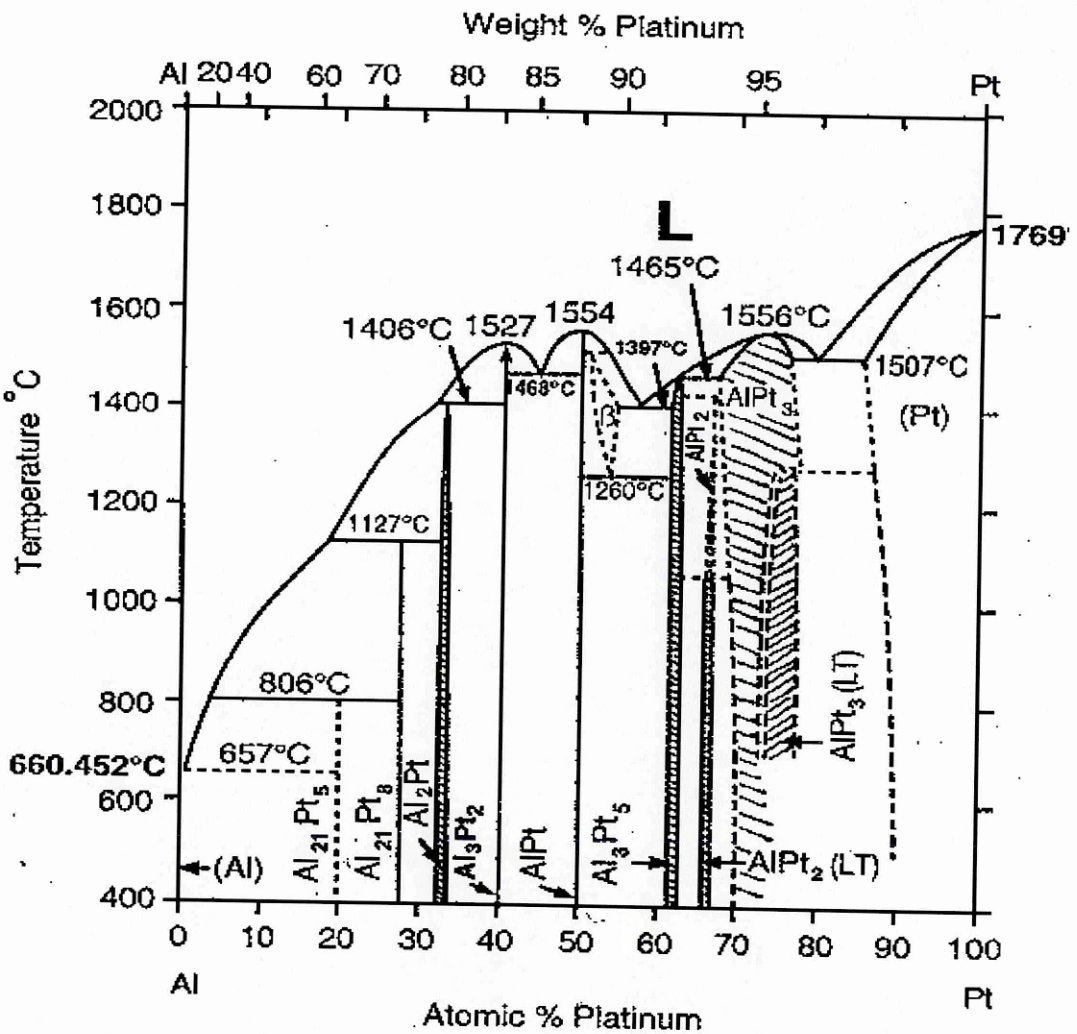

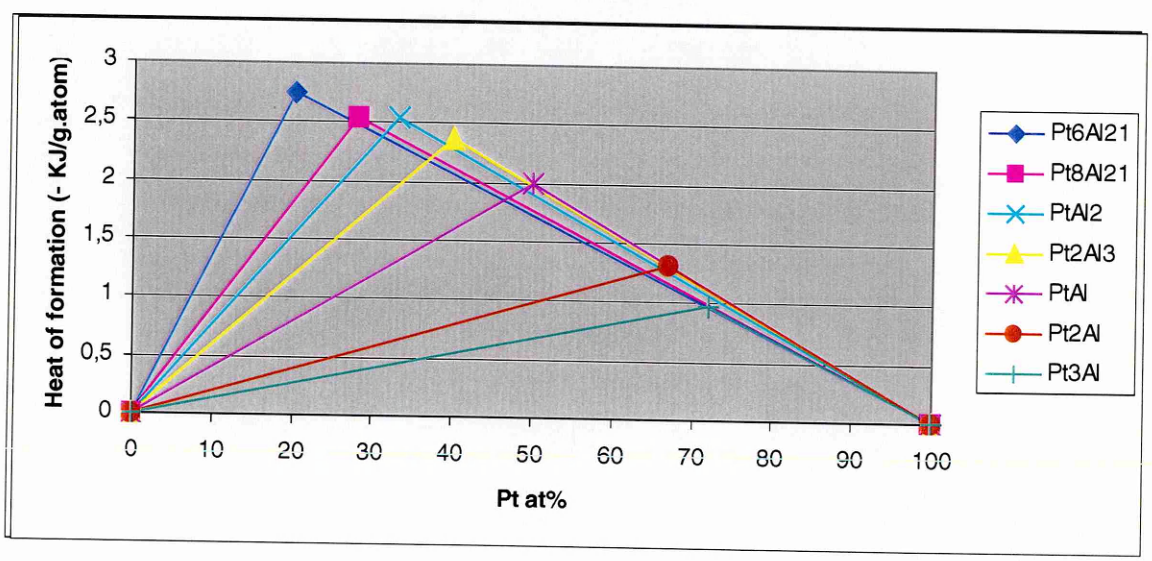

Figure 47: Triangulation of Enthalpies of formation

5.2. X-Ray characterisation of intermetallic compounds

As explained in the 'experimental procedure' chapter, X-Ray diffraction analysis is performed to characterise the different compounds present in the coatings. In the case of the low-mass bondcoat work, it is indeed relevant to recognise and emphasise the platinum aluminides which could have formed after the reaction treatment.
The X-Ray diffractomer results for an analysed sample are usually represented by a spectrum made up of peaks at specific location and intensity according to the compounds. A compound is then detectable if the peak parameters are known, but in the case of the platinum aluminides, only few compounds have been studied, such as $PtAl_2$ or Pt_8Al_{21}.

Because the work on low-mass bondcoat has led to the formation of platinum aluminides with a wide range of platinum and aluminium concentrations, the spectra of 3 intermetallic compounds (Pt_2Al_3, PtAl, and Pt_5Al_3) are also needed.

Intermetallic	Weight percentage of Pt (%)	Atomic percentage of Pt (%)
Pt_2Al_3	82.8	40
PtAl	88.3	50
Pt_5Al_3	92.3	62/63

Table 12: Composition of the studied intermetallic compounds

The procedure, which has been implemented to determine the spectra, involved the melting of platinum and aluminium pieces to form an intermetallic droplet. The experimental steps are described as follows:

- Small pieces of high purity platinum and aluminium were cut, weighted and cleaned. They were gathered then to respect the stoichiometry of each intermetallic compound.
- A graphite crucible to contain the pieces of material was shot drilled to form cylindrical holes with a flat bottom. These holes were then coated with boron nitride to inhibit a reaction between the aluminium and the graphite.
- The crucible was placed in a Hot Isostatic Press (HIP) and heated up to 1800°C (**above the melting temperature of both aluminium and platinum and all the intermetallic compounds**) for ½ hour or 1 hour under a pressure of 250 bar.

The result of the melting process is the formation of a single droplet for each intermetallic compound. A weight measurement was then carried out in order to detect any loss of material. As shown in the Table 13, the weight before and after the treatment is virtually the same.

Each droplet was then polished in order to have a flat surface for analysis and heat treated at 600°C for 15 minutes. This annealing treatment is very important because it increases the accuracy of the analysis by relieving the internal stresses present on the surface after the polishing step.

A X-Ray diffraction analysis (between 20 and 90° θ) of the polished and treated surfaces was finally performed, resulting in the desired spectra.

The droplets were then embedded in Bakelite and an EDS quantitative analysis was carried out to check the final stoichiometry of the compounds. As shown in the Table 13, the final stoichiometry corresponds quite accurately to the expected one.

Intermetallic	**Weight before melting (mg)**	**Weight after melting (mg)**	**EDS quantitative analysis after melting**	
			Pt	**Al**
Pt_2Al_3	275.7	275.6	40.28	59.72
PtAl	193.9	195	50.97	48.94
Pt_5Al_3	268	268.8	62.67	36.99

Table 13: *mass change and composition of the intermetallic compounds formed*

Traces of iron were found, but were < 0.3%.

3 droplets were produced per platinum aluminides in order to reduce the dispersion of the results.

The following data are given in the 2-theta scale. The highlighted number corresponds to the peak with the highest intensity.

Pt_2Al_3													
24,4	25,5	30	**43**	53,2	61,5	88							
PtAl													
25,9	31,9	37	**41,5**	45,6	56,8	60	72,5						
Pt_5Al_3													
23,5	30	32,5	**40,5**	47,9	53,8	63							

The following spectra account for the peaks relative to the Pt_2Al_3, PtAl and Pt_5Al_3 compounds

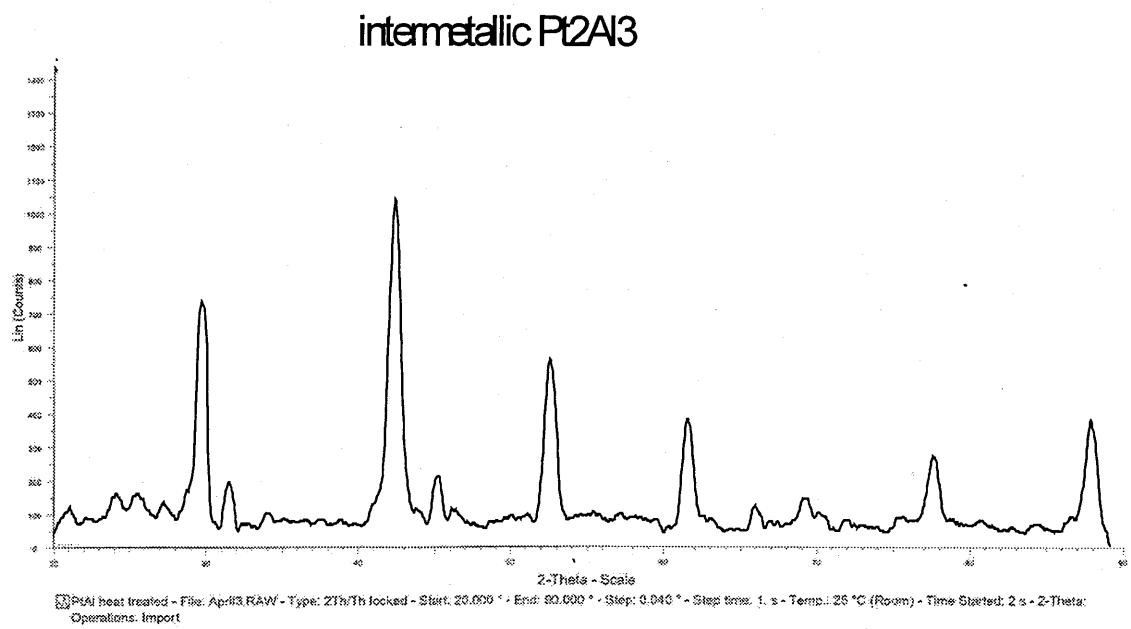

Figure 48: X-Ray spectrum of the Pt_2A_3 intermetallic compound

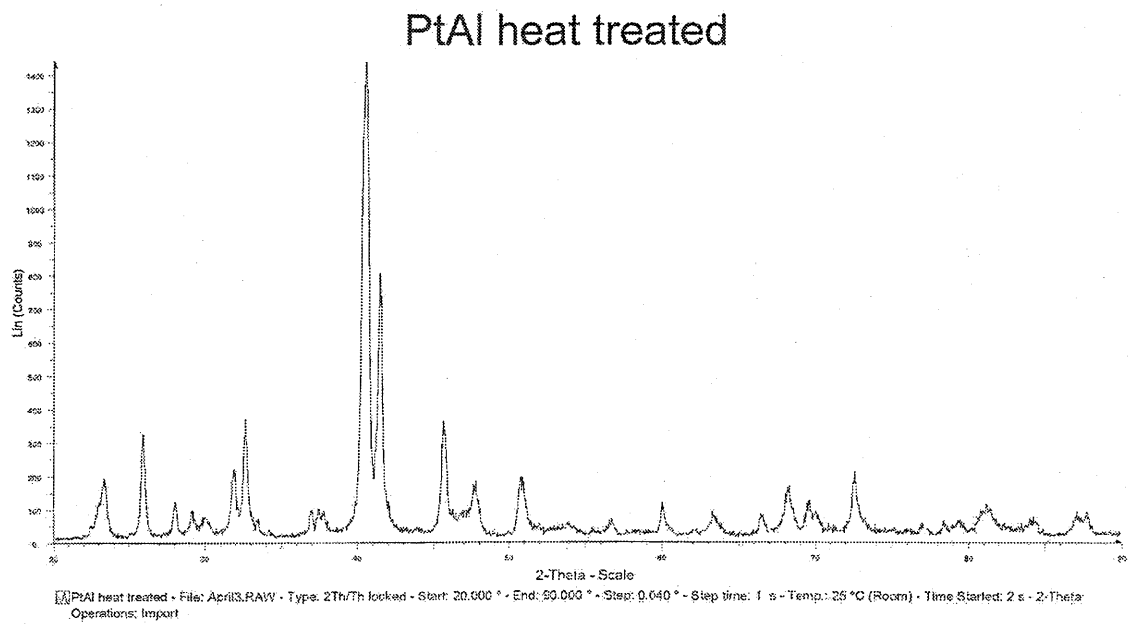

Figure 49: X-Ray spectrum of the PtAl intermetallic compound

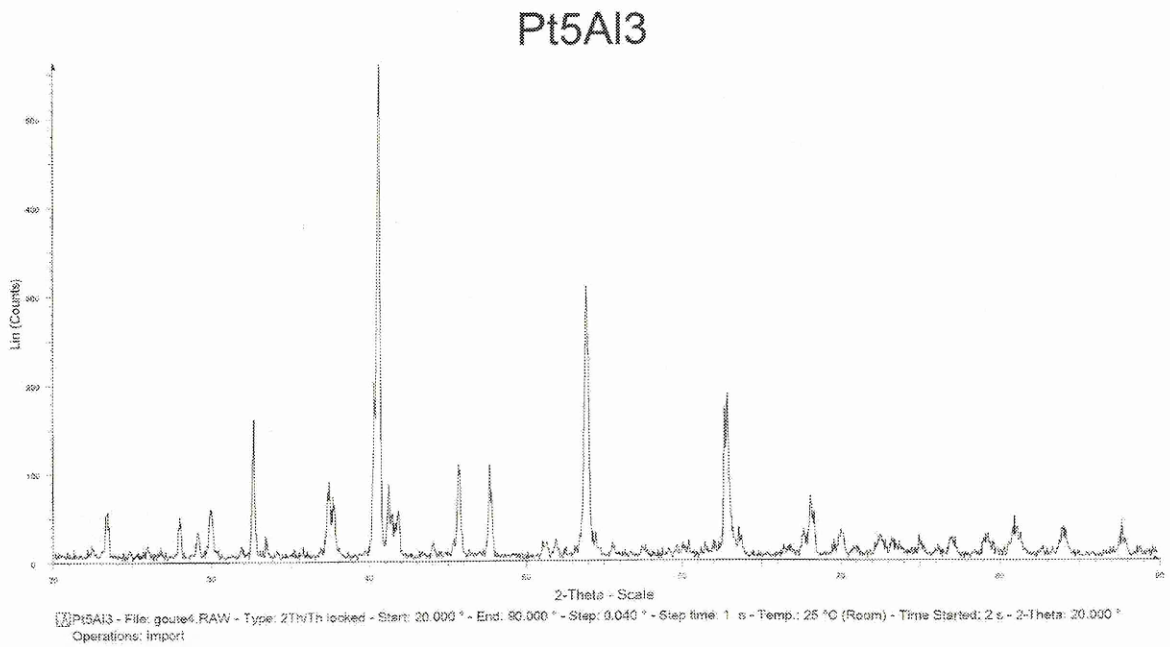

Figure 50: X-Ray spectrum of the Pt_5Al_3 intermetallic compound

The following data correspond to the peaks observed on the X-Ray diffraction spectra taken from the literature or from experimental work. These data has been extensively used in this low-mass bondcoat work.

Pt_6Al_{21}													
23,8	**30,1**	41,8	44,8	45,8									
Pt_8Al_{21}													
22,2	25,8	**26**	26,2	27,7	29,7	38,2	39,2	41,9	43,2	45,2	45,7	54,5	73,8
$PtAl_2$													
26,2	30,1	43,2	51	53,7	62,9	69							
Platinum													
39,8	46,2	67,2	81,5										
Superalloy AM1													
51													
Bondcoat CN91													
30,8	**44**												

The set of peaks given for the superalloy and bondcoat structure is not complete. For the superalloy, the single peak corresponds only to the texture of the cut and coated rod pieces.

5.3. Differential Thermal analysis results

5.3.1. Interpretation of DTA results

The differential thermocouple produces a differential temperature between the sample and the reference. These data are gathered by the DTA recorder, which draws a *Differential temperature-Heating temperature* curve (Figure 51).

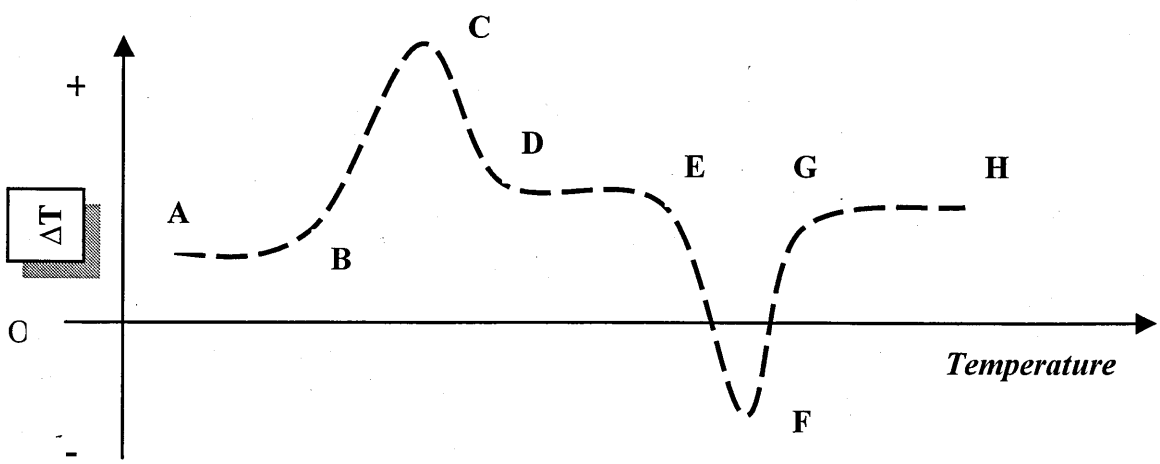

Figure 51: Heating curve of a material or compound

The curve is made up of **baselines (A,B,D,E,G,H)** and **deflections** of these baselines (downward or upward peaks e.g. C or F).

The baseline:

The baseline is a small and steady temperature difference (segments AB, DE, GH), which depends on:

- The ***heat capacity*** of the sample (vertical shift of the baseline)
- The ***thermal conductivity*** of the sample (rotation of the baseline)

For example, the height of the 2 baselines AB and DE differs because of a change in heat capacity of the sample during the heating.

The downward deflection of the baseline corresponds to an endothermic reaction.
The upward deflection of the baseline corresponds to an exothermic reaction.

B and E are referred to as the onset temperature of a reaction. However, an extrapolation of the curve is needed to determine the accurate location of these points (see further).

The peaks:

In a solid-solid metal transformation or phase change, the peak formation corresponds to a reaction, which is defined by:

- The onset temperature of the reaction
- The enthalpy change of the reaction

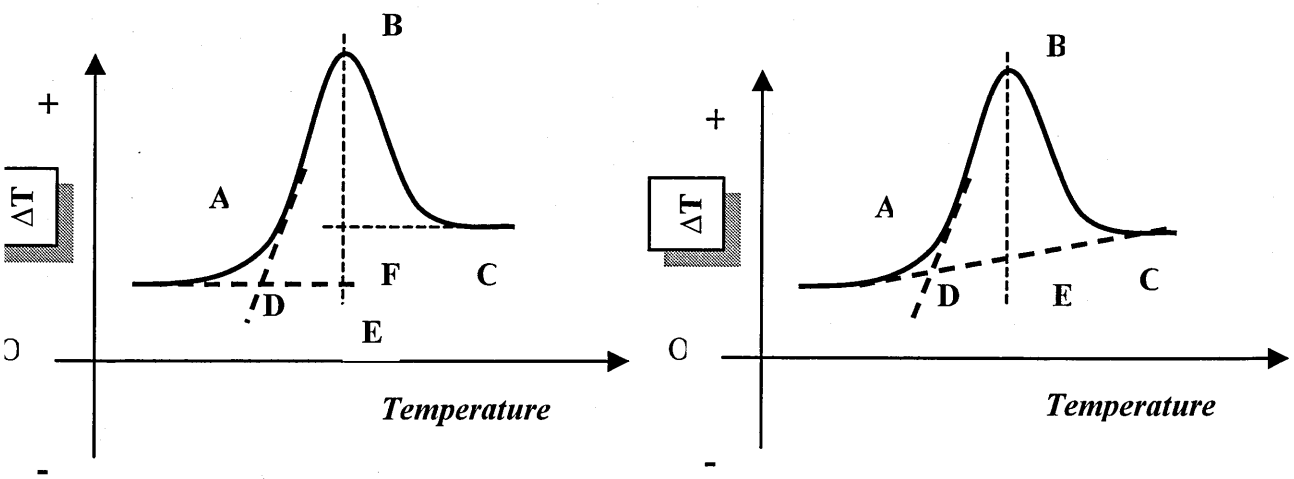

Figure 52: Exothermic reaction peak analysis

On the Figure 52, ABCA or ABCFEA defines the **peak area**, which is directly proportional to the total **enthalpy change** of the reaction, as written in the following equation:

$$Peak \quad area \quad = \int_{T1}^{T2} \theta dT \quad = \frac{mq}{G}$$

D corresponds to the beginning of the reaction and allows us to determine the **onset temperature.**

D is the point of intersection of the tangent drawn at the point of greatest slope on the leading edge of the peak (AB) with the extrapolated baseline (AD).

Computer softwares usually determine the onset point with the tangent and a drawn line between the boundaries of the peak.

5.3.2. Apparatus calibration

5.3.2.1. Calibration procedure

Calibration of the apparatus has to be performed **before launching experimental runs.**
The purposes of the calibration are to adjust the results given by the apparatus in measuring thermal data of **high purity substances**. It means, melting point temperature in most cases, or any endothermic or exothermic known reaction and the relative enthalpy. It is also important to choose reaction temperatures belonging to the range of temperature of the future studies.

The table below gives a non-exhaustive list of calibration pure materials:

Element	Melting point (°C)	Enthalpy of fusion ($J.g^{-1}$)
Indium	156.6	28.5
Tin	231.9	60.7
Lead	327.5	22.6
Zinc	419.5	113
Aluminium	660.2	396
Silver	960.8	105
Gold	1063.0	62.8

Table 14: Thermal data of pure metals used for DTA calibration

The calibration of a DTA apparatus consists of two steps:

1. The baseline calibration, which has to be performed before each series of experiments.
2. The temperature calibration, which is relative to the experiment purposes. It is carried out once and is stored in the DTA memory.

Baseline calibration:
The calibration involves heating the reference and sample cells through the entire temperature range in which it will be operated.
A baseline calibration applies for a given heating rate and has to be performed each time the rate changes.
The baseline calibration measures the amount by which the heat flow curve deviates from zero so that this deviation can be taken into account during operation.
In practice, **empty sample holders** are used for the baseline calibration.

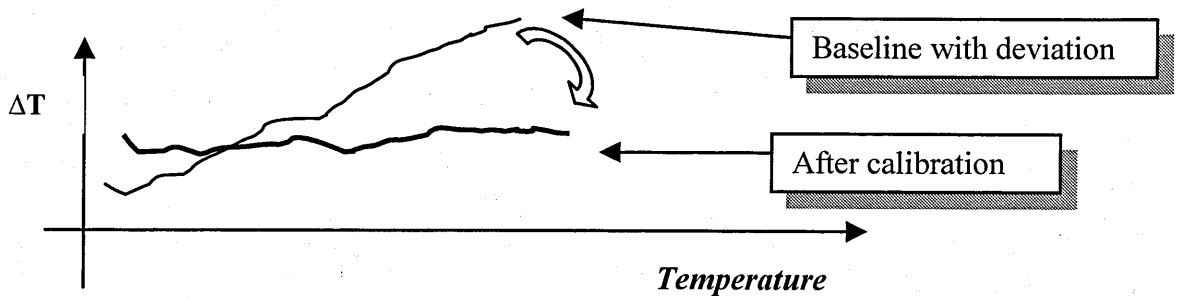

Figure 53: Baseline calibration

Temperature calibration

A known calibration material is heated through its transition temperature.
The extrapolated experimental melting point is gathered and compared to the theoretical value.

5.3.2.2. Experimental calibration

The baseline calibration was performed with empty cells before each series of experiment.
The temperature calibration procedure was carried out in measuring the melting point temperature of pure zinc, aluminium and silver wire pieces. These materials have been chosen because their melting points cover a wide range of temperature, which is compatible with the temperature range of the experimental analysis.

Wire-shape Material	Purity	Melting point (°C)	Enthalpy of fusion ($J.g^{-1}$)
Zinc	99.99%	419.5	113
Aluminium	99.999%	660.2	396
Silver	99.9%	960.8	105

Table 15: materials used for DTA calibration

The melting point of a solid is defined as the temperature at which the liquid and solid phases are in equilibrium. On another hand, the freezing point of a liquid is the same temperature as the melting point of its solid. However, freezing points are rarely measured in practice because they are more difficult to determine. One reason for this is that solidification may not occur at the correct temperature due to the phenomenon of **super cooling**.
Super cooling occurs when a liquid is cooled below its freezing point but does not solidify.

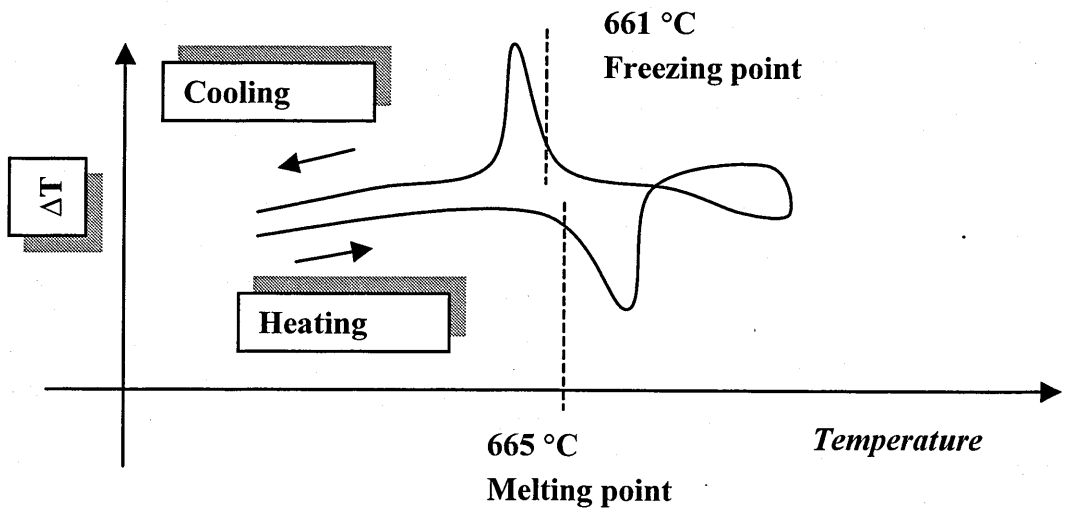

Figure 54: Melting point and freezing point of pure aluminium obtained by DTA

The calibration was therefore carried out with the data collected during the heating step within a temperature range for each pure material beginning usually 100°C below its melting point and finishing at 50°C above it. The other parameters of the calibration are as follows:

Atmosphere	Inert Argon
crucible	Alumina
Heating rate	5°C/min
reference	alumina

Table 16: calibration parameters

The melting point experimental determination was performed three times for each material and the average is gathered in the following table.

Material	**Melting point (°C)**	
	Experimental temperature	**Theoretical temperature**
Zinc	421.08	419.5
Aluminium	661.48	660.2
Silver	970.60	961.78

Table 17: calibration table

The error between the experimental and theoretical data is then used to correlate the results of the other experiments.

5.3.3. As-coated alumina samples analysis

3 and 5-layer coatings were deposited on alumina substrate in order to determine both temperature and energy of formation of the PtAl platinum aluminide.

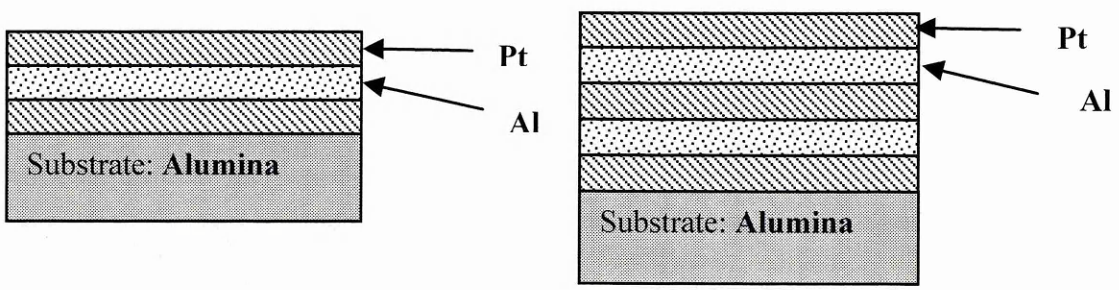

Figure 55: 3 and 5-layer coating systems aimed to the Differential Thermal Analysis

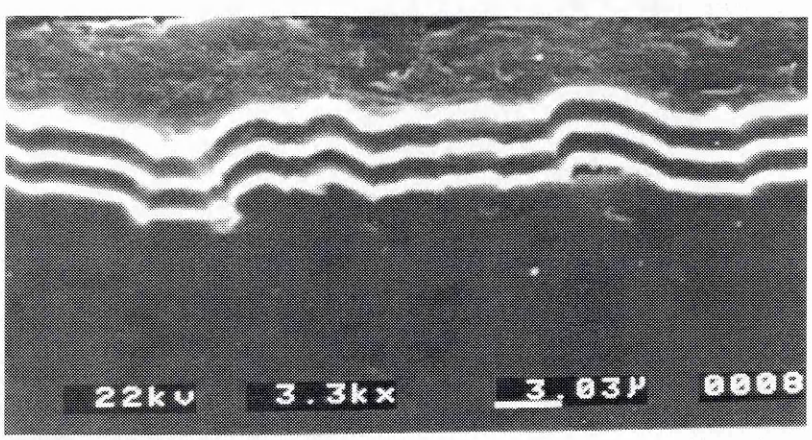

Figure 56: Secondary electron micrograph of an as-deposited 5-layer coating

These coatings had an average Al:Pt thickness ratio of 1.1 (PtAl compound stoichiometry) and their total thickness varied in the range 3-5 microns. Thermal Analysis was then performed using the following parameters:

Sample weight	5 - 60 mg
Heating rate	0.25; 0.5 and 2°C/min
Temperature range	400-1000°C
Isothermal runs	640; 670°C

Usually the analysis were carried out from 400°C, because the reaction was expected to occur at about 700°C

In spite of the different parameters, which were tested, the analysis did not detect any reaction (no peak observed). Even the exothermic reaction observed by Deakin[74] at 700°C was not emphasized.
X-Ray diffraction analysis was then carried out on the samples heated by the DTA:

As-deposited coating	Intermetallic compounds detected after DTA
3-layer	$PtAl$, Pt_5Al_3, $PtAl_2$
5-layer	$PtAl$, Pt_5Al_3, $PtAl_2$

These results show that platinum aluminides have been formed in the coatings. A reaction occurred in the multi-layer coating during the DTA, but the thermal analysis was not sensitive enough to detect it.
The 2 following explanations are relevant:

- The coating /substrate weight ratio is too small. There is indeed only 2.7 wt % of coating relatively to the system (substrate + coating). During the heating step of the DTA, the alumina substrate absorbs the heat released by the exothermic reaction between the coating layers.
- The reaction between aluminium and platinum layers occurs at a lower temperature than expected.

5.3.4. As-coated aluminium foil analysis

The first conclusion, which was drawn in the last section, raises the possibility that the relative thick alumina substrates absorbs the heat of the reaction and distorts the DTA results. In order to test this eventuality, a thin foil of pure aluminium was cleaned and coated both sides with platinum layers (thickness ratio of $PtAl_2$)

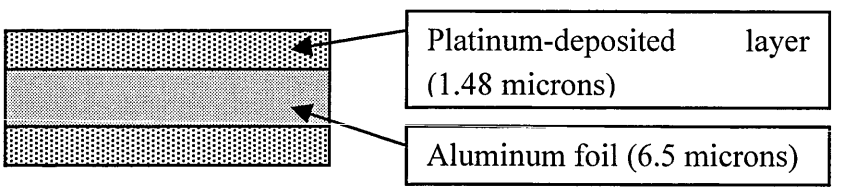

The concept consists of forming a multi-layer coating system with no substrate and the aluminium foil corresponds actually to one of the layer of the coating.

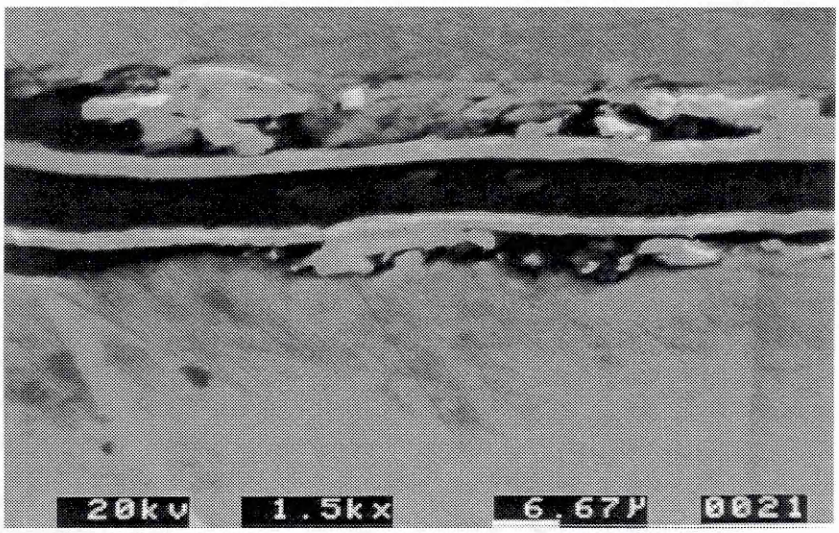

Figure 57: Secondary electron micrograph of an as-deposited 3-layer coating made up of two platinum layer deposited both sides of an aluminium foil

5.3.4.1. The Reaction detection

The as-coated foils, which have been produced, had a thickness ratio corresponding to $PtAl_2$, and were analysed by D*ifferential* T*hermal* A*nalysis* as follows:

DTA runs	**Type of coating**	**Sample Weight (mg)**	**Temperature range (°C)**	**Heating rate (°C/min)**
1	3-layer coating no substrate	7.75	400-1000	5
2	3-layer coating no substrate	8.06	Isothermal run at 675°C (2 hrs)	5
3	3-layer coating no substrate	25.53	400-1000	20
4	**3-layer coating no substrate**	**22.6**	**50-710**	**10**
5	3-layer coating on **alumina**	8	50-710	10

No peaks were detected for the runs 1, 2 and 3, even if the sample weight, the work temperature and the heating rate were varied.

It has however been found in the run 4 that the reaction temperature is lower than expected and stands at approximately 400°C.

Run 5 is carried out with the same conditions as run 4 but with a coating applied on alumina. A peak is observed around 400°C as well but it is very fuzzy and difficult to analyse.
X-Ray diffraction analyses were also performed on the samples after DTA and show the presence of intermetallic compounds such as $PtAl_2$ and Pt_8Al_{21}.

These results highlight eventually **the expected exothermal reaction**; they show that the formation of platinum aluminides is a low temperature onset reaction.

5.3.4.2. Exothermal Reaction study

The next step detailed in this section consisted of study the reaction and its influencing parameters.
The following table gathers the DTA experiments carried out at different heating rates on constant weight samples (as-coated aluminium foil).
All the samples were heated from 50°C to 800°C under argon atmosphere.
In some cases, there are several peak temperatures for one onset temperature. It means that subsequent peaks overlap the peak beginning at the onset temperature.

Heating rate	Weight (mg)	Onset temperature (°C)	Peak temperature (°C)	Integration (°C*min/mg)
20	6.7	442.7	503.3	1.02
10	7.2	424.2	474.2	1.18
			519.7	
5	6.4	413.5	452.8	1.31
			472.5	
			495.7	
0.5	7.9	375.9	393.9	2.58

Table 18: Heating rate influence results

The next figure shows the different DTA curves relative to the tabulated data. It shows as well that the reaction is influenced by the heating rate. **The higher is the rate, the higher the onset temperature of the reaction.**

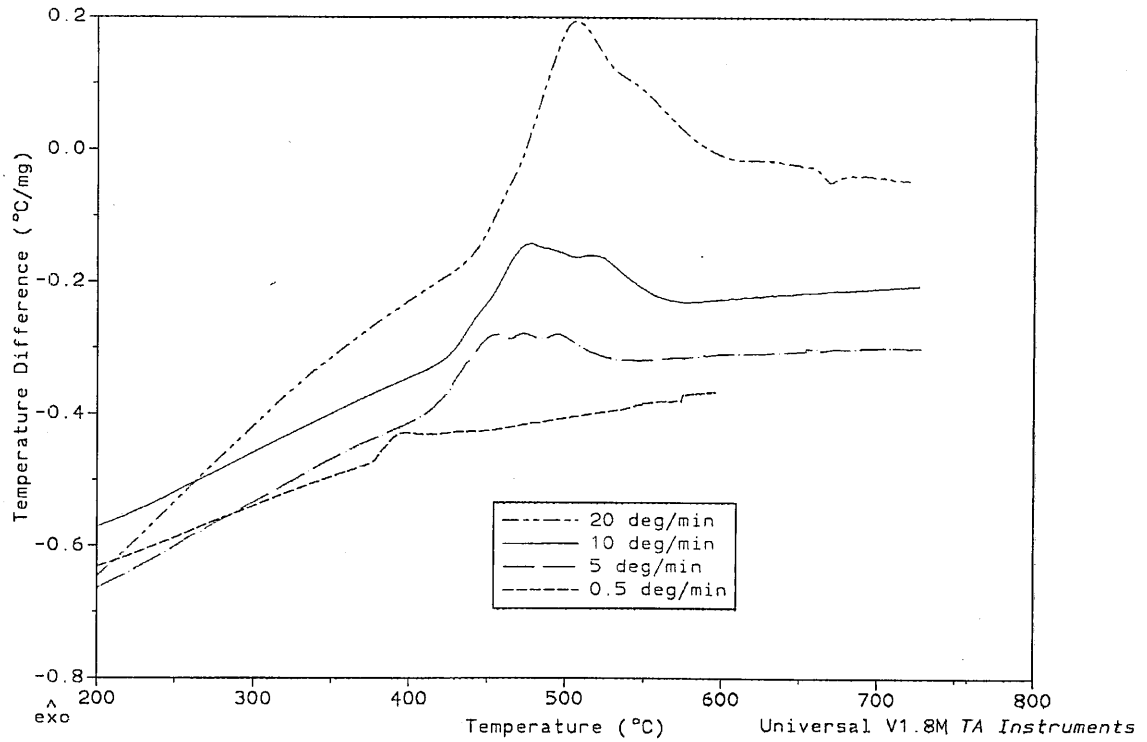

Figure 58: DTA curves of samples heated at different heating rates

X-Ray diffraction analysis was performed on the samples after the DTA and shows the formation of $PtAl_2$, Pt_8Al_{21} and Pt_6Al_{21} intermetallic compounds.

Many other experiments were carried out, but they are not explained in detail because of their relevance:

- The weight of the analysed samples affects the results. Because of its thermal inertia, a heavier coating will need more time and energy to react. However, this variation is slight.
- Isothermal runs at 630, 650 and 670°C were performed and show that the reaction begins faster if the dwell temperature is higher.
- A Differential Scanning Calorimeter head (DSC) was used instead of the DTA one, because it usually gives results with more accuracy and sensitivity. However, the available crucibles were not suitable because they react with aluminium or platinum layers during the heating and distort the results.

5.3.4.3. One-side-coated aluminium foil

6.5 microns thick aluminium foil pieces were coated **on one side** with platinum in order:

- To produce a **bi-layer** coating system with the PtAl thickness ratio (Al:Pt = 1.1) and a **bi-layer** coating system with the $PtAl_2$ thickness ratio (Al:Pt = 2.19).
- To determine the reaction temperature and the enthalpy of formation of the 2 coating systems.
- To correlate the experimental enthalpies with the theoretical ones, because the units of the software used at Cranfield University are not the same than the units referred in the literature.

The coated foils were then heated from 50 to 800°C and analysed using the DTA apparatus. The results are given in the following table:

Samples	**Weight (mg)**	**Onset temperature (°C)**	**Peak temperature (°C)**	**Integration (°C*min/mg)**
2 layers $PtAl_2$	18	486	510	0.84
			663.2	
2 layers PtAl	18	476	506	0.61
			664.7	

Table 19: Thermal analysis results for platinum-coated 6.5- microns thick aluminium foil

As observed in the table and on the following graph, a first peak is detected at a similar temperature to the previous experiments, but a second peak is also discovered close to the melting temperature of aluminium.

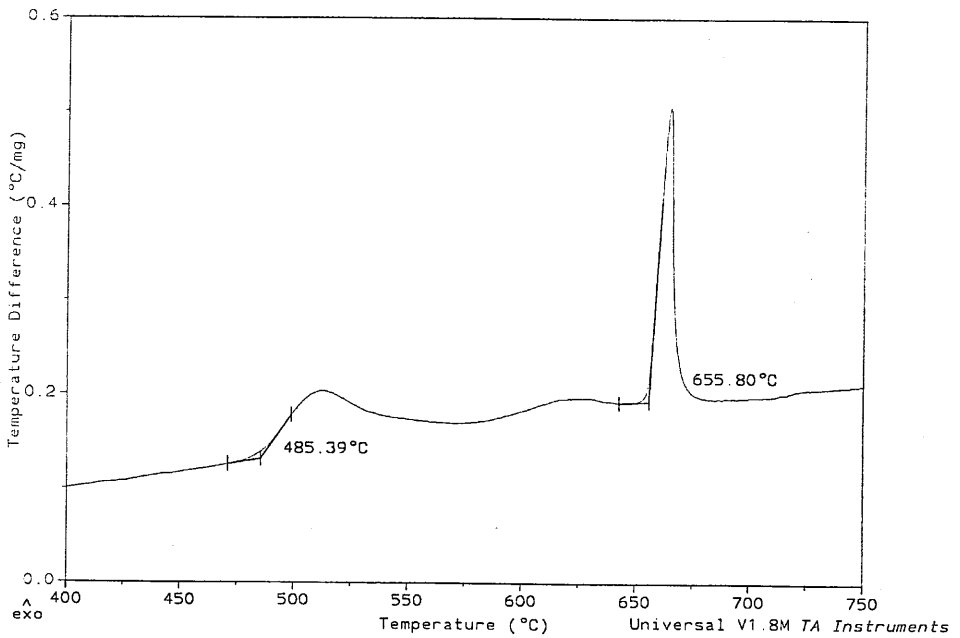

Figure 59: DTA curve of a 2-layer Pt-Al coating

The melting of aluminium at T_m = 660.2°C (which is endothermic) probably triggers the second reaction (which is exothermic). This phenomenon occurs because the thickness of aluminium is too big; the inward diffusion of platinum does not have the time to happen completely before the temperature reaches T_m.

A relation between the integration calculated by the DTA software and the literature data for PtAl and $PtAl_2$ formation enthalpies could not therefore be deduced.

5.3.4.4. Introduction of nickel

A nickel layer was introduced between the aluminium and platinum layer in order to produce a coating more representative of the system low-mass bondcoat + superalloy substrate.
Approximately 40 at % of the coatings consisted of a Nickel layer, which was deposited in 2 different ways as showed in the following table:

Samples	Weight (mg)	Onset temperature (°C)	Peak temperature (°C)	Integration (°C*min/mg)
Pt-Ni-Pt-Al-Pt	18	489.45	517.5	0.6
			650	
			665	
Pt-Ni-Al-Pt	18	552.2	633	0.4

Table 20: Nickel layer introduction

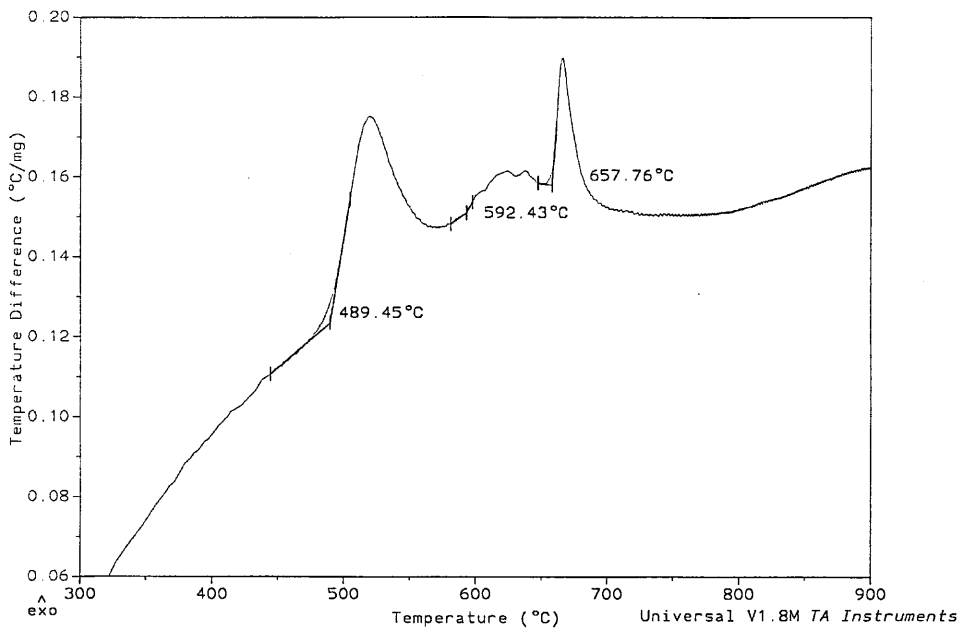

Figure 60: DTA curve of a 5-layer Pt-Ni-Pt-Al-Pt coating

The table and the relative curve for the first coating show that the reaction temperature is higher than for a normal 3-layer Pt-Al-Pt coating.
On other hand, the 3 peaks correspond to the formation of 3 successive compounds, but subsequent X-Ray diffraction did not allow determining them.

5.3.4.5. Use of a thinner aluminium foil

In order to assess the layer thickness influence and to avoid a potential melting of the aluminium during the thermal analysis, other platinum depositions were carried out on thinner aluminium foil (**1.5 microns thick**).
As gathered in the following table, two parameters were varied:

- The number of layers (Pt-Al or Pt-Al-Pt coating systems): a platinum layer was deposited either on one side or both sides of the aluminium foil; however, the total thickness of the coating was kept constant.
- The thickness ratio (Initial stoichiometry of PtAl or $PtAl_2$)

Samples	Weight (mg)	Onset temperature (°C)	Peak temperature (°C)	Integration (°C*min/mg)
2 layers $PtAl_2$	3.3	387.7	414.4	1.54
3 layers $PtAl_2$	3.3	363.3	385.5	1.46
2 layers PtAl	3.3	440	480	0.82
3 layers PtAl	3.3	360	427	0.75

Table 21: Thermal analysis results for platinum-coated 1.5 microns thick aluminium foil

The samples, which were analysed, had the same weight (3.3 mg). They were heated from 20°C to 800°C at a rate of 10°C/min.

The following graph gathers the curves relative to the table and shows the influence of both the number of layer and the initial stoichiometry on the onset temperature of the reaction. As observed, the more aluminium is present in the coating, the lower the onset temperature of the reaction.

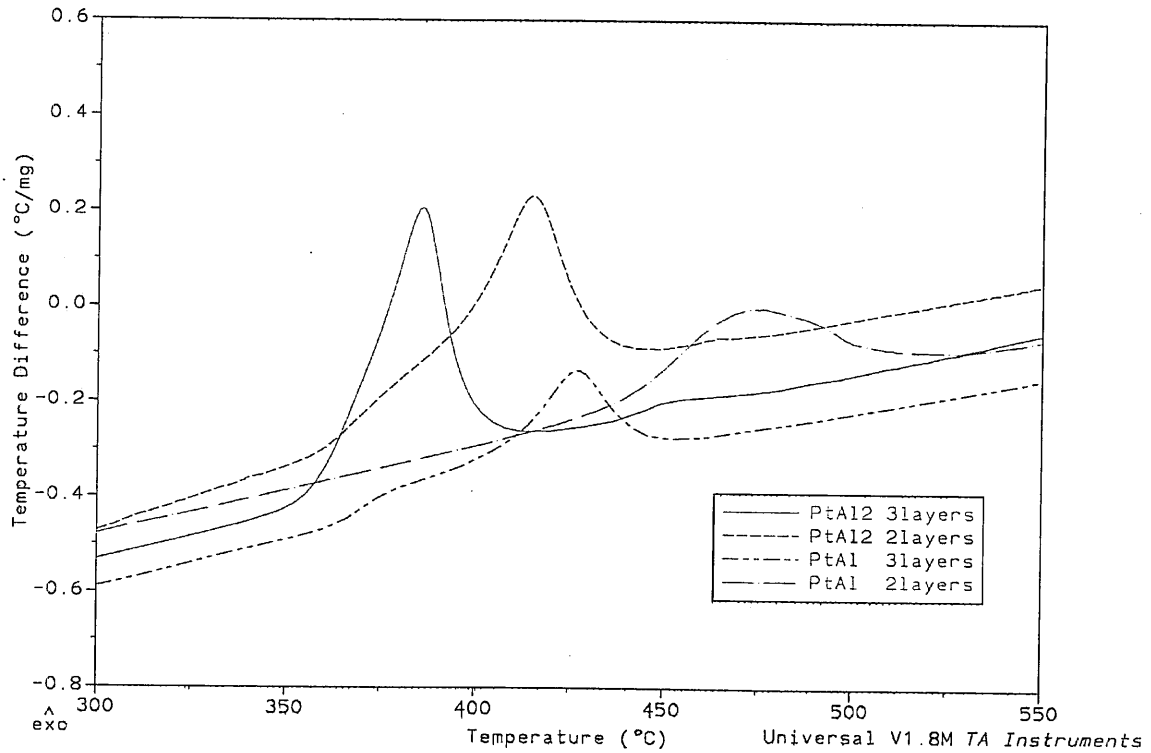

Figure 61: DTA curves of samples with variable number of layers and variable stoichiometry

Compare to the curves observed with the 6.5 microns thick aluminium foil, there is no peak at 660°C, because the foil is thinner and aluminium has the time to diffuse in the platinum layers and to form an intermetallic compound before the temperature reaches its melting point.

Finally, a DTA experiment was carried out with a 300-layer coating deposited on the 1.5 microns thick aluminium foil in order to determine the reaction temperature for a high multi-layered coating system with circa 10nm thick layers. As shown in the following table, the reaction peak was not observed because the exothermic reaction had already occurred during the deposition process.

Samples	Weight (mg)	Onset temperature (°C)	Peak temperature (°C)	Integration (°C*min/mg)
300 layers $PtAl_2$	10	No peaks detected		

Table 22: 300-layer coating Differential Thermal Analysis

5.3.5. Reaction properties

The previous sections have gathered the series of Thermal analysis experiments as well as the observed reactions. The results highlight a low temperature reaction between the platinum and aluminium layers, which is influenced mainly by the heating rate of the DTA, the thickness of the layers and the thickness ratio between aluminium and platinum layers. This section is aimed at detailing the effect of these parameters and at emphasising the thermal properties of the multi-layer platinum aluminides.

5.3.5.1. Influence of heating rate

It has been found that the heating rate affects the onset of the exothermal reaction. It can therefore be related to the diffusion rate at the aluminium-platinum interfaces.
The following graph represents the logarithm of the reaction time in function of the inverse of the onset temperature. The reaction time is the time spent between the experiment start and the onset point of the reaction. The aluminium and platinum layers diffuse in each other until the first intermetallic compound forms.

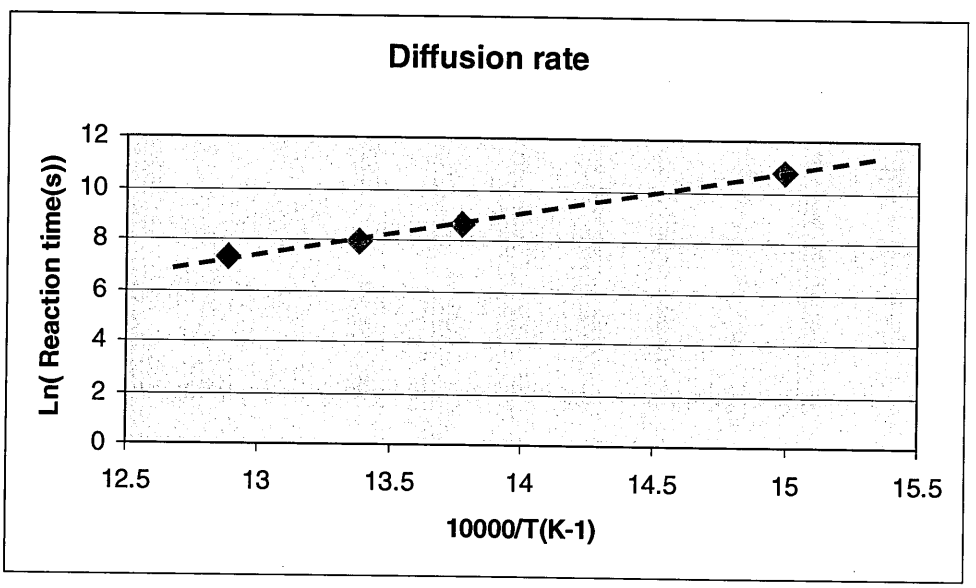

Figure 62: A diffusion law monitored by the DTA heating rate

The graph shows that the reaction onset affected by the DTA heating rate follows a thermodynamic law, which is represented by a straight line. Using this model, it is possible to predict the reaction time and the relative heating rate for a given reaction temperature.

5.3.5.2. Influence of layer thickness

The reaction onset temperatures of the multi-layer produced with 1.5 and 6.5 microns thick aluminium foil are gathered in the following chart.

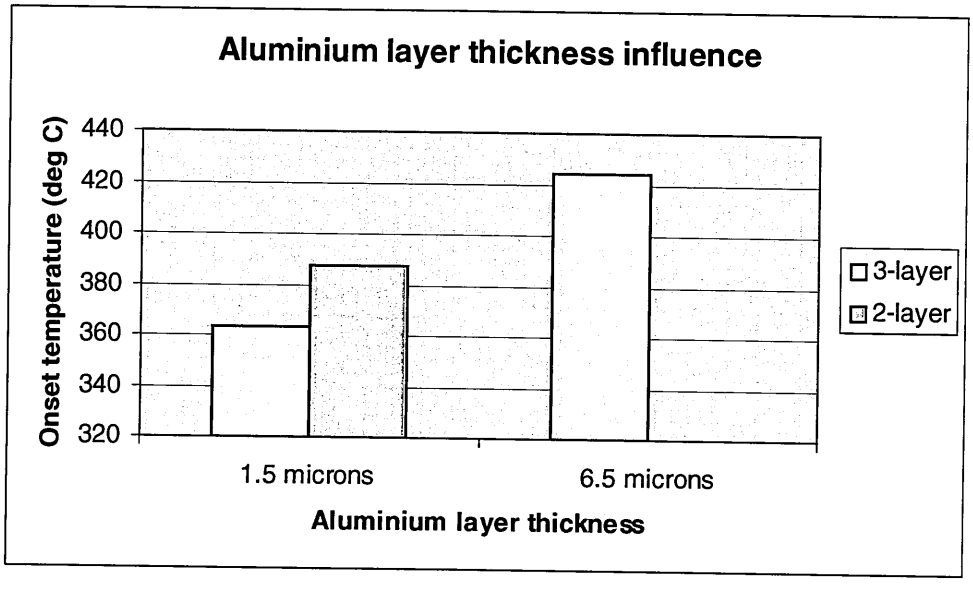

Figure 63: Influence of the layer thickness

In the case of the 3-layer coating (Pt-Al-Pt), a difference of 60°C is observed for the onset temperature between 1.5 and 6.5 microns thick intermediate aluminium layers.
When the aluminium layer is thinner, the reaction occurs at a lower temperature. This has not been proven for the 2-layer coatings.
Furthermore, the peaks observed at 660°C when the 6.5 microns thick foil was used, were not detected in the case of the thinner foil.
The use of a thinner foil avoids therefore any melting reaction of the aluminium.

On other hand, as shown on the Figure 63 and the Figure 64, the onset temperature is also affected by the number of layer: whatever the Al/Pt thickness ratio, the reaction is triggered at a lower temperature if the coating consists of 3 layer instead of 2.

Actually, the 3-layer coatings have 2 Aluminium/platinum layer interfaces, compare to the single interface of the 2-layer coating. This coating structure doubles the surface of contact between the 2 elements and promotes therefore the diffusion as well as the exothermic reaction.

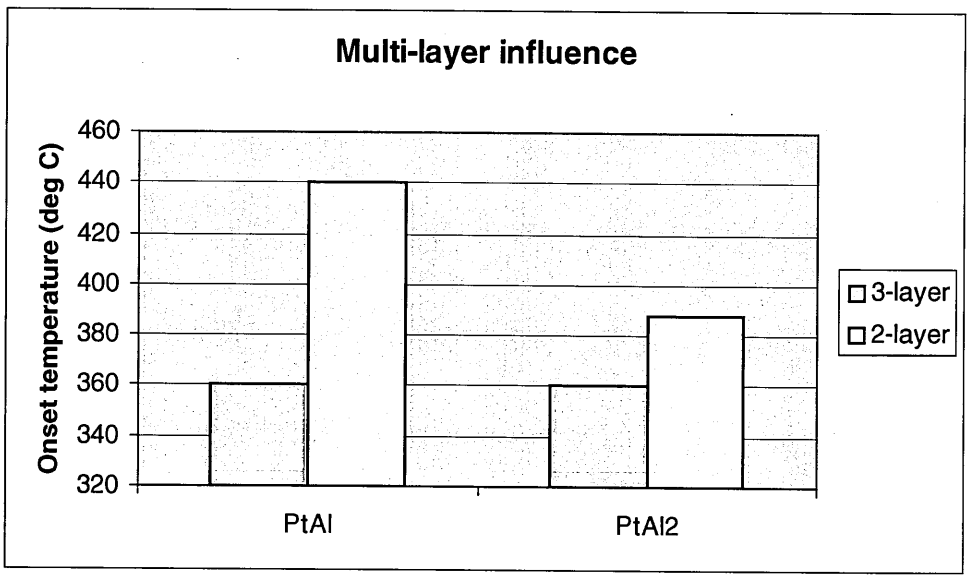

Figure 64: Influence of the number of layer for different coating stoichiometry

The figure 14 gives also a comparison between coatings having different Al/Pt thickness ratios.

In the case of the PtAl coating, the thickness of the platinum layer is virtually twice as big as in the case of the $PtAl_2$ ones. A difference of 60°C is observed between the PtAl and $PtAl_2$ coating for the 2-layer coating systems. However, in the case of the 3-layer coatings, PtAl and $PtAl_2$ form at the same temperature.

It means that the reaction is probably affected by the Al/Pt thickness ratio, but the number of layer (in a constant total thickness coating) plays the most substantial influence.

In the case of the 3-layer coating the system need more layers to decrease the reaction temperature. This has been proven by the 300-layer coating analysis, which shows no reaction over the studied temperature range, because the intermetallic compound was formed during the deposition (which is processed at around 300°C).

6. Low-mass bondcoat experimental development

6.1. Deposition calibration

6.1.1. Deposition rates

Before each multi-layer deposition, a deposition run is carried out to determine the deposition rate of each material to be sputtered.
This deposition is usually longer for platinum because its deposition rate is lower.
The range of deposition rates encountered during the experimental runs is gathered in the following table:

	Aluminium (DC mode)	Platinum (RF mode)
Deposition rate (µm/hr)	**2.0-6.0**	**0.5-1.5**

Table 23: Common deposition rates for aluminium and platinum

6.1.2. Thickness distribution

A deposition was also carried out in order to assess the dispersion of thickness at different locations on the substrate holder.
A strip of nickel (13.3 cm long) was placed on the substrate holder in front of the platinum target and was deposited with a 2 microns thick coating.
Small pieces of adhesive tape were stuck previously at steady intervals and were removed after the deposition. The steps were then measured using a Talisurf apparatus.

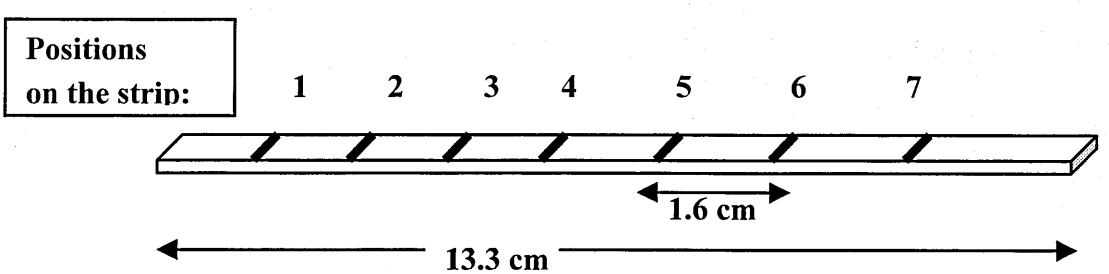

Figure 65: positions of thickness measurement

The position number 4 corresponds to the point facing the middle of the platinum target. Usually, the samples to be deposited are located between the position 2 and the position 6. In this case, the coating thickness varies between 2.4 and 2.8 microns.
The error over this stance stands at **14% and has to be considered before each deposition.**

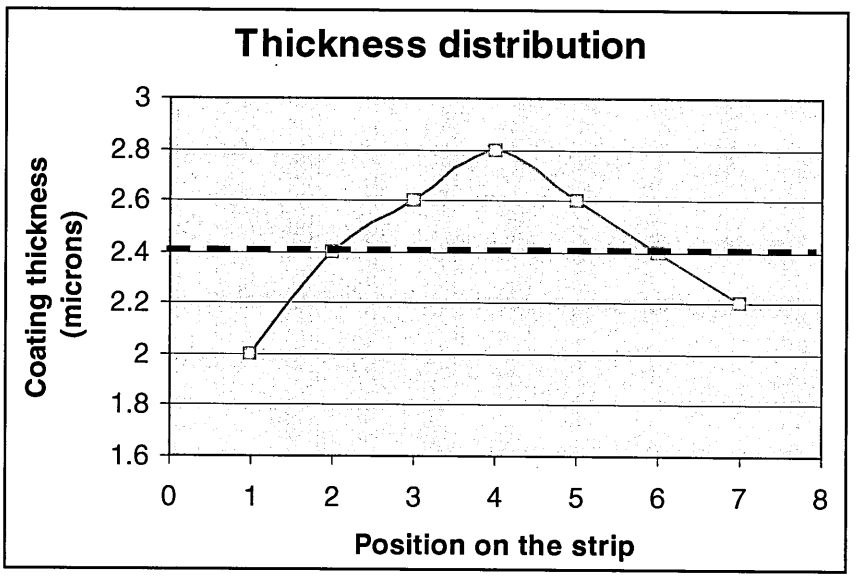

Figure 66: Thickness dispersion along the as-coated strip

6.2. Multi-layered coatings with few layers and the formation of the bondcoat

The 'low multi-layered coatings' correspond to the deposition of 3, 5 and 9 successive layers of platinum and aluminium by the deposition methods detailed in the 'experimental procedure' chapter. Subsequent heat treatment leads to the formation of the low-mass bondcoat.

6.2.1. 3-layer coating system

The first multi-layer coating system to be sputtered consisted of a simple 3-layer Pt-Al-Pt system. The layer in direct contact with the substrate has to be platinum because aluminium can diffuse more easily at high temperature. The layer in contact with the atmosphere has also to be platinum in order to prevent a too fast and uncontrolled oxidation of the aluminium layer.

6.2.1.1. Experimental

These coating systems were applied on alumina and superalloy (AM1) substrates.
The AM1 (Alliage Monocrystallin1) is a nickel-based superalloy developed by SNECMA. Its composition is detailed in the following table (weight %):

	Ni	Co	Cr	Al	Ti	Ta	Mo	W
AM1	base	6.5	7.5	5.3	1.2	8	2	5.5

The **3-layer system** (Pt-Al-Pt) had a total thickness of **9.57 μm.**
Each platinum layer was 1.5 microns thick and the intermediate aluminium layer was 6.57 microns thick.
This thickness ratio corresponds therefore to the stoichiometry of the $PtAl_2$ compound, which requires a platinum to aluminium thickness ratio of 1:2.19.

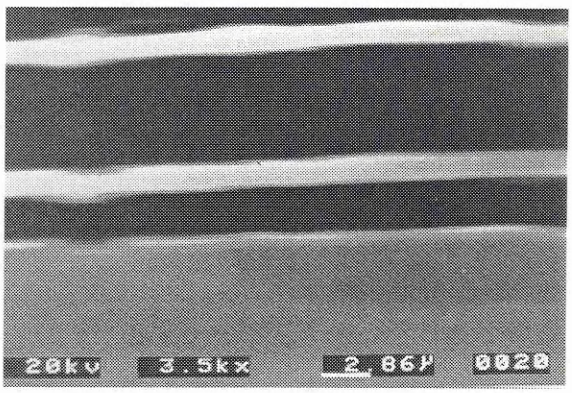

Figure 67:Secondary electron photograph of an as-deposited Pt-Al-Pt coating system

The second step of the low-mass bondcoat process is the formation of an intermetallic compound by reaction between the as-deposited layers. Different heat treatments were therefore carried out to trigger the exothermic reaction. The effects of heat treatment temperature and atmosphere were assessed.

Heat treatment 1: Under Vacuum
Heating rate: 10°C /min
2hrs at 700°C

Heat treatment 2: Under Vacuum
Heating rate: 10°C /min
30 min at 450°C
Heating rate: 10°C /min
2hrs at 700°C

Heat treatment 3: Under Argon atmosphere
2hrs/ 700°C
Heating rate: 10°C /min

Heat treatment 4: Argon atmosphere
2hrs/ 900°C
Heating rate: 10°C /min

The as-deposited and as-reacted coatings were characterised using:

- X-Ray Diffraction analysis on the coating surface
- SEM EDS analysis on the coating surface and cross-sections.

6.2.1.2. Results

After deposition, the coating system seems adherent to the alumina and superalloy substrate, but this adherence is weak in the superalloy case; It is indeed impossible to cut small pieces from the sample without spallation and buckling of the deposited layers.

	Alumina	Superalloy AM1
450°C		No apparent change
700°C	Adherent to the substrate Melting of aluminium Coarse structure of coating Coating decomposes easily	Buckling/ Spallation Melting of aluminium
900°C	Adherent to the substrate Melting of aluminium Coarse structure of coating Coating decomposes easily	Buckling/ Spallation Melting of aluminium

Table 24: Coating observation after heat treatments

After the heat treatment at 450°C, an EDS quantitative analysis was performed on the coating surface, but only platinum was detected. An X-ray diffraction analysis of the coating surface was then carried out but no platinum aluminide compound was present. This means that the reaction did not occur (or slightly at the interfaces between the layers). The previous DTA analysis showed that such a reaction occurs at this temperature for very thin multi-layer coating, but in the case of the 10 µm-thick 3-layer coatings, the layers are too thick and the superalloy substrate must absorb a part of the heat evolved during the heat treatment.

After heat treatment at 700 and 900 °C:

- the coating is not adherent anymore to the **superalloy substrate**, and in few cases the superalloy surface was a little oxidised (superficial traces of cobalt-nickel oxide).
- for the **alumina substrate**, it is more adherent, but the structure of the coating is very brittle and porous (coarse structure).
- a particular and unexpected reaction occurred into the coating (see following photographs) on both substrate (alumina and superalloy). However, this phenomenon is not observed for the very small samples heated by DTA. A reaction involving local attack and the formation of multiple intermetallics was observed.

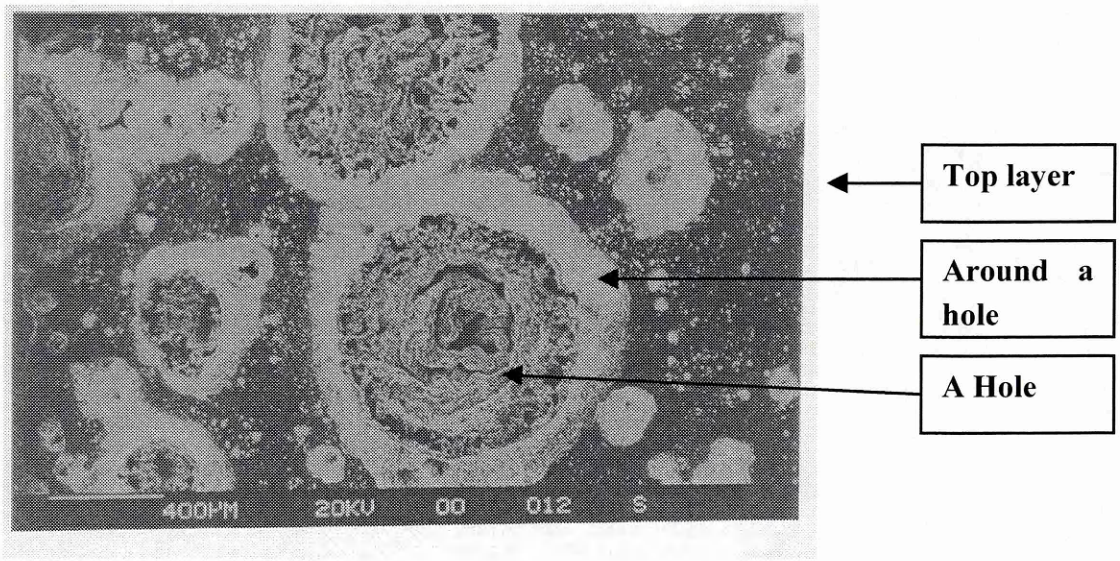

Figure 68: Secondary electron photograph of the coating surface of a 3 layer system after 2 hours at 700 °C

sample	Top layer	Around the holes	Into the holes
Alumina +3 layer 700°C	Pt_2Al	Pt_8Al_{21}	Pt_6Al_{21}
AM1 +3 layers 700°C	Pt/Pt_3Al	$PtAl_2$	PtAl Pt_8Al_{21}

Table 25: Compounds observed by X-ray Diffraction and EDS quantitative analysis

The top layer of the coating after heating is always very rich in platinum. The top layer is also made up of numerous holes. The border of the holes consists of an intermetallic compound with a higher content of aluminium.
Furthermore, the intermetallic compounds into the holes are very rich in aluminium.

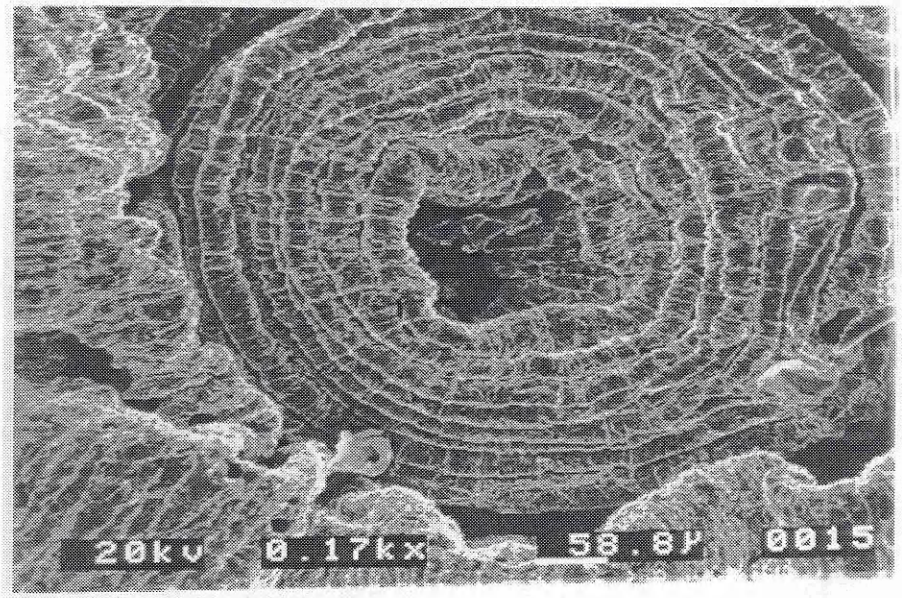

Figure 69: Secondary electron photograph of a specific hole

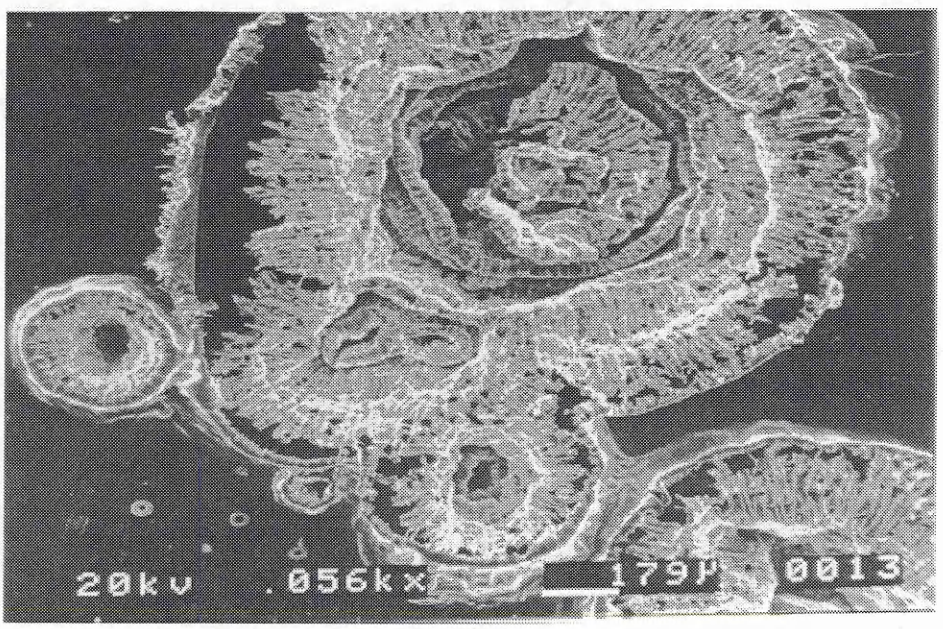

Figure 70: Secondary electron photograph of another batch of holes

6.2.1.3. conclusion for the 3-layer coating systems

When the samples are heated, an exothermic reaction occurs at the interface between platinum and aluminium. The aluminium layer is thick and has not the time to react entirely with the platinum (the aluminium has not the time to interdiffuse with the platinum and to form an intermetallic compound with a higher melting point than the aluminium). It is the reason why it melts.

At some locations, the melting aluminium reacts with the total available top platinum layer, to form circular holes; aluminium reacts on the circular border to form intermetallic compounds, higher in aluminium content.

6.2.2. 5-layer coatings

6.2.2.1. Experimental

In order to overcome the melting problem encountered with the 3-layer coating, a second type of multi-layer coating was introduced: it consists of a **5-layer system** (Pt-Al-Pt-Al-Pt) with the same total thickness than the 3-layer system (9.57 μm), but with the Pt_2Al_3 stoichiometry.

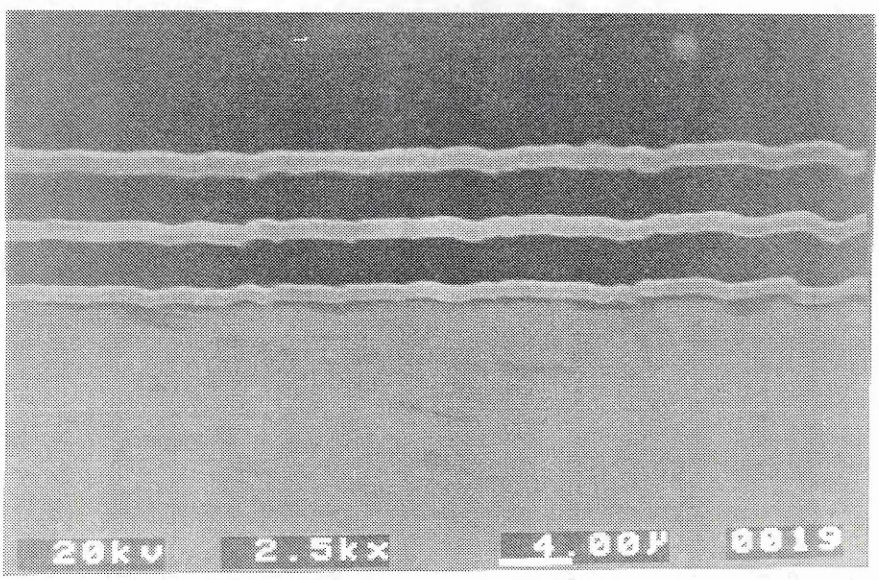

Fig. 2: Secondary electron photograph of an as-deposited 5-layer coating system (on superalloy susbtrate)

The coatings were applied on alumina and superalloy substrates and subsequent heat treatments were then carried out to trigger the exothermic reaction:

Heat treatment 1: Under Argon
Heating rate: 10°C /min
2hrs at 700°C

Heat treatment 2: Under Argon
Heating rate: 10°C /min
2hrs at 900°C

After heat treatment at 700 and 900°C, the coatings were adherent to the **alumina substrate.** However a lack of adherence to the **superalloy substrates** was obvious.

	Alumina	Superalloy AM1
700°C	Adherent Spallation between intermetallic layers	Buckling/ Spallation Surface Rumpling
900°C	Adherent Spallation between intermetallic layers	Buckling/ Spallation Surface Rumpling

Table 26: Observations of the 5-layer systems after heat treatment.

During the heat treatment the first layer of platinum loses contact with the substrate because of a weak interface generated by the sputtering deposition process. Spallation is also induced by the stresses developed in the layer because of a difference in expansion during the heat treatment.
In order to fix this fundamental problem, **a negative bias** was then applied to the substrate during the deposition of the first layer of platinum. This bias increases the ion bombardment on the substrate, which leads to sputter cleaning of any surface contaminants from the substrates, a higher mobility of the sputtered atoms and a better growth of the early deposited film.

Using this technique, another 5-layer coating systems were deposited (10 microns thick /$PtAl_2$ stoichiometry)
The following heat treatments were then carried out:

Heat treatment 3: Under Argon
Heating rate: 10°C /min
2hrs at 700°C

Heat treatment 4: Under Argon
Heating rate: 10°C /min
2hrs at 900°C

6.2.2.2. As-reacted coatings

As observed in the Figure 71, the colour of the coating surface change during the heat treatment. In the case of the samples heated at 700°C, the colour becomes yellow. After a further heat treatment at 900°C for 2 hours the colour becomes red-blue. This colour corresponds to the formation of a very thin oxide, which grew because of the very low amount of oxygen present in the argon atmosphere during heat treatment. This interference coloured oxide highlights moreover the formation of an intermetallic platinum aluminide with the colour characteristic of the type of platinum aluminide intermetallic that is formed.

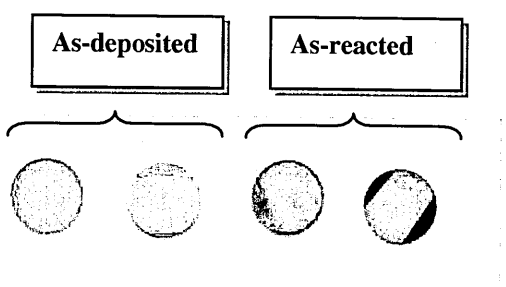

Figure 71: As-deposited and as-reacted coatings (at 700°C)

A DIGIPOINT quantitative analysis of an as-reacted 5-layer coating cross-section (Figure 72) was performed with 10 points of analysis from the outer part of the coating until several microns into the substrate.

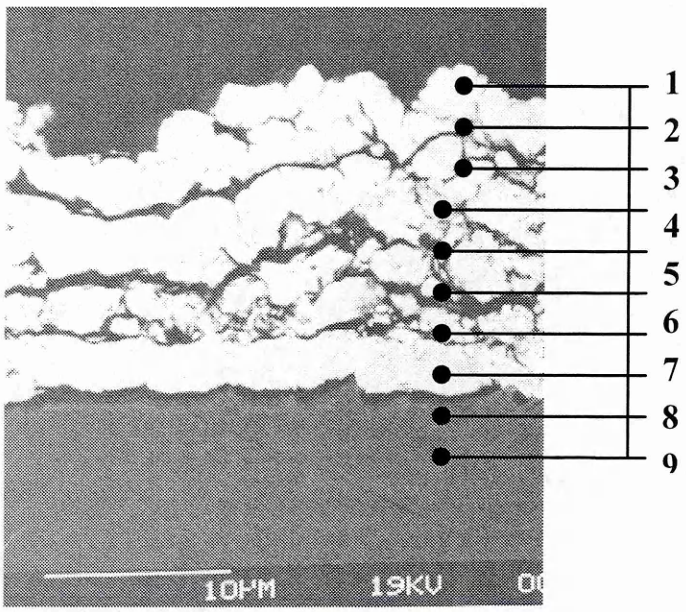

Figure 72: Backscattered photograph of a 5-layer coating system after 2 hrs at 700°C

Observations of the Figure 72 show firstly relevant changes in the structure of the initial multi-layer coating :

- The initial 5-layer coating structure results in a 3-layer coating. The two layer of aluminium seems to have completely diffused in the platinum layers.
- The remaining layers are separated by weak interfaces and cracking spallation occurs. This is evident either by bakelite embedding or relief polishing.
- The adhesive tape test induces spallation of the coating between the remaining layers, but never at the substrate /coating interface. X-Ray diffraction analysis of the interface observable after spallation shows the presence of aluminium rich platinum aluminides, such as Pt_8Al_{21} or Pt_6Al_{21}.

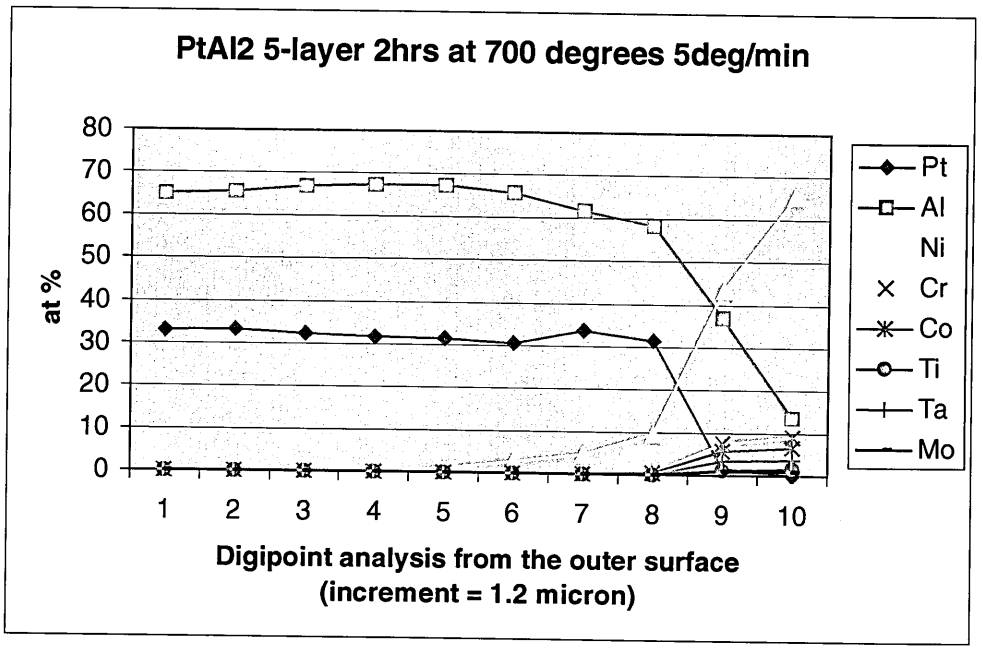

Figure 73: Digipoint analysis relative to the Figure 72 points

The concentration of platinum and aluminium are steady through the coating and the expected stoichiometry is respected.

Virtually no interaction with the substrate occurred during the heat treatment. Even if a slight outward diffusion of nickel is observable in the lower part of the as-reacted coating, the interdiffusion zone is very thin.

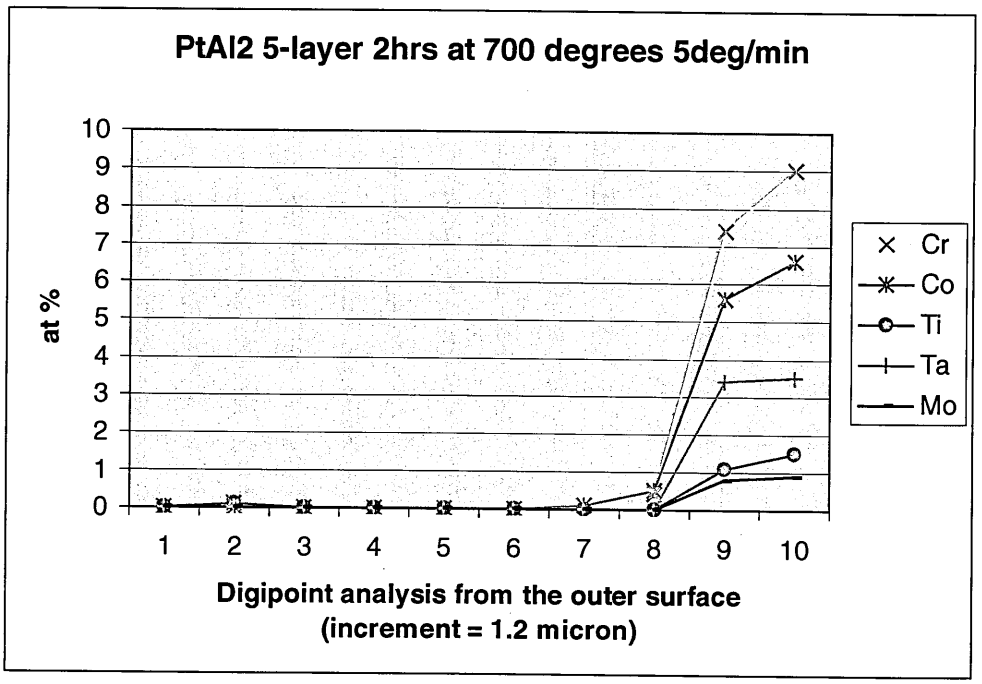

Figure 74: Focus on the diffusion of substrate elements

Figure 74 shows clearly that the diffusion of substrate elements did not occur during the heat treatment. This highlights the efficiency of the process to produce platinum aluminide overlays with a controlled stoichiometry.

6.2.2.3. Influence of a post-treatment

The heat treatment at 900°C was performed on samples already heat treated at 700°C. It was aimed to modify the structure of the coating and to form a single-layer and more homogeneous bondcoat.

As depicted in the Figure 75, the post-treatment resulted in a slight depletion in aluminium: The final stoichiometry corresponds to the Pt_2Al_3 compound whereas $PtAl_2$ was the dominant phase after the treatment at 700°C.

The structure of the coating is still however lamellar, with brittle interfaces. The adhesive test tape shows though that the bond is stronger than for the samples only heat treated at 700°C.

Another important observation is the formation of a relatively deep interdiffusion zone, which seems to be divided in two parts.

The deeper one seems to be made up of intermetallic precipitates, but the outer one seems to be single-phased and could correspond to the (Ni, Pt)Al compound.

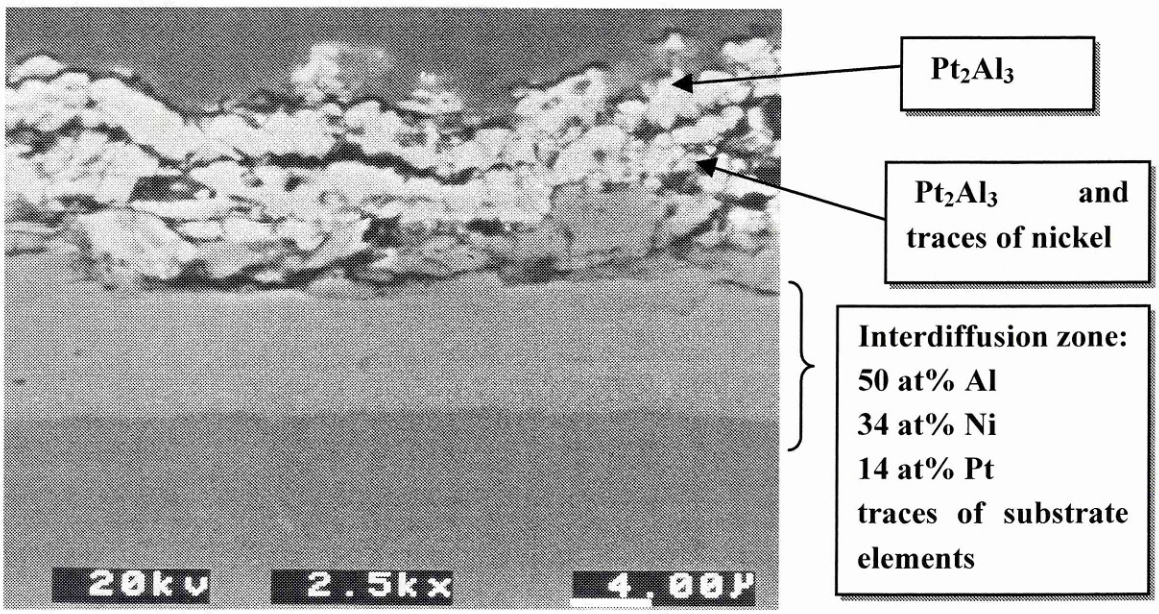

Figure 75: Secondary electron photograph of a 5-layer coating system after 2hrs at 700°C and 2hrs at 900°C

6.2.2.4. Influence of the heating rate

Other heat treatments at 700°C were carried out with as-deposited 5-layer coatings using various heating rates. Thus, the effect of heating rates in the range 5-20°C/min was assessed but no relevant changes in the stoichiometry or in the coating structure were observed.

6.2.2.5. Influence of the substrate thickness

Heat treatments at 700°C were also performed on coatings applied on substrates, which have various thicknesses. Thicknesses in the range 0.25-1mm were tested but no relevant changes were noticed. This set of experiments were undertaken to determine if there was a significant role of the substrate heat capacity in determining the likelihood of reaction.

6.2.2.6. Conclusion for the 5-layer coating system

In increasing the number of layer for a given coating thickness, the expected exothermic reaction was improved and lead to the formation of a platinum aluminide overlay.
Compare to the 3-layer coating system, the 5-layer coating system did not have any problem of melting with the aluminium layers, because for the same total thickness, the aluminium layers are thinner. The complete interdiffusion with platinum can occur before the melting temperature of the aluminium is reached.

The deposition and formation process leads also to a clean coating. The final coating is free of substrate elements and the composition in aluminium and platinum is steady (no gradient).
The structure is however lamellar with brittle interfaces, even after a subsequent heat treatment. A post treatment does improve the bond between the layers, however.

6.2.3. 9-layer coatings

The 9-layer coating system was developed to further improve the bondcoat structure.

6.2.3.1. experimental

The 9-layer coating system was deposited on superalloy AM1 substrates. The total thickness was 10 microns, namely the same as for the 3 and 5-layer coating systems.

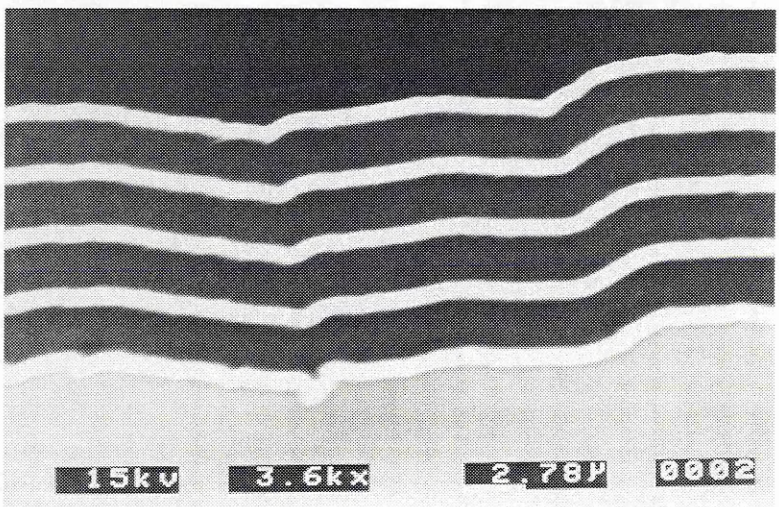

Figure 76: Secondary electron micrograph of an as-deposited 9-layer coating ($PtAl_2$ stoichiometry)

Various thickness ratios were experimented in order to form 3 different platinum aluminide compounds:

- $PtAl_2$
- PtAl
- Pt_8Al_{21}

Each different coating system was applied on superalloy substrates with various thicknesses. After deposition, the coatings were adherent to the substrates and the following heat treatments were performed:

Heat treatment 1: Under Argon
Heating rate: 10°C /min
2hrs at 700°C

Heat treatment 2: Under Argon
Heating rate: 10°C /min
2hrs at 900°C

Heat treatment 3: Under Air
Heating rate: 10°C /min
2hrs at 1100°C
The aim of this last heat treatment was to test the **oxidation resistance** of the as-reacted coating and to analyse the obtained structure.

6.2.3.2. As-reacted $PtAl_2$ coatings:

After 2 hours at 700°C, the initial metallic grey colour of the coating surface becomes yellow/gold.
The Figure 77 depicts a cross-section of the coating system after heat treatment and shows that the coating structure is still lamellar. As for the 5-layer coating system, aluminium diffused in the platinum layers and the initial 9-layer coating consists finally of 5 platinum aluminide layers.
The "scotch tape" strip test was performed on the samples and shows a good adherence of the coatings, but in a few cases some loss of coating occurs with failure between the layers. Even if the structure is not homogeneous, the "scotch tape" strip test emphasises a better bonding between the remaining layers than for the 5-layer coating system.

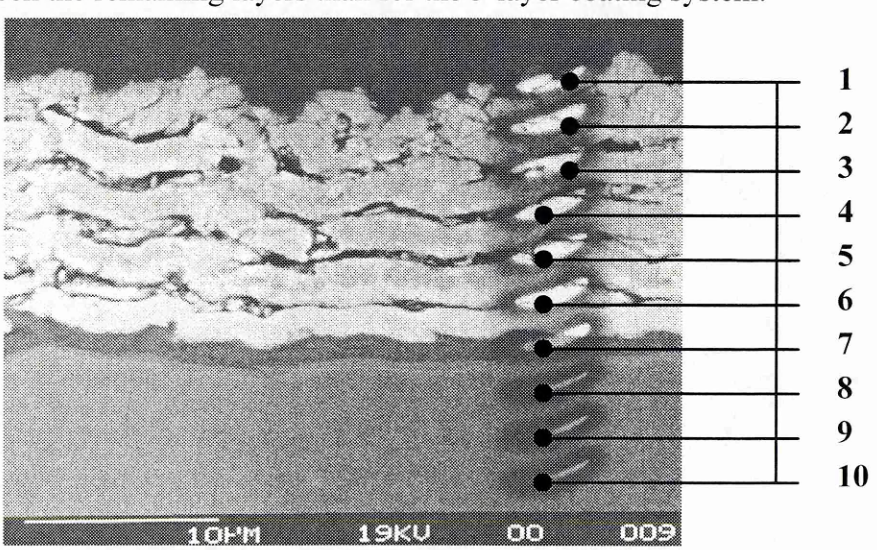

Figure 77: Backscattered micrograph of an as-reacted 9-layer $PtAl_2$ coating after 2hrs at 700°C

The DIGIPOINT graph (Figure 78) highlights a steady concentration of aluminium and platinum through the as-reacted coating and the interdiffusion zone is relatively thin.
The analysis of the point 6 shows a higher level in aluminium, which can correspond to the composition of an interface between two layers.

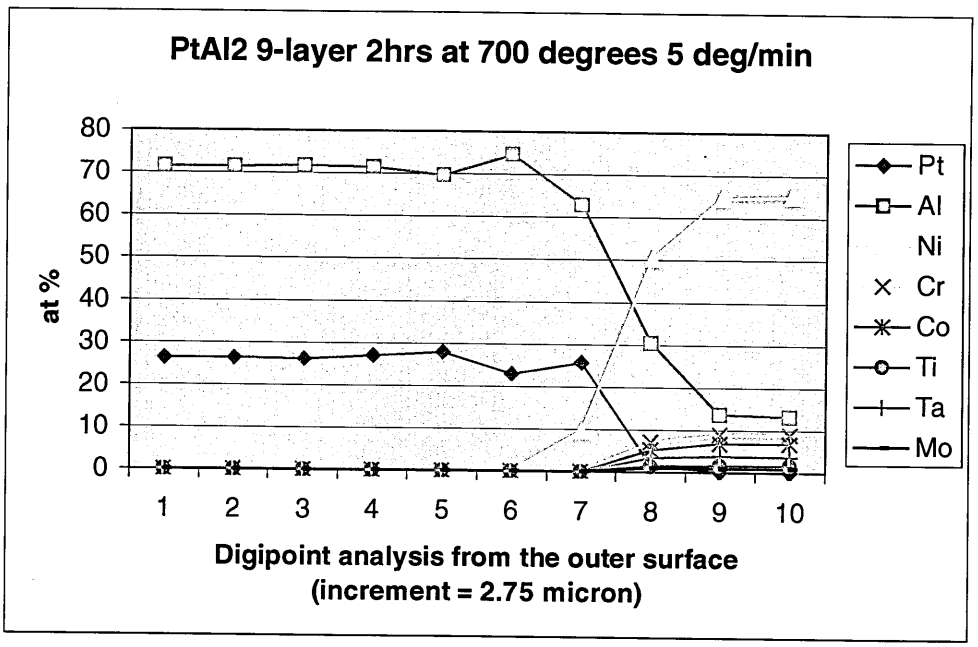

Figure 78: Digipoint analysis relative to the positions marked on Figure 77

The DIGIPOINT graph has to be analysed carefully: the concentrations plotted for each element do not correspond necessarily to a relative compound stoichiometry. If the diffusion and the reaction between the platinum and aluminium layers did not occur completely, or if several different phases have formed at the same time, the correlation between the DIGIPOINT concentrations and a compound stoichiometry is distorted.
This is the reason why an X-Ray diffraction analysis must be carried out in parallel with the quantitative analysis, to identify the compound that is formed.

X-Ray diffraction analysis of the $PtAl_2$ coating heated at 700°C for 2 hours shows the predominant presence of $PtAl_2$ with traces of Pt_8Al_{21}, which is consistent with the Digipoint analysis because the aluminium concentration stands between 60 and 70 at% and the platinum concentration between 30 and 40 at%.

The next figure gives the concentration of the substrate elements apart from nickel. The superalloy substrate/ coating interface lies between the points 7 and 8.

The diffusion of these elements from the substrate into the coating seems to be prevented during the coating process and the reaction heat treatment, or a very small amount could be present but not detectable by the SEM/ EDS apparatus.

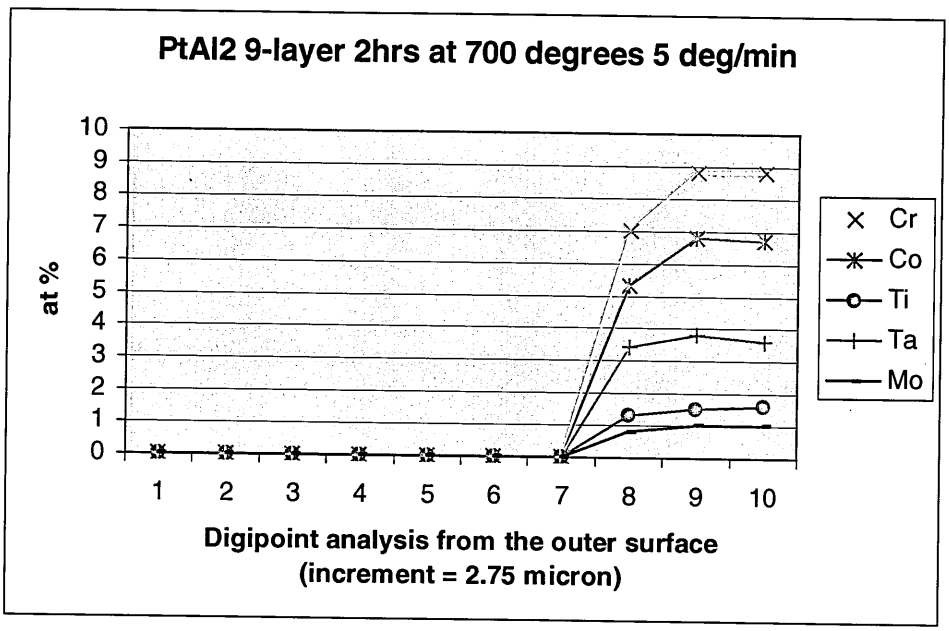

Figure 79: Digipoint Analysis relative to the Figure 77, but focus on the substrate element diffusion

6.2.3.3. As-reacted PtAl coating

A 9-layer coating system with a thickness ratio of 1.5 was deposited in order to form a bondcoat richer in platinum. This corresponds to a stoichiometry that lies between the Pt_2Al_3 and PtAl phases. After 2 hours at 700°C, the coating structure is still multi-layered but seems more compact than the 9-layer $PtAl_2$ system after a similar heat treatment.

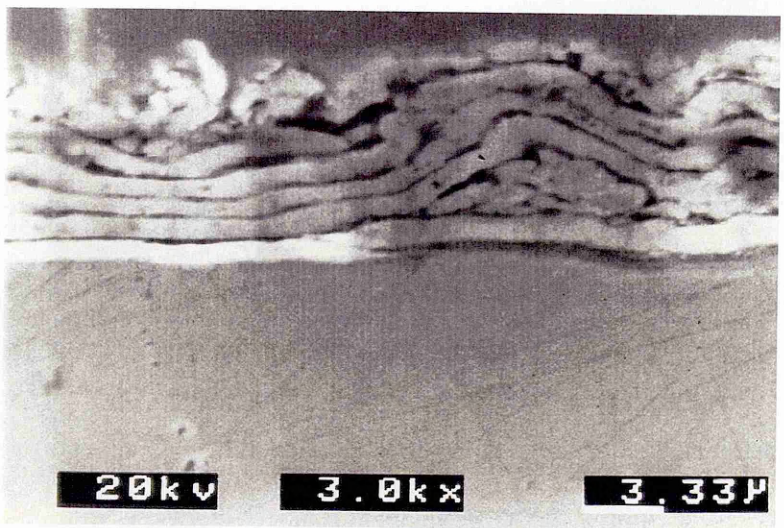

Figure 80: Secondary electron micrograph of a 9-layer PtAl coating system after 2 hours at 700°C

The "scotch tape" strip test was performed on all the heat treated samples and emphasises the good adherence with the substrate and a better bonding between the remaining layers than observed for the 9-layer $PtAl_2$ coatings.

X-Ray diffraction analysis of the notional PtAl coating heated for 2 hours at 700°C shows the predominant presence of Pt_2Al_3 and $PtAl_2$ compounds.

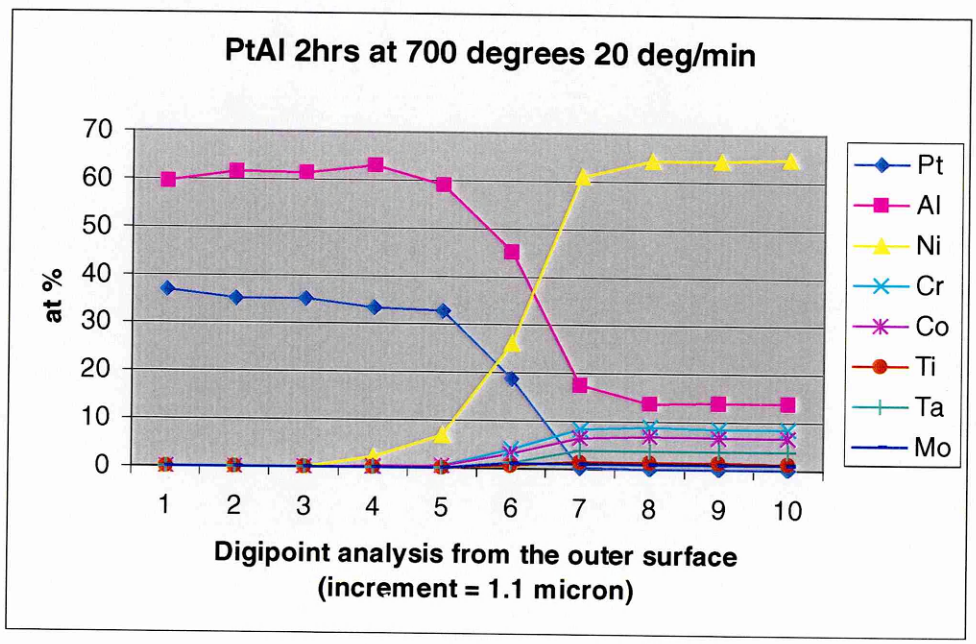

Figure 81: Digipoint analysis of a 9-layer, initially PtAl coating

Digipoint analysis was also carried out and shows a steady concentration profiles for aluminium and platinum (Figure 81). These concentrations are consistent with the X-Ray diffraction results, but shows that the concentration in aluminium is slightly higher than expected.

A thin interdiffusion zone is observable in the Figure 80. It is surprisingly platinum free and seems to be a solid solution of **NiAl** (See following table), assuming that cobalt substitutes for nickel and molybdenum and tantalum substitutes for aluminium. Chromium is assumed to substitute onto both sublattices:

Al	Ni	Pt	Cr	Co	Ta	Mo
36.2	43.8	Nil	8.6	5.9	4.3	1

Concentration in at%

The following figure show the concentration profiles of the substrate elements apart from nickel. As for the other multi-layer coating system, the interaction with the substrate was prevented during the deposition and formation process.

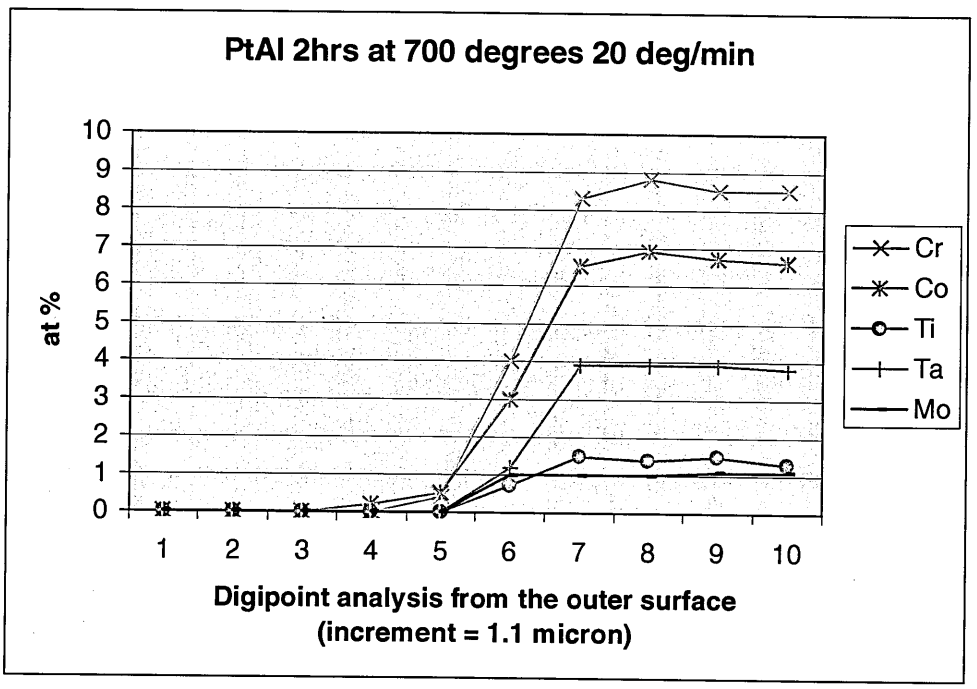

Figure 82: Digipoint Analysis of a 9-layer, initially PtAl coating with focus on the substrate elements diffusion

6.2.3.4. As-reacted Pt_8Al_{21} coating

A third 9-layer coating system was produced with more aluminium than the two previous ones (thickness ratio: 2,9). The initial thickness ratio corresponds to the Pt_8Al_{21} stoichiometry.
The idea of having a higher Al/Pt thickness ratio is to accelerate the diffusion and reaction between the layers, because aluminium diffuses faster than platinum. A change in the coating structure could be therefore expected.
However, after 2 hours at 700 degrees C, **buckling**, **rumpling** and **spallation** phenomena was observed and led to the conclusion that **adding too much aluminium in the coating does not enhance its structure or its adherence.**

On the other hand, these results have to be interpreted carefully because since the thickness of each aluminium layer was increased, a melting phenomenon (similar to the phenomenon observed for the previous 3-layer coatings) could have occurred. Therefore, in order to assess the real benefits of the Pt_8Al_{21} coatings, the number of layer has to be increased to lower the individual aluminium layer thicknesses.

6.2.3.5. Effect of a post-treatment at 900°C

A second heat treatment was performed for some samples, after the samples had been already heat treated at 700°C. 9-layer PtAl and $PtAl_2$ coating systems were thus heated at 900°C for a further 2 hours in order to homogenise their lamellar structures.

After the post treatment at 900°C, only Pt_2Al_3 is detected by X-Ray diffraction on the PtAl sample. A slight depletion in aluminium has thus occurred, since after 2 hours at 700°C, the phase structure consisted of both $PtAl_2$ and Pt_2Al_3.

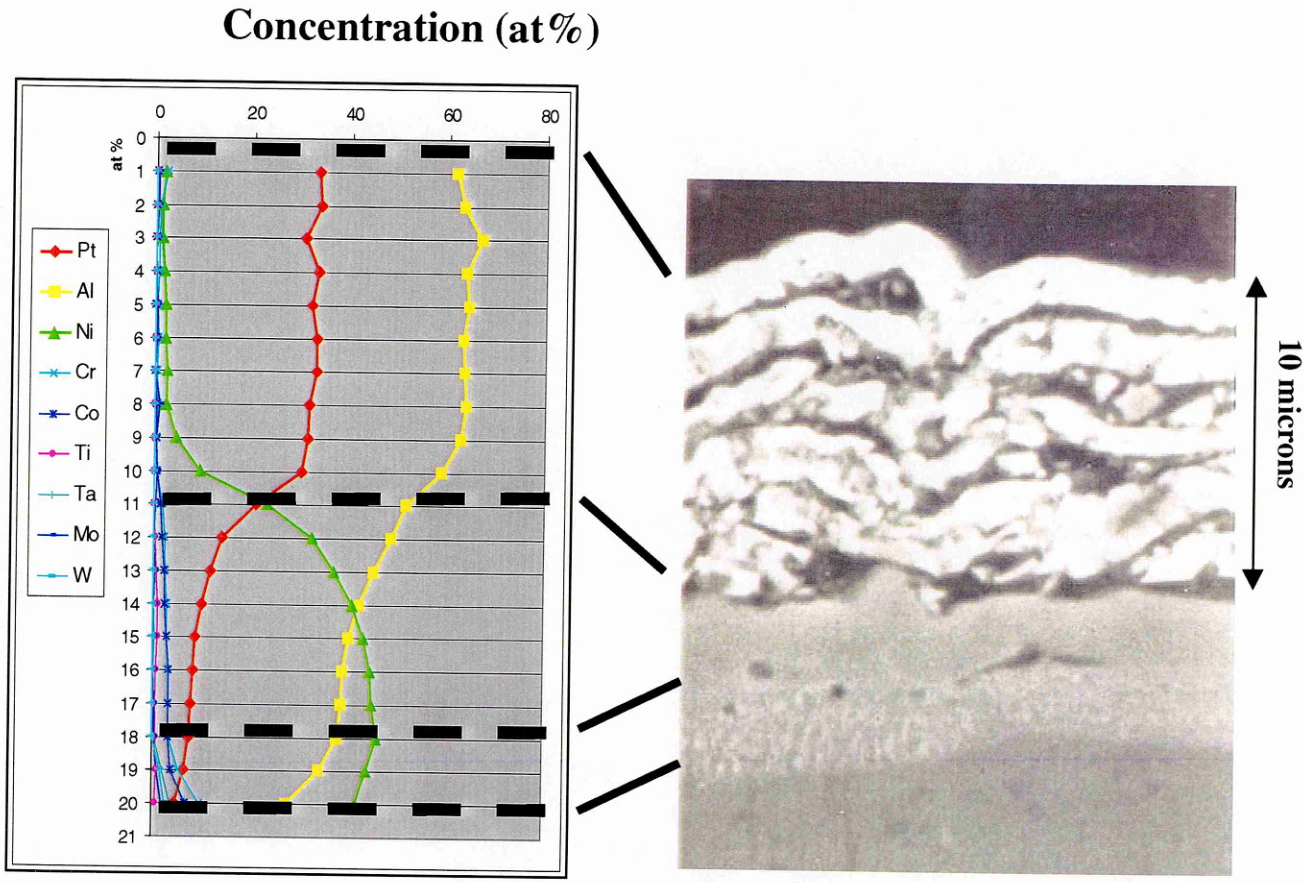

Figure 83: Digipoint analysis of a 9-layer PtAl coating after 2 hrs at 700°C and 2 hrs at 900°C

Digipoint analysis was also performed on a coating cross-section and results in the graphs of Figure 83 and of

Figure ***84***.

The concentration of aluminium and platinum are quite steady through the coatings and correspond to the composition of the Pt2Al3 intermetallic compound detected by X-ray diffraction analysis.

Just underneath the coating, a 2-layer interdiffusion zone is present. The outer zone consists of 3 microns thick **β(Ni,Pt) Al** phase, which acts as a diffusion barrier for the substrate species, except from chromium and cobalt.

A second interdiffusion zone is observed, which is a matrix of β **(Ni,Pt) Al with precipitates containing Cr, Co, W, Ta, Mo; these precipitates are believed to be Laves or σ-phases.**

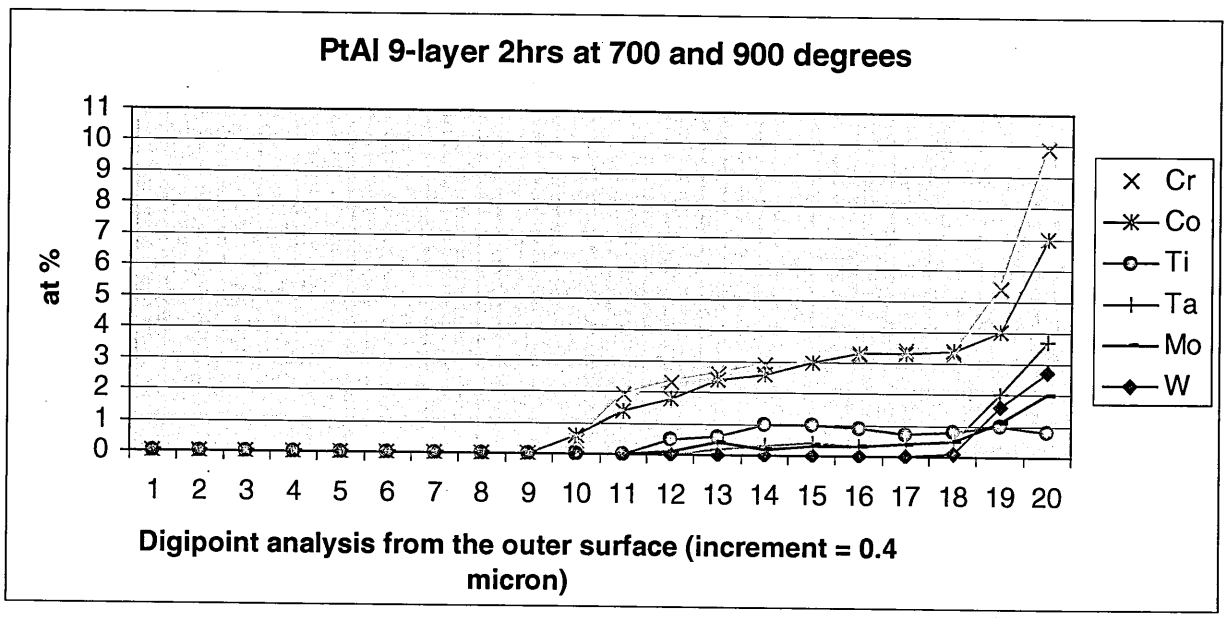

Figure 84: Digipoint Analysis of a 9-layer PtAl coating, after a duplex heat treatment, with focus on the diffusion of substrate elements

These inner 2 zones, which account for the interactions between the substrate and the coating, are similar to the layer structure of the platinum aluminide coatings obtained by aluminizing.

The zone rich in precipitates has appeared during the post-treatment, because it was not observed in the concentration profile of the samples after 2 hours at 700 degrees. It is probably triggered by the inward diffusion of aluminium.

Figure 84 shows however that the substrate elements did not diffuse outwardly in the coating and emphasises the 'diffusion barrier' behaviour of the platinum aluminide overlay.

The following figure shows the 9-layer $PtAl_2$ coating sytem after the 2 heat treatments. As for the PtAl system, the structure is still lamellar and seems brittle.

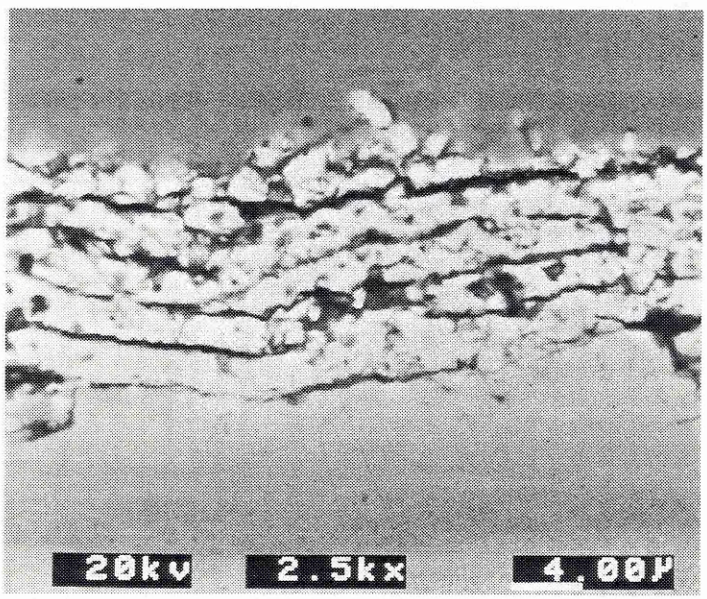

Figure 85: Secondary electron micrograph of a $PtAl_2$ coating after 2 hrs at 700°C and 2hrs at 900°C

Before the post-treatment, the coating consisted of **$PtAl_2$** and Pt_8Al_{21}
After the post-treatment, the coating has **a lower content** of aluminium and **the prevailing phase is Pt_2Al_3.**
Aluminium has obviously diffused inwardly in the interdiffusion zone, which is very rich in aluminium.
The following table gathers the proportion of elements in the interdiffusion zone, which corresponds virtually to the intermetallic compound **(Ni, Pt)Al** (Pt is on the same sublattice as Ni).

Al	Ni	Pt	Cr	Co	Ta	Mo	Ti
45.2	26.1	18.6	4	3	1.1	1	0.7

Concentration in at%

A second interdiffusion is also observable and similar to the one discussed for the PtAl coatings.

Aluminium seems to be the only species to diffuse and the coating is substrate element free after the post-treatment.

6.2.3.6. Heating rate effect

Heat treatments at 700°C were carried out using 2 different heating rates: 20°C/min and 5°C/min. However, no relevant structure and composition changes were noticed, with change in the heating rate.

6.2.3.7. Isothermal Oxidation at 1100°C

Some 9-layer PtAl samples already heat treated at 700°C for 2 hours were oxidised isothermally at 1100°C in Air.

As observed in Figure 86, a substantial degradation occurred through the coating.

X-ray diffraction analysis shows the presence of Pt_8Al_{21}, $PtAl_2$, and Pt_2Al_3. Alumina is also detected and is present even near the coating/substrate interface.

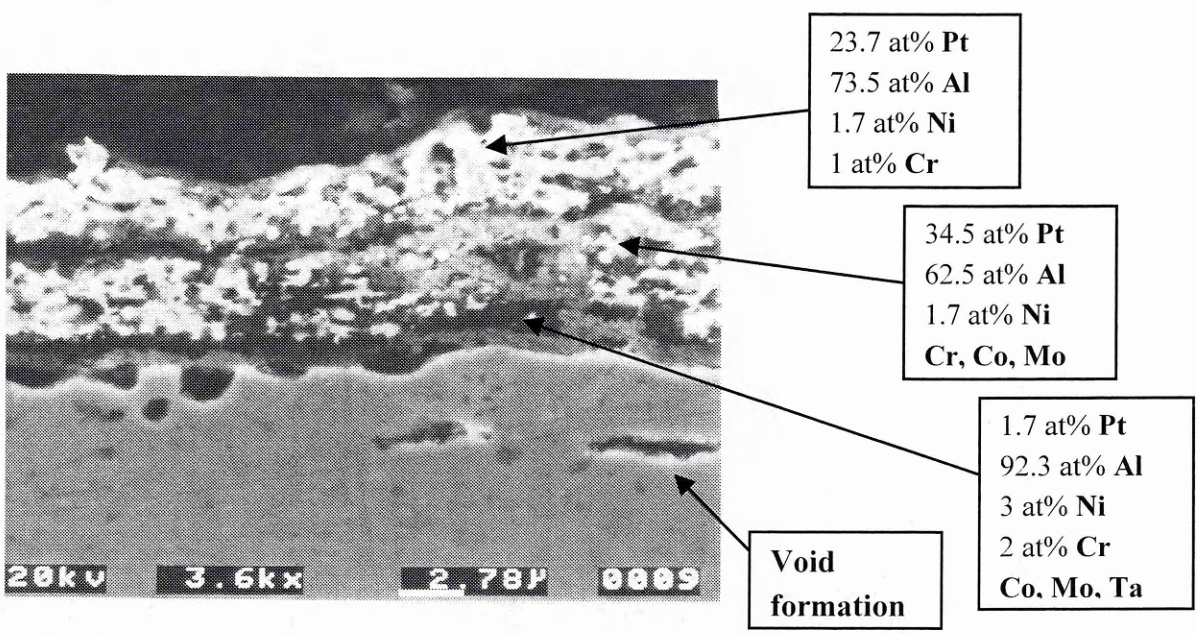

Figure 86:Secondary electron micrograph of an as-reacted PtAl coating after 10hrs at 1100°C

The Figure 86 summarises also the EDS quantitative analysis of different part of the coating and emphasises the high concentration of aluminium.

A few voids are observable in the substrate and could account for a local depletion in aluminium.

6.2.3.8. Auger spectroscopy

It has been pointed out in the previous work that a **multi-layered structure** is present throughout the 5 and 9-layer coating systems even after heat-treatments at 700, 900 and 1100°C. An interface of an aluminium rich intermetallic was suspected to be formed and Auger spectroscopy was carried out in order to determine which elements were present.

The following graphs summarise the Auger spectroscopy results and aimed to determine whether aluminium, platinum and oxygen were present or not at the interfaces between intermetallic layers.

Auger spectroscopy was carried out at the interface between two intermetallic layer of the heat-treated 9-layer coating. This interface was revealed in peeling off the coating using an adhesive tape.

An Auger spectrum plots a function of electron signal intensity versus electron energy.
The **blue line** corresponds to an **intermetallic reference** (Pt8Al21 degraded by the pest phenomenon, namely containing oxygen). The **red and green** lines are related to the coating interface surfaces.

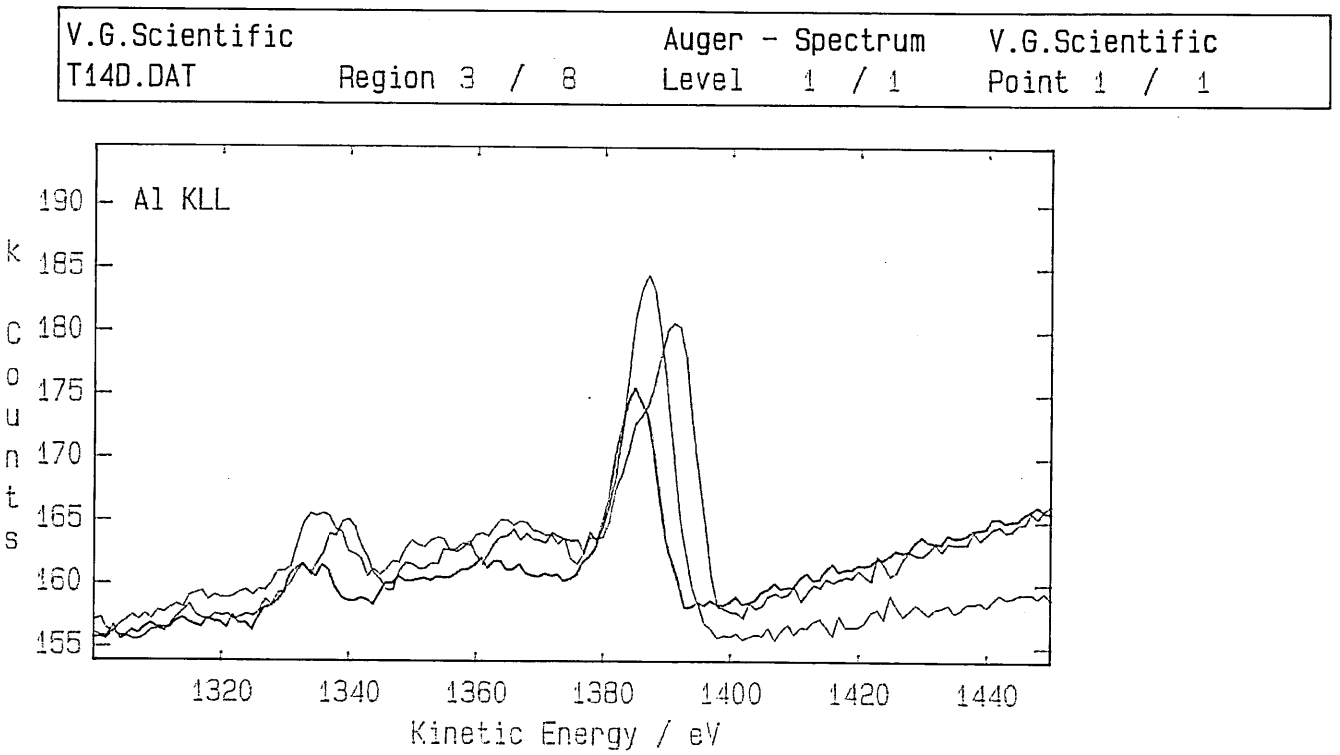

Figure 87: Auger spectra showing an aluminium peak for all specimens

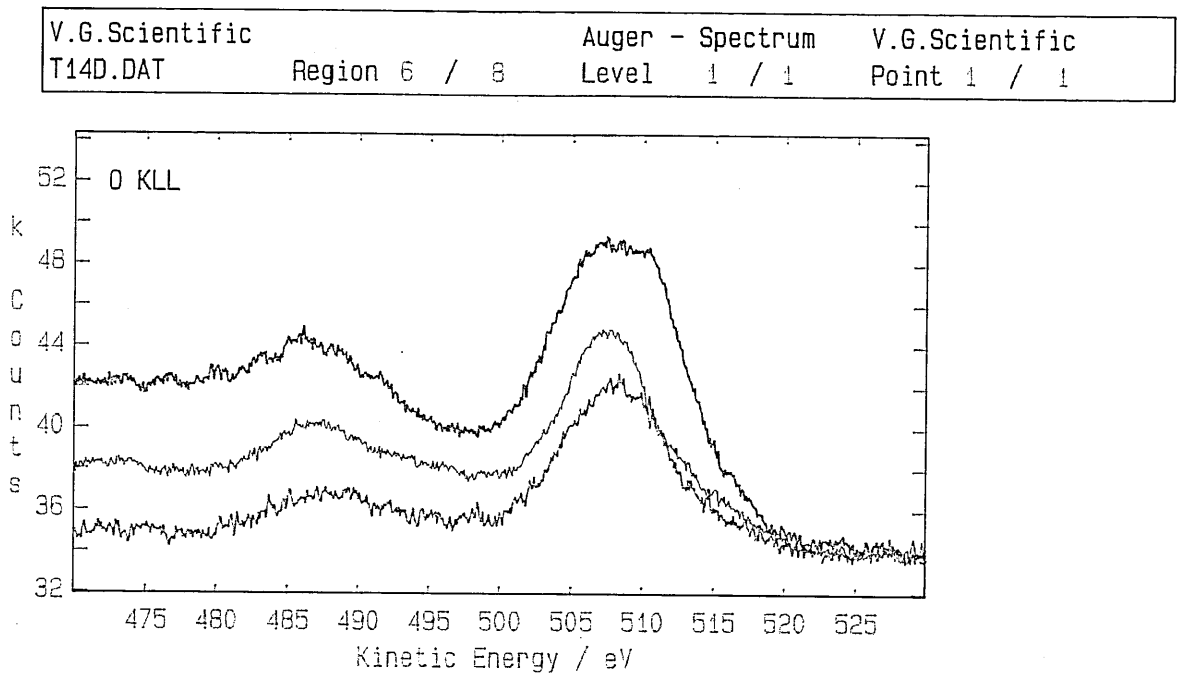

Figure 88:Auger spectra showing the presence of oxygen at the interfaces

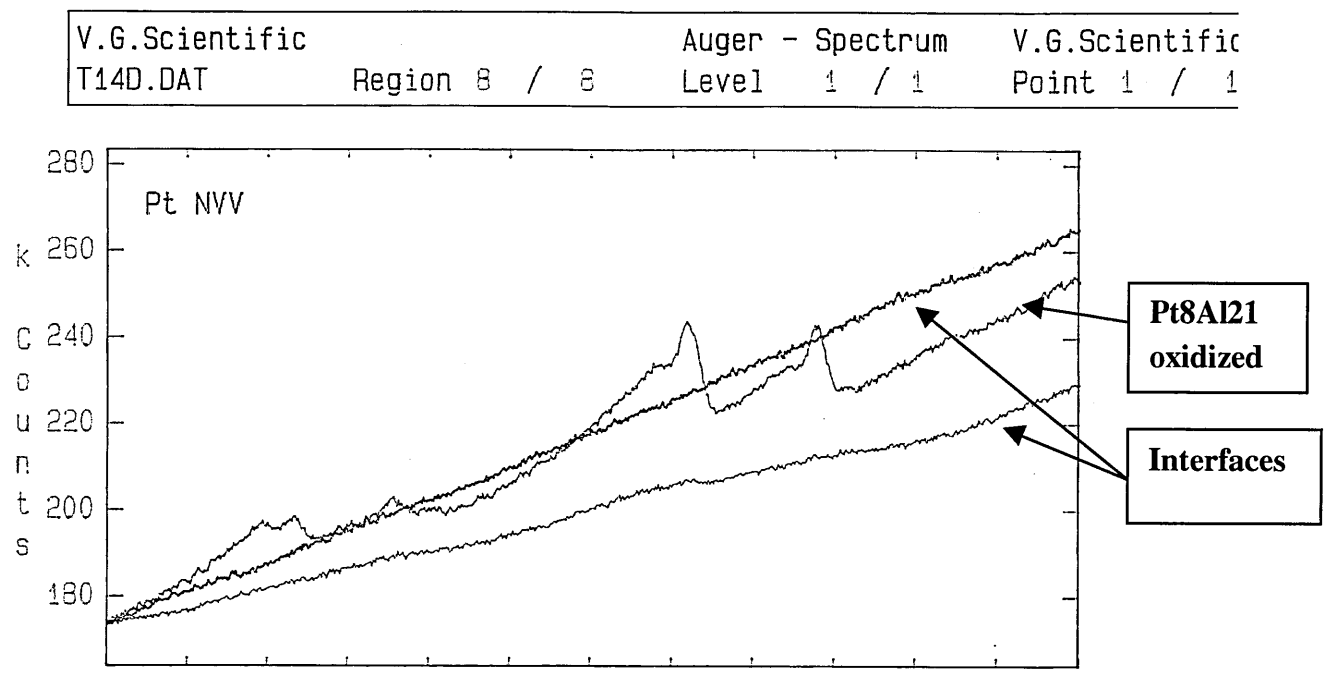

Figure 89: Auger spectra showing no platinum presence at the interfaces

As observed in the previous spectra, the Auger spectroscopy analysis show the presence of aluminium and oxygen at the interface. However, platinum was not detected, which means that the interface consists of an aluminium oxide.

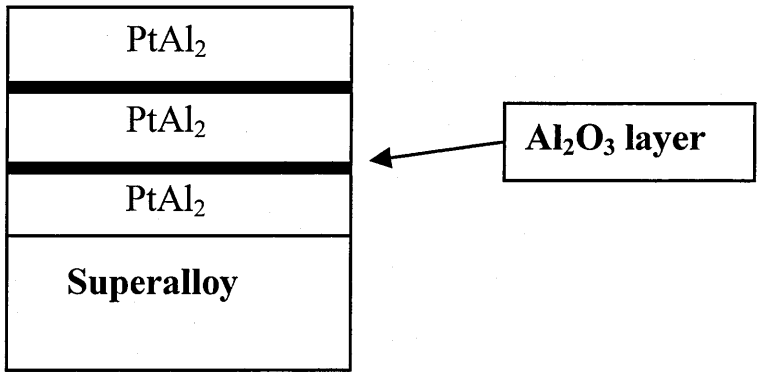

Figure 90: Scheme of a multi-layer platinum aluminide overlay after heat treatment

Several explanations of the phenomenon are possible:

- The oxygen could have been introduced during the deposition process. It would mean that the working gas is not pure enough.
- The oxygen could have diffused in the coating during the heat treatment, because even in an argon atmosphere, a small amount of oxygen is always present.

6.2.3.9. conclusion for the 9-layer coating system

The further increase of the number of deposited layer shows an improvement in the coating properties relatively to the 5-layer coating system.
Even if the structure is still lamellar, the bond between the remaining layers is stronger and the coatings are more compact.
Coating with richer concentration in platinum than $PtAl_2$ were assessed and show the strongest adherence between the remaining layers of the as-reacted coatings.
A post treatment at 900°C does not change the coating morphology, but a relatively deep interdiffusion zone develops in the substrate.

As for the 5-layer coatings, the deposition and formation process leads also to a clean coating. The final coating is free of substrate elements and the composition in aluminium and platinum is steady (no gradient).

6.3. High multi-layered coatings and formation of the bondcoat

The 'high multi-layered coatings' correspond to the deposition of coatings consisting of more than 100 successive layers of platinum and aluminium.
In increasing the number of layers (keeping the same bondcoat thickness) in the coating, the number of interfaces and therefore the surface of reaction are also increased. The rate of reaction between aluminium and platinum is thus improved.

6.3.1. Experimental deposition

The aim of this deposition process is to automatically place for a short time the samples to be coated in front of each sputtering target. A computer program (UNIDEX®) monitors the rotation of the sample holder and allows setting up a specific time spent in front of each target as well as a rotation speed.
3 different multi-layer coatings were produced in order to form 3 different platinum aluminide bondcoats. The expected stoichiometry of the coatings is controlled by the Al/Pt thickness ratio and the characteristics of each as-deposited coating system are detailed in the following table:

	Number of layer	Total thickness	Al layer thickness	Pt layer thickness
Pt_8Al_{21}	240	10µm	30 nm	15 nm
Pt_2Al_3	350	8µm	25 nm	18 nm
PtAl	360	8µm	22 nm	22 nm

Table 27: characteristics of the as-deposited multi-layer coatings

According to the deposition parameters used and to the coating system to be deposited, the deposition time for each aluminium layer varied between 15 and 30s and between 1 min and 2 min for each platinum layer.

6.3.2. 240-layer Pt_8Al_{21} coating system

An EDS quantitative analysis of the as-deposited coating cross-section was performed and emphasizes very steady concentration profiles for aluminium and platinum throughout the coating.

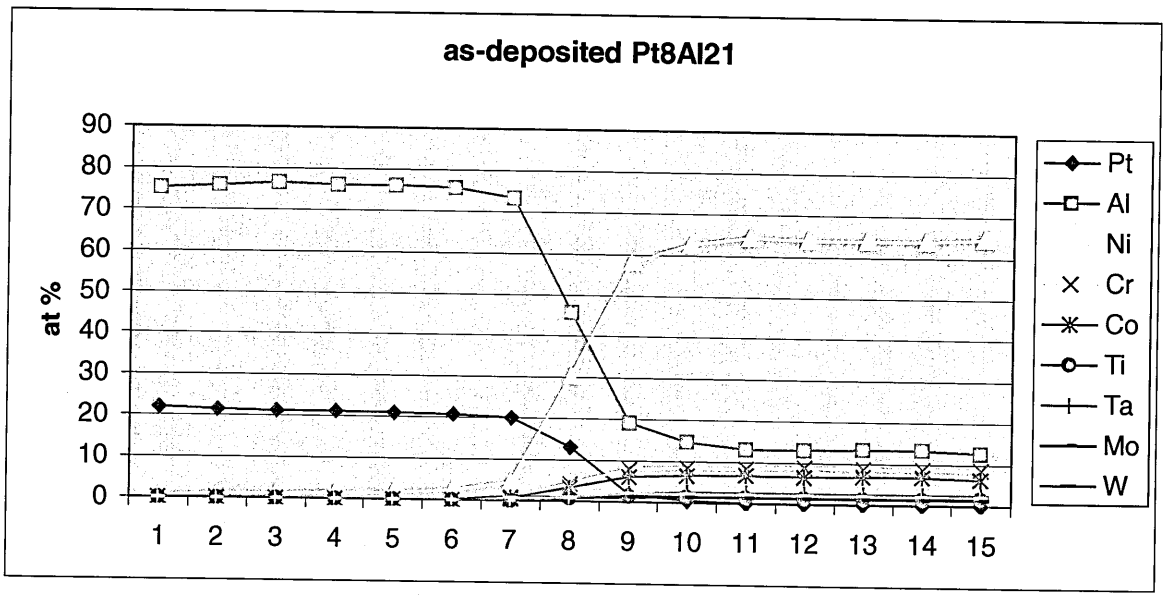

Figure 91: Digipoint analysis of an as-deposited Pt_8Al_{21} coating cross-section

Furthermore, the process prevents the interdiffusion with the substrate and leads to the deposition of a 'clean' coating.

An X-Ray diffraction analysis of the as-deposited coating was also carried out and reveals the formation of an intermetallic compound during the deposition.
The following spectrum shows indeed the fuzzy peaks corresponding to the **Pt8Al21 compound**, which means that the platinum and aluminium layers began to react before the thermal reaction treatment.

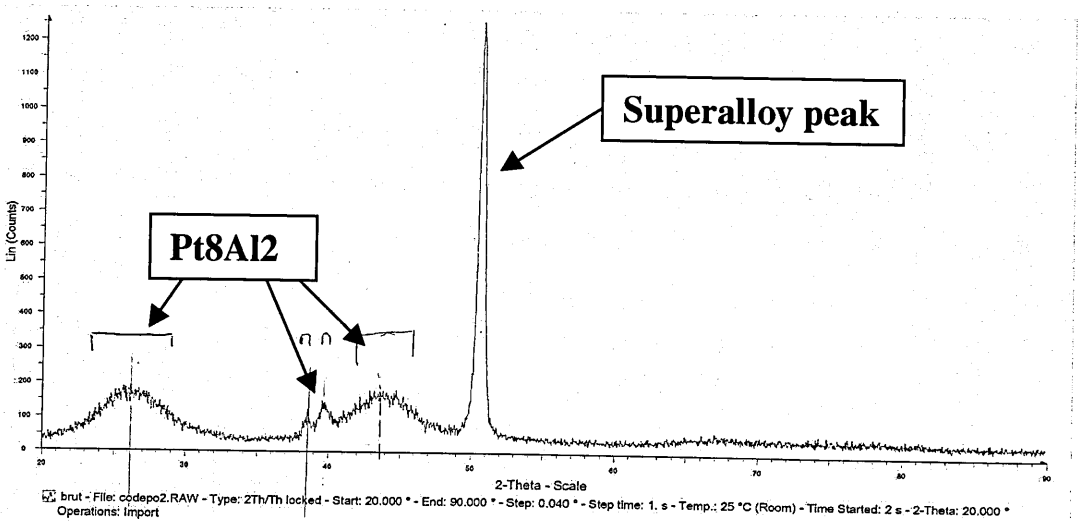

Figure 92: X-ray diffraction spectrum of the as-deposited Pt_8Al_{21} coating

After a reaction treatment at 700°C for 2 hours, the concentrations remain steady throughout the coating. A slight depletion in aluminium is however observable in Figure 93, adjacent to the interface with the surface.

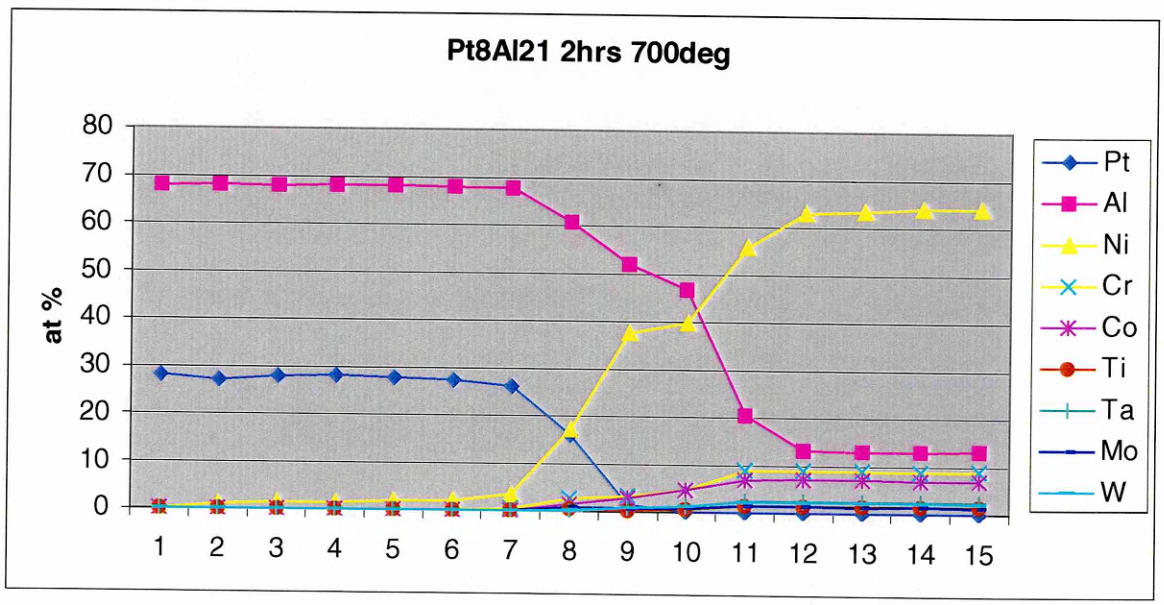

Figure 93: Digipoint analysis of an as-reacted Pt_8Al_{21} coating after 2 hours at 700°C

A 2-microns diffusion zone developed which appeared to correspond to the (Ni, Pt) Al already encountered for the 5 and 9-layer coating systems. This zone is observable in the following photograph:

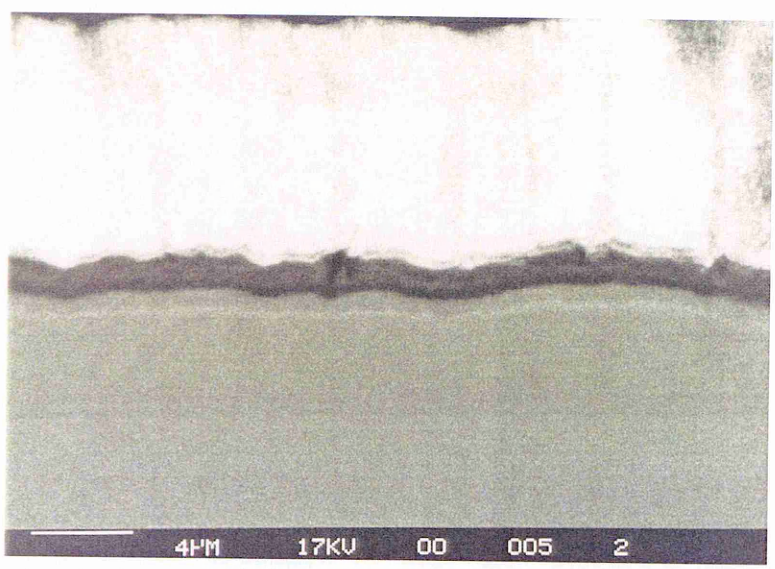

Figure 94: Secondary electron micrograph of an as-reacted Pt_8Al_{21} coating

Figure 94 emphasises also the particular morphology of the coating. As detailed further in the report, the deposition of very thin layers leads to the continuous growth of a thick coating layer, which has a fibrous and columnar structure.

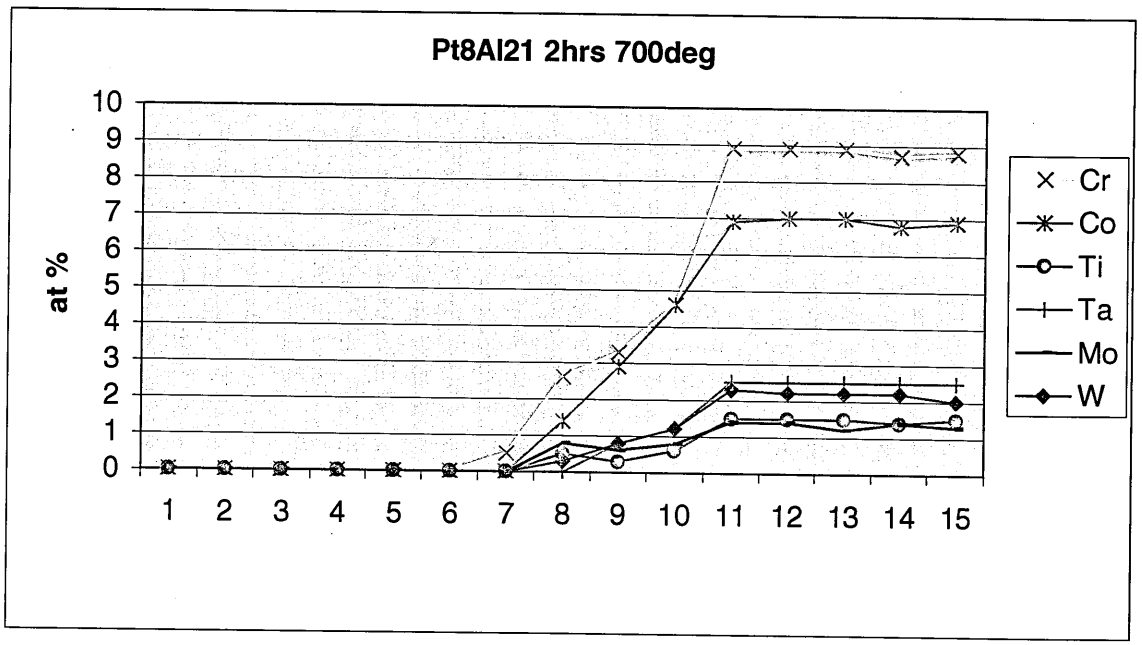

Figure 95: Digipoint analysis of the as-reacted Pt_8Al_{21} coating, with focus on the substrate element diffusion

Figure 95 accounts for the concentration profiles of the substrate elements apart from nickel. It shows that they are not present in the coating and are present at a low level in the thin interdiffusion zone.

The 'scotch' tape test was carried out and all the coatings were adherent before and after the heat treatment.
X-ray diffraction analysis was also performed and shows **the presence of $PtAl_2$**, which is consistant with the quantitative analysis.
The complete process (deposition + reaction treatment) leads therefore to the formation of a 10-microns thick platinum aluminide overlay, free of substrate elements and with a different morphology to the low-multilayered coatings.

After a subsequent heat treatment at 900°C for 2 hours, a depletion in aluminium is observed . The following figures show that the coatings consist of 4 different zones:

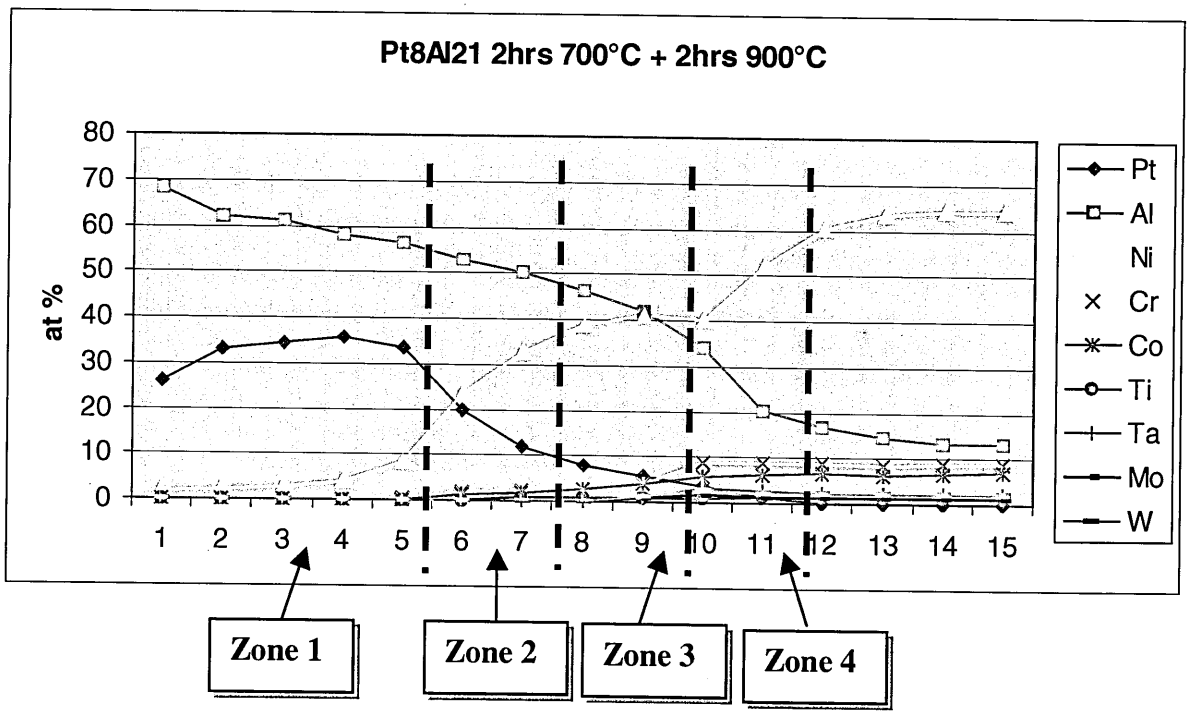

Figure 96: Digipoint analysis of a 240-layer Pt_8Al_{21} after 2 hours at 700°C and 2 hours at 900°C

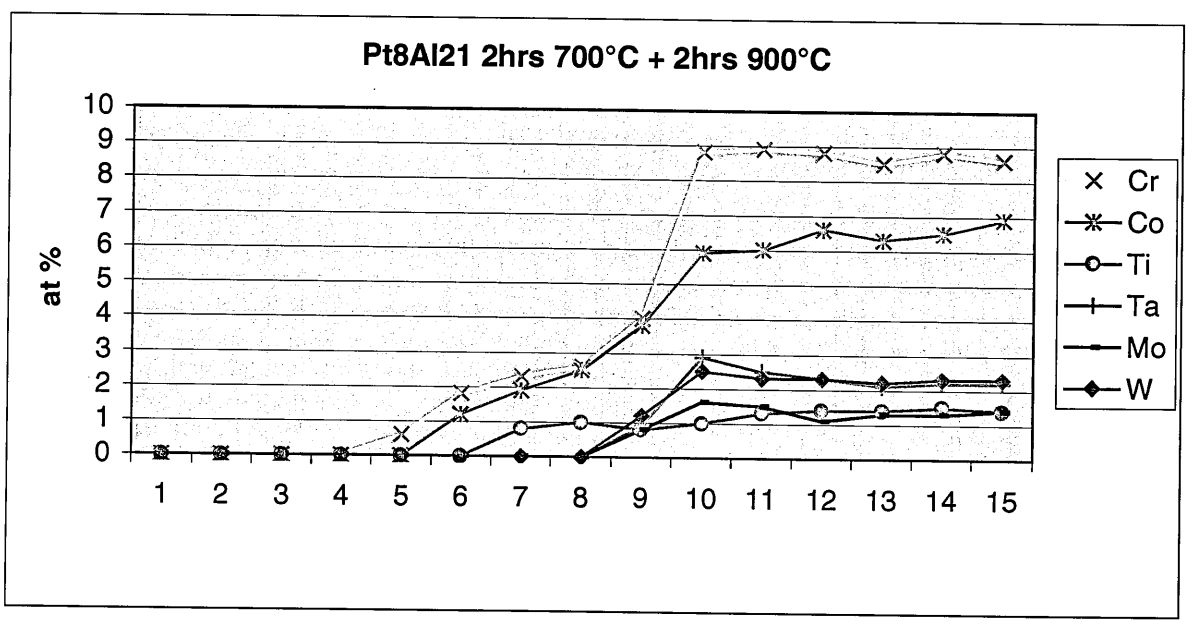

Figure 97: Digipoint analysis of the 240 layer Pt_8Al_{21} coating with focus on the substrate elements diffusion

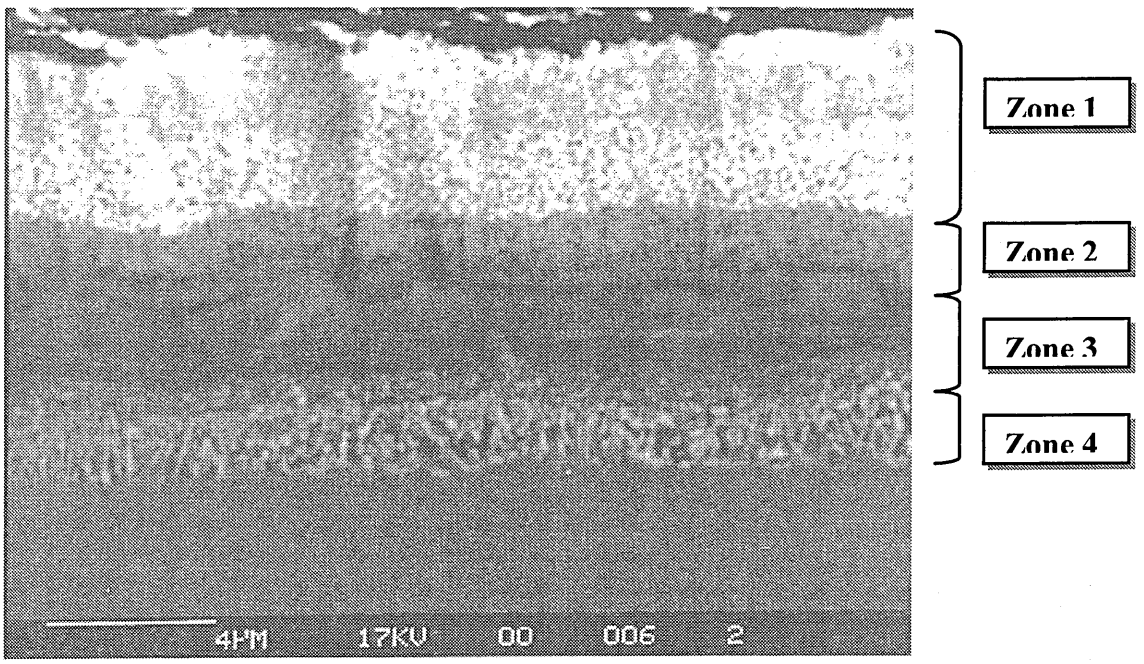

Figure 98: Backscattered micrograph of a Pt_8Al_{21} heat treated 2 hours at 700°C and 2 hours at 900°C

Zone 1: The zone 1 consists of a steady concentration of platinum, and of a decreasing concentration of aluminium, which varies from 70 at% down to 55 at%. This zone is substrate element free. In Figure 98, this zone corresponds to the bright outer layer of the coating.

Zone 2: The second zone is actually the lower part of the initial coating. The change of colour observed in Figure 98 is caused by the outward diffusion of nickel. The aluminium concentration still drops and the platinum concentration decreases as the nickel diffuses outwardly. In this zone, the coating contains some chromium and some cobalt.

Zone 3: In this zone, which corresponds to the first interdiffusion zone, the concentration of nickel is steady, the aluminium level still decreases and the platinum concentration is low. The phase formed could be (Ni, Pt) Al with all the substrate elements in solution. The concentration of these elements increases actually dramatically in this zone from the coating to the substrate.

Zone 4: Thus corresponds to the second diffusion zone. The nickel concentration increases up to its substrate concentration. The aluminium concentration decreases to reach its

substrate concentration. The zone contains also precipitates believed to be Laves and σ phases. These precipitates have a needle-like oriented structure consistent with σ phase.

Compare to the results obtained for the 9-layer systems after the post-treatment, **the aluminium depletion is obviously more marked.** This aluminium depletion causes a phase evolution in the coating and triggers the precipitation and the growth of the Laves phases. The evolution and degradation of the coatings is similar in many ways to the behaviour of the classical platinum aluminide

An X-ray analysis was performed on the coating surface after post-treatment and shows the presence of Pt_2Al_3 and PtAl.

6.3.3. 350-layer Pt_2Al_3 coating system

In order to prevent a too fast degradation of the low-mass bondcoat, another multi-layer system with more platinum was assessed. It consisted of a 350-layer coating with the thickness ratio of Pt_2Al_3.

As observed in the following figure, the aluminium and platinum concentration profiles are steady and no interdiffusion with the substrate occurred during the deposition process.

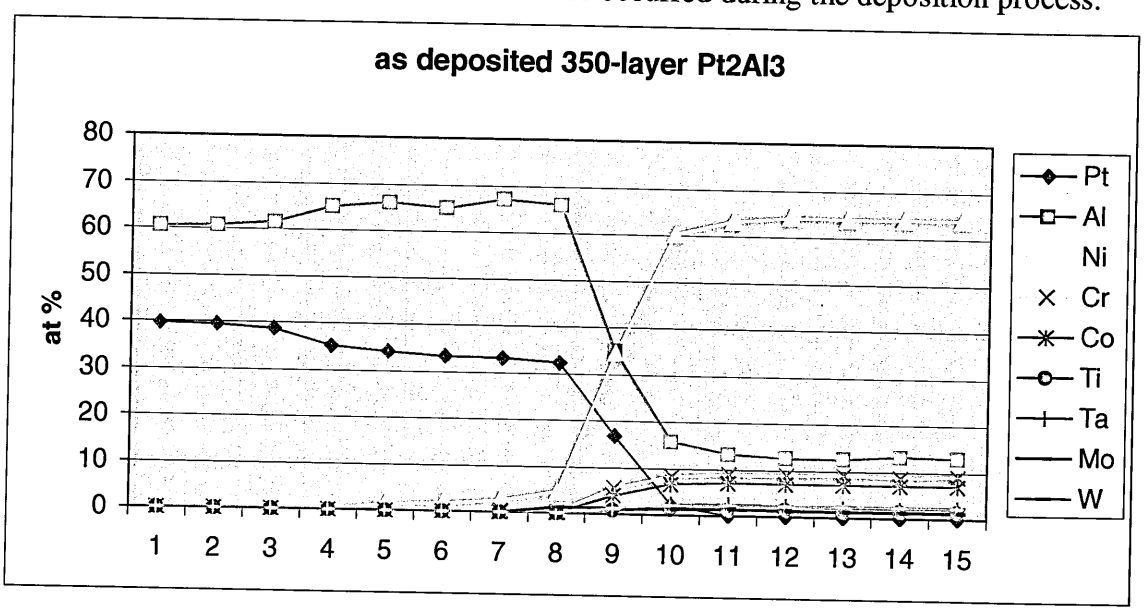

Figure 99: Digipoint analysis of an as-deposited Pt_2Al_3 350-layer coating

An X-Ray diffraction analysis was performed on the as-deposited coating but unlike in the Pt_8Al_{21} multi-layer coatings, no intermetallic compounds was detected, following deposition.

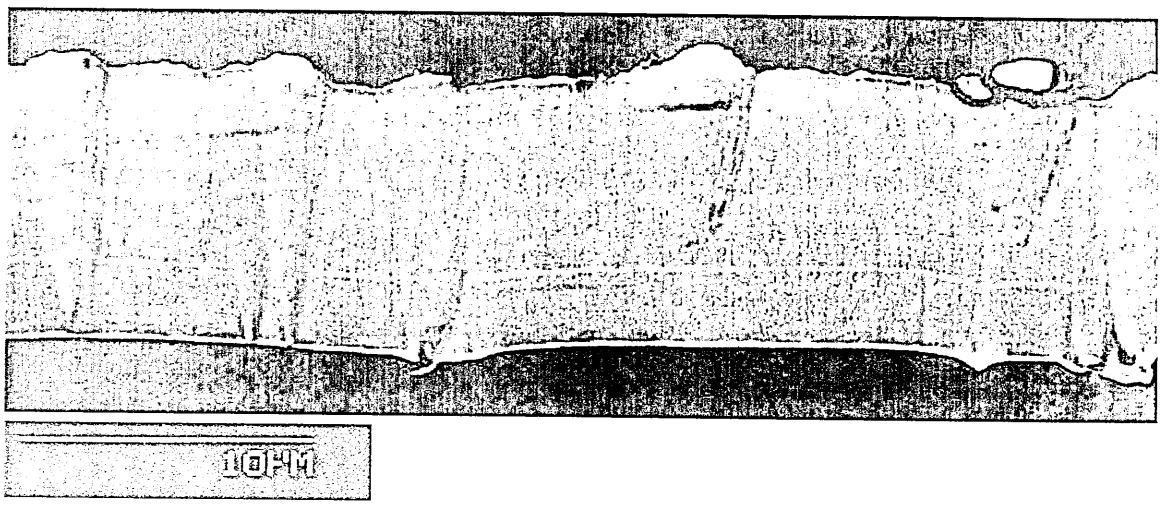

Figure 100: Backscattered micrograph of an as-reacted Pt_2Al_3 coating

Figure 100 is a cross-section micrograph of an as-deposited and reacted coating system. A fibrous and columnar morphology is still obviously remarkable. This structure contains moreover a significant amount of 'leader' defects, whose formation was initiated during the nucleation stage of the coating growth from particles or features on the substrate surface. They are caused by the plasma arcing or by impurities present within the substrate surface.

After a reaction treatment at 700°C for 2 hours, the reaction occurs between the platinum and aluminium layers and the X-Ray diffraction analysis shows the presence of Pt_2Al_3.

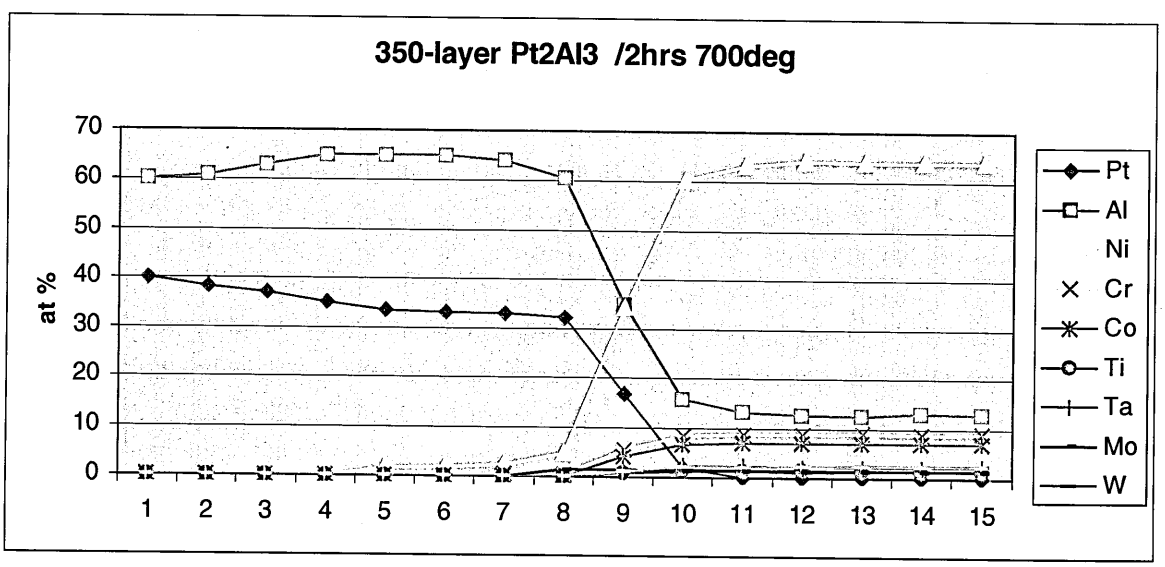

Figure 101: Digipoint analysis of an as-reacted Pt_2Al_3 350-layer coating (2hrs at 700°C)

Digipoint analysis of a coating cross-section emphasises steady concentration profiles. They are moreover consistent with the X-ray analysis.

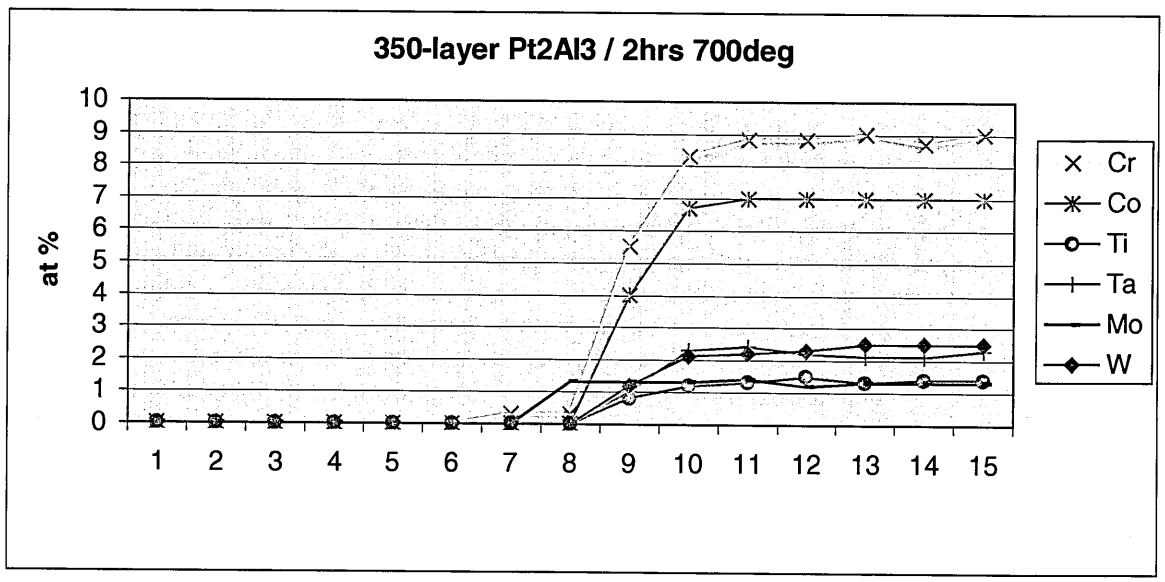

Figure 102: Digipoint analysis focused on the substrate elements diffusion

As observed in the Figure 102, the as-reacted coating is free of substrate elements and compared to the Pt_8Al_{21} coating, there is no significant interdiffusion zone.

After a reaction treatment at 700°C and a subsequent post-treatment at 900°C for 2 hours, the aluminium and platinum concentration profiles are still quite steady and no significant degradation occurred in the coating, unlike that observed for the Pt_8Al_{21} multi-layer coatings.

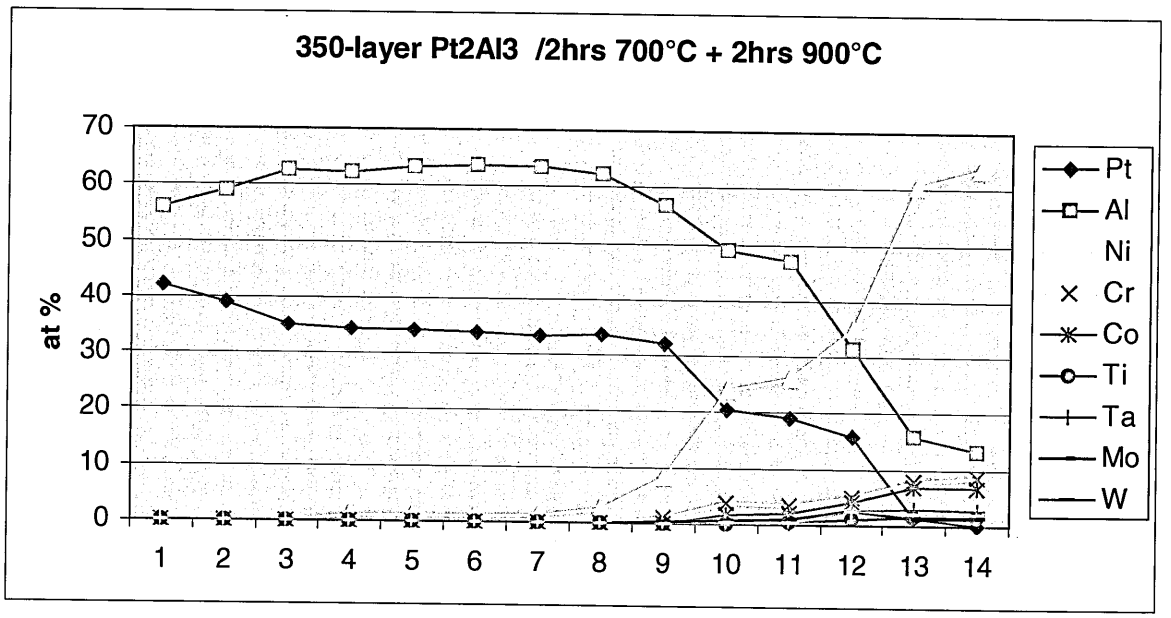

Figure 103: Digipoint analysis of a 350-layer Pt_2Al_3 coating after 2hrs at 700°C and 2hrs at 900°C

As canbe seen in on the Figure 103, a small interdiffusion has formed at the coating/substrate interface and corresponds to the (Ni, Pt) Al phase with 25 at% of nickel, i.e. $NiPtAl_2$ suggesting further ordering in the Ni,Pt lattice.

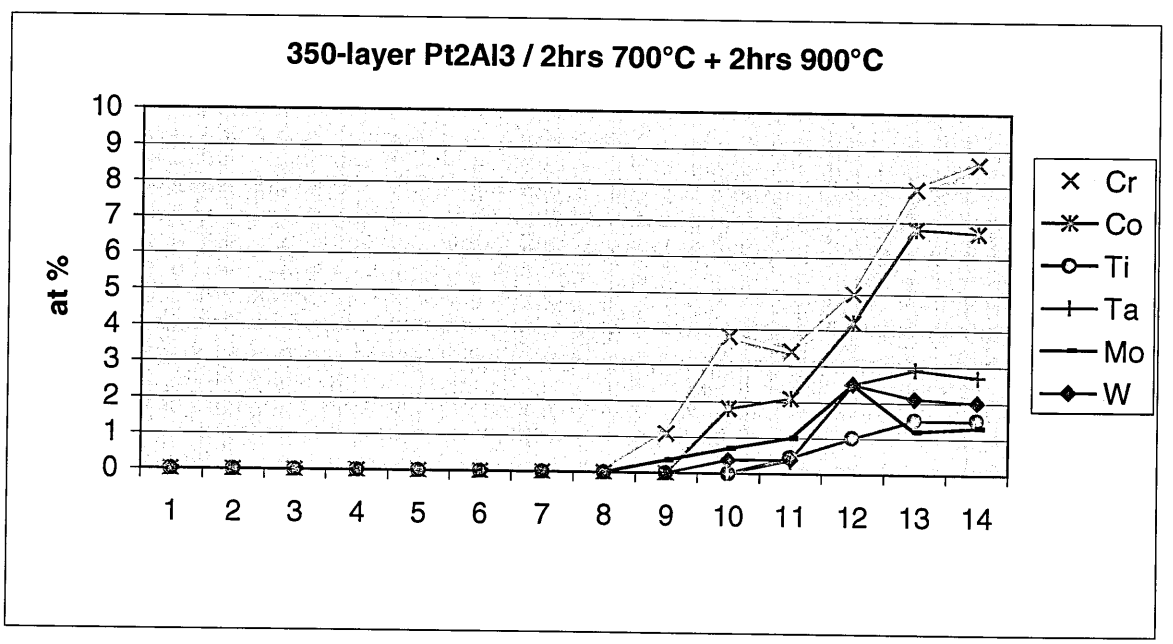

Figure 104: Digipoint analysis focused on the substrate elements diffusion

The Figure 104 accounts for the concentration profiles of the substrate elements throughout the coating; it shows actually that the coating is free of these elements. Only the interdiffusion zone contains chromium, cobalt and low content of molybdenum and tungsten.
An X-ray diffraction analysis was also performed on the coating after heat treatment and the compound Pt_2Al_3 as well as some PtAl were detected.
This means that the coating did not lose any aluminium during the post-treatment as was observed for the Pt_8Al_{21} coatings.

Other heat treatments were carried out in order to assess the stability of the coating. These consisted of 6 hours at 700°C and 16 hours at 700°C, respectively.
X-ray diffraction shows the presence of Pt_2Al_3 in all the heat-treated coatings and the Figure 105 accounts for a quantitative analysis of the coating after 16 hours at 700°C. These results show that the aluminium did not diffuse inward and that the coatings are relatively stable at 700°C.

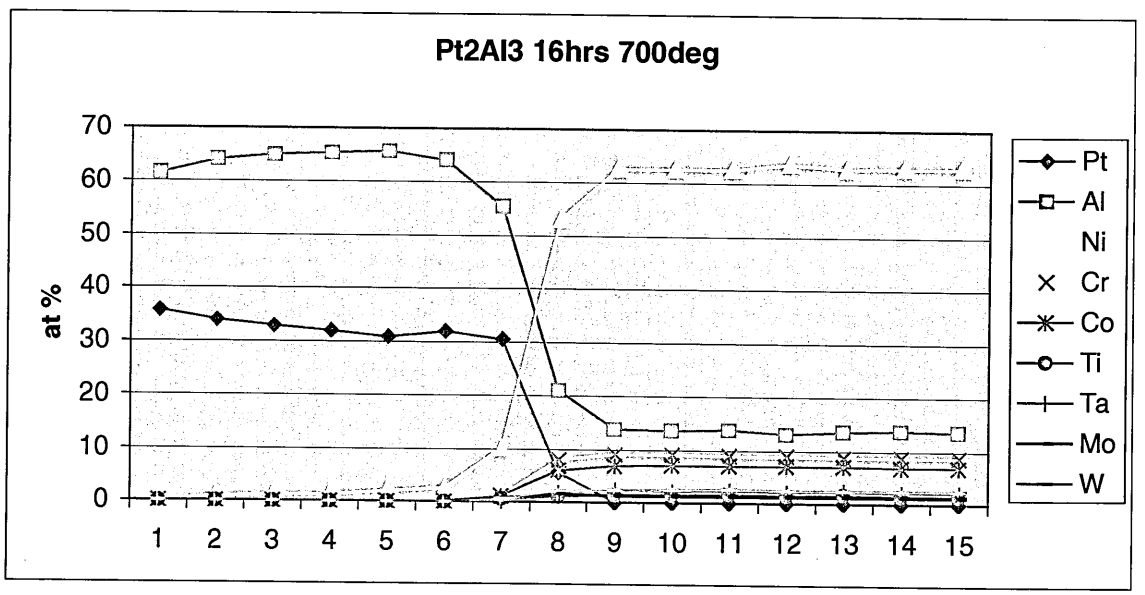

Figure 105: Digipoint analysis of a Pt_2Al_3 coating after 16 hours at 700°C

The degradation of the coating seems thus to be controlled by the initial concentration of platinum. In the case of the Pt_8Al_{21} coatings, the relatively fast inward diffusion of aluminium triggers the formation of NiAl at the interface, with the consequent outward diffusion of nickel. This damages the coating thermal stability. In the case of the Pt_2Al_3 coatings, the stoichiometry remains unchanged after various heat treatments, and this

platinum aluminide compound seems therefore to be very stable, when deposited on a nickel based superalloys.

6.3.4. 360-layer PtAl coating system

In order to study the effect of a further addition of platinum in the low-mass bondcoat, a third high multi-layered system was produced and consisted of a 360-layer coating with the thickness ratio of PtAl. The following Digipoint analysis graph accounts for the concentration profiles of the as-deposited coating:

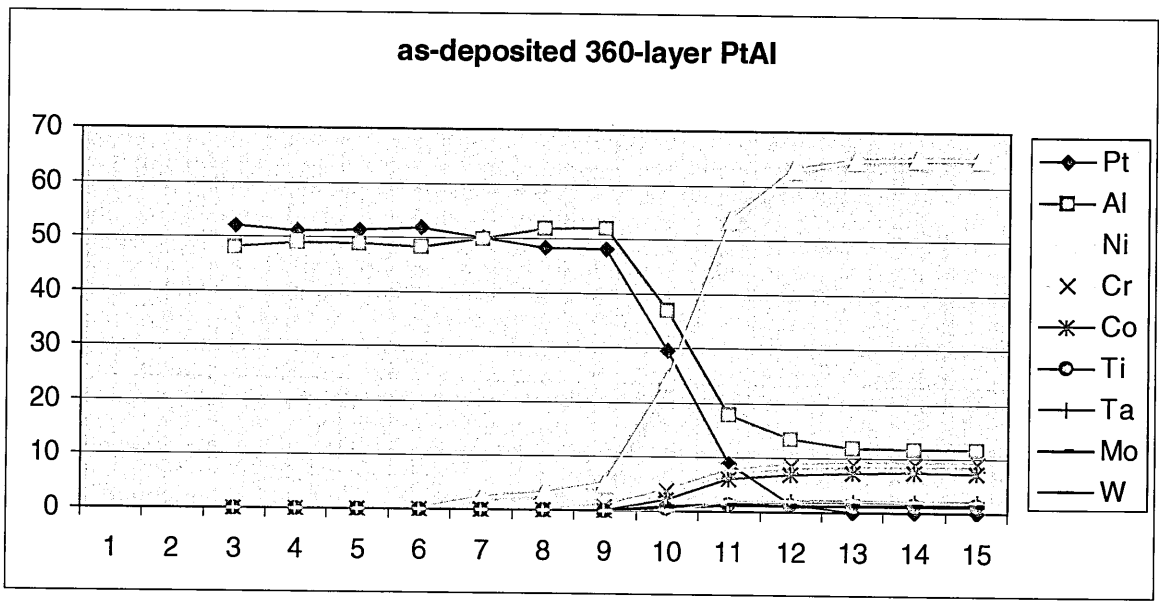

Figure 106: Digipoint analysis of an as-deposited 360-layer PtAl coating

The as-deposited multi-layer coating is again free of substrate elements and has a very steady concentration of aluminium and platinum.

The X-ray diffraction analysis did however not detect the formation of any intermetallic compound follow deposition as was observed for the Pt_8Al_{21} compounds. After a heat treatment at 700°C for 2 hours, the X-ray analysis shows the presence of the Pt_5Al_3 compound and some traces of the PtAl compound.

A Digipoint quantitative analysis was also performed on a coating cross section and the concentration profiles are gathered in Figure 107 and Figure 108. The compounds observed by X-ray diffraction would imply that the coating is thus richer in platinum than the Digipoint results would suggest. This could mean that aluminium oxide precipitates or unreacted aluminium are present in the coating.

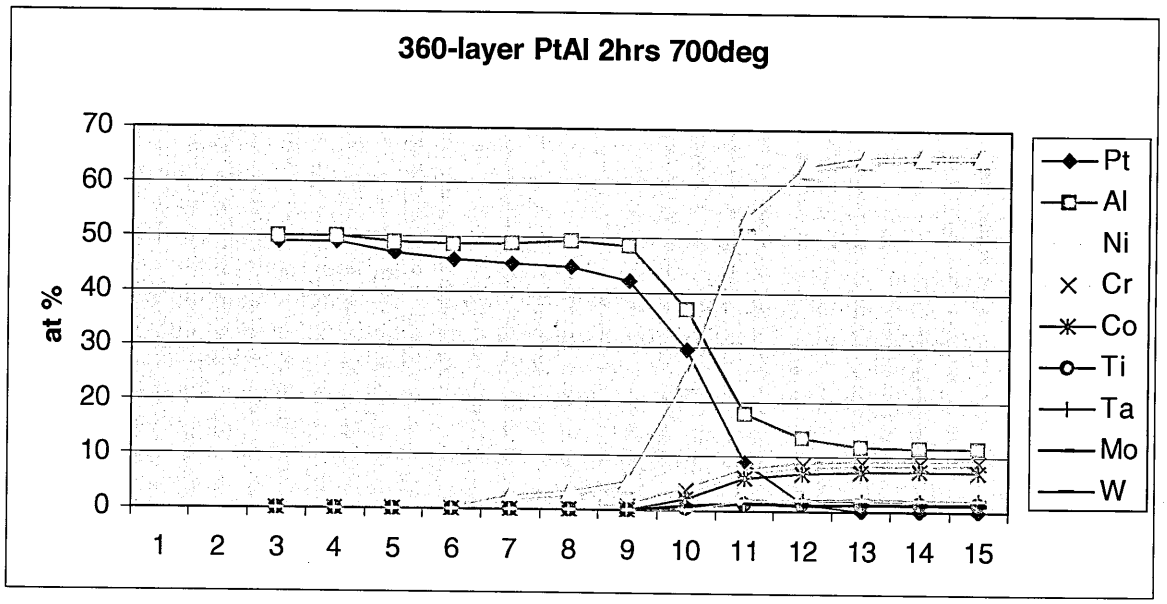

Figure 107: Digipoint analysis of an as-reacted 360-layer PtAl coating

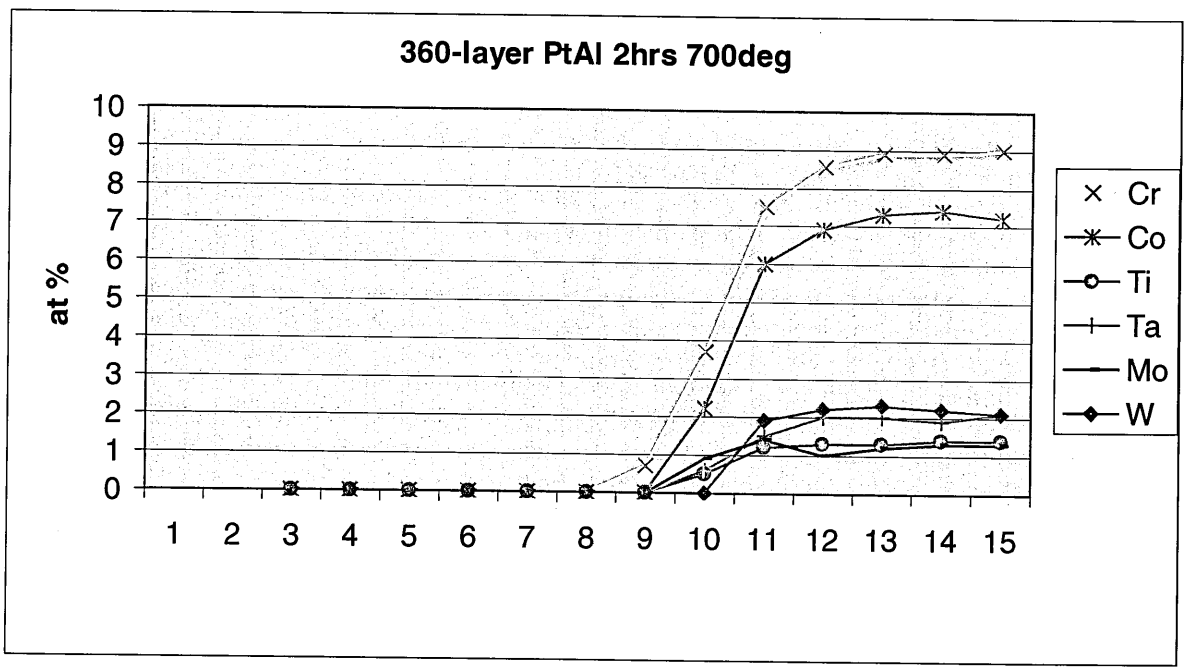

Figure 108: Digipoint analysis focused on the substrate elements diffusion

The concentrations of aluminium and platinum are still very steady throughout the coating and a reaction treatment at 700°C prevented the outward diffusion of substrate elements. After 2hours at 700°C and a subsequent post-treatment at 900°C for 2 hours, the coating composition did not change significantly. X-ray diffraction analysis still shows the presence

of Pt_5Al_3 with some traces of PtAl and the Digipoint analysis results indicated a steady concentration of platinum and aluminium with the stoichiometry of PtAl.

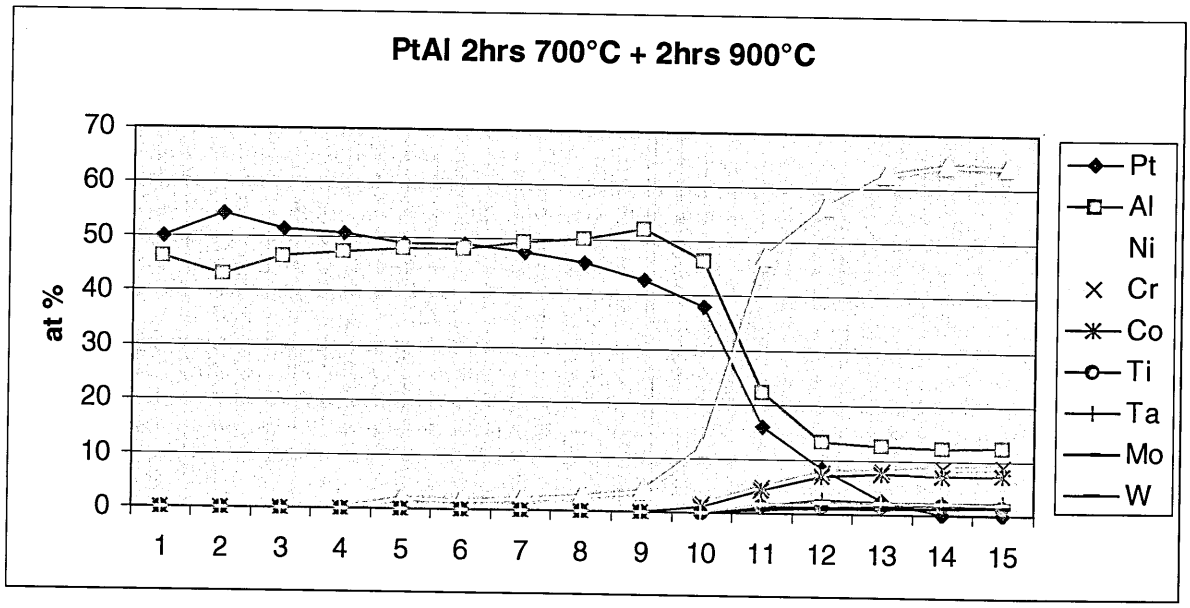

Figure 109: Digipoint analysis of a 360-layer PtAl coating after 2 hours at 700°C and 2 hours at 900°C

Conversely to the Pt_8Al_{21} and to the Pt_2Al_3 coating systems, the interdiffusion zone is very thin after the two heat treatments. This means that the aluminium present in the coating did not diffuse inward any further. This highlights the thermal stability of platinum rich aluminides.

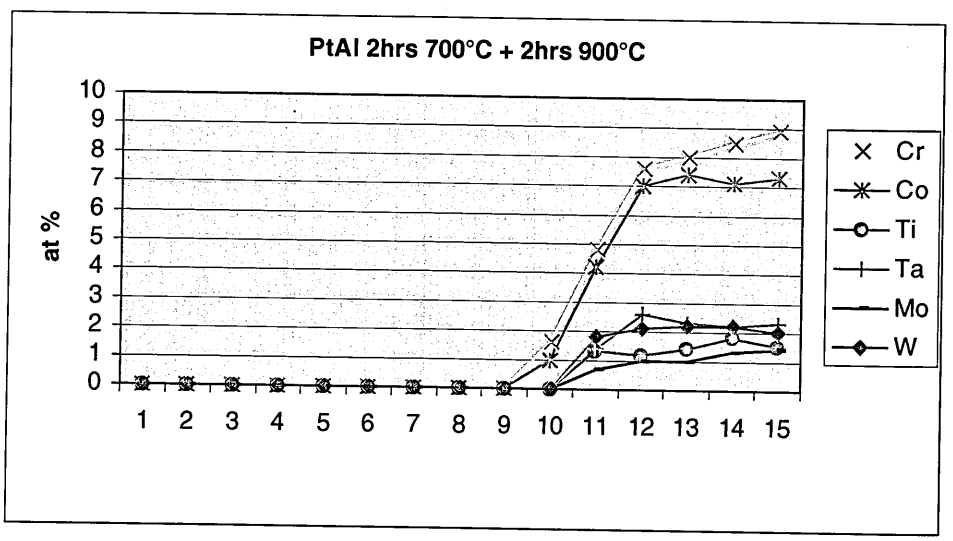

Figure 110: Digipoint analysis focused on the substrate elements diffusion

On another hand, the coating is still 'clean' after both heat treatments. The stable near stoichiometric platinum aluminide compound seems thus to prevent the outward diffusion of substrate elements.

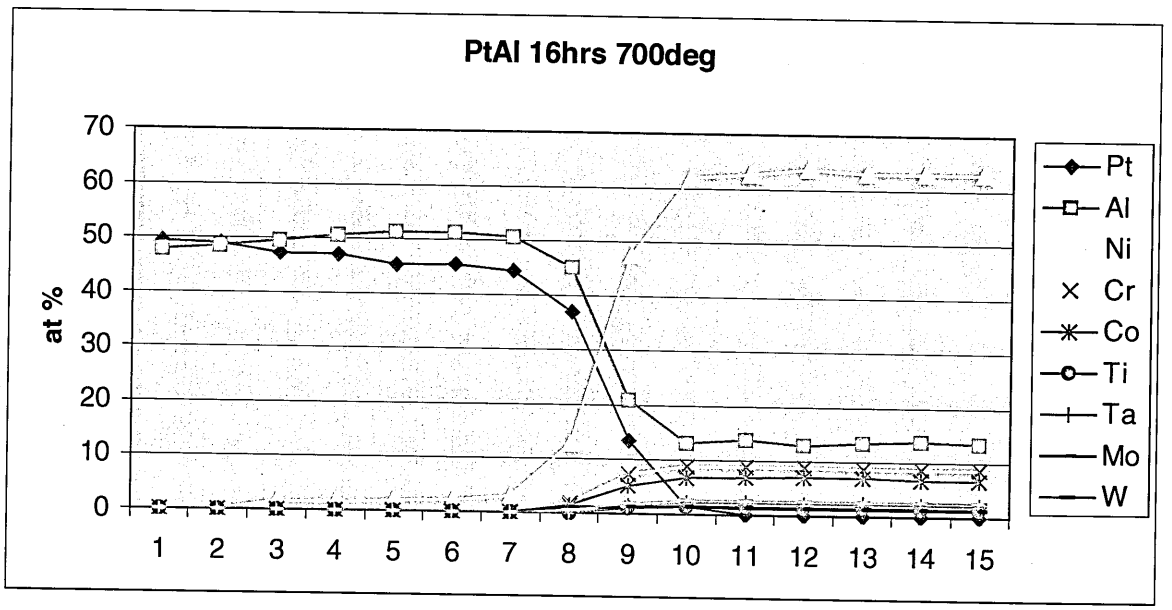

Figure 111: Digipoint analysis of a 360-layer PtAl coating after 16 hours at 700°C

Figure 111 highlights the stability of the coating after 16 hours at 700°C. The concentration profiles are much the same than after 2 hours at 700°C, and the X-ray diffraction analysis has detected the peaks of the Pt_5Al_3 and PtAl compounds.

6.3.5. Morphology study of high multi-layered coatings

This part aims to explain the coating morphology obtained during the high multi-layered coating deposition process. It is also focused on the deposition of a new, high multi-layered, low-mass bondcoat with a different structure.

6.3.5.1. The columnar morphology

The factors promoting the interdiffusion between the coating and the substrate are usually:

- The deposition and substrate temperature
- The nature of the coating
- The structure of the coating

One of the benefits of the sputtering deposition process is that the deposition and **substrate temperatures are relatively low**: it has not been measured but is assumed to be in the range **200-300 deg C**.
The use of substrate bias during the first platinum layer deposition increases slightly the surface temperature of the substrate, **but the interdiffusion with the substrate must be partially inhibited at these conditions.** The sputtering process prevents therefore the coating/substrate interdiffusion during the deposition.

The **nature of the coating** is also substantial: once the layers have reacted to form an **intermetallic** compound, the properties of the coating are not the same. The platinum aluminides are indeed known to prevent or slow down the interdiffusion.

Finally, the **coating structure** is an important factor as well, because **defects** (such as grain boundaries, column boundaries) and **low-density** (porosity) induce usually short-circuit paths for diffusion.
The structure of the low-mass bondcoat (with a high number of layer) can be discussed using both **Mochvan and Demchishin** and **Thornton** Models.
Mochvan and Demchishin (1969) have studied the effect of substrate temperature on the coating structure during sputtering deposition. They have divided the different structures in three zones (relatively to T/Tm, where T is the substrate temperature and Tm is the coating material melting point):

1. **Zone 1 (T/Tm <0.3):** it consists of tapered crystallites with domed tops, which increase, in width with temperature.
2. **Zone 2 (0.3 <T/Tm < 0.45):** it consists of columnar grains with smooth mat surface.
3. **Zone 3 (T/Tm>0.45):** it consists of equiaxed grains and bright surface

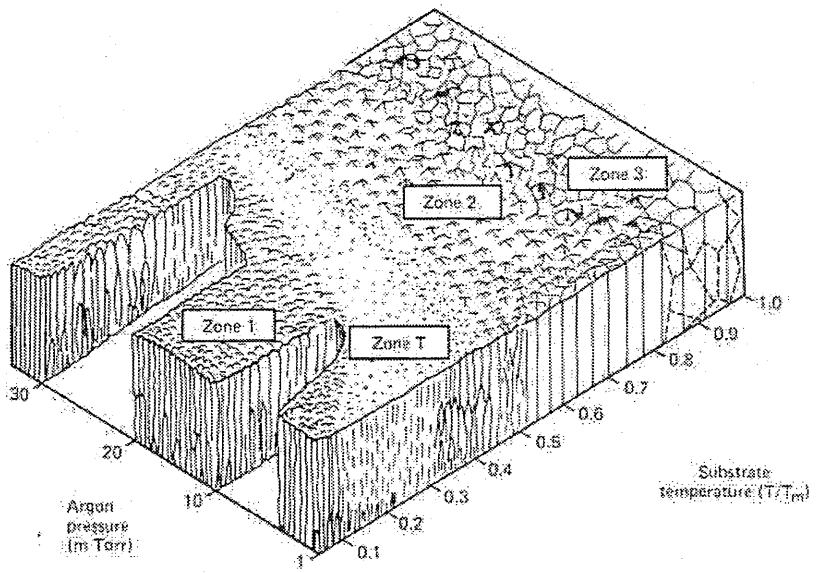

Figure 112: Thornton's Model (1973)

Thornton (1973) studied as well the coating structure dependence on temperature and discovered that **the argon pressure was influencing the morphology**. Thus, at low argon pressures a new zone (called zone T) appears between the previous zone 1 and 2 and consists of densely packed fibrous grains (see Figure 112).

Assuming that the substrate temperature reaches **300 deg C** during the deposition, the different T/Tm ratio for the main platinum aluminides are given as follows:

Intermetallic compound	Melting point (degC)	T/Tm
Pt8Al21	1127	0.26
PtAl2	1406	0.21
Pt2Al3	1527	0.2
PtAl	1554	0.19
Pt5Al3	1465	0.2

Moreover the **argon pressure** used during the sputtering deposition was kept constant at **10^{-2} mbar (namely 7.5 microns or mTorr).**

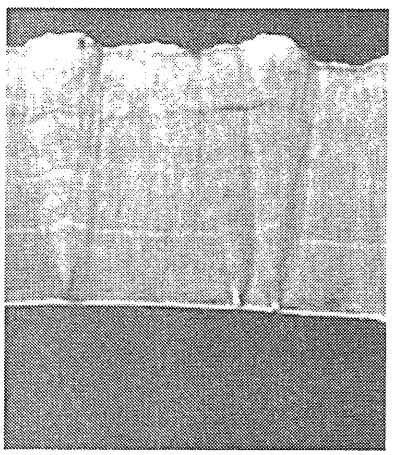

The expected coating structure stands therefore in the **zone T** and is highlighted by the Figure 113.
The coating morphology is a dense array of fibrous, grains, consisting of tapered columns with domed outer surfaces.
This structure has usually a high hardness, a high strength, but a least ductility than the other zones.

Figure 113: as-deposited Pt5Al3 coating (8 microns thick).

The current bondcoat growth and morphology could actually promote the substrate elements outward diffusion (diffusion along extended defects, which are the columnar grains).
Diffusion via line defects is the quickest mode of diffusion and most of diffusion barrier concepts aim to eliminate these defects (De Reus, 1995).

The solution is therefore to avoid or modify the fibrous columnar structure and several ways are possible:

- **Heat the substrate during the deposition:** it would shift the coating structure in the zone 2 or 3 in order to have wider column with less boundary surfaces or equiaxed grains. However, if the substrate surface is heated during the deposition, the interdiffusion is going to be accelerated and the coating could loose its properties. On another hand, the setting of heaters raises a technical problem during automatic rotation of the substrate holder (namely the possible deposition of platinum and aluminium on the heaters!).

- **Use of substrate bias:** Biasing the substrate with a negative potential during deposition results in increasing the ion bombardment on the substrate and the growing deposit tends to eliminate the columnar growth morphology (Thornton 1973)(Bland, Kominiak, Mattox, 1973). However, this solution is not suitable with the deposition process: indeed, during automatic rotation of the substrate holder, both aluminium and platinum plasmas are switched on and substrate bias interferes with the DC bias used for aluminium sputter deposition.

- **Structured multi-layer coating:** a third solution would be to interrupt the growth morphology throughout the coating: To understand this idea, the performance of the 5 and 9-layer coating systems has to be remembered. These coatings appear more brittle than the 300-layer ones, but their morphology was denser. Their structure was **layered** in a macroscale (even after several heat-treatments) and **columnar** in a microscale (in each layer).

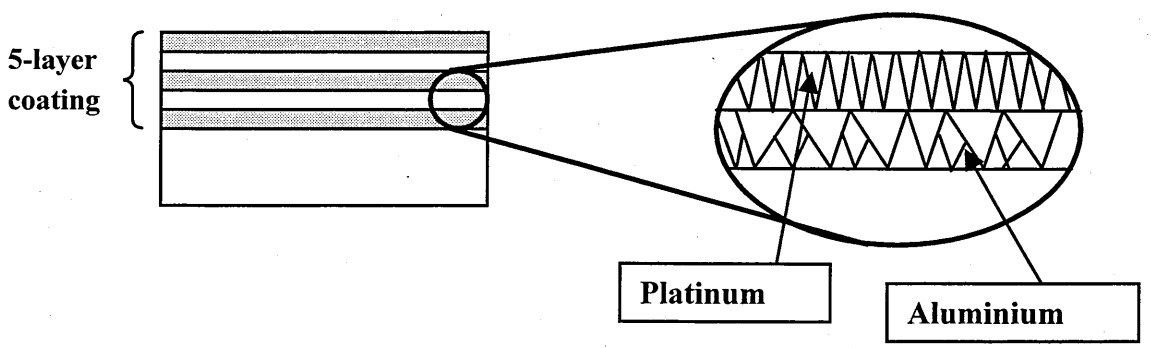

Figure 114:Focus on the microstructure of an as-deposited 5-layer coating system

For each layer, the growth of the tapered and fibrous columns is different because of the material: Aluminium layers have a coarser structure than platinum layers. However, a **new growth begins for each layer** and no continuous vertical defects are present throughout the coating, **inhibiting the defect diffusion.**

In the case, of the 300-layer coatings, each layer has a thickness of few nanometers and a continuous growth can occur. To avoid this, thicker layers of platinum could be introduced at regular intervals in the coating in order to interrupt the columnar growth.

- **Moderate number of layer**: another way to find a compromise between the structure of the low and high multi-layered coatings is to produce a multi-layer coating made up of layers thick enough to prevent a continuous and columnar growth, but thin enough to prevent the formation of brittle interfaces within the coating, i.e. use a moderate number of layers.

6.3.5.2. Growth interruption at regular intervals

A 10-microns thick 300-layer coating was produced with the thickness ratio of Pt_2Al_3. Every 2 microns, a 0.5 microns thick platinum layer as well as a 0.5 microns thick aluminium layer were deposited in order to interrupt the columnar growth of the coating.

As observed in Figure 115, large fibrous columns are still noticable in the as-deposited coating structure, but the whole multi-layer structure seems more compact than the previous 300-layer deposited without growth interruption.

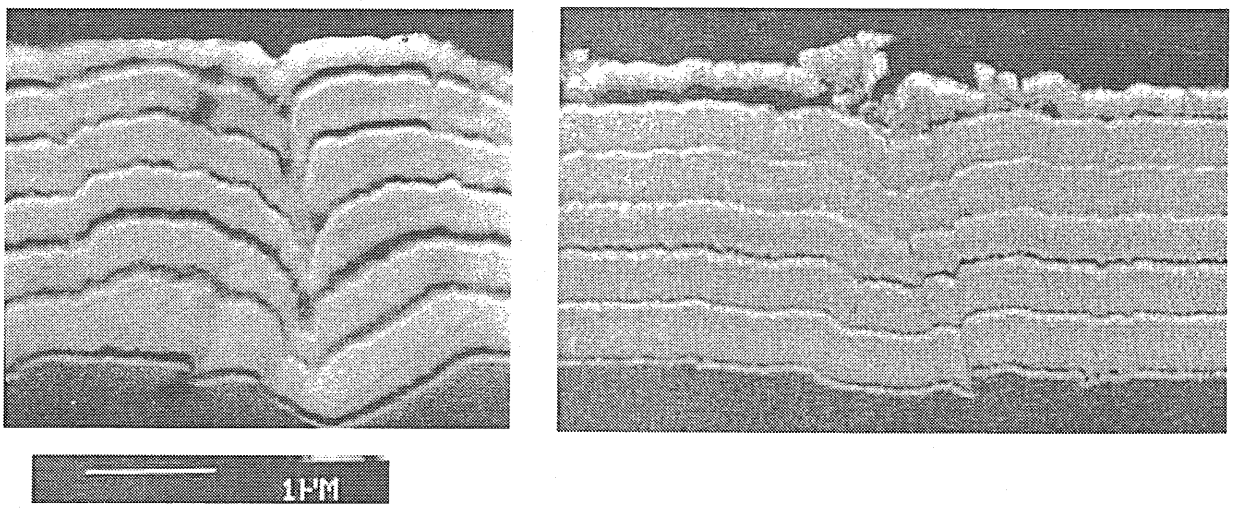

Figure 115: Comparative secondary electron micrographs of an as-deposited and an as-reacted Pt_2Al_3 at 700°C for 2 hours

After 2 hours at 700°C, the thicker layers of platinum and aluminium diffused in each other and seem to form a platinum aluminide layer separated from the remaining parts of the coating.
X-ray diffraction analysis and Digipoint analysis show moreover, that Pt_2Al_3 has formed in the coating.
As observed in Figure 116, delamination caused by the cross-section polishing, can however occur between the different layers, suggesting each set of layers are less well bonded.

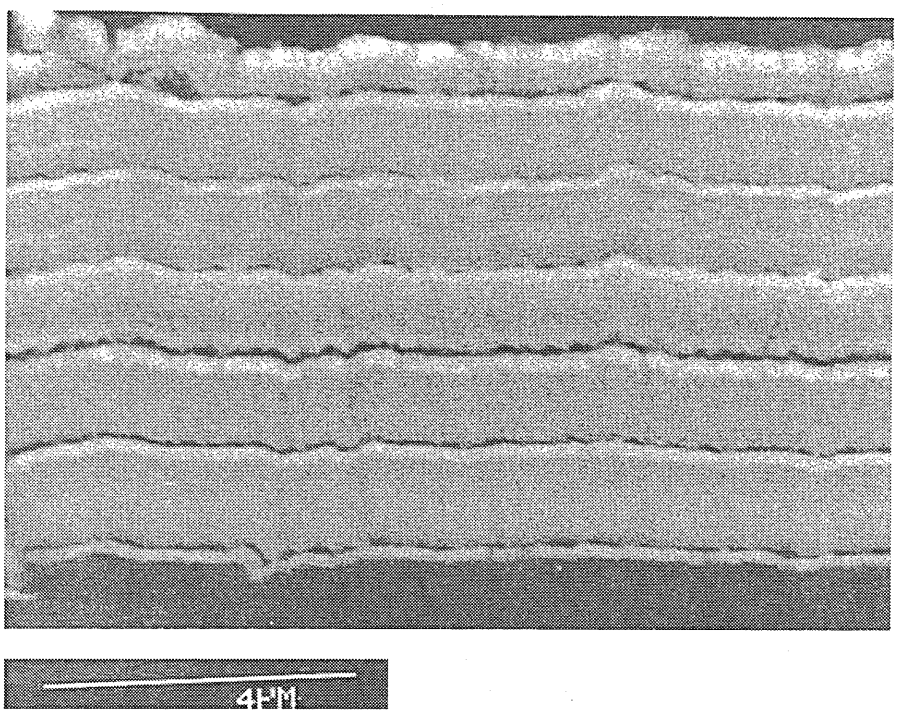

Figure 116: Secondary electron micrograph of an as-reacted growth interrupted Pt_2Al_3 coating

To sum up, the introduction of thicker layers at regular intervals within the low-mass bondcoat promote partially the interruption of columnar growth but leads also to the formation of a multi-layer coating with brittle interfaces.

6.3.5.3. Moderate number of layers

A second interesting way to modify the bondcoat structure, is to find an optimal thickness for the aluminium and platinum layers in order to prevent the columnar growth and to avoid the formation of brittle interfaces.

A 10 microns thick coating made up of 100 layers was then deposited with the thickness ratio of Pt_2Al_3.

The following photograph accounts for the as-deposited coating and conversely to the 300-layer coating, the platinum and aluminium layers are distinguishable. At some locations (fuzzy white patches), the layers seem however to have reacted.

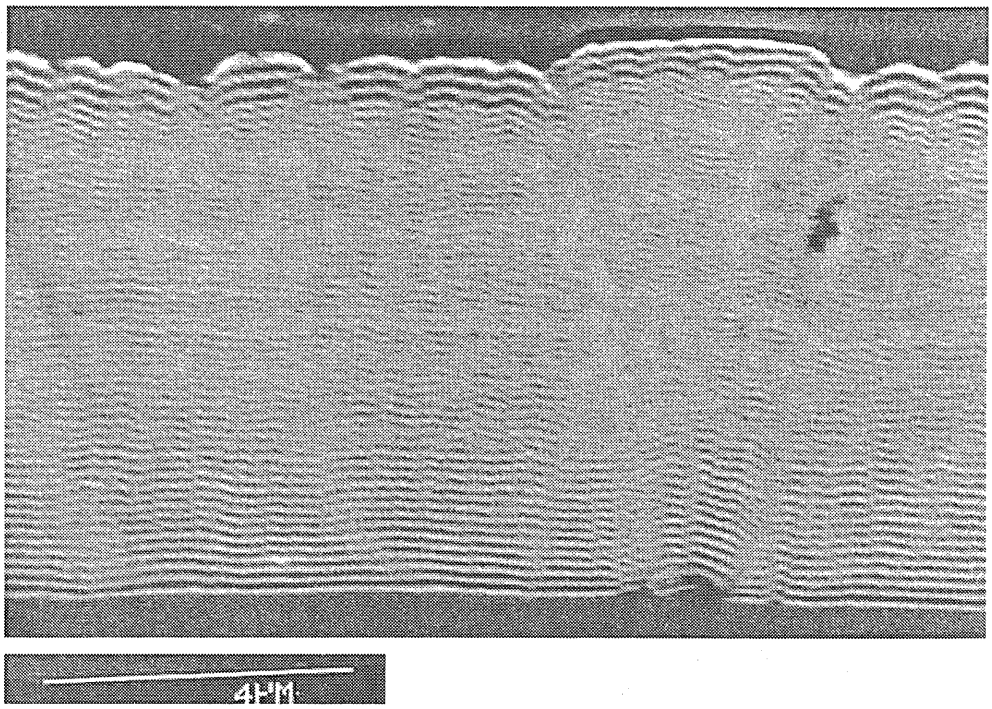

Figure 117: Secondary electron micrograph of an as-deposited 100-layer Pt_2Al_3 coating

A growth defect is also observable, which means that a continuous growth has still occurred but the columnar structure seems more compact than for the 300-layer coatings.

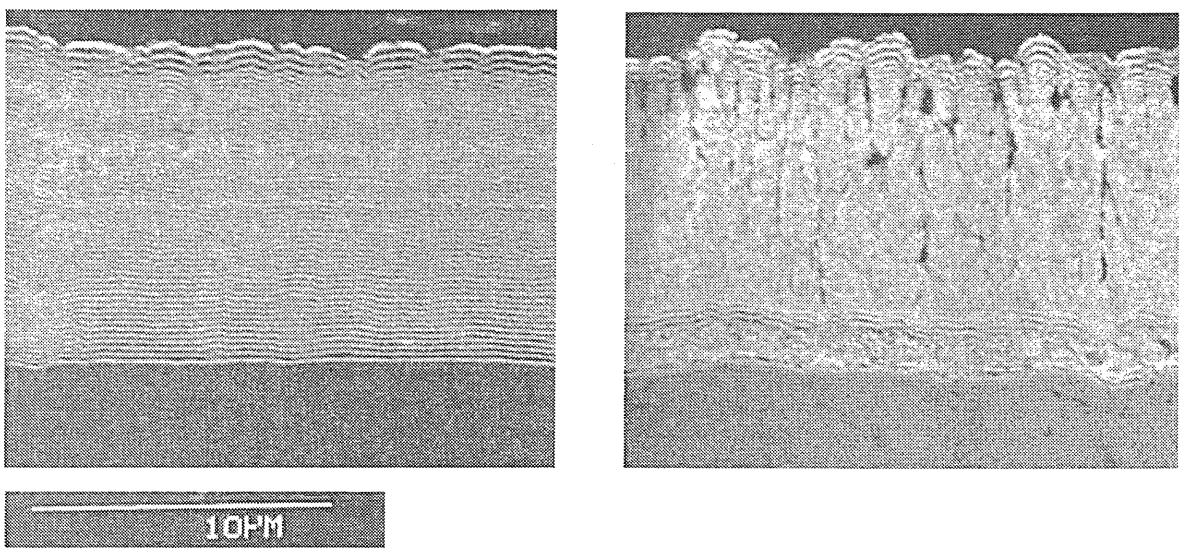

Figure 118: Comparative secondary electron micrographs of an as-deposited and an as-reacted 100-layer Pt_2Al_3 at 700°C for 2 hours

After 2 hours at 700°C, most of the layers have diffused and reacted and the coating structure is denser than in the previous coatings.
Defects and cracks are however present in the middle part of the coatings. This phenomenon could be caused by the coalescence of the thin fibrous columns, and the formation of dense blocks of platinum aluminides separated by relatively large interfaces.
In the lower part of the coating, some layers seem to be still present and means that:

- The thickness of the layers was higher than in the middle of the coating. This thickness could be critical and as we increase them overall in the coating, the bondcoat could remain multi-layered.
- The substrate absorbed the heat during the reaction treatment and the local temperature did not allow the layers to diffuse and react completely.

In the outer part of the coating, a similar phenomenon occurred and seems due to the too large thickness of the layers.

A Digipoint analysis was carried out throughout a cross-section of the as-reacted coating and results in very steady concentration profiles of aluminium and platinum, corresponding to the Pt_2Al_3 compound.
X-ray diffraction analysis was also performed and shows the presence of Pt_2Al_3 and Platinum. This means therefore that some platinum did not react with the aluminium.

6.4. Introduction of a reactive elements in the low-mass bondcoat

The introduction of a small amount of a reactive element to the low-mass bondcoat has been reviewed in the 'Bondcoat selection' chapter. The addition of less than 1 wt% of yttrium, zirconium or hafnium to an alumina-former alloy can sharply improve the oxide scale adherence, reduce the scale growth and prevent the sulphur segregation at the scale/alloy interface.

6.4.1. Co deposition technique

As detailed in the 'experimental chapter', the chosen way to introduce the reactive element in the multi-layer coating is to deposit it at the same time than the aluminium or platinum elements.
A clamp system was then developed to be able to place a piece of Reactive element wire on the platinum or the aluminium target.

The concept of the co-deposition was to control the concentration of Re element in the as-deposited platinum or aluminium layer by:

- Choosing a specific length and diameter of the wire (surface taken by the wire on the target)
- Placing the wire at a specific location on the target (because of the **magnetron effect**: if the wire is placed where the magnetron is the most efficient, namely where the sputtering is the fastest, the sputtering of Re element is accelerated.)

The following data have then been used to implement the fitting out:

Dimension of the target:	183*87 mm
Diameter of the wire:	1 mm
Length of the wire:	100 mm
Effective length of the wire:	96 mm (length to be sputtered)
Higher sputtering rate location:	at 50 mm from the target middle (accounted for the dotted line on the target scheme in the 'experimental part')
Target area:	15921 mm^2
Wire area:	96 mm^2

A single wire placed on the highest deposition rate location occupies therefore **0.6 %** of the total surface of the target. This percentage has then to be correlate with the sputtering yield of the materials to be co-deposit. The following table give thus the minimum concentration expected in the as-deposited coating:

	Expected Concentration (wt%) of the material co-deposited with:	
	Platinum target	**Aluminium target**
Single wire of Al	0.54	0.6
Single wire of Pt	0.6	0.66
Single wire of Y	0.42	0.46
Single wire of Hf	0.43	0.48
Single wire of Zr	0.34	0.37

Table 28: Expected concentration of the added material in the as-deposited coating

These concentrations are moreover proportional to the number of wire pieces placed on the target.

The coatings were deposited on glass plate and on 100-mm long nickel strips (pure nickel 99.9%) in order to assess the concentration distribution all along the substrate holder.
In order to detect the presence of aluminium in the coating, a quantitative analysis (SEM/EDS) was performed at different locations of the strips.

6.4.2. Co-deposition with platinum

As the reactive elements (zirconium, Hafnium, Yttrium) are very expensive materials, aluminium was firstly co-deposited with platinum.
The sputtering mode was then the same used to deposit a single layer of platinum, namely the RF mode.
Wires of aluminium were placed on the platinum target as explained in the previous section, and quantitative analysis was performed on the as-coated nickel strips.
In the case of the co-deposition with 4 pieces of wire, a concentration of 2,5 wt% of aluminium was expected.
However, in all the cases, aluminium was not detected.

Another deposition was run in order to check if the problem was coming from the material to be co-deposited: Instead of using a piece of aluminium wire, a **zirconium one was placed at the higher sputtering rate location of the target.**

However quantitative analysis did not reveal any trace of zirconium on the 2 microns thick platinum coating.

A last deposition was eventually performed using a large strip of aluminium (100*20 mm) on the platinum target, in order to check if the geometry of the wire was not a problem.
This strip was placed where the deposition rate was the faster and a minimum of **12 wt% of aluminium** in the platinum coating was **expected**.
Unfortunately, aluminium was still not detected.

These experiments show that aluminium and zirconium can not be co-deposited with platinum using the RF deposition mode. The aluminium atoms are dislodged from the target, but they are probably backscattered as well from the substrate.
This backscattering can be generated by the substrate ion bombardment produced during the RF sputtering deposition.

6.4.3. Co-deposition with aluminium

As the aluminium is deposited using the DC sputtering mode in the experimental deposition chamber, co-deposition runs were performed in placing pieces of different material in the aluminium target.
Platinum strips (50*20mm) were clamped on the aluminium target and the subsequent quantitative analysis showed the presence of 15 at% of platinum in the final aluminium coating.
Another deposition runs were then carried out using wires of copper, and zirconium.
The copper was successfully sputtered but the wires melted during the deposition. It is actually difficult to place properly the wire in contact with the aluminium target and if the wire is located in the high energy area produced by the magnetic field, this can raise dramatically its temperature.
On another hand, the aluminium coating deposited with zirconium did not contain the reactive element.

It was then assumed than the sensibility of the SEM/ EDS apparatus was not accurate enough to measure very small concentration (<1%) of elements and 2-microns thick aluminium coatings deposited with either yttrium or hafnium were sent to SNECMA in order to detect the presence of reactive element.
Both coatings were deposited on glass plate and were expected to contain at least 0.46 wt% of yttrium in the first case and 0.48 wt% in the second case.

A quantitative analysis was thus carried out using a Glow Discharge Mass Spectrometer and the results are given in the following table:

	Concentration (wt%) of reactive element in the aluminium coating	
	yttrium	**hafnium**
expected	0.46	0.48
experimental	0.25 +/- 0.05	0.60 +/- 0.10

Table 29: Concentration of reactive element in a 2-microns thick aluminium coating

6.4.4. Conclusion

The co-deposition of hafnium and yttrium with aluminium has been successfully implemented and the experimental technique allows the introduction of a small amount (<1wt%) of reactive element in the aluminium layers of the low-mass bondcoat.
This co-deposition was carried out by DC sputtering in placing a wire of re element on the aluminium target.
The co-deposition of reactive element with the platinum using the RF sputtering mode was conversely inefficient.

7. Cyclic oxidation test

Cyclic oxidation tests have been performed at 1100°C and 1200°C on samples coated with various low-mass bondcoats and with CN91 bondcoats. The purpose of these tests was to assess the oxidation behaviour in thermal cycling of the novel low-mass bondcoats relatively to commercial bondcoats.

7.1. Cyclic oxidation samples

7.1.1. As-deposited coatings

According to the process described in the 'experimental procedure ', which involves the computer assisted rotation of the samples between two plamas (rotation 1 of the Figure 119), different coatings have been deposited.

The substrates consisted of AM1 single crystal superalloy coupons (thickness: 2mm / diameter:14mm) and they were coated on both sides. In order to achieve a uniform deposition all around the samples, a second rotative motor was mounted to the sputtering chamber and connected to the samples to make them rotated in front of each target. This corresponds to the rotation 2 in the Figure 119.

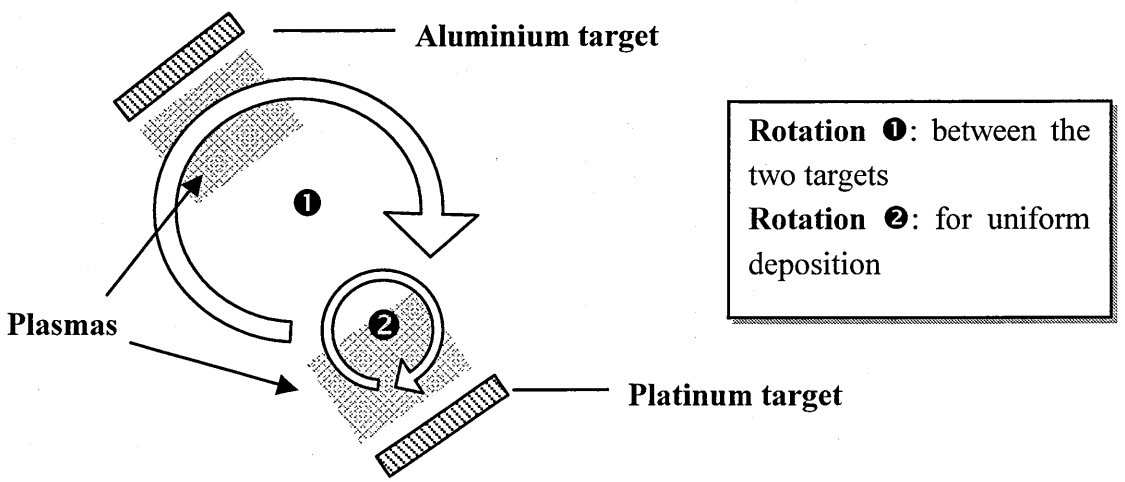

Figure 119: coating process for oxidation test samples

A deposition calibration of both platinum and aluminium target was carried out on rotating polished superalloy substrates to calculate the deposition rate during the rotation 2.

Target material	Sputtering mode	Power (W)	Deposition rate

Aluminium	DC	300	2.26µm/hr
Platinum	RF	420	0.64µm/hr

Table 30: Deposition calibration

3 different coating systems have been produced using the process and deposition data are gathered in the following table:

Expected Stoichiometry	Number of layers	Thickness	Pt layer thickness	Al layer thickness	Deposition duration
PtAl2	9	7.5 µm	0.45 µm	1.23 µm	5h40
PtAl2	167	7.5 µm	0.03 µm	0.066 µm	5h40
PtAl	180	7.75 µm	0.053 µm	0.05 µm	8h

Table 31: Deposition and coatings characteristics

7.1.2. As-reacted coatings

All the samples were hung in a furnace and heated at 700°C for 2 hours under an argon atmosphere. This heat-treatment is the reaction treatment detailed in the 'experimental procedure part'. It triggers the interdiffusion between the layers of platinum and aluminium and leads to the intermetallic formation via an exothermic reaction.

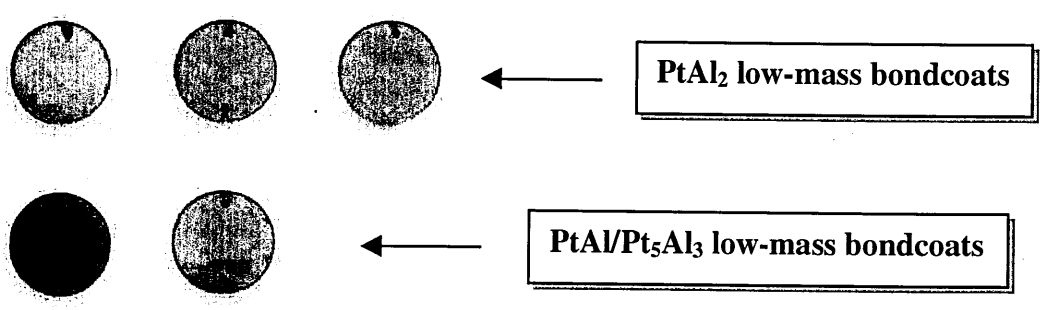

Figure 120: As-reacted 200-layer low-mass bondcoats

The Figure 120 shows the high multi-layered coatings PtAl and $PtAl_2$ after the reaction treatment. In the case of the $PtAl_2$, a shiny yellow colour has appeared and replaced the

initial grey colour. This is consistent with the previous results for such a coating system and it emphasises the formation of the $PtAl_2$ intermetallic compound.
In the case of the PtAl coatings, this phenomenon is less marked, but a slight yellow tinge is observable.
X-Ray diffraction analysis was carried out on the surface of the as-reacted samples to characterise the intermetallic compounds formation. Figure 121 accounts for the phases structure of the as–reacted 200-layer $PtAl_2$ and emphasises the formation of the single $PtAl_2$ phase.
Figure 122 accounts for the structure of the as-reacted 200-layer PtAl samples and emphasises the formation of PtAl and Pt_5Al_3.
These results show that the expected stoichiometry is observed for both coating systems after the layer reaction. The whole amount of material incorporated in the initial multi-layer coatings has reacted with a minimal interaction with the substrate. It proves thus that the bondcoat deposition and formation process controls accurately the final stoichiometry and structure of the bondcoat

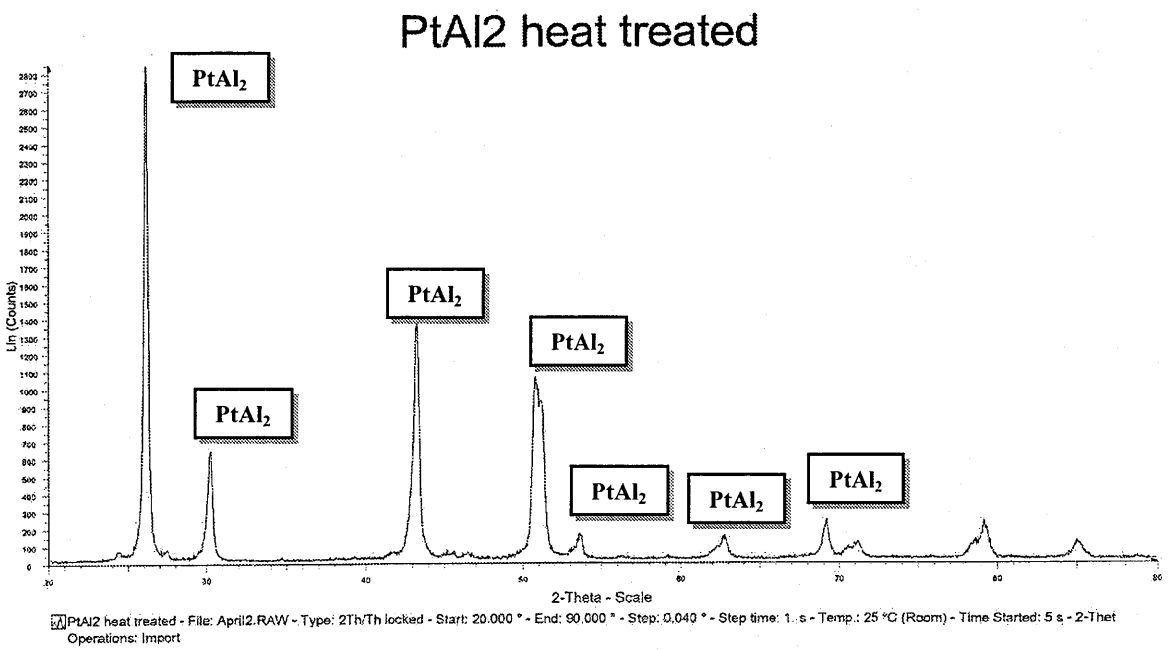

Figure 121: X-Ray diffraction spectrum of as-reacted 200-layer $PtAl_2$

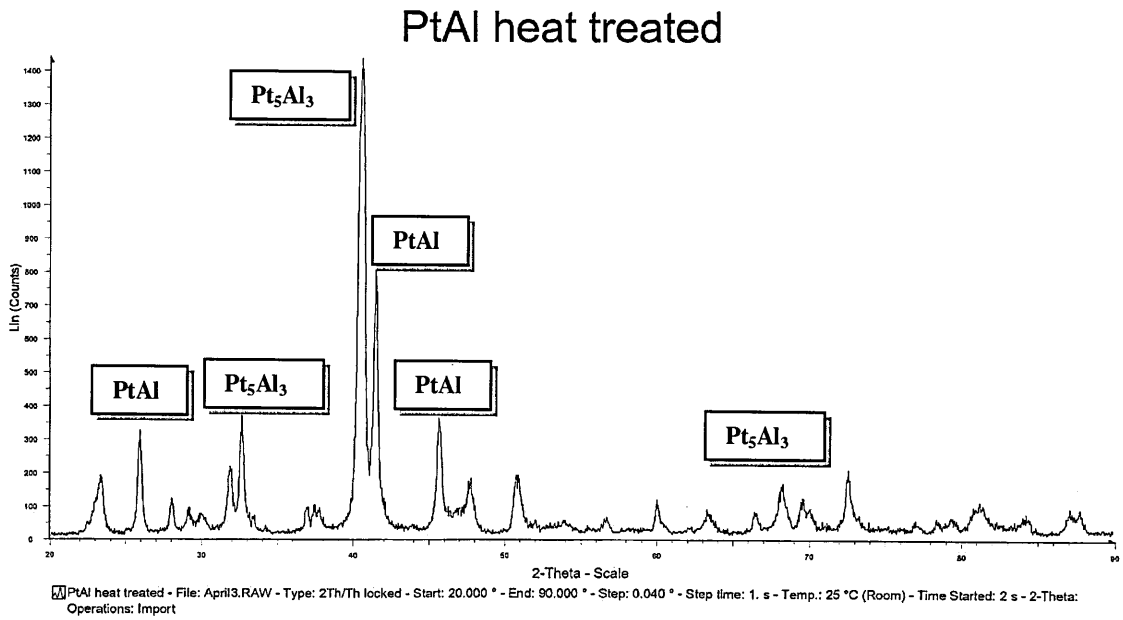

Figure 122: X-Ray diffraction spectrum of as-reacted 200-layer PtAl/Pt_5Al_3

Figure 123 depicts the 9-layer coatings after the reaction treatment. Delamination obviously occurred between the substrate and the multi-layer coating. Although bias sputtering was performed at the early stage of the deposition for this coating system, the bonding at the interface did not withstand the heat treatment and sufficient interdiffusion between the first platinum layer and the substrate did not have the time to happen. The lack of adherence, coupled with the multi-layer relieving the internal stresses, led to a wrinkled surface texture.

Figure 123: as-reacted 9-layer bondcoats

These 9-layer samples were not used in the further oxidation study.

7.1.3. CN91 bondcoats

These bondcoats, to be compared to the low-mass bondcoats, were deposited by Chromalloy UK. It consisted of single phase (Ni,Pt)Al platinum aluminides applied on the same substrates as the ones used for low-mass bondcoats deposition (2mm thick AM1 superalloy coupons/ diam. 14mm). Their thickness is about 80 microns (10 times as thick as the low-mass bondcoats)

7.2. Cyclic oxidation tests results

The cyclic oxidation resistance is a most important factor influencing the performance for the coated nickel or cobalt-based superalloy used in aircraft gas turbines. As summarised in Table 32, operation on military or short haul civil duty cycle induce many thermal cycles into the life of components (The duty cycle is defined as the typical mission time per engine start in hours). Cyclic oxidation tests are thus aimed at reproducing these conditions.

Gas turbine application	**Duty cycle(h)**		
	minimum	***mean***	***maximum***
Civil Aero gas turbine	1	2	8
Military Aero gas turbine	1	2	4
Industrial turbine /base power generation	500	2000	8000

Table 32: typical duty cycle for various gas turbine engines[70]

7.2.1. Cyclic oxidation common features

The life of components under thermal cycling condition depends on the laboratory facilities, and the cycle parameters (cooling rate, cycle frequency), but common features can be summarised:

All alloys that are protected by a stable, slow-growing oxide layer conform to a common behaviour under cyclic oxidation. This life cycle of such alloys involves first the formation of a stable protective scale. At a **critical thickness** this may start to spall increasing the rate of scale-forming element consumption. When the activity of such elements falls below a critical level, in the near surface region, internal oxidation results together with the formation of less protective scales. Ultimately, it is not longer possible for the alloy to self repair following a thermal cycle and then breakaway oxidation ensues, making the end of the life of the alloy[70].

During the **oxide growth stage** prior to the onset of spallation, the oxidation is usually parabolic and independent of the cycle freqency. This means that the oxidation kinetic during thermal cycling is virtually similar to the oxidation kinetic during isothermal oxidation.

During the early stage of oxidation, the mass gain and the alloy depletion depends also on the accumulated time at temperature.

The spallation onset is caused in a major part by the stress concentration in the oxide layer and at the interface with the bondcoat.
The oxide and bondcoat are nearly stress free at the peak temperature. However, on cooldown, tensile stress and plastic deformation are produced in the bondcoat leading to compressive stress in the oxide scale. Upon reheating, the enlarged bondcoat forces the oxide into tension[36] and can lead to scale cracking. Spallation usually occurs during the cooling step.
The onset of spallation depends on the cooling rate (the faster the cooling, the earlier the spallation onset) and on the nature of the bondcoat: for a given protective oxide, spallation will occurs readily for a stronger alloy, because it is less able to relieve thermally induced stresses during cooling by creep.

Once spallation has begun, the cyclic oxidation proceeds by continued spalling and rehealing and the mass of spall produced is thus a function of cycle freqency.

7.2.2. Furnace calibration

The cyclic oxidation tests were carried out using the Cranfield's cyclic oxidation rig depicted in the following figure.

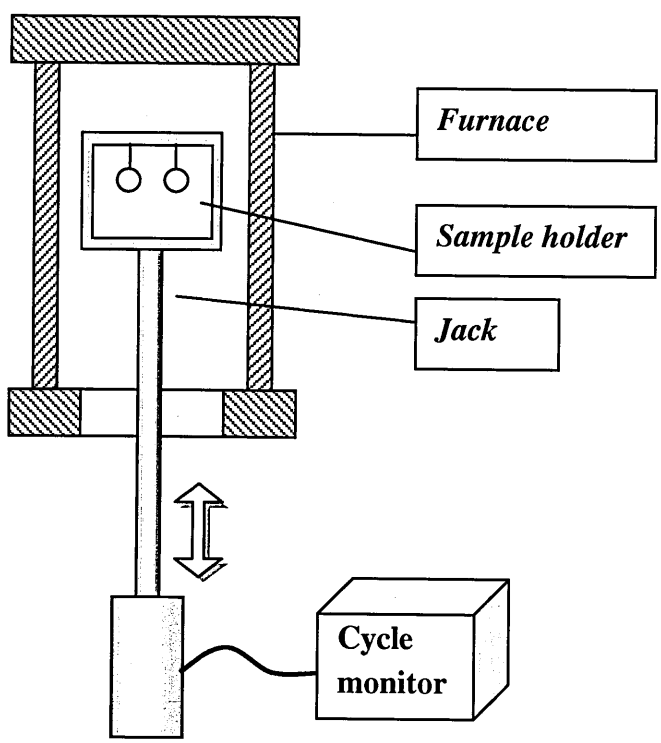

Figure 124: Cyclic oxidation rig

This rig is designed to cool the samples by air or water injection in the lower part of the apparatus. This functionality has however not been used because SNECMA's cyclic oxidation tests do not involve forced-air cooling.

A sample holder is mounted on a shaft, whose motion is controlled automatically to let the samples enter the hot part of the furnace as well as to bring them back to ambient temperature.
The temperature in the hot part of the furnace was checked by placing a thermocouple on the sample holder. A coupon of AM1 superalloy was actually welded to the top of the thermocouple in order to measure the closest temperature to the real temperature suffered by the coated samples during the thermal cycling.
A temperature evolution during a 1h-cycle run at 1200°C was recorded and it is represented on the following graph:

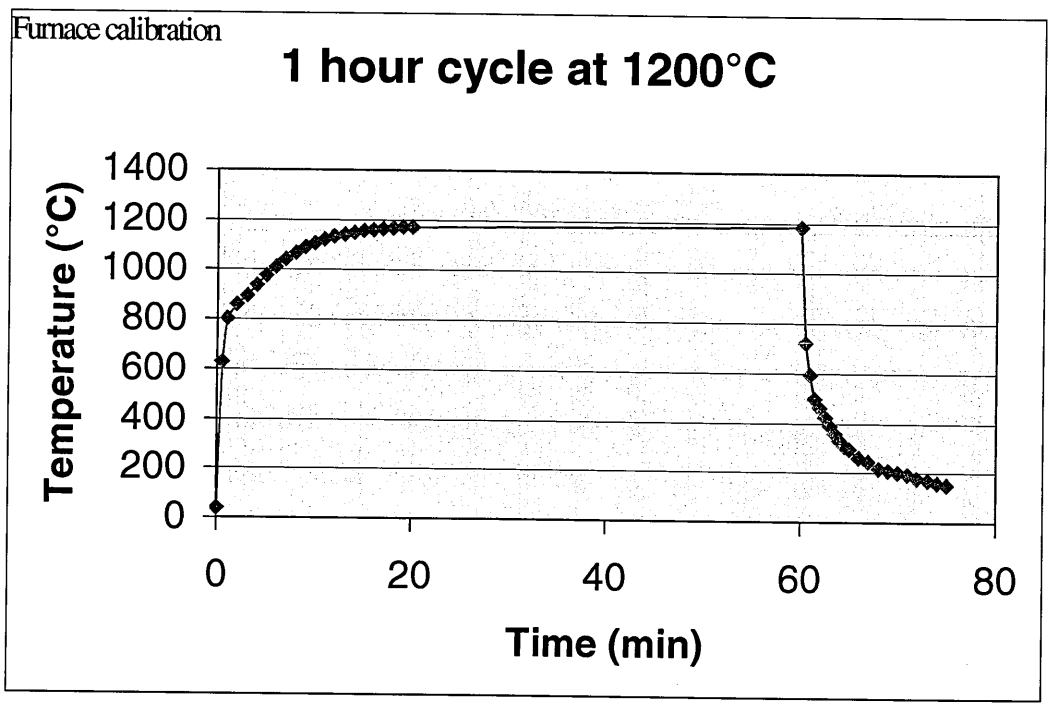

Figure 125: Temperature evolution during a 1hr-cycle run at 1200°C

The heating rate stands at 800°C/min during the first minute and then decreases progressively. 90% of the exposure temperature (1200°C) is reached in 9 minutes.
After 60 min., the temperature reaches 1190°C and the cooling step begins. The sample temperature drops from 1190 to 150°C in 15 minutes. This corresponds to a mean cooling rate of 69°C/min but it cools at 260°C/min during the first 3 minutes of cooling.

7.2.3. Oxidation at 1200°C

The following graph summarizes the weight changes during the first cycles of the test. As referred in the legend, 7 samples are plotted and consist of 3 SNECMA's bondcoats, 2 low-mass $PtAl_2$ and 2 low-mass PtAl bondcoats.

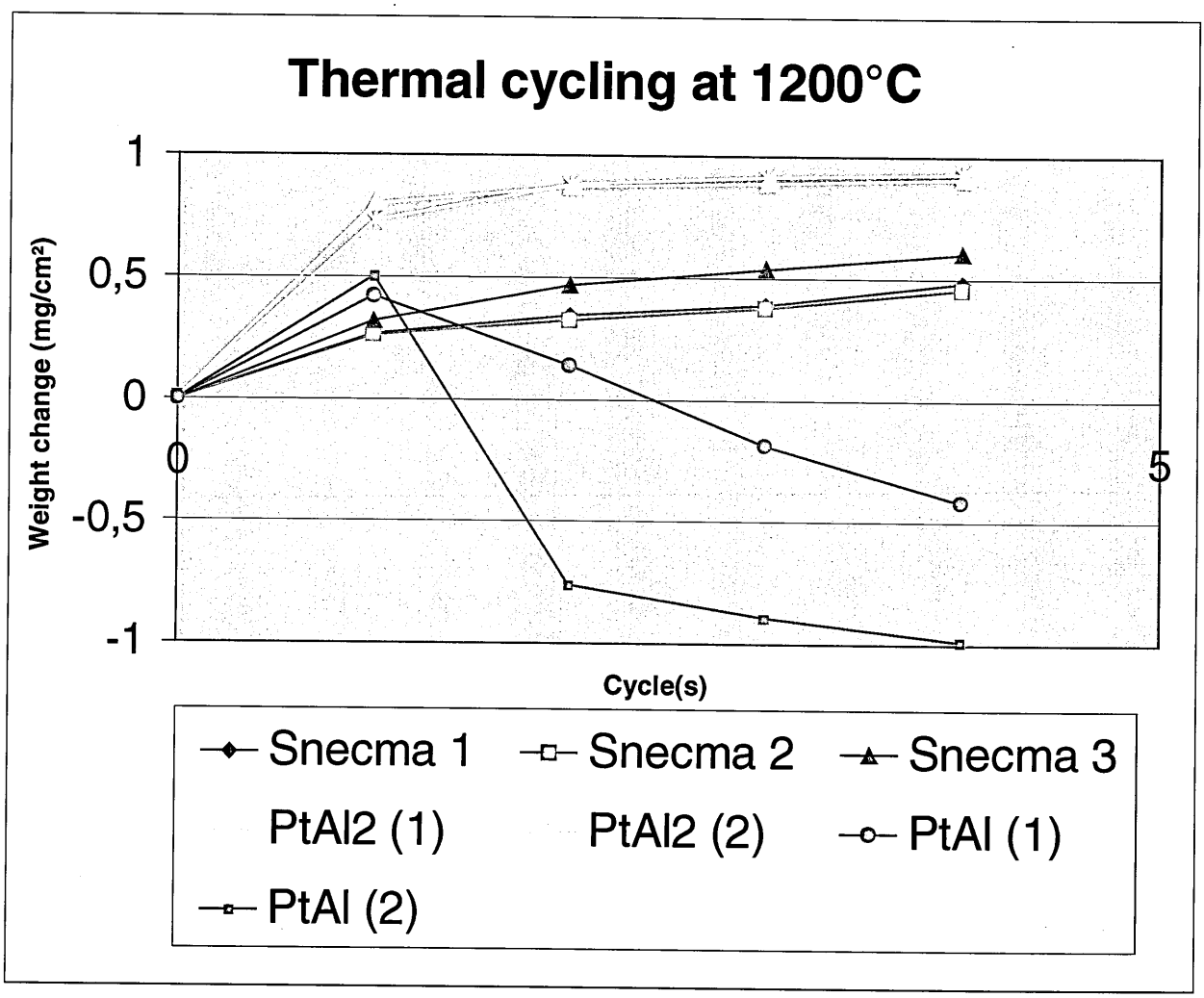

Figure 126: Weight changes for the first cycles

The first weight gain measurement indicates that the low-mass bondcoats have a higher oxidation rate that the SNECMA's platinum aluminides. This observation is especially true for the aluminium-rich $PtAl_2$, whose oxide scale is 3 times as thick as the oxide scale of the SNECMA's bondcoats after the first cycle.

The following cycles show however that the oxidation rate of the $PtAl_2$ low-mass bondcoat decreases significantly and becomes slower than the one of the SNECMA's bondcoats.

The former emphasises actually a non-parabolic oxidation kinetic for these low-mass bondcoats: they form very quickly a relative thick oxide scale, whose thickness remains virtually steady afterwards.
Conversely, the SNECMA's coatings have a parabolic oxidation rate and the oxide scale continues to grow progressively after a few cycles.
The SNECMA's bondcoat were initially dark blue and become grey during the cycling. The low-mass bondcoats lose their initial shiny yellow colour for a dark blue one after the first cycle.
The low-mass PtAl bondcoats failed after 2 cycles showing locally a few millimeters-large patches of spallation . This may be caused by :

- A lack of adherence between the bondcoat and the substrate
- A quick aluminium depletion in the bondcoat

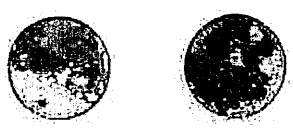

Figure 127: PtAl low-mass bondcoat after spallation

The explanation for the rapid spallation is however uncertain because no measurement has been made on failed samples.
The following graph accounts for the totality of the test until the failure of all samples.

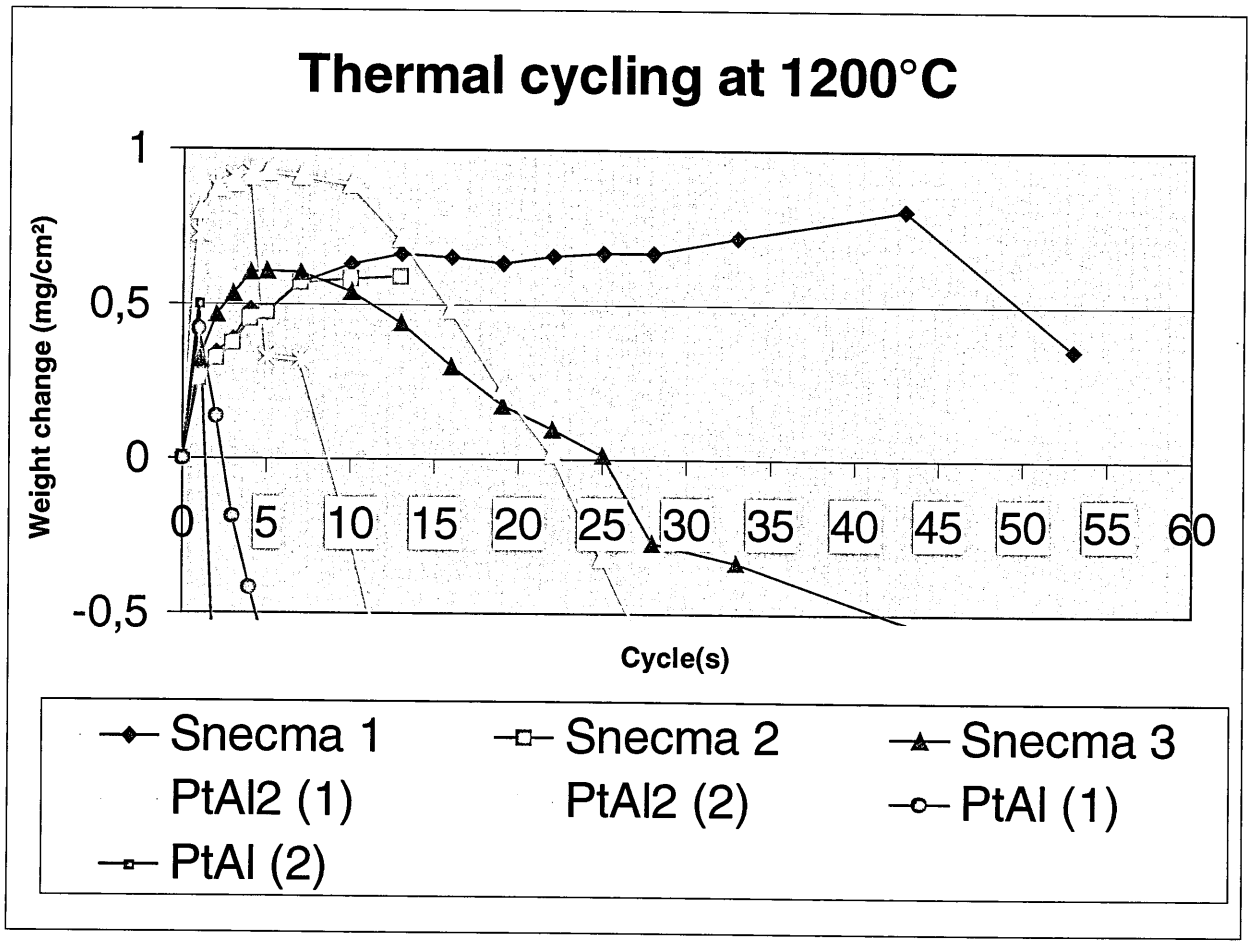

Figure 128: Weight changes for cyclic oxidation at 1200°C

In order to compare the life of the different coating systems, a failure indicator has to be defined. Usually, it can be set at the crossover between the weight change curve and the X-axis (cycles axis), or at the beginning of a dramatical weight loss. However, in the case of bondcoat oxidation for EB-PVD TBCs, oxide spallation means TBC failure; so, **the best life-indicator is the onset of spallation** and the first decrease in weight change will thus be used to assess the coatings systems. It has however to be noticed that it does not correspond exactly to the spallation onset: the weight change accounts indeed for the weight gained by oxide growth and also for the weight lost by spallation during a cycle thus spallation may commence before the peak in the weight change curve.

As observed in Figure 9, the first samples to fail are the low-mass PtAl, then the low-mass $PtAl_2$ bondcoats and finally the SNECMA's samples.

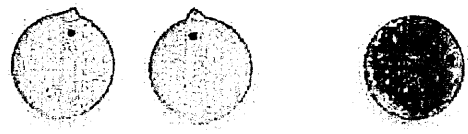

Figure 129: CN91 and $PtAl_2$ low-mass bondcoats after failure

As for the PtAl coating systems, the $PtAl_2$ ones exhibit a spallation by patches. At some locations, the coatings came off completely and the substrate can be seen.
The CN91 coating spalls are conversely smaller and evenly scattered but they are however numerous.
Even if the results show some dispersions, it is possible to draw few conclusions:

- The conditions were severe and could promote a rapid degradation mechanism due to phase instability, phase transformation, stress relaxation.
- At 1200°C, the cycle life of the PtAl2 low-mass bondcoat is 3 times as long as the PtAl low-mass bondcoat and are 5^{th} of that of the CN91 bondcoats (Table 30)
- The degradation is more accentuated for the $PtAl_2$ low-mass bondcoats than for the CN91 bondcoats. This mean that the latter have a better self-repair capability, which is probably due to their higher reservoir of aluminium. This phenomenon should not be taken into account because the desired oxide scale should not spall!

The mass changes record enables to calculate the oxide thickness which has grown until spallation. As we know the oxide density and the total surface of the sample, the critical thickness can be defined as follows:

$$Critical\ thickness = \frac{weight\ gain\ before\ spallation}{Total\ surface \times Oxide\ Density}$$

The following table gathers the different critical thicknesses relative to the tested samples:

samples	Cycles to spallation onset	Maximum weight gain (mg/cm^2)	Critical oxide thickness (µm)
SNECMA1	43	0,8	2,07
SNECMA3	7	0,6	1,55
$PtAl_2$ (1)	7	0,9	2,33
$PtAl_2$ (2)	5	0,9	2,33
PtAl (1)	2	0,5	1,37
PtAl (2)	2	0,5	1,37

Table 33: oxidation data

From these data, it is possible and relevant to calculate the total amount of aluminium consumed in the bondcoat during the high temperature oxidation. The number of oxide molecules can be determined from the oxide critical thickness using the following equation:

$$m_{Al_2O_3} = Oxide\ molecules \times \left(\frac{2 \times M_{Al} + 3 \times M_O}{Avogadro's\ number} \right) = \rho_{Al_2O_3} \times a \times S$$

a: critical thickness
S: oxide surface
ρ: density
M: molecular mass
m: weight

Once the number of moles of Al_2O_3 is known, the aluminium weight consumption is given by:

$$Al\ weight\ consumption = Al_2O_3\ molecules \times 2 \times M_{Al}$$

The following table gathers the aluminium consumption calculations for the tested samples:

samples	Aluminium consumption (g/cm²)	Initial Aluminium reservoir (g/cm²)	% of aluminium depletion
$PtAl_2$	$4{,}8.10^{-4}$	$13{,}45.10^{-4}$	36 %
PtAl	$2{,}8.10^{-4}$	$10{,}09.10^{-4}$	28 %
SNECMA1	$4{,}3.10^{-4}$		
SNECMA2	$3{,}2.10^{-4}$		
SNECMA3	$3{,}2.10^{-4}$		

Table 34: aluminium consumption data

The initial reservoir of aluminium was calculated using the sum of aluminium layers thickness for each coating system (5 µm for $PtAl_2$ and 3,75 µm for PtAl) and the density of aluminium (2,69 $g.cm^{-3}$).

The consumption of aluminium for the CN91 samples is not relevant, because spallation and self-repair cycles have already occurred a few times before a dramatic weight loss begins.

Finally, the aluminium content remaining in the bondcoat should allow the maintaining of the scale.

7.2.4. Cyclic oxidation at 1100°C

A cycle oxidation run was also performed at 1100°C with a 15 min cooling at ambient temperature.

The following graph emphasises the oxidation kinetics during the first few cycles of the test:

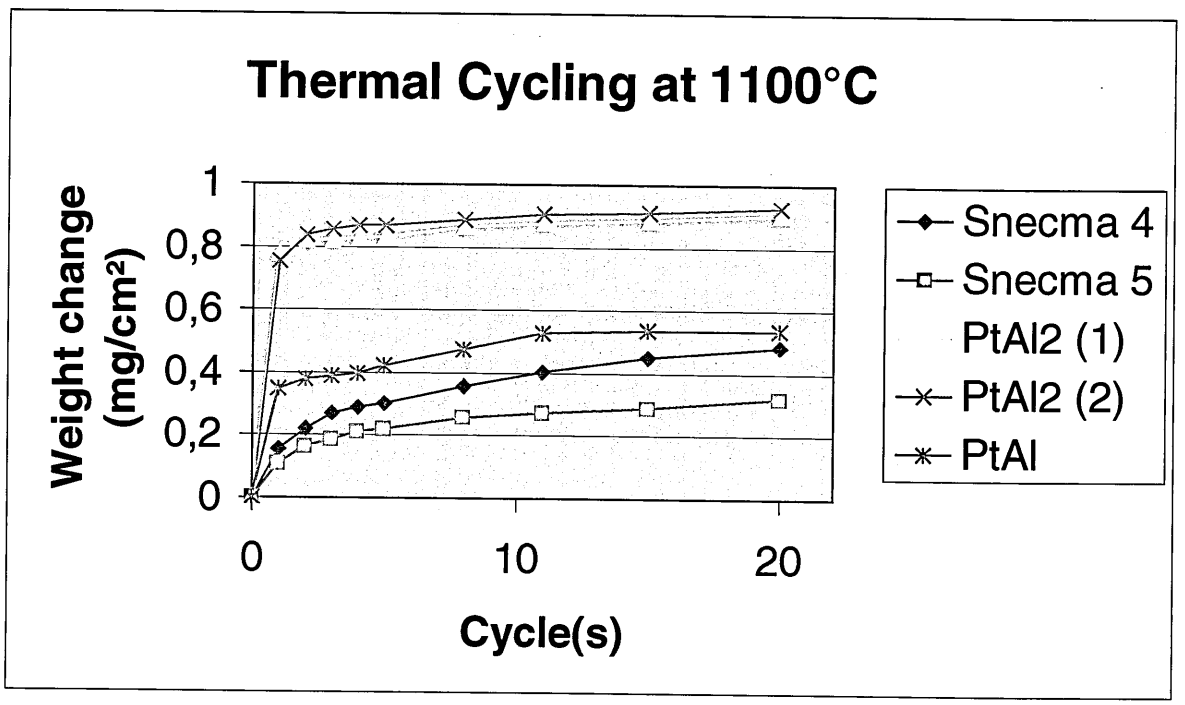

Figure 130: Weight changes for the first cycles at 1100°C

As for the test at 1200°C, the oxidation rate of the low-mass bondcoats is significantly higher during the first cycle, but decreases dramatically during the following cycles.

The weight gain is actually very similar at 1100°C and at 1200°C and the formation of the oxide scale seems independent of the temperature, which would be very unusual.

Figure 131 accounts for the results obtained after 100 cycles and highlights the onset of oxide spallation for the low-mass bondcoats. Because the exposure temperature is lower, the lifetime of the samples is longer, but the oxidation seems to exhibit the same relative evolution as seen at 1200°C.

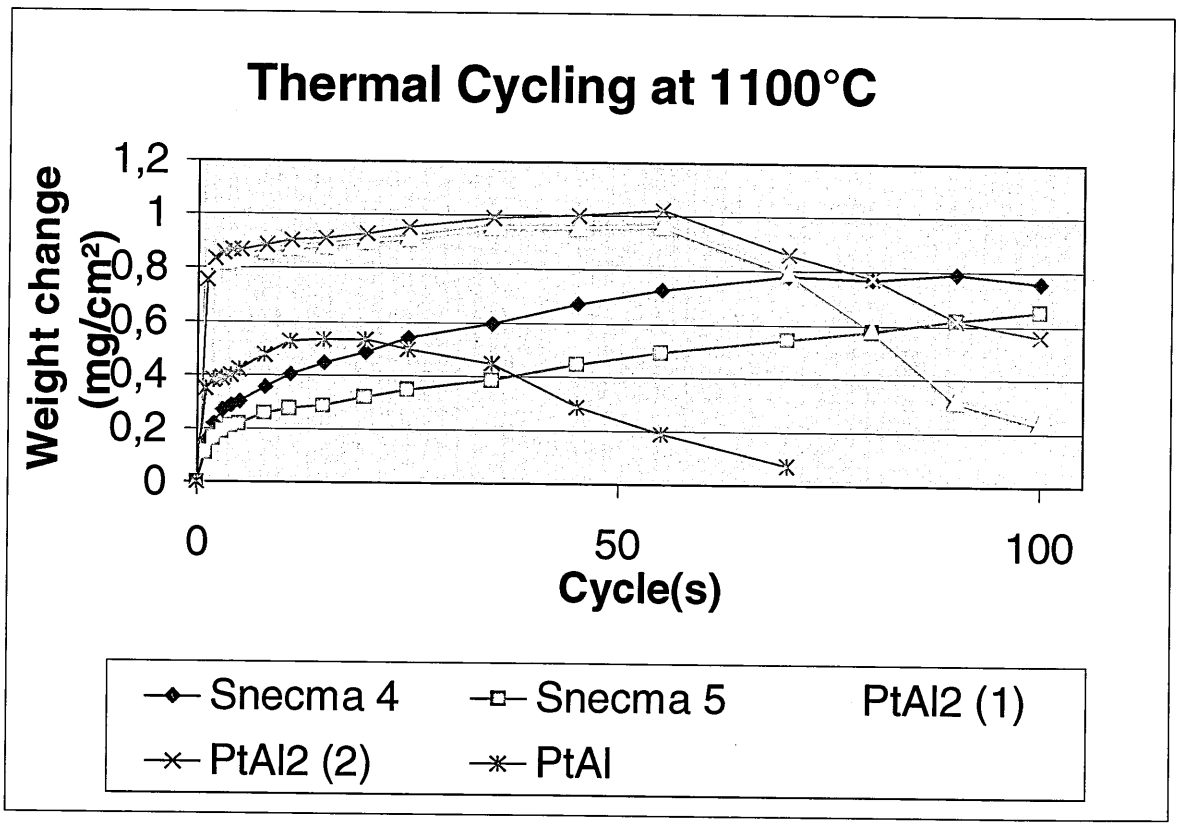

Figure 131: Weight changes for the first 100 cycles at 1100°C

As observed in Figure 131 and detailed in the Table 35, the life time of the low-mass bondcoats - whatever their stoichiometry- is ten times longer at 1100°C than at 1200°C. The critical oxide thickness is however virtually the same for both tests. Namely the aluminium depletion due to oxidation is about the same as the values calculated in the Table 34.

samples	Cycles to spallation onset	Maximum weight gain (mg/cm^2)	Critical oxide thickness (µm)
SNECMA 4			
SNECMA 5			
$PtAl_2$ (1)	70	0,96	2,46
$PtAl_2$ (2)	70	1,02	2,62
PtAl	25	0,53	1,37

Table 35: critical oxide thickness of the samples tested at 1100°C

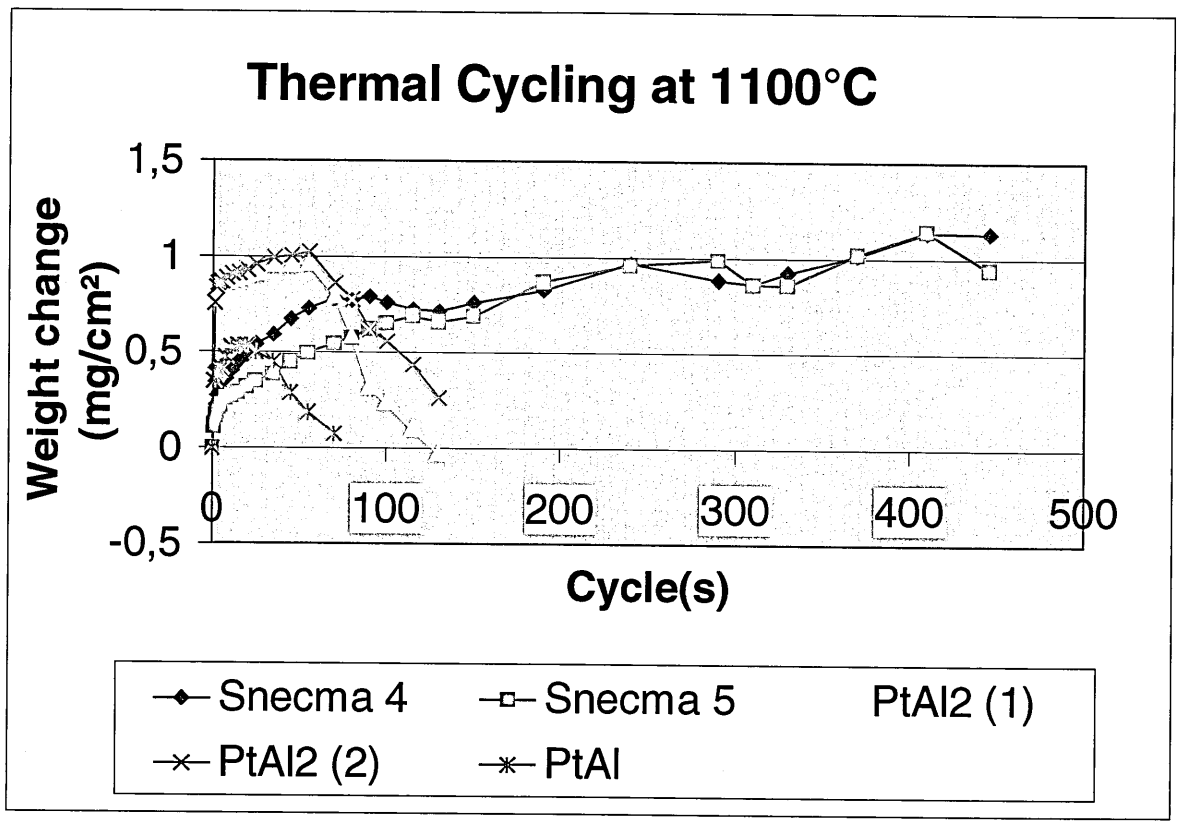

Figure 132: Weight changes for the complete cyclic oxidation test at 1100°C

Figure 132 shows the results of the test stopped after 450 cycles. The CN91 showed several weight change fluctuations, but did not begin a dramatical weight loss. The test had actually to be stopped because the time available for testing was too short.

7.3. Cyclic oxidation discussion:

In the case of the EB-PVD TBC application, the requirements for the bondcoat oxidation differs significantly from the oxidation of a protective coating. The self-repair capability for

instance is less relevant, because if the oxide layer spalls, the ceramic spalls as well and the TBC system fails.
The requirements for the optimal oxide scale are therefore to be:

- strongly adherent to the bondcoat
- rapidly formed, but slow-growing afterwards
- pure and dense as long as possible

The cyclic oxidation of the low-mass bondcoats exhibits a non-parabolic behaviour. The scale reaches virtually its final thickness during the first cycle and then grows very slowly. Such an oxidation mechanism could reduce the growth stress accumulation during service and prevent spallation.
The best way to assess the benefits of this scale is to test the bondcoat coated with a ceramic layer deposited on top.

The aluminium level in the low-mass bondcoats influences the initial oxidation rate. As observed in the results, the more aluminium in the bondcoat, the thicker the initial oxide scale, and the thicker the critical oxide thickness.

This aluminium concentration seems to affect also the spallation onset, since the PtAl scale fails before the PtAl2 one.
The bondcoat is actually an aluminium reservoir for the oxidation, but below a critical level, the stable alumina scale can not be maintained anymore.
For a simple aluminide coating[99], this critical level stands approximately at 17 %wt. Chan and al.[17] have modelled the degradation of platinum aluminide and determined that the aluminium critical level drops to about 9%wt (19%at).
Assuming these critical concentrations could be applicable for the low-mass bondcoats, the % of depletion from the Table 34 accounting for the oxidation at 1100°C and 1200°C show however that the aluminium level in the bondcoats after oxide spallation does not drop below this threshold. Even if the $PtAl_2$ bondcoats lose 38 % of aluminium and the PtAl 27%.
The scale should thus still be maintained by the bondcoat aluminium reservoir.

Possible explanation for oxide spallation are given below:

- The aluminium could diffuse in the substrate. Because it is thin, the low-mass bondcoat would be rapidly depleted in aluminium by inward diffusion.

- The thermal expansion mismatch between the bondcoat and the oxide could lead to the formation of cracks in the scale or to the propagation of voids at the interface with the bondcoat.

A X-ray diffraction analysis was performed on top of the $PtAl_2$ and PtAl bondcoats after failure and the predominant phase is alumina. Ni_3Al and traces of $NiAl_2O_4$ were also detected.

The X-ray analysis of the CN91 bondcoat after failure at 1200°C only showed the presence of alumina.
An Auger spectroscopy analysis of the failed low-mass bondcoat surface was also performed and emphasised the presence of the alumina phase. Some traces of chromium oxide were also detected (but no nickel oxide).

The predominant observation of the aluminium oxide phase is however expected because the other transcient oxides form at the interface between the alumina scale and the coating.

A further study of the low-mass bondcoat was then undertaken by carrying out SEM/EDS quantitative analysis of the coating surface and cross-section.
The surface analysis does not give reliable quantitative data because of gradients present in the coating, but it shows the presence of platinum, chromium, nickel, and titanium in, or under, the oxide scale.

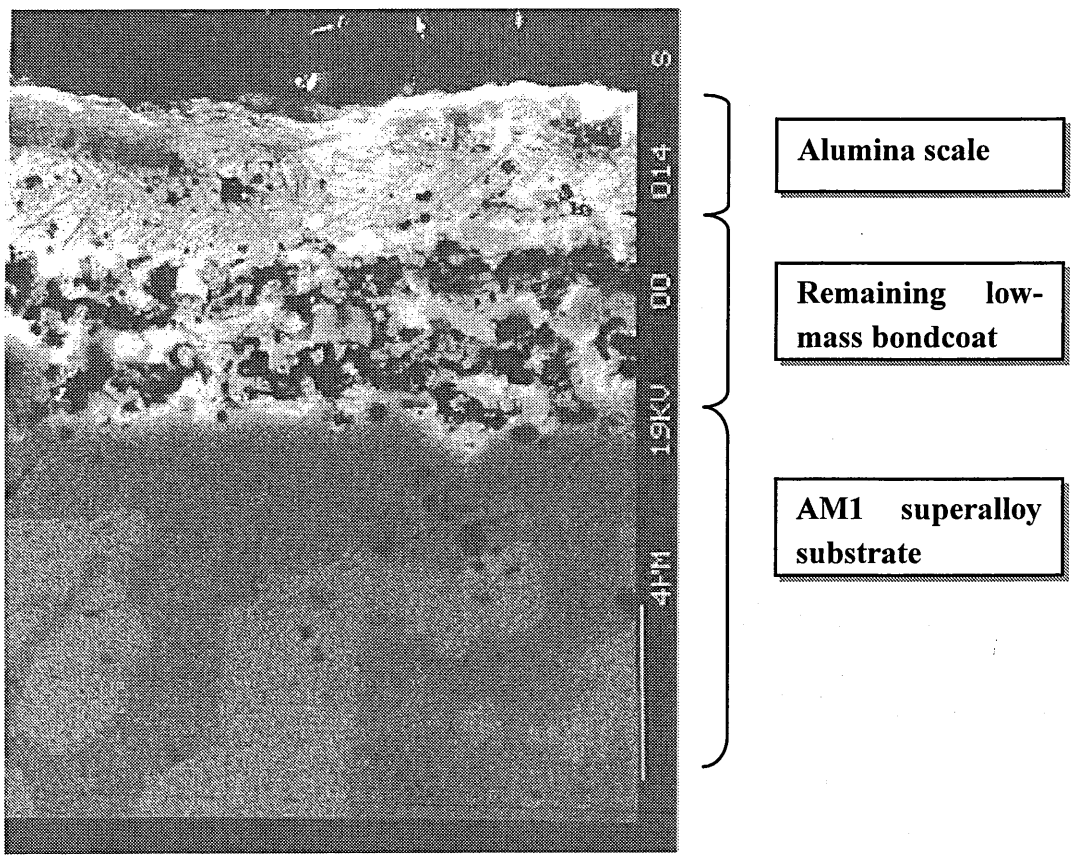

Figure 133: Secondary electron photograph of a $PtAl_2$ bondcoat failed at 1100°C

The cross-section analysis of the $PtAl_2$ bondcoat referred to the different zones of the Figure 133. The 2,5 microns thick outer zone consists of the **alumina scale**. Its thickness is coherent with the critical one calculated using the weight gain at the spallation onset. Apart from oxygen, it contains between 93 and 96 at % of aluminium, between 1 and 2 at% of chromium, between 1 and 4 at% of nickel, between 0,3 and 0,5 at % of platinum and traces (<1 at%) of titanium.

The underlying zone seems obviously less dense and more porous than the alumina scale. It consists of the remaining bondcoat layer. This micrographical observation has however to be carefully interpreted because the porosity could actually corresponds to a phase which has been removed during the sample polishing.

Its thickness is about 4 microns, which is less thick than the as-reacted coating before the cyclic oxidation test.

The quantitative analysis of this zone results in the following composition, from the oxide scale to the substrate: between 50 and 35 at% of aluminium, between 30 and 50 at% of nickel, between 1 and 3 at% of platinum, between 4 and 6 at% of cobalt, around 6 at% of chromium, between 3 and 4 at% of titanium, traces of molybdenum, tungsten and tantalum in the lower part.
The substrate composition near the bondcoat interface shows however more platinum (around 5 at%).

The bondcoat is therefore depleted in platinum, which diffused in the substrate. The composition of the remaining bondcoat could correspond to the Ni_3Al detected by X-ray diffraction, and to an internal oxidation promoted by the porosity.
The porosity is probably due to the outward diffusion of aluminium to maintain the alumina scale and to its inward diffusion into the substrate. This porosity is dramatic and led probably to the spallation of the oxide.

Finally, it is important to remember that the cyclic oxidation test undertaken in this work was not the best test to assess a bondcoat for a TBC system. However, relatively to the given time of the thesis, it was the only relevant test available to assess and compare the low-mass bondcoat to a commercial bondcoat.

8. Discussion

The development of a low-mass bondcoat for EB-PVD TBC was aimed to produce a thinner and more efficient bondcoat than the available commercial ones. For that purpose, the bondcoat requirements were:

- **Thermal stability**, that relies on the formation of an intermetallic structure. This structure is dependant on the composition which consists mainly of platinum and aluminium.
- The formation of a **pure, slow-growing alumina scale** on top of the bondcoat. The mechanism of oxidation has then to be controlled by the bondcoat composition and structure and is known to be improved by the introduction of a reactive element.
- The formation of an **thin overlay bondcoat**, whose deposition and formation does not imply an interaction with the substrate. This requirement comes along with the choice of a relevant deposition technique as well as the development of a multi-layer deposition concept

8.1. Bondcoat deposition and formation process

8.1.1. Accurate control of the deposition process:

The choice of the suitable deposition process drives the formation of a reliable low-mass bondcoat. Because Sputtering is a Physical Vapour deposition technique undertaken at a relative low temperature (300-400°C), diffusion processes are not activated and the substrate does not interact with the material ,which is deposited. Thus, each layer is built by condensations of atoms on top of the substrate. Such a coating can be referred as to an ***overlay coating***.

It is therefore possible to control accurately the thickness of each deposited layer and the bondcoat total thickness before the reaction treatment.

This control of the deposited material allows also to set up the stoichiometry before the deposition by calculating a thickness ratio between the layers.

The work detailed in this thesis highlights the successive deposition of platinum and aluminium layers with a thorough individual and total thickness control.

Moreover, the flexibility of the Cranfield's sputtering facility allows the deposition of another two different materials without opening the chamber held under vacuum. In other terms, successive layers of four different materials can be deposited to build a bondcoat

with an improved composition. Materials, such as nickel or rhenium could thus be added in order to improve the thermal stability.

Finally, the sequential depositions can be carried out automatically using a computer assisted rotation of the samples to be coated in front of each target. This technological improvement of the process offers a wide industrial scope, and enables also the alternate deposition of a multitude of very thin layers.

8.1.2. Control of the formation process

Complementary and subsequently to the deposition phase, a reaction treatment is carried out in order to trigger a reaction between the elements chosen for the bondcoat composition. This heat treatment leads to the formation of one or several intermetallic compounds, which was furthermore revealed to be exothermic. This allows to undertake the heat treatment at a relatively low temperature, which prevents, as for the deposition phase, any interdiffusion mechanism with the superalloy substrate.
Moreover this bondcoat formation technique has been proven to be accurately controllable and reproducible. The formation of a range of stable intermetallic bondcoats containing platinum and aluminium and with a control thickness has been carried out successfully in the thesis experimental work.
The final stoichiometry is directly connected to the thickness ratio fixed before the deposition phase, because of the low temperature of heat treatment, this does not initiate any interdiffusion with the substrate.
Moreover, the multi-layering has been shown to be a very important parameter of the process, since:

- It affects the temperature needed to trigger the exothermic reaction: when the number of layers is higher for a given total thickness, the number of interfaces and therefore the surface of reaction is increased and less energy is then needed to trigger the reaction between the two materials.
- It affects the bondcoat morphology as detailed in the next part of the discussion

Finally, a patent has been submitted in order to protect the potential industrial applications or subsequent developments of this coating formation process as well as the resulting bondcoat.

8.2. Low-mass bondcoat morphologies

The use of multi-layer systems with variable layer thicknesses has led to the development of bondcoats with different morphologies.
The following figure collates the microstructures obtained after the heat treatment to the initial number of layer (for a given bondcoat total thickness).

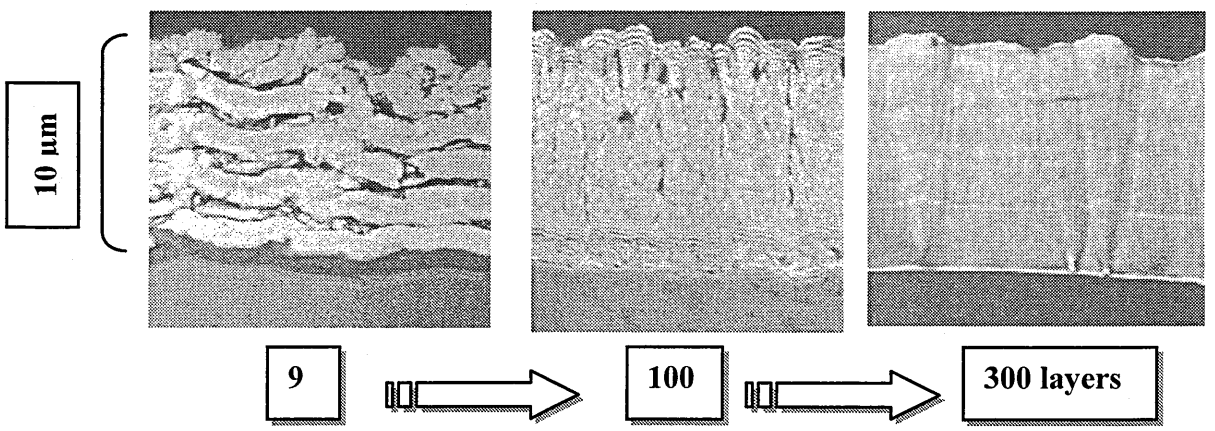

Figure 134: As-reacted coating morphologies

As observed here above and detailed in the thesis, two different bondcoat morphologies can be produced by the mode of layering:

8.2.1. Bondcoat with multi-layered structure

The first type of microstructure is observed when the ***initial number of layer is relatively small*** (9-layer of Figure 134) for a given total thickness –usually 10 microns-. After the reaction treatment, the structure still remains multi-layered and interfaces are present between the as-reacted layers of platinum aluminide. This structure was produced with initial 5- to 100-layer PtAl and $PtAl_2$ coatings, but the morphology is actually directly connected to the individual aluminium layer thickness.
During the reaction treatment, the aluminium, whose mobility is higher than the platinum one, diffuses in the platinum layers forming there platinum aluminide intermetallic compounds. However, interfaces remains between each intermetallic layer. These interfaces are thermally stable, because even after a further heat treatment at 700°C or 900°C (up to 16 hours), the multi-layered structure is still there.
In order to explain this phenomenon, X-ray analysis as well as Auger spectroscopy were carried out at the interfaces and showed the unique presence of alumina. The information

gathered by these analysis along with micrographies and adherence tests lead to the following **models for interface formation**:

1. During the sputtering deposition of aluminium, the very small amount of oxygen present in the chamber reacts spontaneously with the aluminium atoms, leading to the formation of alumina. This oxide is then deposited simultaneously with aluminium and the resulting layer embeds a second phase. During the subsequent reaction treatment usually at 700°C, the aluminium diffuses from the amorphous layer to the platinum layers, but the alumina phase does not diffuse because it is very stable and even more stable than any platinum aluminide compounds. When the former aluminium layers have been completely emptied, a thin interface made up of the deposited alumina remains between the platinum layers, which have swollen as a result of the aluminium diffusion.

The following figure illustrates the formation of an alumina interface in the case of a 3-layer initial coating and accordingly to this first model.

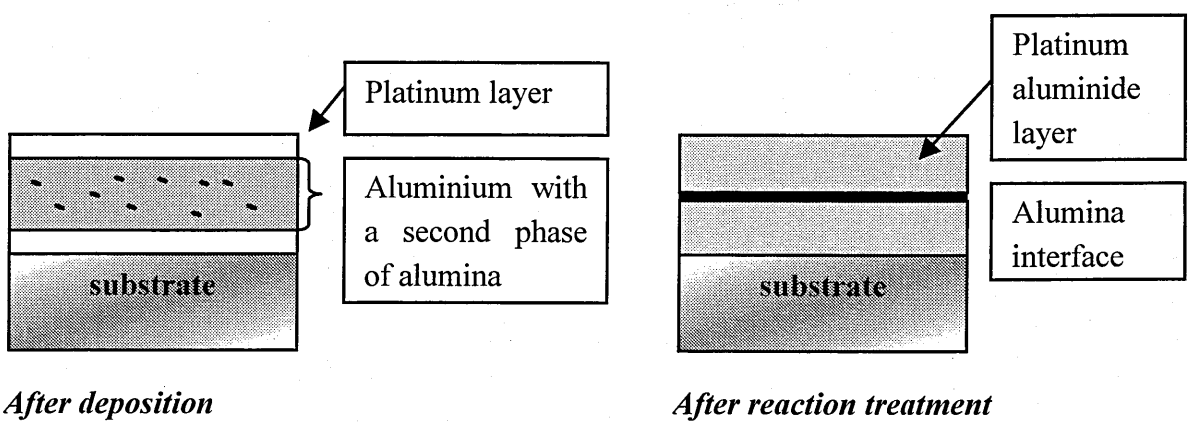

Figure 135: Formation of interfaces

2. the formation of an alumina film as interface between the platinum aluminide layers can also be produced when aluminium melts within the layers. This melting is promoted by the reaction treatment temperature being above the melting point of aluminium, but also by the heat released during the exothermic platinum aluminide formation. (this phenomenon occurred dramatically for the initial 10µm-thick 3-layer coating). The oxidation of molten aluminium is very fast and would explain the high diffusion of oxygen into all the aluminium layers. It would also explained the convoluted aspect of the coating after heat treatment, because the melting of a material induces a variation of volume.

Both models of interface formation are supported by the observations made on 3, 5 and 9-layer coatings. The relatively large number of adherence tests carried out on these samples showed that for a given total thickness, the higher the number of layers, the stronger the interfaces. When the aluminium layers are thinner, the proportion of alumina is the same but its amount is smaller. This means, that less alumina is present to form the interfaces, which will be thinner and therefore stronger. Thinner aluminium layers are also less prone to melt.

In order to avoid the presence of interfaces,

- a better vacuum is needed and a higher purity of the introduced argon gas must be obtained; these requirements are however difficult to fulfil because even a very low partial pressures of oxygen can generate the formation of alumina.
- The multi-layer coatings could be heat treated at a lower temperature but for a longer time (i.e. 10hrs @ 650°C).

The advantages and disadvantages of the above-detailed multi-layered type bondcoat are given are reminded as follows:

Advantages:

- After deposition and formation, the bondcoats are free of substrate elements such as W, Ti, Ta, Mo, Co, which are deleterious to the oxide scale adherence.
- Due to the bulk diffusion of relative thick aluminium layers into platinum layer, the morphology is not columnar and should be relatively dense.

Disadvantages:

- brittle interfaces between each layer can form
- relative weak adherence to the substrate may result from the lack of diffusion

8.2.2. Bondcoat with homogeneous structure

The second type of morphology is the microstructure of the **high multi-layered coatings**. Successive very thin layers (20-100nm) of platinum and aluminium have been deposited successively on superalloy substrate leading to more than 300 layers within a 10 microns coating.

An automatic rotation and dwell of the substrate holder has been programmed and implemented in the deposition chamber. The initial stoichiometry of the coatings is therefore controlled and any platinum aluminide intermetallic compound can be deposited easily.
The layers are so thin that:

- The exothermic reaction between aluminium and platinum begins already during the deposition (X-rays diffraction results).
- The growth of the coating is not interrupted by the layering, and leads to a columnar morphology which is characteristic to the PVD process.

Advantages:

- coating homogeneity and strength
- the bondcoat is free of substrate elements after its formation
- the bondcoat is strongly adherent to the substrate

Disadvantages:

- the columnar and fibrous morphology can probably promote oxygen diffusion and thus coating degradation.
- the more aluminium in the intermetallic composition, the sharper the aluminium depletion after subsequent heat treatments.

8.3. cyclic oxidation further analysis

The lifetime assessment of a coating in cyclic oxidation condition depends on its service function. In the case of a protective coating, the life time does not correspond to the first spallation: this coating is indeed design to maintain partially its protective function even after spallation. Its lifetime can thus be assessed at the inflexion point of the weight gain curve, when the weight loss becomes dramatic.
In the case of a bondcoat, the lifetime can be assessed at the first spallation, but it must be tested with the ceramic on top of it.
At SNECMA, the bondcoat without ceramic thermal barrier are always tested using the protective coating criteria, because even if the ceramic spalls, the underlying bondcoat must still protect partially the superalloy.
The duration of the cyclic oxidation test performed with the Cranfield's rig was not long enough to compare the life time of the SNECMA's and low-mass bondcoats as protective

coatings with the criteria detailed previously. These coatings were therefore compared by taking into account the onset of spallation of the oxide scale.

The lifetime indicator chosen for the Cranfield's test, was **the first loss of net mass gain** after the peak of the mass change curve. The net mass gain corresponds actually to the difference between the gross mass gain and the spalls weight. The thermally grown oxide can however spall before the first loss of net mass gain, if the gross mass gain is bigger than the mass of the spalls.

In order to assess more accurately the real spallation onset, a new original data representation has been evaluated. It consists of plotting the mass change relative to each cycle as a function of the time. Thus, each mass change/ time is the difference between the net mass gain after and before a cycle.

Mass change /time = Net mass gain at the end of a cycle – net mass change just before the cycle

When the mass was measured after several cycles, the mass change/time has to be divided by the number of cycles.

Such a representation is shown below for the results of the Cyclic oxidation test at 1100°C:

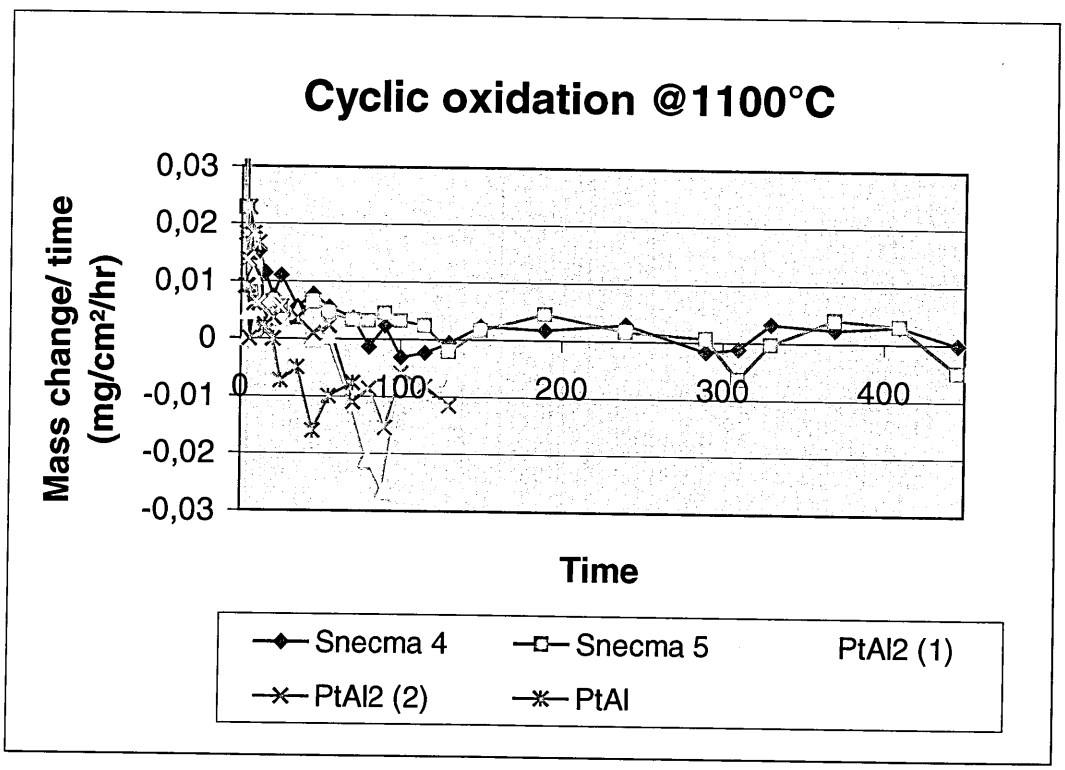

Figure 136: Relative mass change representation

This indicator accounts actually for the 'instantaneous' mass gain rate.
When the curve drops below the X-axis after a cycle, it means that the net mass gain has decreased and that the spallation mass was higher than the gross mass gain during this cycle. However it does not mean that spallation started at this point. Spallation can occur actually beforehand, but its value is hidden by the gross mass gain. A relevant point to look at is therefore an inflexion point located before the intersection of the curve with the X-axis.
The following figure provides a focus on the first few cycles of Figure 136 and enables the estimation of the first spallation for the studied samples:

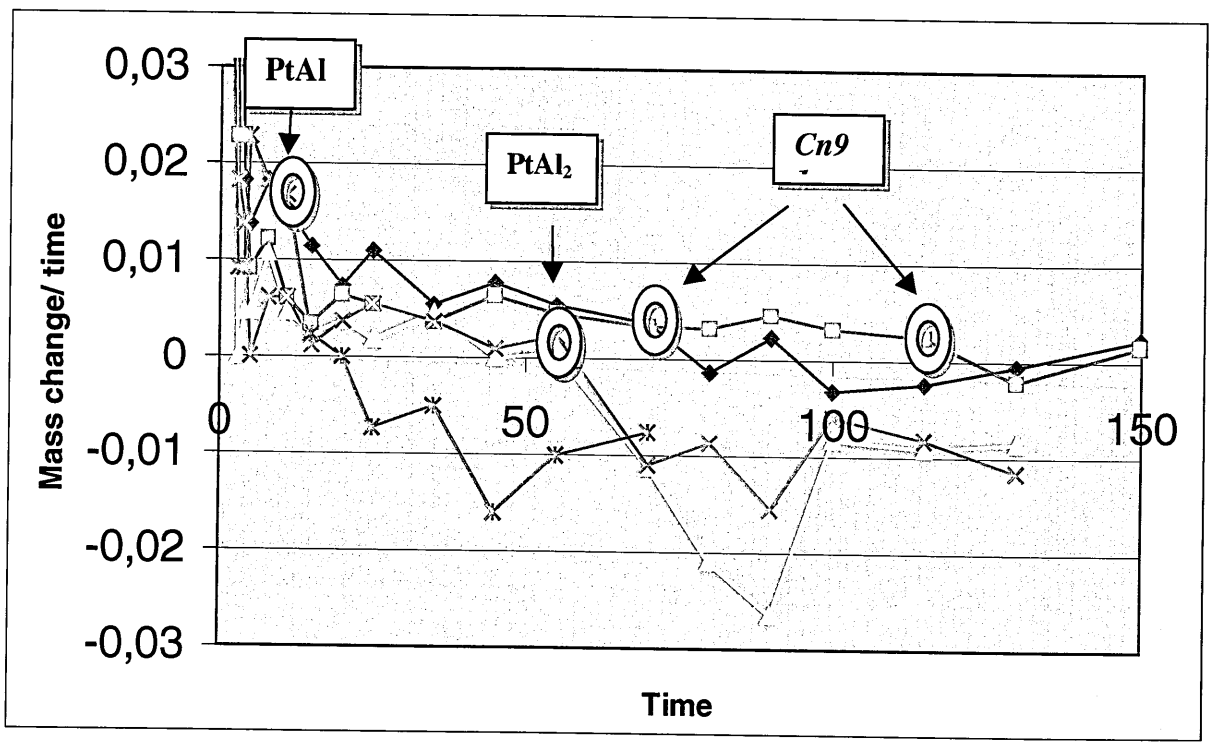

Figure 137: estimation of the first spallation

Figure 137 allows to rank more accurately the coatings performance for use under a TBC and can stimulate the behaviour as if the test was carried out with a real TBC system. This model assumes however that the spallation of the oxide induces directly the spallation of the ceramic topcoat.
These new results show firstly that the PtAl bondcoats still have a very short lifetime compared to the other bondcoats. Conversely, the lifetime of the $PtAl_2$ low-mass bondcoat comes closer to the Snecma diffusion Pt-Al bondcoats. On average, the Snecma's bondcoat lifetime is twice as long as the low-mass bondcoats to first spall. But in the cyclic oxidation

chapter and with the previous representation, it was reported to have more than 4 times the life.
If we consider these results relatively to the bondcoat thickness (80 microns for the CN91 and 10 microns for the low-mass bondcoats), the performance of the $PtAl_2$ low-mass bondcoats looks really promising with an increase in total thickness.

8.4. Factors of improvement

The work detailed in the thesis and synthesised in the present discussion have reported the properties and first performance of a new type of bondcoat. The potential of development of such a coating remains however significantly broad and is outlined in this following section:

Multi-layering

The multi-layering has shown its advantages and limitations, but has especially highlighted its major influence on the final bondcoat structure. During the deposition stage, the coating growth is dictated by the PVD processing and is affected by the temperature of the substrate. This latter parameter play a crucial role on the final density of the bondcoat: the higher the temperature, the higher the density. When the layers that composed the coating are thin and numerous, the reaction is promoted because of the multitude of interfaces. It has moreover been shown that this exothermic reaction could even be triggered during the deposition. This exothermic reaction brings heat by definition and raised the temperature where the deposited atoms condensate. It should therefore increase the density homogeneously through the coating made up of very thin layers!
The intrinsic density of the bondcoat is a most important parameter affecting its stability and diffusion barrier performance. It has however to be kept in mind that fibrous or columnar morphologies should be avoided because it is well known that such defects are short-cut path for diffusion. The intrinsic density is therefore not the only parameter to be taken into account. A trade-off must be found between the structure and the density.

Nickel addition

The deposition process enable the addition of nickel layers in the coating design and allows therefore the formation of ternary intermetallic compounds made up of platinum, aluminium and nickel. The bondcoat performance and thermal stability of platinum aluminide diffusion coatings have already been proven in aeronautical applications and it

would be extremely interesting to produce them without any interaction with the substrate material.

Graded bondcoat

The deposition and formation process enables also to vary the relative composition of the elements through the coating. This flexibility gives the opportunity to build a bondcoat by separating each of its functions and by producing a composition gradation.
The following figure accounts for an example of such a bondcoat gradation:

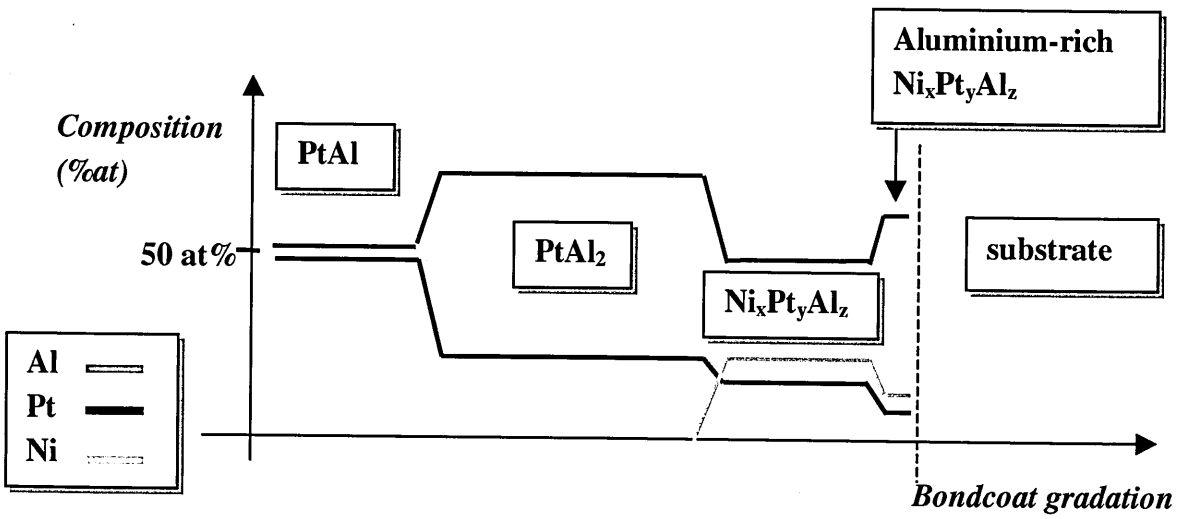

Figure 138: optimisation of the bondcoat performance by composition gradation

Referring to this gradation, an optimised bondcoat would consist of:

- A first layer of a platinum-rich intermetallic such as PtAl, that could control the oxidation rate and growth.
- A second layer, significantly thicker with a higher content in aluminium (i.e. $PtAl_2$), that would act as the aluminium reservoir.
- A third layer of a $Ni_xPt_yAl_z$ intermetallic compound, more stable than the previous layer, that would inhibit the interdiffusion with the substrate during service (the composition of the compound is arbitrary indexed, because it has not been studied yet).
- A last thin layer of an aluminium-rich intermetallic is incorporated to promote the adherence of the bondcoat with the superalloy substrate.

This bondcoat would be deposited in a continuous manner using the technique developed in this thesis and would have a subsequent reaction treatment at a temperature chosen in the range 700-900°C for a couple of hours.

Reactive element

The uniform introduction of a very small amount of a reactive element could also be taken into account in the bondcoat design. However, the current experimental work only allows to co-deposit such an element with aluminium but does not prove whether it influences the oxidation mechanism or gives any performance improvement in the lifetime duration of a TBC system.

Bondcoat thickness

Even if the oxide scale growth does not consume all the aluminium from the low-mass bondcoat, it induces phase transformation and vacancy coalescence through it. This leads to the formation of interconnected porosity, defects and contributes therefore to the bondcoat degradation.

A solution to improve the bondcoat stability would be to increase its whole thickness: the aluminium reservoir would be more consequent and its consumption would affect less significantly the atomic and morphological bondcoat structure.

This improvement in performance has however to be considered relatively to its cost if the bondcoat application is undertaken in an industrial context.

Conclusions:

- A new concept of coating has been developed for a bondcoat application as part of a Thermal Barrier system.
- This bondcoat has been produced by depositing alternatively platinum and aluminium layers using the sputtering technique and by carrying out a heat treatment in order to trigger an exothermic reaction between the layers.
- The choice of the materials, the technique of deposition as well as the process of formation lead to a thin intermetallic layer whose expected properties are extremely promising and beneficial to fulfil the bondcoat requirements within a TBC system.
- For a given total bondcoat thickness, the structure is controllable by decreasing the thicknesses of the deposited layers: the structure remains multi-layered when the number of layer is relatively low, but can be homogeneous when the number of layers is relatively high.
- The composition of the bondcoat is controllable -even during the deposition- by modifying the thickness ratio between the platinum and aluminium layers.
- The composition and microstructure of the bondcoat can be programmed and automatically carried out using a computer-assisted rotation of the samples to be coating during the sputtering deposition.
- A reactive element, which consists of either zirconium, yttrium or hafnium has been introduced into the aluminium layer by sputtering co-deposition and it has been therefore demonstrated the possibility of improving the efficiency of the low-mass bondcoat by adding such an element evenly through the coating.
- Whatever the composition or its structure, the low-mass bondcoat is adherent to the substrate and does not interact with the substrate during the deposition and the formation process.
- The bondcoat is thermally stable for a significant time of aging at 700°C, 900°C and 1100°C.

Further Work:

Bondcoat improvements

- Further experimental work has to be done to control the morphology of the bondcoat using the deposition parameters and the coating structure design.
- A third metallic element such as nickel can be added in the bondcoat using the process detailed in this thesis and the flexibility of the Cranfield's sputtering facilities. The introduction of such an element should improve the thermal stability of the bondcoat under high temperature conditions.
- A graded coating can be produced to optimise the bondcoat design.
- A reactive element has to be added evenly in the bondcoat in order to slow the oxide scale growth.
- The thickness of the bondcoat can be increased in order to obtain a bigger aluminium reservoir
- Longer reaction treatment at a lower temperature (6hrs at 650°C) can be assessed to prevent the melting of aluminium and to avoid the formation of a multi-layered bondcoat.

Study of the oxidation mechanism

- The degradation mechanism has to be better understood in order to target the directions of improvement.
- For this purpose, it would be interesting to study the oxide scale at different stage of the oxidation, especially through the earlier stages.

Assessment in a TBC system

- The assessment of the low-mass bondcoat within a Thermal Barrier system is the best way to highlight its performance: for this purpose, a ceramic topcoat has to be deposited onto it and a subsequent cyclic oxidation test has to be carried out.
- A number of commercial TBC systems have to be included in the test in order to give a relevant comparison.

Reference List

1. Allam, I. M., Akuezue, H. C., and Whittle, D. P. *Influence of small platinum additions on Al_2O_3 scale adherence*. Oxidation of metals 14(6), 517-530. 1980.

2. Alperine, S., Derien, M., Jaslier, Y., and Mevrel, R. *Thermal Barrier coatings: The Thermal conductivity challenge*. Proceeding of the 85th meeting of the Agard Structures and Materials panel . 1997.

3. Arana, C. A. *The effect of TBC utilization in the design of robust aircraft combustors*. AGARD. Proceeding of the 85th meeting of Agard structures and material panels. 1997.

4. Aurrecoecha, J. M., Hsu, L. L., and Kubarych, K. G. *Field experience of platinum aluminide coated turbine blades*. Materials and Manufacturing Processes 10(5), 1037-1051. 1995.

5. Bauer, R., Schneider, K., and Grunling, H.W. *Experience with platinum aluminide coatings in land-based gas turbines*. High Temperature Technology **3**, 59-64 .1985.

6. Bell, S.R., Wing, R.G., and Wood, J.L. *EB-PVD TBC for industrial gas turbine*.

7. Bennett, A. *Properties of thermal barrier coatings*. Materials Science and Technology 3(2), 257-261. 1986.

8. Berstein, H.L. and Allen, J.M. *Analysis of cracked gas turbine blades* . Journal of Engineering for gas turbines and power **114**, 293-300 .1992.

9. Bessot, J.J. *Depots par pulverisation cathodique*. Techniques de l'ingenieur **M1657**, 1-24 .1985.

10. Blocher, J.M. *Chemical Vapor Deposition*. Metals Handbook: Surface cleaning, finishing and coatings.1982.

11. Boone, D. H. *Physical vapour deposition processes*. Materials Science and Technology 2(3), 220-223. 1986.

12. Brentnall, W. D., Aurrecoecha, J. M., Rimlinger, C. M., Harris, K., Erikson, G. L.,

and Wahl, J. B. *Extensive industrial gas turbine experience with second generation single crystal alloy turbine blades.* International Gas Turbine and aeroengine Congress and Exhibition, Orlando, Florida . 1997.

13. Broomfield, R. W., Ford, D. A., Bhangu, H. K., Thomas, M. C., Frasier, D. J., Burkholder, P. S., Harris, K., Erikson, G. L., and Wahl, J. B. *Development and turbine engine performance of three advanced rhenium containing superalloys for single crystal and directionally solidified blades and vanes.* International Gas Turbine and aeroengine Congress and Exhibition, Orlando, Florida . 1997.

14. Budinski, K.G. Surface Engineering. *Engineering Materials: Properties and Selection.*

15. Bull, S.J. *Microscopy of failure in the scratch adhesion testing of oxide scales.* Microscopy of oxidation 3 309-319.1996.

16. Chalker, P.R. *Characterisation of coatings and interfaces.* In Rickerby, D.S. and Matthews, A. (eds.) Advanced Surface Coatings: a handbook of surface engineering. Glasgow and London .1991.

17. Chan, K.S., Cheruvu, N.S., and Leverant, G.R. *Coating life prediction under cyclic oxidation conditions.* Journal of Engineering for gas turbines and power **120**, 609-614 .1998.

18. Chapman, B. *Glow Discharge Process, Sputtering and Plasma etching.* John Wiley & Sons, New York .1980.

19. Chen, J.H. and Little, J.A. *Degradation of the platinum aluminide coating on CMSX4 at 1100°C.* Surface and Coatings Technology **92**, 69-77 .1997.

20. Crabos, F., Marin, F., and Monge-Cadet, P. *Les revetements MCrAlY dans les Turbines a Gaz* . Surfair XII . 1998.

21. Czech, N., Fietzeck, H., Juez-Lorenzo, M., Kolarik, V., and Stamm, W. *Studies of the bondcoat oxidation and phase structure of TBC.* Surface and Coatings Technology 113, 157-164. 1999.

22. Deakin, M. J. *Surface coatings on Titanium alloys to limit oxygen ingress.* PHD Thesis, Cranfield University . 1995.

23. Deakin, M. J. and Nicholls, J. R. *Diffusion Barrier Layers.* Patent n° US 5741604 .1998.

24. Dearnaley, G. *Ion implantation and ion-assisted coating.* In Rickerby, D.S. and Matthews, A. (eds.) Advanced Surface Coatings: a handbook of surface engineering. Glasgow and London .1991.

25. Dinwiddie, R. B., Beecher, S. C., Nagaraj, B. A, and Moore, C. S. *Thermal Transport in Zirconia Thermal Barrier Coating.* NASA TBC Workshop . 1995.

26. Doychak, J. *Oxidation behavior of high temperature intermetallics.* Nasa Lewis Research center **1**, .1994.

27. Duret, C., Mevrel, R., and Pichoir, R. *Aluminide coatings on superalloys.* In Kossowsky, R. and Singhal, S.C. (eds.) Surface Engineering.1983.

28. Eaton, H. E., Bornstein, N. S., and DeMasi-Marcin, J. T. *The effects of environmental contaminants on industrial gas turbine thermal barrier coatings.* International Gas Turbine and aeroengine Congress and Exhibition, Birmingham, UK . 1996.

29. Fauchais, P., Vardelle, A., and Vardelle, M. *Recent developments in plasma sprayed TBC.* Proceeding of the 85th meeting of the Agard Structures and Materials panel . 1997.

30. Felten, E.J. and Pettit, F.S. *Development, Growth, and Adhesion of Al_2O_3 on platinum-aluminium alloys.* Oxidation of metals **10**, 189-223 .1976.

31. Fisher, G. *The optimisation of bondcoat oxides for improved thermal barrier coating adhesion* . PHD Thesis, Cranfield University . 1998.

32. Fisher, G., Datta, P.K., Burnell-Gray, J.S., Chan, W.Y., and Soares, J.C. *The effects of active element additions on the oxidation performances of a platinum aluminide coating at 1100°C.* Surface and Coatings Technology **110**, 24-30 .1998.

33. Foutain, J.G., Golightly, F.A., Stott, F.H., and Wood, G.C. *The influence of platinum on the maintenance of α–Al_2O_3 as a protective scale.* Oxidation of metals **10**, 341-345 .1976.

34. Freborg A.M., Ferguson, B.L., Brinley, W.J., and Petrus, G.J. *Modeling oxidation induced stresses in thermal barrier coatings.* Materials Science and Engineering 182-

190 .1998.

35. Gallagher, P.K. Instrumentation, techniques and methodology.

36. Gell, M., Vaidyanathan, K., Barber, B., Cheng, J., and Jordan, E. *Mechanism of spallation in platinum aluminide/EB-PVD TBC.* Metallurgical and materials transactions A **30A**, 427-435 .1999.

37. Gobel, M., Rahmel, A., Schutze, M., Schorr, M., and Wu, W.T. *Interdiffusion between the platinum-modified aluminide coating RT 22 and nickel-based single-crystal superalloys at 1000 and 1200°C.* Materials at high temperatures **12**, 301-309 .1994.

38. Golightly, F.A., Stott, F.H., and Wood, G.C. *The influence of yttrium additions on the oxide adhesion to an iron-chromium-aluminium alloy.* Oxidation of metals **10**, 163-187 .1976.

39. Goward, G. W. *Protective coatings- purpose, role, and design.* Materials Science and Technology 2(3), 194-200. 1986.

40. Goward, G. W. *Progress in coatings for gas turbine airfoils.* Surface and Coatings Technology 108, 73-79. 1998.

41. Haubold, T., Gans, H., Schwingel, D., and Taylor, R. *On thick Thermal Barriers for combustor application.* Proceeding of the 85th meeting of the Agard Structures and Materials panel . 1997.

42. Hitchman, M.L. and Jensen, K.F. *Chemical Vapor Deposition: Principles and Applications.* 1993.

43. Hochman, R.F. *Ion implantation.* Metals Handbook: Surface cleaning, finishing and coatings.1982.

44. Hochman, R.F. and Mattox, D.M. *Ion plating.* Metals Handbook: Surface cleaning, finishing and coatings.1982.

45. Honnorat, Y. and Morbioli, R. *Corrosion and oxidation protections in aeronautical engines by vapor phase processes.* Coatings for heat engines, NATO Advanced Workshop.

46. Hoppin, G.S. and Danesi, W.P. *Future of superalloys.* Superalloy II .1987.

47. Hou, P.Y. and Smialek, J.L. *Effect of sulphur removal by H2-annealing on the oxidation behaviour of a Ni-25Cr alloy.* Scripta Metallurgirca et Materiala **33**, 1409-1416 .1995.

48. Huenecke, K. *Jet Engines: Fundamentals of theory, design and operation.* Airlife publishing .1997.

49. Jaslier, Y. and Alperine, S. *EB-PVD TBCs: a comparative evaluation of competing deposition technologies.* AGARD, 85th meeting of the structures and materials panel . 1997.

50. Katsman, A., Grabke, H.J., and Levin, L. *Penetration of oxygen along grain boundaries during oxidation of alloys and intermetallics.* Oxidation of metals **46**, 313-331 .1996.

51. Kaysser, W. A., Peters, M., Fritscher, K., and Schulz, U. *Processing, characterisation and testing of EB-PVD thermal barrier coatings.* Proceeding of the 85th meeting of Agard structures and material panels. 1997.

52. Khanna, A.S., Wasserfuhr, C., Quadakkers, W.J., and Nickel, H. *Addition of Yttrium, Cerium and Hafnium to combat the deleterious effect of sulphur impurity during oxidation of an Ni-Cr-Al Alloy.* Materials Science and Engineering **A120** .1989.

53. Kingswell, R. and Scott, K.T. *Thermal spraying.* In Rickerby, D.S. and Matthews, A. (eds.) Advanced Surface Coatings: a handbook of surface engineering. Blackie, London and Glasgow .1991.

54. Krishna, G.R., Das, D.K., Singh, V., and Joshi, S.V. *Role of Pt content in the microstructural development and oxidation performance of Pt-aluminide coatings produced using a high activity aluminizing process.* Materials Science and Engineering **A251**, 40-47 .1998.

55. Larikov, L.N. *Diffusion.* In Westbrook, J.H. and Fleischer, R.L. (eds.) Intermetallics compounds: Principle and Practice.1994.

56. Lawson, K. J., Nicholls, J. R., and Rickerby, D. S. *The effect of coating thickness on the thermal conductivity of CVD and PVD coatings.* 4th International Conference on Advances in Surface Engineering. 1996.

57. Le Gall, R., Saindrenan, G., and Roptin, D. *Les segregations interfaciales du soufre*

au cours de la restauration de la structure du nickel ecroui. Memoires et etudes scientifiques Revue de metallurgie 99-107 .1991.

58. Lees, D.G. *On the reasons for the effects of dispersions of stable oxides and additions of reactive elements on the adhesion and growth mechanisms of chromia and alumina scales.* Oxidation of metals **27**. 1987.

59. Leyland, A. and James, A.S. *Evaporation.* In Rickerby, D.S. and Matthews, A. (eds.) Advanced Surface Coatings: a handbook of surface engineering. London and Glasgow .1991.

60. Lugscheider, E., Barimani, C., and Dopper, G. *Ceramic thermal barrier coatings deposited with the electron beam-physical vapour deposition technique.* Surface and Coatings Technology , 1221-1227. 1998.

61. Malie, A. and Arnault, V. *Influence sur la conductivite thermique de la morphologie des couches ceramiques obtenues par EBPVD.* Conference SURFAIR XII. .1998.

62. Mazars, P. *Les procedes industriels de protection des superalliages.* Traitement thermique 37-42 .1980.

63. Mazars, P., Manesse, D., and Leroy, M. *Les differents traitements thermochimiques d'aluminisation.* Traitement thermique 25-32 .1987.

64. McMordie, B. G. and Kircher, T. A. *Platinum enriched, silicon-modified corrosion resistant aluminide coating.* Patent n° US9502226 .1995.

65. Mochvan, B. A. and Demchishin, A. V. *Study of the structure and properties of thick vacuum condensates of nickel, titanium, tungsten, aluminium oxide and zirconium oxide.* Physics Metals Metallurgic 4, 83-90. 1969.

66. Mora, M.M., Sisson, R.D., and Biederman, R.R. *A microstructural study of MCrAlY coatings. In Kossowsky,* R. and Singhal, S.C. (eds.) Surface Engineering .1983.

67. Morrell, P. and Rickerby, D. *Advantages/disadvantages of various TBC systems as perceived by the engine manufacturer.* Proceeding of the 85th meeting of Agard structures and material panels . 1997.

68. Nagaraj, B. A, Katz, G., Maricocchi, A. F., and Rosenzweig, M. *Evaluation of high pressure turbine blade coatings on an LM2500 Rainbow rotor.* International Gas

Turbine and Aeroengine Congress and Exposition .1995.

69. Newcomb, S.B. and Stobbs, W.M. *The degradation of aluminide and platinum aluminide diffusion coatings on CMSX-4*. Elevated Temperature Coatings: Science and Technology II 265-274 .1996.

70. Nicholls, J.R. and Bennett, A. *Cyclic oxidation: Guidelines for test standardisation, aimed at the assessment of service behaviour*. IOM Communications. Cyclic oxidation of high temperature materials .1999.

71. Nicholls, J.R., Deakin, M.J., and Rickerby, D. *A comparison between the erosion behaviour of thermal spray and electron beam physical vapour deposition thermal barrier coating*. Wear **233-235**, 352-361 .1999.

72. Nicholls, J. R., Lawson, K. J., Rickerby, D., and Morrell, P. *Advanced processing of TBC's for reduced thermal conductivity*. Proceeding of the 85th meeting of the Agard Structures and Materials panel . 1997.

73. Nicholls, J.R. and Stephenson, D.J. *High temperature coatings for gas turbines*. In Westbrook, J.H. and Fleischer, R.L. (eds.) Intermetallics compounds: Principle and Practice .1994.

74. Nicholls, J. R., Winstone, M. R., Deakin, M. J., and Kerry, S. *A platinum aluminide diffusion barrier for the oxidation protection of titanium and titanium intermetallic alloys*. Elevated Temperature Coatings: Science and Technology II , 199-208. 1996.

75. Pint, B. *Experimental observations in support of the dynamic segregation theory to explain the reactive element effect*. Oxidation of metals **45** .1996.

76. Pint, B. *On the formation of interfacial and internal voids in alpha-Al2O3*. Oxidation of metals .1996.

77. Pint, B. *The oxidation behavior of oxide-dispersed ß-NiAl: Short-Term performance at 1200°C*. Oxidation of metals **49**, 531-559 .1998.

78. Pint, B., Martin, J. R., and Hobbs, L. W. *O/SIMS characterization of the growth mechanism of doped and undoped α-Al_2O_3*. Oxidation of metals 39(3/4), 167-195 .1993.

79. Pint, B., Treska, M., and Hobbs, L.W. *The effect of various oxide dispersions on the*

phase composition and morphology of Al_2O_3 scales grown on β-NiAl. Oxidation of metals **47**, 1-19 .1997.

80. Pint, B. *et al. Substrate and Bondcoat compositions: Factors affecting alumina scale adhesion.* TBC workshop .1997.

81. Pope, M.I. and Judd, M.D. *Differential thermal analysis: a guide to the technique and its application.* Heyden and Son .1977.

82. Prasanna, K. M. N., Khanna, A. S., Chandra, R., and Quadakkers, W. J. *Effect of θ-alumina formation on the growth kinetics of alumina-forming superalloys.* Oxidation of metals 46(5/6), 465-480. 1996.

83. Reus, R. *Diffusion barriers.* Intermetallics Compounds: Principle and Practice **2**, 603-635 .1994.

84. Rickerby, D.S. and Bull, S.J. *Evaluation of coatings.* In Rickerby, D.S. and Matthews, A. (eds.) Advanced Surface Coatings: a handbook of surface engineering. Glasgow and London .1991.

85. Rohde, S.L. and Munz, W.D. *Sputter deposition.* In Rickerby, D.S. and Matthews, A. (eds.) Advanced Surface Coatings: a handbook of surface engineering. Glasgow and London .1991.

86. Rolls Royce. *The Jet engine.* 1987.

87. Rossnagel, S.M. *Use of plasmas in deposition technologies.* In Rickerby, D.S. and Matthews, A. (eds.) Advanced Surface Coatings: a handbook of surface engineering. Glasgow and London .1991.

88. Sahoo, P., Carr, T., Martin, R., and Dinh, F. *Thermal Spray Manufacturing Issues in Coating IGT Hot Section Components.* Journal of Thermal Spray Technology **7**, 481-483 .1998.

89. Sauthoff, G. *Intermetallics.* 1995.

90. Schulz, U., Fritscher, K., Leyens, C., Peters, M., and Kaysser, W. A. *The thermocyclic behaviour of differently stabilized and structured EB-PVD TBCs.* Journal of Metals 49(10). 1997.

91. Schumann, E., Yang, J.C., and Graham, M.J. *Direct observation of the interaction of Yttrium and Sulphur in oxidised NiAl.* 1995.

92. Schwarz, E., Nicoll, A. R., Gruner, H., and Prince, R. *Thermal spraying: Component design and process considerations for plasma spraying.* First International Conference on Surface Enginering. 1985.

93. Shillington, E.A.G. and Clarke, D.R. *Spalling failure of a thermal barrier coating associated with aluminium depletion in the bondcoat.* Acta Materiala **47**, 1297-1305 .1999.

94. Silva, M. F. O. V. *Multilayer TiB2/X hard coatings by sputtering deposition.* PHD Thesis, Cranfield University . 1998.

95. Singhal, S. C. *High-temperature protective coatings.* Corrosion and environmental effects committee of the Metallurgical Society of AIME. 1983.

96. Smeggil, J.G., Funkenbush, A.W., and Bornstein, N.S. *A relationship between indigenous impurity elements and protective oxide scale adherence characteristics.* Metallurgical transactions **17**, 923-931 .1996.

97. Smeggil, J.G. and Peterson, G.G. *Nature of indigenous sulphur segregated to the free metal surface and to the scale-metal interface.* Oxidation of metals **29** .1987.

98. Smialek, J. L. *Oxidation resistance and critical sulfur content of single crystal superalloys.* International Gas Turbine and Aeroengine Congress and Exhibition. 1996.

99. Smialek, J. L. and Meier, G. H. *High-temperature oxidation.* Superalloy II ch 11, 293-326. 1987.

100. Smothers, W.J. and Chang, Y. *Differential thermal analysis: theory and practice.* Chemical Publishing and Co .1958.

101. Stoever, D. and Funke, C. *Directions of the development of thermal barrier coatings in energy applications.* Materials Processing Technology 92-93, 195-202. 1999.

102. Streiff, R., Boone, D.H., and Purvis, L.J. *Structure of platinum modified aluminide coatings.* In Kossowsky, R. and Singhal, S.C. (eds.) Surface Engineering .1983.

103. Streiff, R., Cerclier, O., and Boone, D.H. *Structure and hot corrosion of platinum-*

modified aluminide coatings. Surface and Coatings Technology **32**, 111-126 .1987.

104. Streiff, R., Farrel, M.S., and Boone, D.H. *Oxide adhesion and growth characteristics on platinum-modified aluminide coatings*. Surface and Coatings Technology **32**, 69-95 .1987.

105. Tawancy, H.M., Sridhar, N., Abbas, N.M., and Rickerby, D. *Comparative thermal stability characteristics and isothermal oxidation behavior of an aluminized and a Pt aluminized Ni-base superalloy*. Scripta Metallurgirca et Materiala **33**, 1431-1438 .1995.

106. Tawancy, H.M., Sridhar, N., Tawabini, B.S., Abbas, N.M., and Rhys-Jones, T.N. *Thermal stability of a platinum aluminide coating on nickel-based superalloys*. Journal of materials science **27**, 6463-6474 .1992.

107. Thornton, J. A. *Influence of apparatus geometry and deposition conditions on the structure and topography of thick sputtered coatings*. Journal of vacuum science and technology 11(4), 666-670. 1974.

108. Thornton, J.A. and Munz, W.D. *Sputtering.Metals Handbook: Surface cleaning, finishing and coatings*.1982.

109. Van Dal, M.J.H. and Pleumeekers, M.C. *Intrinsic diffusion and Kirkendall effect in Ni-Pd and Fe-Pd solid solutions.* Acta Materiala **48**, 385-396 .2000.

110. Wang, J.S. and Evans, A.G. *Effects of strain cycling on buckling, cracking and spalling of a thermally grown alumina on a nickel-based bond coat*. Acta Materiala **47**, 699-710 .1999.

111. Westbrook, J.H. *Intermetallic compounds*. 1967.

112. Whittle, D.P. and Stringer, J. *Improvement in properties: additives in oxidation resistance; improvements in high temperature oxidation resistance by additions of reactive elements or oxide dispersions*. 1980.

113. Wing, R. *Advances in thermal barrier coating technology for gas turbine engine applications*. 1998.

114. Wood, G.C., Foutain, J.G., and Stott, F.H. *Oxidation resistance of aluminized coatings on a directionally solidified Ni-Al-Cr_3C_2 eutectic alloy*. Oxidation of metals

14, 47-63 .1980.

115. Wood, J. H. and Goldman, E. H. *Protective Coatings*. Superalloys II , 359-383. 1987.

116. Wright, P.K. and Evans, A.G. *Mechanisms governing the perfomance of thermal barrier coatings*. Current opinion in solid state and material science **4**, 255-265 .1999.